

Research to Evaluate Nitrous Oxide (N₂O) Emissions from Compost in Support of AB 32 Scoping Plan Composting Measure



California Department of Resources Recycling and Recovery

October 2015

Contractor's Report
Produced Under Contract By:
William R. Horwath
Xia Zhu Barker
Shannon K. Bailey
Martin Burger
Eric R. Kent
Kyaw Tha Paw U
Department of Land, Air, and Water Resources
University of California
Davis, CA

S T A T E O F C A L I F O R N I A

Edmund G. Brown Jr.
Governor

Matt Rodriguez
Secretary, California Environmental Protection Agency

DEPARTMENT OF RESOURCES RECYCLING AND RECOVERY

Scott Smithline
Director

Department of Resources Recycling and Recovery
Public Affairs Office
1001 I Street (MS 22-B)
P.O. Box 4025
Sacramento, CA 95812-4025
www.calrecycle.ca.gov/Publications/
1-800-RECYCLE (California only) or (916) 341-6300

Publication #DRRR 2015-01544

-  To conserve resources and reduce waste, CalRecycle reports are produced in electronic format only. If printing copies of this document, please consider use of recycled paper containing 100 percent postconsumer fiber and, where possible, please print images on both sides of the paper.

Copyright © [2015] by the California Department of Resources Recycling and Recovery (CalRecycle). All rights reserved. This publication, or parts thereof, may not be reproduced in any form without permission.

Prepared as part of contract number DRR CIWMB; IWM09027

The California Department of Resources Recycling and Recovery (CalRecycle) does not discriminate on the basis of disability in access to its programs. CalRecycle publications are available in accessible formats upon request by calling the Public Affairs Office at (916) 341-6300. Persons with hearing impairments can reach CalRecycle through the California Relay Service, 1-800-735-2929.

Disclaimer: This report was produced under contract by the University of California Davis. The statements and conclusions contained in this report are those of the contractor and not necessarily those of the Department of Resources Recycling and Recovery (CalRecycle), its employees, or the State of California and should not be cited or quoted as official Department policy or direction.

The state makes no warranty, expressed or implied, and assumes no liability for the information contained in the succeeding text. Any mention of commercial products or processes shall not be construed as an endorsement of such products or processes.

Table of Contents

Table of Tables	5
Table of Figures	8
Acknowledgments	12
Executive Summary	13
Chapter 1. Introduction.....	20
Chapter 2. Greenhouse Gas Fluxes from Compost Windrows.....	21
Introduction	21
Flux Chamber Background.....	22
Micrometeorological Background	23
Materials and Methods.....	24
Experimental Site and Sampling Description General Information	24
Compost Sampling and Analyses.....	25
Temperature and Oxygen Measurements.....	26
Greenhouse Gas Measurements Flux Chamber Theory and Methods	27
Flux Chamber Experimental Sampling Design.....	29
GHG and Uncertainty Analyses	32
Results.....	32
Compost Analysis.....	32
Seasonal Variation	34
Oxygen, Temperature and Moisture Trends.....	34
Greenhouse Gas Emissions.....	37
Discussion	46
Conclusions	51
Chapter 3. Measurements of Greenhouse Gas Fluxes from Composting Green Materials Using Micrometeorological Mass Balance and Comparison to Flow-Through Chambers.....	53
Introduction	53
Materials and Methods.....	54
Experimental Site and Timeline.....	54

Micrometeorological Mass Balance Method	56
Micrometeorological Mass Balance Method Set-Up.....	57
Fetch Calculation.....	59
Upwind/Downwind Gas Sampling Tower Classification	60
Flux Calculations	60
Data Filtering	61
Open Flux Chamber Measurements	62
Results and Discussion.....	64
Temperature Dependence of Gas Concentration Conversion.....	64
Mean Concentration Profiles	64
Effects of Filtering Criteria	66
Wind Velocity	67
Temporal Patterns.....	68
Comparison with Chamber Technique	73
Conclusions	78
Chapter 4. A Study on Biofilter Efficiency and Flux Emissions from Composting.....	79
Introduction	79
Materials and Methods.....	82
Experimental Site	82
Greenhouse Gas Measurements – Mass and Flow Balance Theory	86
Mass and Flow Balance Measurement Methodology	89
Mass and Flow Balance Experimental Sampling Design	91
Gas Analysis	95
Results.....	96
Greenhouse Gas Concentrations	96
CO ₂ Calculated Entrainment Factor	100
Removal Efficiency.....	101
Greenhouse Gas Emissions.....	104
Discussion	106
Conclusions	111

Chapter 5. Monitoring N ₂ O Emissions Following Yard Trimmings Compost Amendment in Tomato Fields and Almond Orchards	113
Introduction	113
Methods and Materials.....	114
Russell Ranch Sustainable Agricultural Facility	115
Leslie J. Nickels Soil Laboratory.....	117
Farmer Sites.....	120
Nitrous Oxide Monitoring.....	121
Statistics.....	123
Results and Discussion.....	123
Background	123
Tomatoes at RRSAF	124
Tomato Grower Fields.....	127
Almonds	132
Conclusions	135
Chapter 6. Using Laboratory Incubations to Assess N ₂ O Emissions from Yard Trimmings Compost Application to California Agricultural Soils.	136
Introduction	136
Materials and Methods.....	137
Soil and Compost Sampling	138
Soil Extraction and Analysis	140
Study 1: Effect of Compost Additions on N ₂ O Production	140
Study 2: Determining Sources of N Contributing to N ₂ O Production	140
Determining the Role of Soil Properties on N ₂ O Production in Compost Amended Soils	142
N ₂ O Sampling and Analysis	143
Statistical Analyses	143
Results and Discussion.....	144
Statistical Analysis of Soil Properties	144
Study 1: Effect of Compost on N ₂ O Emissions Across a Range of Agriculture Soils	146
Original Soil Properties and Change in Response to Applied Treatments	150

Key Soil Properties Driving N ₂ O Emissions.....	151
Study 2: The Source of N for Production of N ₂ O in Compost-Amended Soils	153
Inorganic N Concentrations, Net Nitrification, and Gross N Mineralization.....	153
Production of N ₂ O	157
Sources of N ₂ O from Heterotrophic Denitrification and Ammonia Oxidation	158
Quantifying the N ₂ O Emitted from the Soil, Fertilizer, and Compost Pools	161
Conclusions	164
Conclusions and Recommendations.....	165
Abbreviations and Acronyms.....	170
Appendices	172
A.2.1 Materials and Methods Supplemental Information.....	173
A.2.1.1 Flux Calculations.....	173
A.2.1.2 Contribution Ratios	173
A.2.1.3 Details of the Pile Size	173
A.2.1.4 Surface Area Calculations.....	175
A.2.1.5 Integration	177
A.2.2 Supplemental Data	178
A.4 Appendix for Chapter 4	199
A.4.1 Materials and Methods Supplemental Information.....	199
A.4.1.1 Pipe Flow Averaging Method for Biofilter Equations	199
A.4.2 Supplemental Data	206
Bibliography	214

Table of Tables

Table 1 - ES. California statewide methane emissions factors (\pm expanded uncertainty) ..	15
Table 2 - ES. California statewide nitrous oxide emissions factors.	16
Table 2.1. Characteristics of the input and output material for each experiment.	33
Table 2.2: Calculated grams CO ₂ equivalents (\pm expanded uncertainty) day ⁻¹ DW tons ⁻¹ using the AR5 global warming potentials, 25 for CH ₄ and 310 for N ₂ O.	46
Table 3.1. Mean downwind-upwind concentration differences at each height and p values from t-test testing if mean upwind and downwind concentrations are significantly different from one another while a) the compost pile was in place and b) during the zero source test period.....	66
Table 3.2. Coefficients of the piecewise nonlinear weighted least squares curves fit to the concentration differences (at 0.7m) and fluxes of the CO ₂ , CH ₄ , and N ₂ O averaged across periods in between turn events.	73
Table 3.3. Integrated emissions of CO ₂ , CH ₄ , and N ₂ O during period 5 using chamber fluxes, MMB fluxes, MMB fluxes averaged around chamber sampling events, and MMB fluxes averaged into 3.5 hour periods	76
Table 4.1: Calculated grams removal efficiency, expressed as a fraction.	103
Table 4.2: Calculated grams CO ₂ equivalents day ⁻¹ DW tons ⁻¹ for the ASP using the AR4 GWPs equaling 25 for CH ₄ and 298 for N ₂ O.	106
Table 5.1. Soil characteristics (0–30 cm) tomato cropping system.	115
Table 5.2. Soil characteristics (0–30 cm) almond system.	118
Table 5.3. Timing, quantities, and types of fertilizer applied in the almond experiment.	119
Table 5.4. Soil characteristics (0–30 cm) at the Esparto site.....	121
Table 5.5. Soil characteristics (0–30 cm) at the Woodland site.....	121
Table 6.1. Soil characteristics used in lab incubation.	139
Table 6.2. Correlation matrix of the soil properties evaluated in this study.....	145
Table 6.3. Results of simple linear regression of cumulative N ₂ O emissions (as ng N ₂ O-N g ⁻¹ soil) against iron, across ten soils and under 12 different conditions.....	146
Table 6.4. Effects of soil, compost, water content, and nitrogen (N) fertilization on cumulative N ₂ O emissions.	147
Table 6.5. The effect of compost, water content, and N fertilization and their interaction on soil pH, DOC, and IN.....	150
Table 6.6. Soil gross mineralization and net nitrification rates in soils during the incubation period.....	156

Table 6.7. Cumulative N ₂ O emissions from different treatment during incubation period.	158
Table A.2.1: CH ₄ flux data from Experiment I for each sampling day.....	178
Table A.2.2: CH ₄ flux data from Experiment II for each sampling day.....	180
Table A.2.3: Methane flux data from Experiment III for each sampling day.	182
Table A.2.4: N ₂ O Flux Data from Experiment I for each sampling day.....	184
Table A.2.5: N ₂ O Flux Data from Experiment II for each sampling day.....	186
Table A.2.6: N ₂ O Flux Data from Experiment III for each sampling day.....	187
Table A.2.7: Summary of integration data for CH ₄ from each experiment.....	189
Table A.2.8: Summary of integration data for N ₂ O from each experiment.....	190
Table A.2.9: Summary of the annual N ₂ O and CH ₄ emissions calculation.	191
Table A.2.10: Summary of Experiment I: moisture, nitrate/nitrite, ammonium, dissolved organic carbon and carbon nitrogen ratio.....	192
Table A.2.11: Summary of Experiment II: moisture, nitrate/nitrite, ammonium, dissolved organic carbon, and carbon nitrogen ratio.....	193
Table A.2.12: Summary of Experiment III: moisture, nitrate/nitrite, ammonium, dissolved organic carbon, and carbon nitrogen ratio.....	194
Table A.2.13: Calculated surface area for Experiment I for each location and total surface area.	195
Table A.2.14: Calculated surface area for Experiment II for each location and total surface area.	196
Table A.2.15: Calculated surface area for Experiment III for each location and total surface area.	197
Table A.2.16: Weight measurements of compost piles for each experiment.....	198
Table A.4.1. Raw measurements in fpm, and fractions of pipe diameter, starting from the sample port to the opposite pipe wall.	203
Table A.4.2. Coefficients from profile near beginning of study.	203
Table A.4.3. Coefficients for the velocity profile taken near end of experiments.	204
Table A.4.4. All biofilter CH ₄ concentrations for each sampling day.....	205
Table A.4.5. All biofilter N ₂ O concentrations for each sampling day.....	206
Table A.4.6. Wind speed for the time period of sampling from the Esparto, Calif., CIMIS site.....	207
Table A.4.7. Average of the measured pipe velocity by day and those values after being converted using information given in Appendix A.4.1.1 and then to m ³ min ⁻¹	208
Table A.4.8. CO ₂ Entrainment Factors for each section and the average daily R factor. Calculated using equation EQ 3.11.	209

Table A.4.9. All biofilter CH₄ filter efficiencies (f_i) for each section and average for each sampling day calculated using equation EQ 3.9..... 210

Table A.4.10. All biofilter N₂O filter efficiencies (f_i) for each section and average for each sampling day calculated using equation EQ 3.9..... 211

Table A.4.11. All biofilter CH₄ emissions originating from the compost source for each section and average for each sampling day calculated using formula EQ 3.10a. 212

Table A.4.12. All biofilter N₂O emissions originating from the compost source for each section and average for each sampling day calculated using formula EQ 3.10b. 213

Table of Figures

Figure 2.1. Photograph of scarab turning the experimental windrow pile (left) and the water truck spraying the experimental windrow pile (right)..... 25

Figure 2.2. Photograph of experimental windrow, showing variation in uniformity. 25

Figure 2.3. Visual representation of a windrow cross section showing the sampling locations for oxygen and temperature. 27

Figure 2.4. Representation of the flux chamber used in this study..... 28

Figure 2.5. Visual representation of the nine open chamber sampling locations on the compost windrow..... 31

Figure 2.6. Experiment I-III air temperature (°C) and precipitation (mm/hr) vs. date from the Esparto, CA CIMIS site. 35

Figure 2.7. Average internal oxygen percentage (%) vs. internal temperature (°C) for each experiment..... 36

Figure 2.8. Average oxygen concentration for all experiments at a three foot depth from the top of the surface of the compost pile vs. time. Experiment I (a), Experiment II (b), and Experiment III (c). 39

Figure 2.9. Average temperature for all experiments at a three foot depth from the top of the surface of the compost vs. time. Experiment I (a), Experiment II (b), and Experiment III (c). 40

Figure 2.10. Average moisture percent after turning events for all experiments vs. time. Blue boxes represent periods of rain events leading to 0.6 mm/day or higher, solid green lines represent known watering days, and dotted green lines represent suspected watering days. 40

Figure 2.11. Methane emissions (g CH₄ day⁻¹) for each experiment over the age of the pile..... 42

Figure 2.12. Nitrous oxide emissions (g N₂O day⁻¹) for each experiment over the age of the pile..... 42

Figure 2.13. Averaged methane (CH₄) and nitrous oxide (N₂O) daily fluxes for the three compost piles. (CH₄ emissions in g CH₄ day⁻¹ DW tons⁻¹ (a) and N₂O emissions in mg N₂O day⁻¹ DW tons⁻¹ (b) divided by experiment and location: top, upper side, and lower side..... 45

Figure 2.14. Averaged CH₄ daily emissions in g CH₄ day⁻¹ DW tons⁻¹ (a) and N₂O emissions in mg N₂O day⁻¹ DW tons⁻¹ (b) divided by experiment. 46

Figure 3.1. Relative positions of the compost pile (large rectangle) and the wind and gas sampling towers (numbered 1-4)..... 54

Figure 3.2. Experiment timeline. Month, day, and time (in 2012) are given along the horizontal axis. 55

Figure 3.3. Schematic of gas sampling and analysis system. Air is drawn from the intake tubes (4 of 16 shown) through the valve manifold system by the vacuum pump	59
Figure 3.4. Mean upwind (black circles) and downwind (red triangles) profiles of CH ₄ , N ₂ O, and CO ₂ concentration as measured using the micrometeorological technique for a-c) when the compost was present and d-f) during the zero source test when the compost pile was not present.....	65
Figure 3.5. Hourly averages of concentration differences at each height and flux of CO ₂ (a, b), CH ₄ (c, d), N ₂ O (e, f).	70
Figure 3.6. Half-hourly concentration differences (left) and fluxes (right) of CO ₂ , CH ₄ , and N ₂ O averaged across periods in between turn events.	72
Figure 3.7. Fluxes of CO ₂ , CH ₄ , and N ₂ O calculated with the chamber and micrometeorological mass balance method during turn period 5 (see Figure 3.2).	77
Figure 4.1. Compost pile laid out over the CompDog™ by ECS and covered by the ECS tarp.	83
Figure 4.2. Biofilter layout containing 19 lines of misting sprinklers on top and an inflated tube that releases the gases underneath the biofilter.....	85
Figure 4.3. Photographs of the biofilter.	86
Figure 4.4. Photographs of flux chamber on compost pile.	90
Figure 4.5. Photograph of the pipes bringing the compost gases into the main feeder pipe and finally to the biofilter.....	91
Figure 4.6. Blueprint of the biofilter semi-randomized sampling locations (numbered 1 to 89).	93
Figure 4.7. The average CH ₄ concentrations in g L ⁻¹ for the pipe, the biofilter surface concentrations of the north, south, side, and the ambient concentrations (a). The average CH ₄ concentrations in g L ⁻¹ for the pipe, the total daily average of the biofilter surface, and the ambient concentrations (b).	97
Figure 4.8. The average N ₂ O concentrations in mg L ⁻¹ for the pipe, the biofilter surface concentrations of the north, south, side, and the ambient concentrations (a). The average N ₂ O concentrations in mg L ⁻¹ for the pipe, the total daily average of the biofilter surface and the ambient concentration (b).	98
Figure 4.9. The average CO ₂ concentration (g L ⁻¹) in the pipe vs. time.....	99
.....	99
Figure 4.10. Averaged daily CO ₂ calculated entrainment factor (R) vs. daily averaged wind speed in m s ⁻¹ from the Esparto, California CIMIS site.....	100
Figure 4.11. CO ₂ calculated entrainment factor (R) vs. time, delineated by location (north, south, and side).	101
Figure 4.12. Removal efficiency (RE _e) of CH ₄ vs. date of sampling.	103
Figure 4.13. Daily emissions of CH ₄ from the biofilter vs. date of sampling.	105
Figure 5.1. A picture of tomato plots at the RRSAF site.....	116

Figure 5.2. Shows randomly assigned replicate plots containing 4 trees. Within each plot, treatments were assigned randomly.....	118
Figure 5.3. Picture of the various compost treatments at the Nickels Soil Laboratory.	119
Figure 5.4. Picture of a typical sampling event in tomatoes showing the vented chamber.....	122
Figure 5.5. Emissions of N ₂ O during the summer and winter from the tomato/winter fallow/tomato/winter wheat system in 2010 to 2011.....	125
Figure 5.6. Emissions of N ₂ O during the summer and winter from the tomato/winter fallow/tomato/winter wheat system in 2011 to 2012.....	126
Figure 5.7. The daily N ₂ O flux in the conventional tomato during the summer of 2010.....	126
Figure 5.8. The daily N ₂ O flux in the conventional tomato during the summer of 2011.....	127
Figure 5.9. Emissions of N ₂ O during the summer and winter from the cover crop/tomato/winter wheat two year rotation system in 2010 to 2012.....	128
Figure 5.10. The daily N ₂ O flux in the cover crop tomato rotation during summer 2011. Fertilizer N applied the end of May.....	128
Figure 5.11. The daily N ₂ O flux in the cover crop tomato rotation during winter 2011-2012.....	129
Figure 5.12. Total N ₂ O emissions for winter and summer (Esparto winter only; no tomato) at both grower sites.....	129
Figure 5.13. The daily N ₂ O emissions over the winter of 2010-2011 at the Esparto site.....	130
Figure 5.14. The daily N ₂ O emissions over the winter of 2010-2011 at the Woodland site.....	130
Figure 5.15. The daily N ₂ O emissions over the summer tomato crop of 2012 at the Woodland site.....	131
Figure 5.16. Total N ₂ O emissions in the four treatments (control/no compost, 3 Mg ha ⁻¹ , 6 Mg ha ⁻¹ and the tractor row) in 2011 to 2012.....	133
Figure 5.17. Total N ₂ O emissions in the four treatments (control/no compost, 3 Mg ha ⁻¹ , 6 Mg ha ⁻¹ and the tractor row) in 2012 to 2013.....	133
Figure 5.18. Daily N ₂ O emissions from all treatments during the first year (2011-2012) of the almond trial.....	134
Figure 5.19. Daily N ₂ O emissions from all treatments during the second year (2012-2013) of the almond trial.....	134
Fig. 6.1. Quantifying the effects of compost application, water content, and nitrogen fertilization on nitrous oxide emissions in ten agricultural soils.....	149
Fig. 6.2. Quantifying the effects of compost application, water content, and nitrogen fertilization on nitrous oxide emissions in ten agricultural soils.....	152

Figure 6.3 Change in NH_4^+ and NO_3^- concentrations over incubation time in different soils incubated with or without compost, and with different N fertilizer type. 155

Figure 6.4. Dynamics of soil N_2O emissions under various compost and fertilizer treatments. 157

Figure 6.8. Fraction of the N_2O flux derived from denitrification and ammonia oxidation. 160

Figure 6.10. Total N_2O emissions from denitrification and ammonia oxidation in different soil types and treatments. 161

Figure 6.11. N_2O emissions from soil, fertilizer and compost N in different soils and treatments. 162

Figure 6.12. Total N_2O emissions from soil, fertilizer, and compost N in different soil types and treatments..... 163

Figure A.2.1: (a) All possible measurements taken in Experiment I and II. (b) The additional measurements taken in Experiment III..... 174

Figure A.2.2: Compost pile measurements diagram. 175

Figure A.2.3: Visualization of the surface areas that the previous formulas are calculating. 177

Figure A.4.1: Flow velocity in feet per minute plotted against normalized distance from the sample port, showing the asymmetric flow profile. 199

Figure A.4.2: Cross-sectional view of the flow regimes used for the integration method. 200

Acknowledgments

The authors would like to thank everyone who assisted with this research and/or the production of this report, including Xue Meng Chen, Tad Doane, Lucas Silva, Dave Paige, Michael Mata, Thomas Shapland, and Richard Snyder. Also, this work would not have been possible without the assistance of Grant Ingalls and the rest of the crew at Northern Recycling in coordinating access to the field site and turning of the compost pile.

This research was funded under California Department of Resources Recycling and Recovery Agreement #IWM09027. Additional funding was supplied by the J.G. Boswell Endowed Chair in Soil Science.

Executive Summary

Composting is a preferred alternative to disposal of green materials in landfills and has several benefits, including the use of the resulting compost as a soil amendment. Although ample literature exists describing measurements of greenhouse gas (GHG) fluxes from other sources, including soils and composted or stored animal manure, limited studies have quantified GHG emissions from the process of composting green materials. In this contractor's report, we examine nitrous oxide (N_2O) and methane (CH_4) emissions, both from the composting process and after its application to soil.

In consultation with CalRecycle staff, a composting facility managed by Northern Recycling in Zamora, Calif., was selected to conduct GHG emissions studies from both open air and an aerated static pile system (ASP). The compost facility feedstock is green materials from surrounding areas and the City of Napa, Calif. Seasonally, the waste includes grape pomace from Napa Valley wine operations. The facility uses a mechanically turned windrow system and may be expanding into ASPs to compost a mixture of green and food materials. During this study, the amount of food in the compost feedstock ranged from five to fifteen percent of the total feedstock.

Monitoring of N_2O , CH_4 and carbon dioxide (CO_2) emissions from standard windrow composting was done using two methodologies: an open-flow flux chamber technique modified to include a sweep gas, and a micrometeorological mass-balance (MMB; micro-met) approach. Both methodologies required the development or alterations of gas sampling methods and new, or revised, mathematical equations to estimate GHG emissions. The micro-met approach has numerous technical challenges, and some of these data require further analysis.

In addition to the standard compost windrow monitoring, GHG emissions were monitored from the ASP composting system, which pulls composting gases from the bottom of the pile and routes them through a biofilter. The purpose of this effort was to determine the capability of the biofilter to remove N_2O and CH_4 produced during the composting process. Again, novel mathematical interpretations were developed to estimate GHG filtration capacity of the biofilter.

Field investigations to monitor emissions of N_2O , CH_4 , and CO_2 from applications of yard trimmings compost to California agricultural crops were done on both university research and private grower fields. The crops included almonds and tomatoes in various rotations that included cover crops. A site located at Russell Ranch Sustainable Agricultural Facility (RRSAF) at UC Davis was chosen to represent a tomato-based row-crop rotation with either wheat or wheat and leguminous cover crops as entry points to the rotation. The UC Davis site represents a 20-year study comparing conventional cover cropping and organic agricultural systems. The plots at RRSAF were complemented with additional sites on the farm to reflect more applied agronomic management. The on-farm sites rotated tomatoes and sunflowers, a typical rotation in the Sacramento Valley region. Commercial tomato growers use compost to improve soil

properties. Some growers, especially those who own their land, apply yard trimmings compost to select fields on a three- to five-year schedule.

An almond orchard located on the Leslie J. Nickels Soil Laboratory (NSL) in Arbuckle, Calif., a research and educational facility administered jointly by the Colusa County Water District and the University of California, was used to determine the effect of compost application on N₂O emissions. Local almond growers buy the majority of compost sold from the Northern Recycling facility as a standard soil amendment.

The results from the field studies represented a limited appraisal of the effects of yard trimmings compost on N₂O emissions from soils and crops. Limitations include the small number of soils and crops examined. To broaden the observations of the field study, ten 10 agricultural soils from diverse regions and cropping systems throughout California were used in controlled lab studies to determine the effect of yard trimmings compost on soil GHG emissions. In the controlled study, fertilizer type, soil moisture, and compost amendments were examined across a range of soil textures.

The following are the major conclusions of the study:

The bulk of the data obtained in the chamber study of compost windrows falls within the range of previous emissions studies of these materials. Performing this experiment with different feedstock materials and during different seasons allowed the research team to obtain three seasonal fluxes. The findings suggest that environmental and seasonal influences, as well as composting process management, have a large impact on GHG emissions.

We used a modified chamber with a sweep gas to estimate CH₄ emissions from compost piles. Daily methane emissions ranged from about 30 ± 10 to 340 ± 120 grams CH₄ per day per dry weight ton of composted material depending on the season in which composting occurred. The low estimate represents emissions for the non-winter time periods of the year. The high estimate represents composting during the winter (wetter) pile, when appropriate turning of the pile did not occur throughout the composting period and emissions spiked as a result of this situation. The winter pile was turned less frequently than the other seasonal piles due to lack of equipment accessibility for the compost windrow turner (scarab), which resulted in a prolonged CH₄ emissions profile compared to the other seasonal piles and other published results. Therefore, two scenarios of CH₄ emissions are presented that reflect the results as collected and one that reflects the emissions profile expected to occur (a gradual decline or level response) during the latter stages of the composting in windrows (see details in table footnote below). Assuming approximately 150 compost facilities receive about 5.0 Mt of yard waste (wet wt.; 45% avg. moisture) per year currently, the total yearly emissions range from about 10,000 ± 1,400 Mg CH₄ per year (extrapolating assuming the winter pile was able to be turned appropriately) to 20,000 ± 6,100 Mg CH₄ per year (extrapolating using the raw winter pile data, which was not able to be appropriately turned during the late stages of composting). The 2012 California Air Resources Board (CARB) estimate for CH₄ emissions from composting approximately 4.4 Mt green waste in California is 16,000 Mg per year

(http://www.arb.ca.gov/cc/inventory/doc/docs4/4b_solidwastetreatment_composting_feedstockprocessed_ch4_2012.htm); the results reported in this study are comparable to CARB estimates. The average emissions factor for CH₄ in this study is 4.5 ± 0.12 grams per kilogram of material (wet weight). This compares favorably to 4.1 grams per kilogram from organic wastes (wet weight) reported by CARB (2012).

Table 1 - ES. California statewide methane emissions factors (± expanded uncertainty). The expanded uncertainty was based on a standard uncertainty multiplied by a coverage factor k = 2, providing a level of confidence of approximately 95%.

	Total statewide CH ₄ emissions (Metric tons/yr)	Emissions factor (%)		Emissions factor (g/kg)		Emissions factor (lbs/ton)	
		Based on wet weight	Based on dry weight	Based on wet weight	Based on dry weight	Based on wet weight	Based on dry weight
Non adjusted winter pile emissions ¹	20,000 ±6,000	0.45 ±0.12	0.65±0.17	4.5±1.2	6.5±1.7	8.9±2.4	13±3.5
Adjusted Winter pile emissions	10,000 ±1,400	0.21±0.03	0.30±0.04	2.1±0.3	3.0±0.4	4.2±0.56	6.1±0.81

¹The winter pile experienced less frequent turning due to equipment accessibility issues that led to emissions that were higher than expected. An emissions spike occurred in this winter pile after three weeks of composting. This extrapolated estimated value is calculated based on the assumption that CH₄ emissions would level off instead of spiking. We extrapolated estimates for the days after the three-week period that more closely followed the emissions patterns present in the spring and summer piles.

1. The same modified chamber with which we monitored CH₄ emissions was used to estimate N₂O emissions from the three compost piles. Daily nitrous oxide emissions estimates ranged from about 240 ± 50 to 1100 ± 300 mg N₂O per dry weight of composted material. Assuming that approximately 150 compost facilities in the state receive 5.0 Mt green waste (wet weight) per year, total annual N₂O emissions from composting of organic waste in this study were about 120 ± 20 tons per year, while the 2012 CARB estimates for N₂O emissions from composting organic waste in California are 362 tons per year (http://www.arb.ca.gov/cc/inventory/doc/docs4/4b_solidwastetreatment_composting_feedstockprocessed_n2o_2012.htm). The average emissions factor for N₂O in this study is 0.02 ± 0.0004grams per kilogram of material (wet weight). This compares to 0.09 grams per kilogram from organic wastes (wet weight) reported by CARB (2012). For comparison, the total annual N₂O

emissions represent 0.25 ± 0.04 percent of total N₂O agricultural soil management emissions annually in California.

Table 2 - ES. California statewide nitrous oxide emissions factors.

Total statewide N ₂ O emissions (metric tons/yr)	Emissions Factor (%)		Emissions Factor (g/kg)		Emissions Factor (lbs/tons)	
	Based on wet weight	Based on dry weight	Based on wet weight	Based on dry weight	Based on wet weight	Based on dry weight
120± 20	0.002± 0.0004	0.003± 0.0006	0.02± 0.004	0.03± 0.006	0.04± 0.008	0.06± 0.01

2. The MMB approach results are only reported for Experiment I. Difficulties with equipment and data analysis prevented comparison for Experiment II. Data for Experiment III requires further analysis. Experiment I data are highly variable and dependent on consistent wind. In many data pairings, upwind N₂O measurements were higher than those downwind of the pile. Although overall MMB estimates for CH₄ and N₂O are 163 percent (62.9 kg t⁻¹ vs. 40 kg t⁻¹) and 261 percent (3,103 mg t⁻¹ vs. 1,189 mg t⁻¹) higher than estimates obtained using the chamber technique, direct comparison of the approaches is not validated here or anywhere in the literature. This approach requires further validation, particularly in order to measure N₂O emissions, before any conclusions may be drawn.
3. The ASP system produced similar CH₄ and N₂O emissions when compared to mechanically turned windrow composting. The ASP biofilter removal efficiency for CH₄ and N₂O was 73 ± 0.03 percent and 32 ± 0.05 percent, respectively, based on measured concentrations before and after biofiltration. This biofilter had open sides, however, and was subject to entrainment of ambient air, which could dilute emissions exiting the biofilter, leading to a potential overestimation of biofilter efficiency. In addition, the difficulty in sealing the bottom of the chamber on the coarse biofilter likely resulted in additional air from the top of the biofilter being drawn into the sampling chamber. Novel calculations, based in part on wind data and emissions measurements of ambient air, were devised to correct the biofilter exit GHG concentrations for entrainment of ambient air from both sources. These calculations revised the removal efficiency of the biofilter to 11 ± 0.05 percent for CH₄ and 50 ± 0.05 percent for N₂O. These calculations have not been validated but suggest that as a GHG mitigation practice, biofilters may be

more effective to reduce N₂O emissions than CH₄. Another consideration is that the biofilter examined was composed of wood chips designed originally to reduce VOC emissions. Additional research on biofilter substrates and system design could lead to further reductions of CH₄ and N₂O. However, since the emissions of N₂O and CH₄ from all composting sources are 0.2 to 1 percent or less of total statewide emissions, respectively, a greater implementation of potentially improved ASP type systems would have a small overall effect on reducing both CH₄ and N₂O emissions statewide.

4. Suggested practices to reduce GHG emissions during composting in mechanically turned windrows and windrow systems would focus on improved aeration. Though ASPs theoretically should aerate piles more effectively than static windrows, preferential flow through the pile could occur, causing areas within the piles to become oxygen-deprived. Smaller piles (height by width) may produce fewer emissions; however, some studies show the opposite, suggesting this is an area where additional research is needed. In windrows, a smaller cross section would reduce the path length of fresh air moving through as a result of convective processes produced by the self-heating composting process. However, smaller piles may produce less total heat, retarding the convective flow process when compared to larger piles. Alternatively, aeration could be improved in negatively aerated static piles by running a perforated pipe through the pile and pumping in fresh air to combine with the existing convective flow. The additional aeration would likely reduce both CH₄ and N₂O emissions.
5. The application of finished yard trimmings compost as a soil amendment to agricultural lands was studied in tomato fields and almond orchards to determine whether it affected soil N₂O emissions. Overall, compost application to soils had no significant effect on N₂O emissions in tomato or almond systems. Though compost had no effect on N₂O emissions in the crops examined in this study, growers remarked they use compost for a variety of reasons, namely to improve soil properties. The most notable improvement after compost application was said to be a more even infiltration of irrigation water and greater soil water-holding capacity, which was perceived to increase irrigation efficiency. Secondly, growers remarked that crop growth was generally improved following compost applications, likely from the addition of a wide variety of macro- and micro-nutrients and the buildup of soil organic matter, which positively affects soil properties. The application of compost may help to promote crop resilience to variable climatic conditions of excessive growing season rainfall, and prolonged periods of high temperatures that will likely occur as California's climate changes.
6. Lab studies using ten different agricultural soils to assess the effect of compost applications on CH₄ and N₂O emissions were done to broaden the results of the field compost application studies. Two studies (1 and 2) were

conducted to examine the interaction of compost with fertilizer nitrogen (N), and to determine the sources (fertilizer vs. compost N) contributing to CH₄ and N₂O emissions. Methane was examined to determine whether compost-amended soils became a greater sink. Compost appeared to have no effect on CH₄ consumption. The results of Study 1 show compost application, water content, and N fertilization have important effects on N₂O emissions from agricultural soils. The application of compost increased N₂O emission in soils with low N availability and low background N₂O emissions. These soils generally had higher sand contents. For soils in which the compost application caused a decrease (more clay fraction) in N₂O emissions, this decrease was larger than any of the increases caused by compost application across all soils. In soils fertilized with ammonium sulfate ((NH₄)₂SO₄), N₂O emissions were greater than in soils fertilized with potassium nitrate (KNO₃), even under 100 percent water-holding capacity (WHC; the maximum amount of water a soil can retain), resulting in a 3- to 44-fold increase, indicating ammonium oxidation is the main pathway of N₂O production. Among all studied variables, extractable iron proved to be the most important factor regulating soil N₂O emissions, followed by changes in pH, available N, changes in dissolved organic carbon (DOC), and original DOC.

In Study 2, the complex relationships between green material compost, N fertilizer type, and N₂O emissions were examined. The results suggested the application of compost increased nitrification rates and N₂O emissions from sandy soils, while no significant effect was found in clay loam soils, confirming the results of Study 1. Greater N₂O emissions were observed in fertilizer treatments receiving fertilizer in the form of ammonium (NH₄; NH₄⁺) compared to nitrate (NO₃; NO₃⁻) in sandy soils, suggesting N₂O production was mainly attributable to ammonia oxidation in these soils. In sandy soils, compost N was a significant source of N₂O production. In addition, the application of compost increased N₂O emitted from fertilizer N in the form of (NH₄)₂SO₄ in sandy soils, whereas N₂O emitted from soil N was decreased by compost application. These results indicate the source of N₂O emissions in sandy soils with compost applied, is mainly from the compost itself. The results of the lab studies indicate that to mitigate N₂O emissions, if compost application is to be paired with fertilizer application, nitrate fertilizers are a better choice than ammonium. This is particularly true for sandy soils. In soils where there is an elevated background concentration of NH₄, compost application may elevate N₂O emissions because of ammonia oxidation during the nitrification process.

Overall, this study confirms that composting of green materials produces both CH₄ and N₂O. The results are comparable to other studies, though in general the number of total studies is limited. From the perspective of statewide emissions, the total estimated CH₄ and N₂O contributions from green material processing facilities is small, contributing less than 0.01 to 0.1 percent of total emissions for N₂O and CH₄, respectively. Although there were technical

difficulties using the MMB approach in this application, this may be a method worth further study to capture a more complete profile of emissions in comparison to the standard chamber approach. The use of the finished compost as a soil amendment proved to have no effect on N₂O production at standard application rates in both research and farmer fields for tomato and almond crops. Lab studies indicated that sandy soils could be prone to increased N₂O emissions following the addition of compost compared to finer-textured loam and clay soils. In summary, composting of green materials and its use as a soil amendment are recommended to reduce waste and improve soil productivity.

Chapter 1. Introduction

Composting is an alternative to disposal of green materials in landfills, having benefits including use as a soil amendment and reserving more landfill capacity for non-compostable waste. In this contractor's report the greenhouse gases (GHG) nitrous oxide (N_2O) and methane (CH_4), which are produced during the composting process and following its application to soil, were examined. The goal was to provide improved GHG emission estimates from the composting process and to examine the GHG impacts on agricultural soil when compost is used as a soil amendment.

Monitoring of N_2O , CH_4 , and carbon dioxide (CO_2) emissions from standard windrow composting was done using two methodologies that include a sweep gas flux chamber technique (Chapter 2) and a micrometeorological mass balance (MMB; micro-met) approach (Chapter 3). In addition to the standard compost windrow monitoring, the emissions of GHG were monitored from an aerated static pile (ASP) system to determine the removal capacity for N_2O and CH_4 of the associated biofilter (Chapter 4). All methodologies required the development or alteration of gas sampling methods, and new, or revised, mathematical relationships to improve GHG emissions estimates.

Field investigations to monitor emissions of N_2O from applications of yard trimmings compost to California agricultural soils was done on University of California Davis (UCD) research facilities and on private grower fields. The crops receiving compost as a soil amendment included tomatoes and almonds. The results from the field studies represented a limited appraisal of the effects of yard trimmings compost on N_2O emissions from soils and crops (Chapter 5). To broaden the observations of the field study, ten agricultural soils from diverse regions and cropping systems from around California were used in controlled lab studies to determine the effect of yard trimmings compost as a soil amendment (Chapter 6).

Chapter 2. Greenhouse Gas Fluxes from Compost Windrows

Introduction

Composting is the managed decomposition of organic materials. The diversion of yard and food materials from landfills to composting has been increasing over the past 20 years in California, due to the impacts of a 1989 law, Assembly Bill (AB) 939, which requires all cities and counties to divert half of their waste from landfills annually by 2000. A bill passed by the California Legislature in 2011, AB 341, set a goal of source reducing, recycling, or composting 75 percent of the state's solid waste. In order to accomplish this, the state's organic materials handling infrastructure will need to roughly double (CalRecycle). Methane and N₂O are the main gases of concern when discussing composting. Carbon dioxide emitted from this process is considered neutral in terms of its global warming potential (GWP) because it represents the release of the previously sequestered CO₂ through photosynthesis. (Andersen et al., 2010).

Fossil fuel combustion emitting CO₂ accounted for 79 percent of the GWP in 2010 (U.S. EPA, 2013). Agriculture accounted for the majority of CH₄ and N₂O emissions in the form of enteric fermentation and manure management (CH₄) and agricultural soil management (N₂O) (U.S. EPA, 2013). The waste sector is another source of GHG emissions accounting for 1.9 percent of the total GHG emissions in 2010. Landfills contributed the majority of emissions in this category. However, composting is among these waste management practices, and its contribution to emissions has been increasing since 1990 (U.S. EPA, 2013).

The process by which CH₄ and N₂O are formed and the variables by which they can be controlled during composting is not well understood. Microorganisms under anaerobic conditions generate CH₄ (Hellebrand, 1998; Beck Friis et al., 2000; Jäckel et al., 2005). Nitrous oxide is known to form during the process of incomplete ammonia oxidation (nitrification) and incomplete denitrification. Bacteria that carry out ammonia oxidation are aerobic. The bacteria performing denitrification can be either anaerobic or aerobic (Beck-Friis et al., 2000). The specific pathways contributing to the majority of N₂O emissions that take place in compost remain uncharacterized. Studies have shown that CH₄ emissions are seen to increase when there are lower levels of oxygen availability. (Hellebrand, 1998; Beck-Friis et al., 2000; Beck-Friis et al., 2003). Higher levels of aeration can lead to lower moisture content due to drying, which shows a decrease in CH₄ emissions (VanderGheynst et al., 1998).

There are different ways to conduct large-scale composting. The main two methods are known as windrow and ASP composting. Windrow composting is the main method explored in this study; it is popular because of its simplicity and relatively low expense. In this system, organic material is laid out in long rows known as windrows, with lengths anywhere from 15 meters to 115 meters or greater. Windrows are between two meters in height and five meters in width (Beck Friis et al., 2000; Andersen et al., 2010). In this

method all airborne emissions, including GHGs, are fugitive. There is no way to capture them. Large, diesel-powered windrow turners are used to mix piles for even composting of materials, to incorporate oxygen into the pile, and to increase the porosity of the feedstock in order to lessen the opportunity for the formation of anaerobic conditions (Rynk, 1992). The size, frequency of turning, and overall management of windrows will vary from facility to facility. However, due to CalRecycle's regulation, all windrow facilities must reduce pathogens by performing five turns within a 15-day period, while maintaining windrow temperatures of 55°C (131°F) (Title 14, California Code of Regulations, Division 7, Article 7, Section 17868.3). An ASP system with an insulating cover can perform pathogen reduction by demonstrating three days of pile temperatures above 55°C. Due to the increase in composting over the years, the need for characterizing and understanding this process has become important. The increase in the study of the composting process over the past 20 years has provided insight into multiple ways emissions can be measured, each with their own advantages and disadvantages. The most notable types of measurements can be narrowed down to a flux chamber approach and the MMB approach. In this chapter, the chamber technique to measure CH₄ and N₂O was done on three different compost piles done at different times of the year to assess the effect of season on GHG emissions from the yard trimmings composting process.

Flux Chamber Background

Flux chamber techniques, in general, involve putting a vessel directly on top of the surface of the compost pile to capture emissions. They are limited by a small area in which they capture the emissions, but are mechanically simple and can be quite sensitive to the change of gas concentration (Denmead, 2008). Because of the small area, many replicates can be required. Other issues include compost substrate disturbance when placing chambers and pressure differences that can create artifacts in the data (Denmead, 2008). This technique can be further broken down into two types, closed chambers and open chambers, also known as flow-through chambers.

Closed chambers consist of an open bottom and a sealed top, sometimes including a small vent mechanism. These chambers are most commonly used to measure soil emissions, but have also been used on compost (Andersen et al., 2010; Beck-Friis et al., 2000). The principles are based on the buildup of the concentration of the GHGs over the period of time the chamber is in place. The desired result is a linear increase with time (Denmead, 2008). This technique is sensitive to leaks and the inhibition of gas fluxes due to concentration buildup in the chamber headspace. Due to the rapid accumulation of gases in compost when compared to soil, closed chambers will be more susceptible to the inhibition of flux. This leads to closed chambers giving a potential underestimation of the flux for a given system (Gao and Yates, 1998).

Open chambers are considered flow-through chambers because of the lack of a seal at the top. Emissions are permitted to flow from the surface of the compost out of a chamber chimney or opening. Because of the flow of these gases, the principles used to estimate flux in a closed chamber are not applicable. In order to calculate a flux, the use

of a sweep-gas or flow-through gas is needed. This gas can be composed of ambient air or a gas that does not contain the gases of interest, like nitrogen gas (N₂). Surface flux density (F) can then be defined by the following equation where *v* is velocity of the sweep gas, *C_o* is the concentration of gas leaving the chamber, *C_i* is the concentration of the gas entering the chamber, and *A* is the area of the chamber bottom. (Denmead, 2008; Gao et al., 1997)

$$F = \frac{v(C_o - C_i)}{A} \quad [\text{EQ 2.1}]$$

There are ways the concentration of *C_i*, the gas entering the chamber, must be estimated, but this will be discussed in further detail later on. This method gives only a lower bound, and thus will give an underestimation of the flux. Benefits of this method include that when fluxes are high, as they are in compost, open chambers have a lower risk of the buildup of gas concentration, as is seen in closed chambers. A flow-through chamber tends to underestimate actual flux when the flow rate (*v*) used is low and overestimate if the flow rate used is high (Gao and Yates, 1998). Calibration of these methods has been attempted in different ways such as by creating a known artificial flux or by trying to compare multiple methods on the same emissions source (Gao and Yates, 1998; Park et al., 2009; Widén and Lindroth, 2003; Butnor and Johnsen, 2004).

Micrometeorological Background

Micrometeorological techniques include measuring the air around a given source to estimate fluxes. This can be done in different ways and depends on the application involved. Micrometeorological techniques for measuring emissions from compost piles are based on the principles of conservation of mass as applied to the emitted gases, as well as wind flow and direction. A variety of techniques have been used or proposed, but the most appropriate to individual compost piles are the mass balance and backward Lagrangian methods (Denmead, 2008). Backward Lagrangian dispersion models employ basic turbulent transfer theory, and simulate the trajectory of the gases backward from the measurement location to the source (Flesch et al., 1995; Denmead, 2008). The mass balance method involves measurement of the vertical profile of gas concentrations upwind and downwind of the gaseous emission source, in parallel with a vertical profile of wind velocity. Emissions are essentially determined by subtracting the vertically integrated upwind horizontal gaseous fluxes from the downwind fluxes (Denmead, 1995; 2008). This method has been applied to small field plots of fertilizer, chemical treatments, animal waste, and composted animal materials (Khan et al. 1997, Brown et al. 2002, Wagner-Riddle et al. 2006, Park et al. 2010a, b, VanderZaag et al. 2011, Sommer et al. 2004). In general, micrometeorological techniques do not involve some of the potential problems of chamber measurements (pressure, flow, and micrometeorological changes caused by the chambers), but require a greater amount of equipment, more complex set up than for chambers, and intensive analysis of large data sets.

Materials and Methods

Experimental Site and Sampling Description General Information

Greenhouse gas emissions and compost chemistry were monitored at the Northern Recycling compost facility (11220 County Road 94; latitude 38.77564° N, longitude 121.88007° W) in Zamora, Calif. The windrow was comprised of yard trimmings collected from surrounding cities and the north end of San Francisco Bay, which was then mixed with wood chips or chopped branches to increase porosity, allowing for higher aeration.

In the course of this study three windrow piles were monitored during three different seasons. The first pile represented a summer pile (57 days old, gas sampled over 55 days), and is referred to as Experiment I throughout this report. The second pile represented a winter pile (43 days old), and is referred to as Experiment II throughout this report. The third pile represented a spring pile (54 days), and is referred to as Experiment III throughout this report. The exact pile start and end dates are shown in Table 2.1.

The compost was laid out in a windrow and turned using a windrow turner, a rotary drum with flails, shown in Figure 2.1 (Rynk, 1992). The pile was weighed using a truck scale operated by Northern Recycling, with the weight measured both before and after the composting process. The ends of the pile were shaped with a loader to obtain the trapezoidal shape on the ends. At times the loader was also used to narrow the pile when the turning widened it. Test piles were approximately 18 m x 3.5 m x 1.3 m (L x W x H), reduced in length from the normal commercial piles, to allow for micrometeorological measurements to be made simultaneously with the methods described here. The pile was oriented in the north-to-south direction. A truck was used to add water according to the specifications determined by facility management (Figure 2.1). The goal was to maintain the pile at approximately 50 percent moisture. Moisture content was determined gravimetrically following drying at 80°C for 24 hours. Water applications mostly occurred before turning, so the newly wetted material could be mixed into the rest of the pile. Exact size fluctuated, for each pile, due to turning and the composting process (Figure 2.2).

Figure 2.1. Photograph of scarab turning the experimental windrow pile (left) and the water truck spraying the experimental windrow pile (right).



Figure 2.2. Photograph of experimental windrow, showing variation in uniformity.



Each pile was turned five times within the first 15 days of initial construction, and then the pile was turned weekly. On a few occasions the piles were not turned because of weather conditions or equipment malfunction. This occurred once during Experiment I, when the pile should have been turned on day 29, and twice during Experiment II, when the pile should have been turned on day 19 and day 29. (The pile was turned on day 23.) In Experiment III, on the last day of sampling, the pile was mixed with a loader because the windrow turner broke down.

Compost Sampling and Analyses

Compost material was sampled to quantify the moisture content, ammonia, nitrate, dissolved organic carbon (DOC), total carbon, and total nitrogen on a mass-specific basis. Immediately following each turning event (unless otherwise noted), grab samples were taken from five different sections of the pile starting from the north and working to

the south. In each of these sections, five different locations from the cross sections of the pile were mixed together to fill a one-gallon bag (for the extractions and analysis described below) and one metal tin (for oven drying, described below), to equal five bags and five tins for each turning date. These locations were approximately 15 cm below the surface of the pile. Each bag was stored in a cold room at 4°C within five hours of obtaining the samples. Experiment I samples were not analyzed until three to nine weeks later, while Experiment II and III samples were analyzed within zero to five days. The lag in analysis for Experiment I could have affected the results; however, this was evaluated with other samples and found not to influence the results. Experiments I and III contained 55 compost analysis samples total, at five samples per pile, while Experiment II contained 45.

To determine moisture content, the samples taken in the metal tins were oven-dried at 105°C for 48 to 120 hours. Moisture content was calculated gravimetrically from the mass loss. Chemical analysis for nitrate, ammonia, and DOC were performed on the bag samples; the compost material was first hand-chopped and cut to mix the material. Part of this mixture (~60g wet weight compost, ~30g dry weight) was extracted using 500 mL of 0.05 M potassium sulfate (K₂SO₄). Nitrate (Doane and Horwath, 2003) and ammonia (Verdouw et al., 1978) concentrations were determined colorimetrically, with a Shimadzu UV mini 1240 spectrophotometer. Dissolved organic carbon was determined by UV persulfate digestion (Teledyne-Tekmar Phoenix 8000).

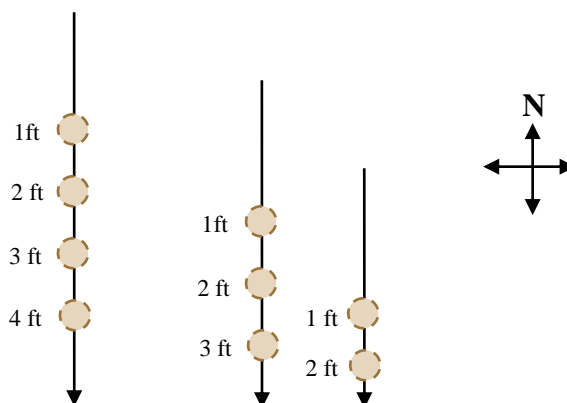
The remaining amount of sample not used for the extraction was then dried at 60°C in preparation for total carbon and nitrogen analysis. After the samples were completely dry, they were milled down to two-millimeter aggregates, and later ground down to a fine powder using individual ball mills. Samples were then analyzed for total carbon and nitrogen in the Costech Analytical Technologies ECS 4010, an elemental combustion system with an atropine standard used in Experiment I and an acetanilide standard used for Experiment II and III for calibration.

Temperature and Oxygen Measurements

Temperature and oxygen profiles were taken in parallel with each sampling. On turning days, where two samplings would occur, temperature and oxygen measurements were also taken twice. The measurements were taken using the ReoTemp OxyTemp probe (Manufacturer stated specifications - oxygen: accuracy [0-100±2%]; temperature [0-90°C±1%]).

Measurements were taken at different depths at the same locations as the chamber measurements (see below for details of the chamber methods). The top measurements were taken at one, two, three, and four feet (0.30 meters, 0.61 meters, 0.91 meters, and 1.22 meters, respectively) below the surface of the compost. The side was taken at one, two, and three feet for the upper part of the slope and one and two feet for the lower part of the slope (Figure 2.3). Occasionally the water content of the pile would lead to clogging of the oxygen sampling head and measurements could not be taken for that section. Also, as the pile shrank due to the composting process the depths of measurement were lessened.

Figure 2.3. Visual representation of a windrow cross section showing the sampling locations for oxygen and temperature.



Greenhouse Gas Measurements Flux Chamber Theory and Methods

Open flow-through chambers were used to study windrow emissions focusing on CH₄, N₂O and CO₂. Open chambers are thought to measure emissions more accurately by allowing better pressure and flow equilibration with the substrate emissions being monitored (Schmidt, 2012). The chamber design is composed of a main, large cylindrical chamber with a small cylindrical chimney that is open to the atmosphere (Figure 2.4). The large chamber has a diameter of 28.5 cm and a height of 31.7 cm. The chimney has a diameter of 5.25 cm and a height of 20.5 cm. A small fan is inside the large chamber for circulation of the headspace. Nitrogen gas was used as a sweep gas in this system at a rate of 8 L min⁻¹ by dispersing it into the main chamber. This flow rate was chosen based on open chamber work by Pumpanen et al. (2001) and Gao et al. (1997) and initial lab testing.

Flow rate is critically involved in the estimation of the surface flux density from the open chamber. One derivation of the flux density calculation requires the assumption that the sweep gas has a much greater flow than the flow from the compost source (see [EQ 2.3]). Equation 2.4 [EQ 2.4] below gives a lower bound to the flux density estimation using this assumption (Playa Vista Dev. Regional Geochemical Assessment, 2001).

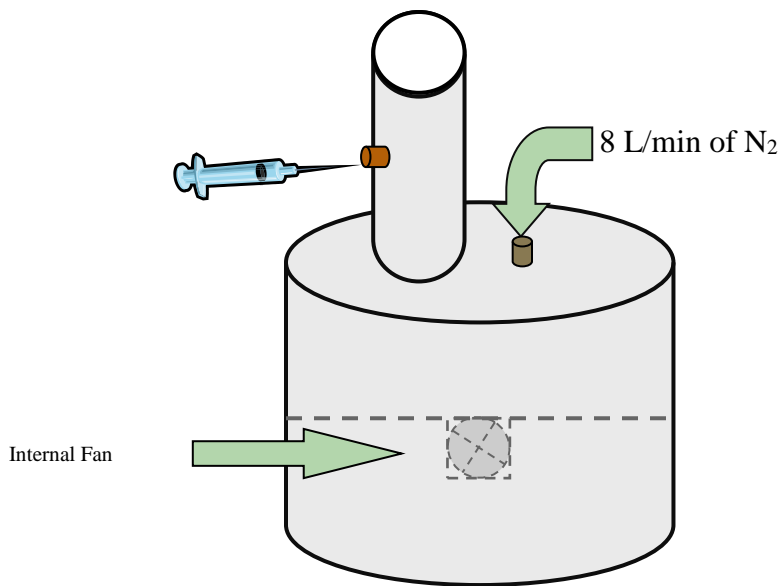
$$E = \frac{(Q_{Sweep} + Q_{Source})Y_{Sample}}{A} \quad [EQ 2.2]$$

$$Q_{Sweep} + Q_{Source} \approx Q_{Sweep} \quad [EQ 2.3]$$

$$E1 \approx \frac{Q_{Sweep} Y_{Sample}}{A} \quad [EQ 2.4]$$

Where E is the surface flux density from the source in $\text{g m}^{-2}\text{s}^{-1}$, Q_{sweep} is the flow rate of the N_2 sweep gas, going into the chamber in L min^{-1} , Q_{source} is the flow rate of the gas coming from the surface of the compost being emitted into the chamber in L min^{-1} , Y_{sample} is the concentration of the gas sampled from the chamber in mg L^{-1} , and A is the surface emissions area of the bottom of the chamber in m^2 .

Figure 2.4. Representation of the flux chamber used in this study. The bottom of the chamber is placed on the desired surface for measurement. The chimney-like top is left open, and syringe samples are taken from the port on the chimney as gases travel out of the chamber.



Equation 2.8 for flux density estimation gives an even greater lower bound than the formula above (Playa Vista Dev. Regional Geochemical Assessment, 2001). The concentration of the GHG of interest in the sample was assumed to be less than the concentration in the source. The source was also assumed to be 100 percent of the GHG of interest. These assumptions are reasonable when there are gas emissions because the sample gas will be a dilution of the concentration at the source. Because these assumptions give a closer approximation, although still a lower bound to the desired flux density, all flux estimations in this paper used EQ 2.8 for the calculation. We also used this equation as the upper bound of the flux density. Below shows the derivation after some substitutions.

$$E = \frac{Q_{\text{sweep}} (C_{\text{source}} / (C_{\text{source}} - C_{\text{sample}})) Y_{\text{sample}}}{A} \quad [\text{EQ 2.5}]$$

$$C_{Sample} < C_{Source} \leq 1 \quad [EQ 2.6]$$

$$C_{Source} \approx 1 \quad [EQ 2.7]$$

$$E2 \approx \frac{Q_{Sweep}(1/(1 - C_{Sample})) Y_{Sample}}{A} \quad [EQ 2.8]$$

Where C_{source} is the concentration of the gas from the surface of the compost being emitted into the chamber in vol/vol, C_{sample} is the concentration of the gas sampled from the chamber in vol/vol, and all other previously defined variables remain the same (Playa Vista Dev. Regional Geochemical Assessment, 2001).

Flux Chamber Experimental Sampling Design

The windrow area was assumed to be a trapezoidal prism. Over time it was made irregular by frequent turning and the composting process, but it kept the general shape. The pile was measured at nine different locations, by first visually dividing it into three different sections, north, south, and middle. Three chamber measurements were done in each section, at least one meter from the edge of the pile to prevent measuring end effects. As shown in Figure 2.5 one chamber was located directly on top of the pile, the second and third was located on the side of the pile at an angle perpendicular to the pile surface, one on the upper half of the slope and one on the lower half of the slope. Andersen et al. (2010) demonstrated the majority of windrow emissions are emitted from the top of the pile. From this we determined that measuring on one side of the pile would be a sufficient estimate of the flux for both sides. If the pile was assumed sufficiently mixed and homogeneous, bilateral symmetry could also be assumed. The piles were sampled only on the top and the east facing side.

During Experiment I each chamber was run individually, with serial measurements one after another (unlike the photo in Figure 2.5). In Experiments II and III, chambers were placed and run simultaneously on the top, upper side, and lower side using a manifold to split the gas and a flow controller for each of the gas lines to ensure the flow was maintained (Figure 2.5). When chambers were placed on the side positions, a small metal rod was inserted into the pile and through the chamber to secure the chambers to the sloping surface. The fans were turned on, and the N_2 sweep gas was run at 8 L min^{-1} for eight minutes. This equilibration time was calculated to allow for three exchanges of the nitrogen gas to pass through the chamber based on its volume. Preliminary chamber measurements with varying run times confirmed this was an adequate duration.

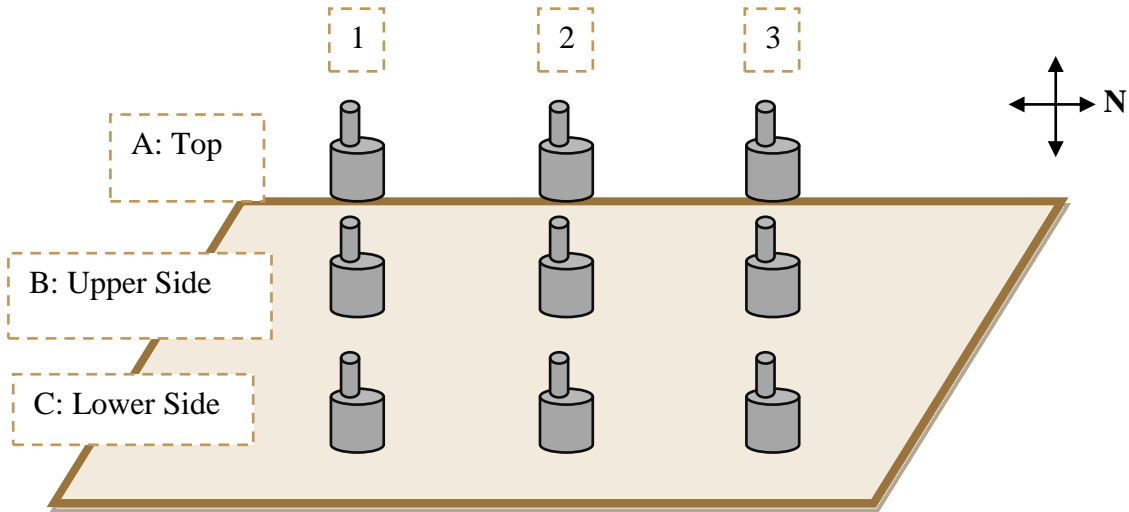
Ambient samples (n) near the compost pile were taken as well ($n = 5$ for most days). A control chamber was also used in each study ($n = 1$ for Experiment I, $n = 3$ for subsequent studies). This control method consisted of putting the open chamber on the soil approximately five meters from the pile (Experiment I), or on a polyurethane tarp (Experiments II and III). These chambers were treated and sampled in the same way as if they were on a pile. The purpose of this control is to determine the concentrations

where there are negligible emissions to use as a baseline for background level emissions.

Samples were taken out of a small rubber septa located along the chimney of the open chamber, using a 20 mL syringe, and injected into a previously evacuated Exetainer vial. In Experiment I, duplicate samples were taken with each chamber; the average relative standard deviation was eight percent for CH₄, ten percent for CO₂, and four percent for N₂O. During analysis these values were averaged, and then treated similarly to samples from Experiments II and III when only one gas sample from the chambers was taken.

Chamber temperature measurements were taken at the time of sampling with a Fluke 51II Thermometer using a type K thermocouple near the gas removal septa by inserting the thermocouple wire downward, 14 cm from the chimney top. Ambient temperature was also captured during ambient air sampling using the same thermocouple.

Figure 2.5. Visual representation of the nine open chamber sampling locations on the compost windrow. Three chambers were run at a time (A, B, and C) starting with Section 1 on the southernmost side of the compost pile (top). Photograph of the three chamber placement on Section 2, micrometeorological tubing seen on the left (bottom).



GHG and Uncertainty Analyses

The Exetainer vials were stored at a temperature range of 19°C to 25°C from five hours to three weeks before analysis on a gas chromatograph (GC). The GC was fitted with an electron capture detector (ECD) for N₂O measurement, a thermal conductivity detector (TCD) for CO₂ measurement, and a flame ionization detector (FID) for CH₄ measurement (GC-2014, Shimadzu). Calibration gases (AirGas Inc., Sacramento) were run in tandem with the samples to act as standards with a known concentration. These standards were treated in the same manner as the samples, by injecting 20 mL of gas into an evacuated Exetainer vial. The GC gives an output of peak area for each standard and sample run on the instrument. Using the known concentration of the standard (independent variable) and the peak area of the result (dependent variable), a calibration curve is made. A total of 1,126 samples were analyzed in this fashion over the three experimental periods.

Gas fluxes measured on each sampling date were used to estimate cumulative mass-based gas emissions using trapezoidal integration of daily fluxes under the assumption that the measured fluxes represented mean daily fluxes, and that mean daily fluxes changed linearly between measurements. The daily average mass-based gas emissions were calculated as the cumulative mass-based gas emissions divided by number of sampling days. The annual GHG emissions were calculated as the sum of three seasonal cumulative gas emissions based on the assumption that the annual yard green waste was equally distributed in each season. The uncertainty in this report was calculated as the expanded uncertainty based on a combined standard uncertainty multiplied by a coverage factor $k = 2$, providing a level of confidence of approximately 95 percent. The combined standard uncertainty of the annual GHG emissions was calculated from the combined standard uncertainty of the seasonal GHG emissions by assuming the sources of uncertainty were uncorrelated, and then the variance of the annual GHG emissions equals the sum of the variances of seasonal GHG emissions. The combined standard uncertainty of the seasonal GHG emissions was calculated from the standard uncertainty of daily GHG flux using the same method as discussed above, and the standard uncertainty of daily GHG flux was calculated as the standard deviation of the mean value from the three replicates used in each sampling event.

Results

Compost Analysis

Table 2.1 shows a summary of the input and output characteristics of the compost material measured when the windrow was constructed and when the windrow monitoring was ending.

Table 2.1. Characteristics of the input and output material for each experiment.

	Experiment I		Experiment II		Experiment III	
	5/22/12	7/19/12	11/5/12	12/18/12	2/21/13	4/16/13
	Input	Output	Input	Output	Input	Output
Material, Mg (DW*)	13.2	9.50	11.6	10.6	10.5	13.2
Pile Dimension (L x W x H, m)	18.3 x 3.3 x 1.7	13.7 x 3.7 x 1.7	17.7 x 3.8 x 1.5	18.0 x 3.7 x 1.2	20.8 x 3.6 x 1.4	15.4 x 3.4 x 0.96
C:N ratio**	31.5 ± 1.5	21.9 ± 0.4	30.1 ± 0.4	19.5 ± 0.2	27.5 ± 0.2	21.7 ± 0.3
Total C, kg (DW)	4400	2500	3600	2500	3200	3100
Total N, kg (DW)	140	115	120	130	120	140
Ammonium-N, kg (DW)	2100	1700	12000	470	20	200
{Nitrate +Nitrite}-N, kg (DW)	430	5.1	100	Below Detection	Below Detection	Below Detection
DOC, Mg (DW)	160	33	340	28	69	19

*DW indicates dry weight

** ± indicates standard error between five experimental replicates.

In Experiment III on 3/19/2013, while the pile was being shaped, the loader introduced a visible amount of excess soil into the pile. This could explain the unexpected gain in dry weight from the input to the output. All measured compost material composition data, with the exception of the N₂ for Experiments II and III and ammonium-N for Experiment III, exhibit a drop. This is expected because of the release of carbon and N₂ in the form of gases, such as the ones measured—CO₂, N₂O and CH₄, as well as others such as carbon monoxide (CO) and ammonia gas (NH₃) (Hellebrand, 1998), that were not measured in this study.

Seasonal Variation

Each experiment occurred during a different time of year, and therefore the feedstocks of each pile varied based on the initial plant material. Not surprisingly, the diverse seasons were associated with different weather for the duration of each pile. Figure 2.6 graphs the temperature (°C) and precipitation (mm/hr) for each of the three experiments. Experiment I experienced a hot and dry climate with an average temperature of 24.1 °C (75.4 °F), and overall rain of just 1.4 mm (0.05 inches). Note the different scale when looking at Experiment I precipitation. Rain events were frequent during Experiment II, and the duration was characterized by cooler temperatures with an average of 12.3°C (54.1 °F) and total rain of 1,187.6 mm (46.8 inches). Experiment III experienced a climate in-between that of Experiment I and Experiment II. It had a range of medium to high temperatures, averaging 15.5°C (59.9 °F), with occasional rain events, 33.2 mm (1.3 inches) total. Turning operations during Experiment II were often delayed because of the frequent rain events.

Although feedstock was not a measured variable of this study, it was changing with the seasons and most likely affected GHG emissions. According to the facility manager, Experiment I was comprised of the most diverse feedstock, containing grass clippings and shrub and tree branches. Experiment II was performed in the fall, and leaves were the main feedstock, estimated as high as 90 percent. Finally, leftover leaves and chopped pine trees made up the feedstock for Experiment III.

Oxygen, Temperature, and Moisture Trends

Internal temperature and oxygen concentrations are thought to affect emissions of GHGs (Beck-Friis, 2003; Jackel, 2005; Andersen, 2010). Measurements of internal temperature and oxygen levels were taken during each pile sampling. The analysis was simplified by only looking at the measurements from the top section at three feet deep (Figure 2.1) taken in the three different sections (north, middle, and south). By averaging these values over the whole of each experiment, a correlation between internal temperature and oxygen percentage was observed (Figure 2.7). This correlation implies the lower the internal temperature, the lower the oxygen percentage, with an R squared value of 0.9377. Experiment II, which experienced the most rain, had the lowest internal temperatures and internal oxygen percentage, where Experiment I, which was exposed to very little rain, had the highest of each variable. The low internal oxygen of Experiment II was $1.7\% \pm 0.25\%$ with a temperature of $53.7 \pm 0.58^{\circ}\text{C}$, whereas Experiment I had $5.1\% \pm 4.6\%$ oxygen and a temperature of $61.3 \pm 0.63^{\circ}\text{C}$. The median internal oxygen percentage and temperature of Experiment III was $3.3\% \pm 0.42\%$ and $55.5 \pm 0.59^{\circ}\text{C}$, respectively. The temperatures at the center of the piles in each experiment were in the thermophilic range (between 45 and 70°C) for microbial activity (mesophilic conditions with temperatures between 20 and 45°C could have been present on the far edges or closer to the surface).

Figure 2.6. Experiment I-III air temperature (°C) and precipitation (mm/hr) vs. date from the Esparto CIMIS site. Note that Experiment I has a different scale for precipitation to more effectively show the low amount of rain during that time.

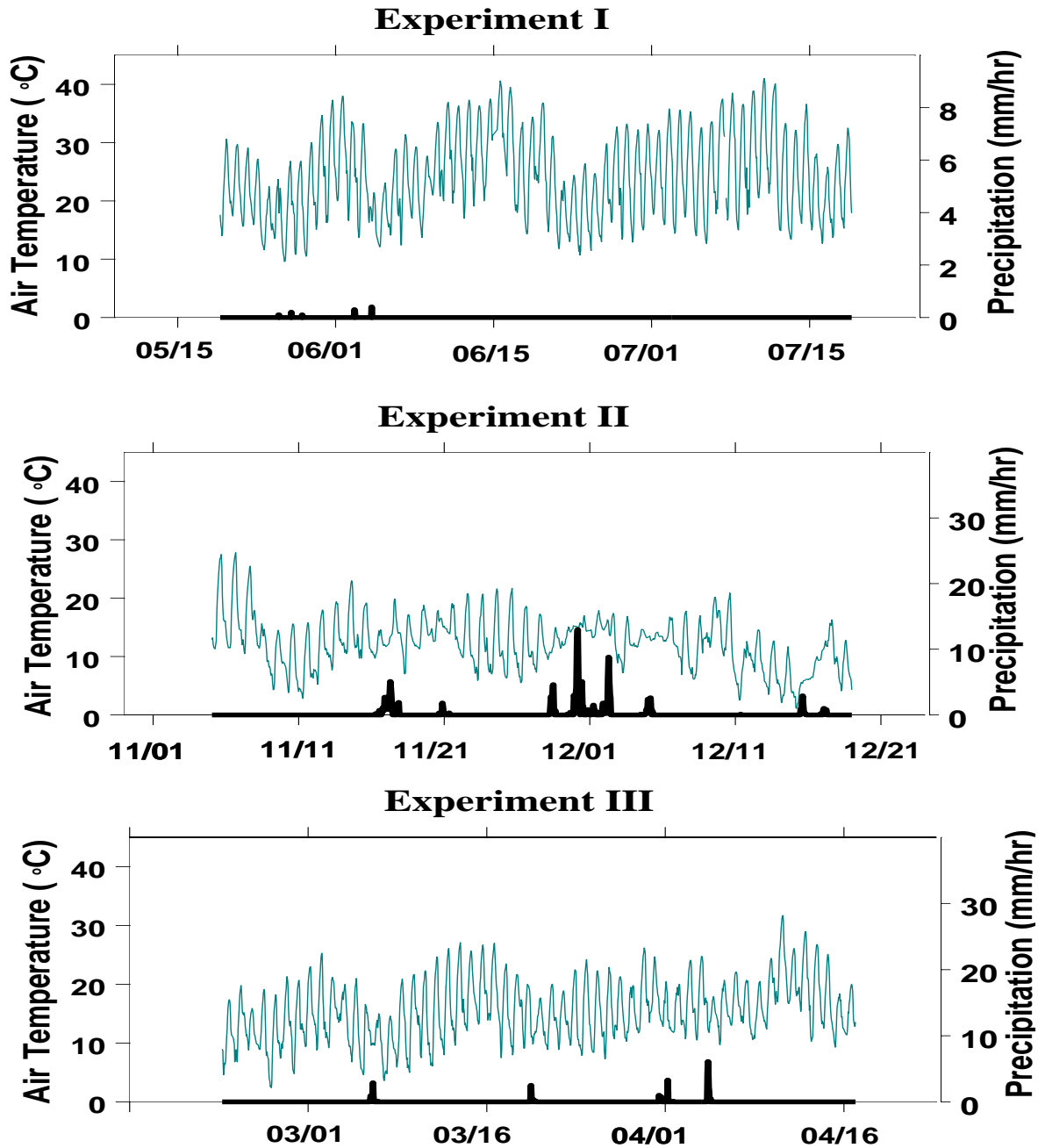
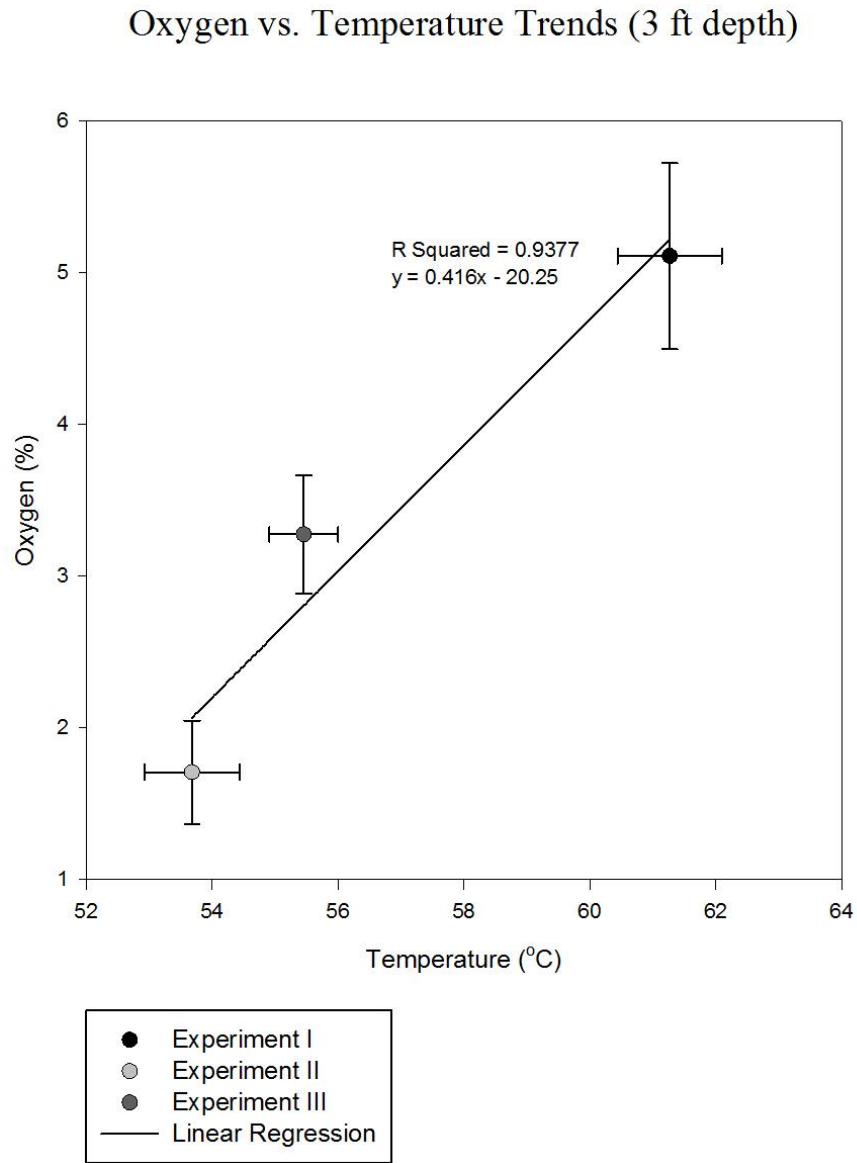


Figure 2.7. Average internal oxygen percentage (%) vs. internal temperature (°C) for each experiment. Error bars display standard deviation.



Oxygen, temperature, and moisture changed over the course of composting. Oxygen was consumed by microbes, especially during the first few weeks after windrow formation. Figure 2.8 shows the change of oxygen over the course of monitoring of each pile for the three-foot depth from the top of the pile surface. On many of the turning days the piles were measured before and following the turn (different symbols). Samples taken after the turning are marked in gray. In Experiment II, on one occasion samples were taken 2.5 hours after the turn as well as both immediately before and after the turn. This 2.5-hour post-turn sample is marked in red. Experiment I (Figure 2.8a) shows

a high level of variability in the oxygen concentration. Experiment II (Figure 2.8b) and III (Figure 2.8c) show similar patterns of higher oxygen concentrations during the first few weeks, especially for sampling after turning, which then tapers down to a low oxygen level. Average temperature at the three-foot depth is shown in Figure 2.9. These measurements were taken simultaneously with the oxygen measurements in Figure 2.8. Experiment II (Figure 2.9b) had a lower average temperature than the other piles and also had a decrease in temperature near the end of the monitoring period. Experiment III (Figure 2.9c) also experienced a late decrease in temperature. Experiment I (Figure 2.9a) experienced higher variations in temperature as well as the highest average temperature. At times during Experiment I, there was a greater separation of pre-turn temperatures and post-turn temperatures than was observed in the other two experiments.

Figure 2.10 displays the moisture percentage over the monitoring time. Symbols are similar to the previous graphs. Moisture concentrations were always taken after a turn, or in the case of 4/16/13, after mixing by a loader. On occasion watering events would occur immediately prior to turning to incorporate moisture. A truckload of water, maximum of 2,500 U.S. gallons (9.5 ML), was used for each watering event. Watering was not a focus of this study and was determined by the management of the composting facility. Watering events were well documented for Experiment I. Documented watering events of Experiment I were on 7/6/12 and 7/12/12; however, any previous rise in moisture before these dates was most likely due to undocumented watering events since no rain events greater than 0.6 mm/day occurred during this experiment. Blue boxes represent rain events, solid green lines represent known watering days, and dotted green lines represent suspected watering days (although other turning days may have received water). With these watering events moisture was kept fairly constant in Experiment I, although slightly lower than that at the beginning (Figure 2.10a). Rain events halfway through the monitoring of Experiment II (Figure 2.10b) contributed to a higher moisture content at these later times. Moisture in Experiment III (Figure 2.10c) started high due to watering by the facility, but the subsequent rain events were not large enough to keep the moisture from slowly decreasing over time.

Greenhouse Gas Emissions

Methane, CO₂, and N₂O were measured from the windrows in each experiment. The focus of the following figures is on CH₄ and N₂O. Figure 2.11 displays CH₄ emissions in grams per day for each pile versus the age of the pile in days. Symbols are similar to those seen on previous graphs. Turning events are marked with a red dotted line. Note that the scale on Experiment II is different from the others and involves a break because the CH₄ emissions in this experiment were large. There is much variability in the data over time (Figure 2.11). However, each pile consistently starts with low CH₄ emissions and begins to increase approximately ten days into the composting process. Experiments I (Figure 2.11a) and III (Figure 2.11c) have similar post-turn results on day 14 of 760 ± 180 g CH₄ day⁻¹ and 660 ± 170 g CH₄ day⁻¹ respectively, where Experiment II (Figure 2.11b) has a higher value at 1900 ± 370 g CH₄ day⁻¹. Also, post-turn sampling

revealed most CH₄ emissions decreased after turning, although not present in every occasion. Other increases in CH₄ emissions are not uniformly observed. Experiment II experienced large CH₄ emissions during the last 15 days of composting, with a high of 17,000 ± 2,900 g CH₄ day⁻¹. The average flux per unit area for each experiment over the time frame shown in Figure 2.11 was 4.2 ± 3.6 g CH₄ m⁻² day⁻¹, 34 ± 52 g CH₄ m⁻² day⁻¹, and 5.4 ± 4.7 g CH₄ m⁻² day⁻¹ for Experiments I, II, and III, respectively.

Figure 2.8. Average oxygen concentration for all experiments at a three-foot depth from the top of the surface of the compost pile vs. time. Experiment I (a), Experiment II (b), and Experiment III (c). Standard deviations are show with sample size (n) ranging from one to three.

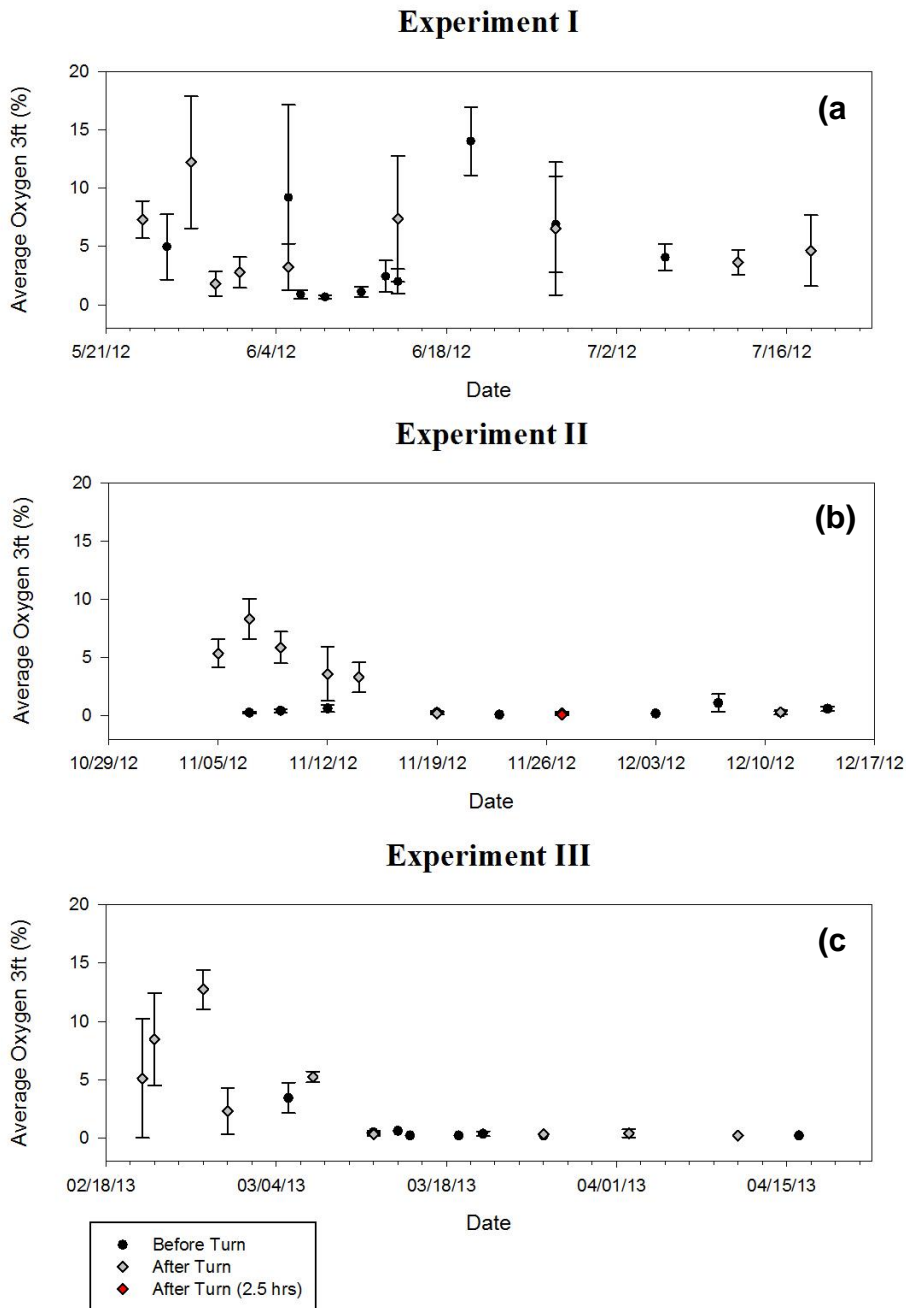


Figure 2.9. Average temperature for all experiments at a three-foot depth from the top of the surface of the compost vs. time. Experiment I (a), Experiment II (b), and Experiment III (c). Standard deviations are shown with n ranging from one to three.

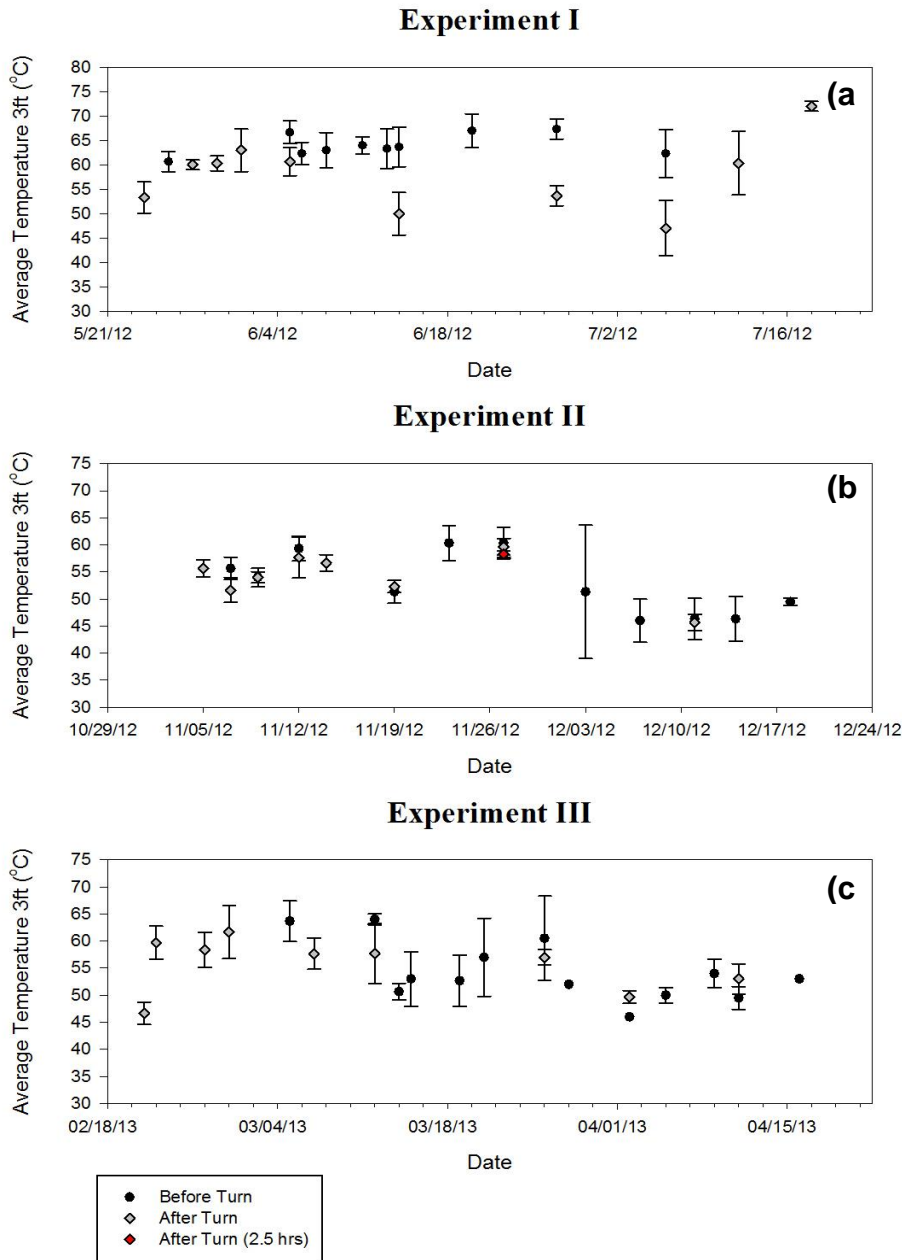
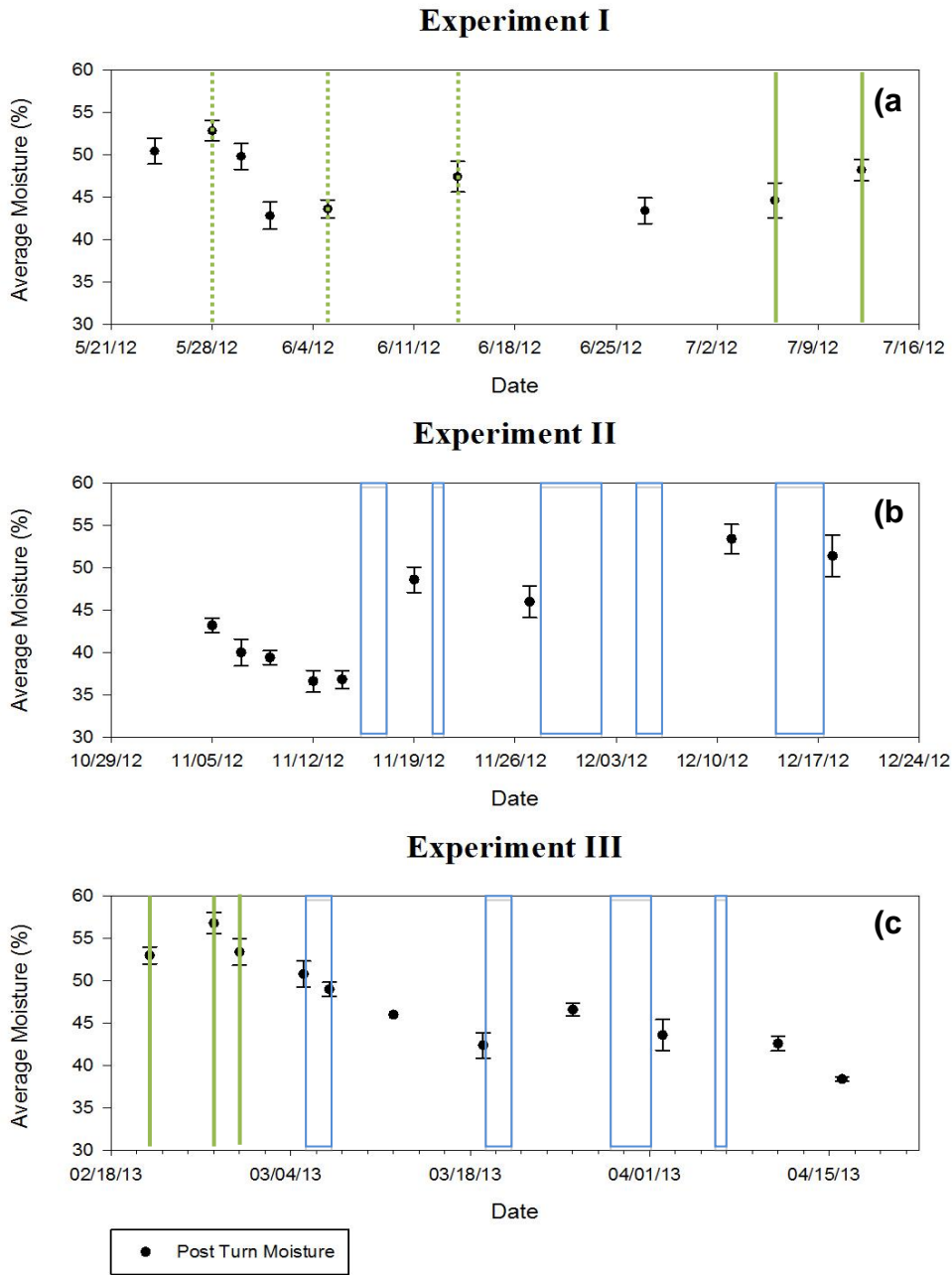


Figure 2.10. Average moisture percent after turning events for all experiments vs. time. Blue boxes represent periods of rain events leading to 0.6 mm/day or higher, solid green lines represent known watering days, and dotted green lines represent suspected

watering days. Experiment I (a), Experiment II (b), and Experiment III (c). Standard deviations are shown with $n = 5^*$.



*Except 3/12/13 which is an estimation because samples were compromised.

Figure 2.11. Methane emissions ($\text{g CH}_4 \text{ day}^{-1}$) for each experiment over the age of the pile. Turning days are marked with a red dotted line. Note the scale change after the break in Experiment II. Experiment I (a), II (b) and III (c). Error bars display standard deviations ($n = 3$).

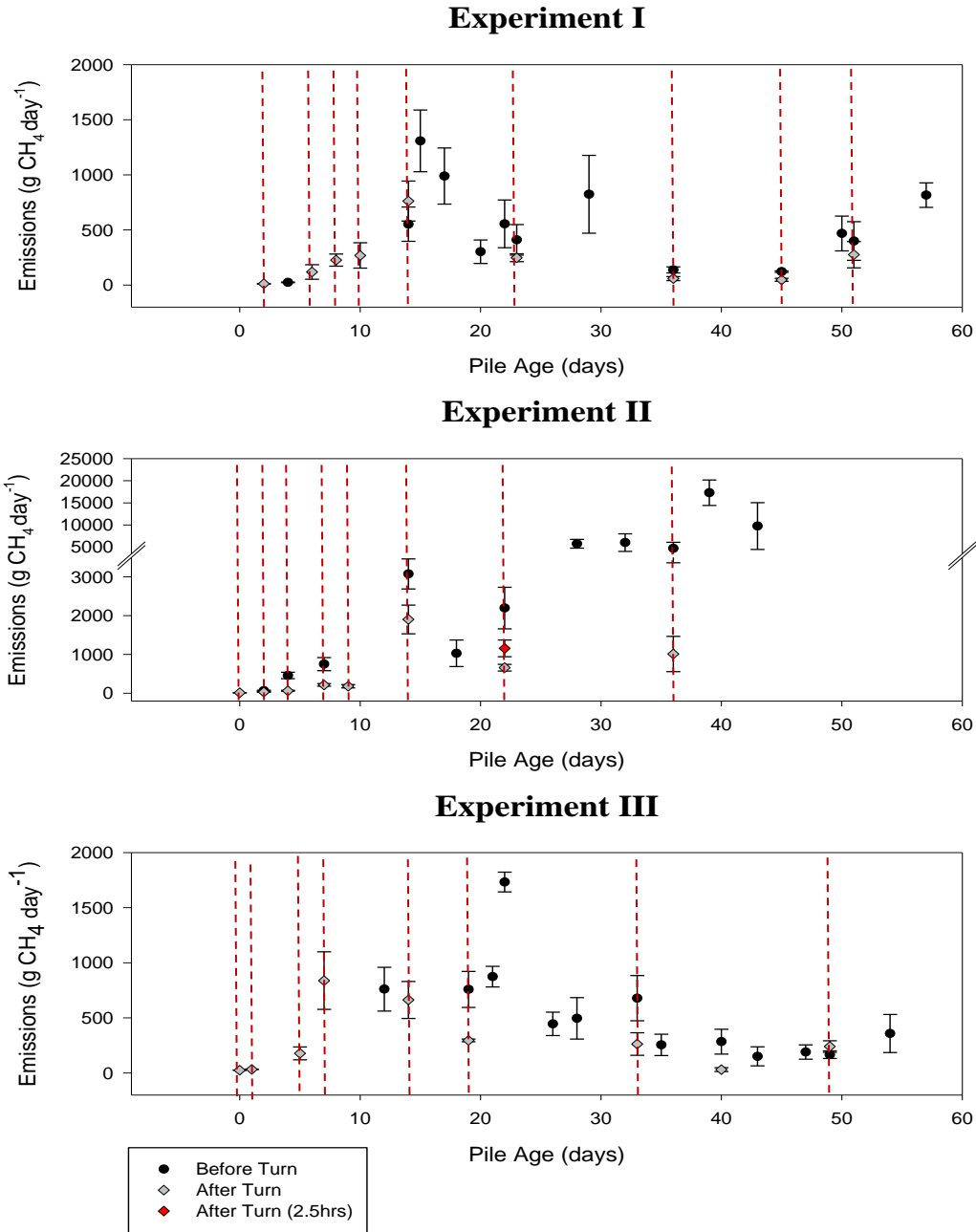
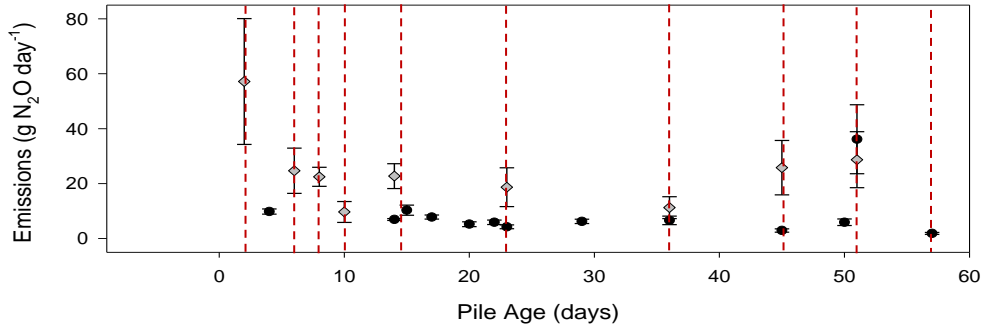
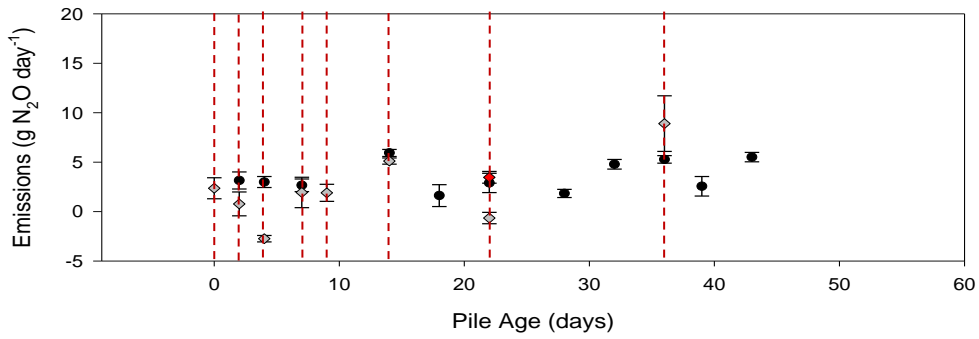


Figure 2.12. Nitrous oxide emissions ($\text{g N}_2\text{O day}^{-1}$) for each experiment over the age of the pile. Turning days are marked with a red dotted line. Note the scale difference in Experiment II. Error bars display standard deviations ($n = 3$).

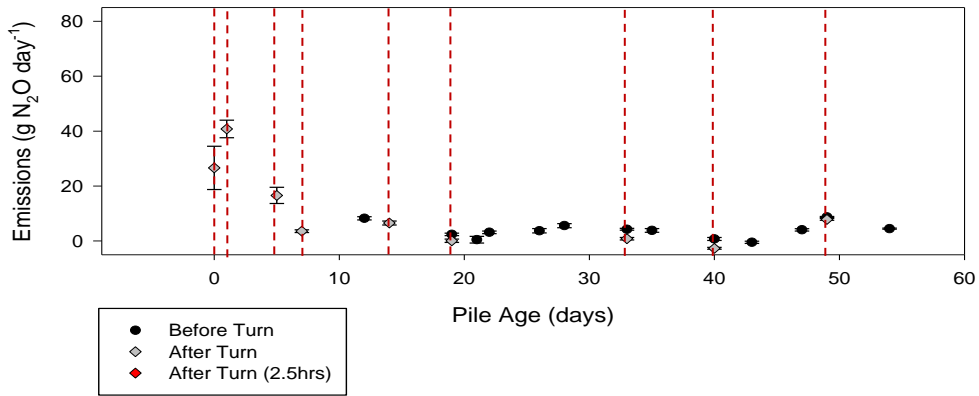
Experiment I



Experiment II



Experiment III



- Before Turn
- ◇ After Turn
- ◆ After Turn (2.5hrs)

Figure 2.12 presents the N₂O emissions for each experiment in grams per day versus the age of the pile in days. Experiment II (Figure 2.12b) contained low N₂O emissions (note the smaller scale), only reaching a high of 8.9 ± 2.8 g N₂O day⁻¹. It is difficult to interpret a pattern from such low emissions, however the other two experiments were characterized by higher N₂O emissions at the start of the pile then tapering off within the first ten days. Experiment I (Figure 2.12a) has a peak of 57 ± 23 g N₂O day⁻¹ on day 2, the first sampling day, and Experiment III (Figure 2.12c) has a peak of 41 ± 3.2 g N₂O day⁻¹ on day 1. The emissions pattern nearing the ending of the piles is not consistent, with Experiment I experiencing an increase in N₂O emissions later and Experiment III remaining fairly constant in concentration near the end of the compost process monitoring. The average N₂O flux per unit area for each experiment was 160 ± 150 mg N₂O m⁻² day⁻¹, 36 ± 31 mg N₂O m⁻² day⁻¹, and 75 ± 94 mg N₂O m⁻² day⁻¹ in order of Experiment I-III.

The emissions values in Figures 2.11 and 2.12 were integrated over the duration of the pile, using a trapezoidal area integration method in Sigma Plot 10.0; some quick checks using other integration methods revealed little difference between them and the trapezoidal method. From the information obtained with trapezoidal integration, Figure 2.13a shows CH₄ and Figure 2.13b shows N₂O emissions broken down for each experiment and by each sample location. The experiments are presented in order of increasing average internal temperature and oxygen concentration (Figure 2.7). Methane flux is always highest on the top of the pile. Although the top (area A) has the smallest surface area related to the geometry of a trapezoidal prism, the convection process inherent in a windrow brings most of the airflow out of the top of the pile (Andersen et al., 2010). Nitrous oxide should exhibit the same effect of having the majority of emissions through the top of the pile, and this is observed for Experiment I and III. Experiment II had low N₂O emissions and does not exhibit the same patterns. Experiment II had high CH₄ emissions of 300 ± 51 g CH₄ day⁻¹ DW tons⁻¹. Emissions of CH₄ for location A are close for Experiment I and III, at 29 ± 3.0 g CH₄ day⁻¹ DW tons⁻¹ and 35 ± 2.5 g CH₄ day⁻¹ DW tons⁻¹ respectively. The largest N₂O emissions are from Experiment I, which experienced the hottest and driest weather, with 570 ± 166 mg N₂O day⁻¹ DW tons⁻¹ for section A alone. Control values are shown for both gases to present the background level of emissions, or lack of emissions, as shown with the negative value for Experiment II (too low for quantification).

Total emissions, with all areas of the piles added up by weighting based on surface area (called contribution ratios), show (Figure 2.14b) the N₂O emissions of Experiment I were approximately double that of Experiment III. Experiments are presented in Figure 2.14 in the same order as Figure 2.13. Experiment I had total emissions of $1,100 \pm 300$ mg N₂O day⁻¹ DW tons⁻¹, and Experiment III had 550 ± 61 mg N₂O day⁻¹ DW tons⁻¹. Experiment II had the lowest N₂O emissions, at a total of 240 ± 47 mg N₂O day⁻¹ DW tons⁻¹ and the highest CH₄ emissions at 340 ± 120 g CH₄ day⁻¹ DW tons⁻¹ (Figure 2.14a). Experiment I and III are again very similar in the CH₄ emissions, at a total of 30 ± 10 g CH₄ day⁻¹ DW tons⁻¹, and 56 ± 11 g CH₄ day⁻¹ DW tons⁻¹, respectively.

One goal of this study was to determine the amount of emissions contributing to climate change resulting from the windrow composting process. Table 2.2 below shows the results of each experiment in the calculated CO₂ equivalents (CO₂ eq) using the GWPs from the Fourth Intergovernmental Panel on Climate Change (IPCC) assessment report (AR4) (Solomon et al., 2007).

Figure 2.13. Averaged methane (CH₄) and nitrous oxide (N₂O) daily fluxes for the three compost piles. (CH₄ emissions in g CH₄ day⁻¹ DW tons⁻¹ (a) and N₂O emissions in mg N₂O day⁻¹ DW tons⁻¹ (b) divided by experiment and location: top, upper side, and lower side. Experiments are in order of increasing internal average internal temperature and oxygen concentration for three-foot depth. Control values are also included for each experiment.) Error bars display expanded uncertainty.

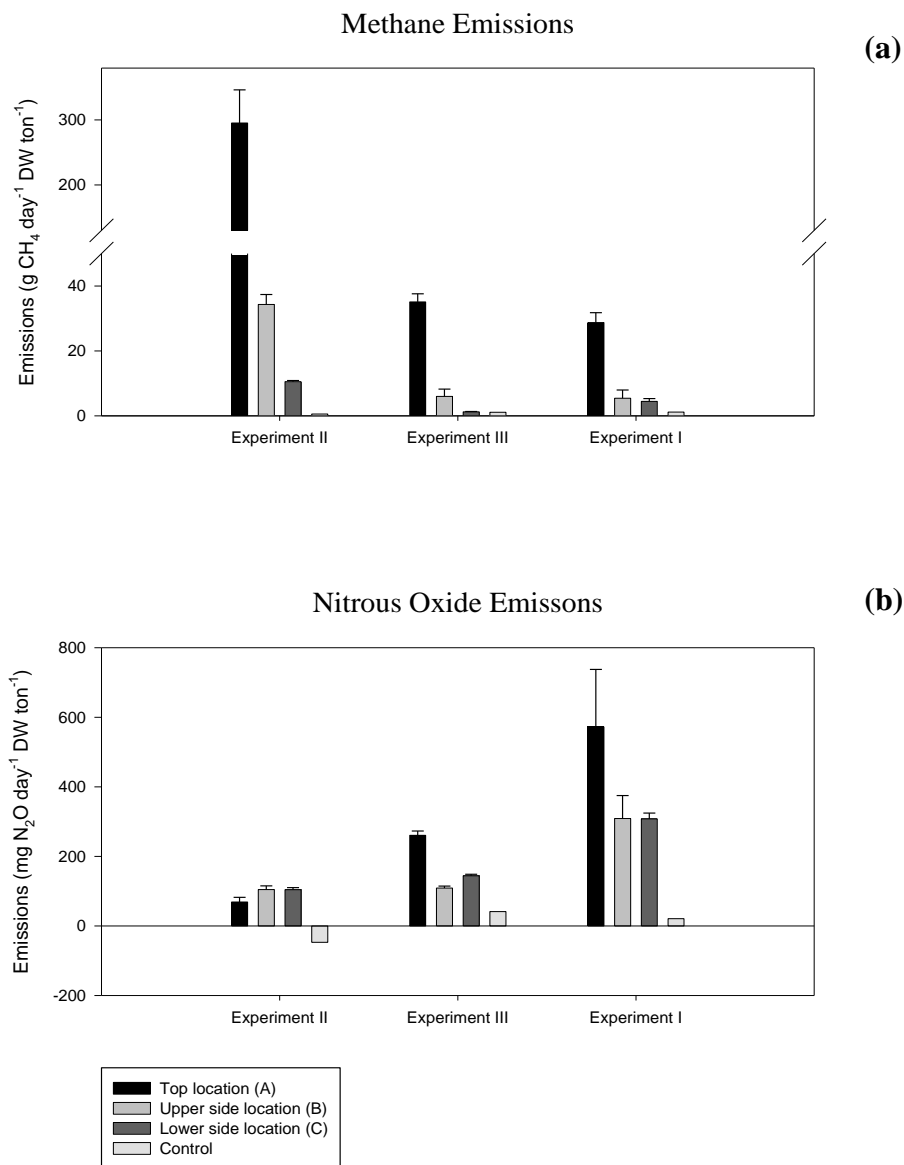


Figure 2.14. Averaged CH₄ daily emissions in g CH₄ day⁻¹ DW tons⁻¹ (a) and N₂O emissions in mg N₂O day⁻¹ DW tons⁻¹ (b) divided by experiment. Error bars display expanded uncertainty.

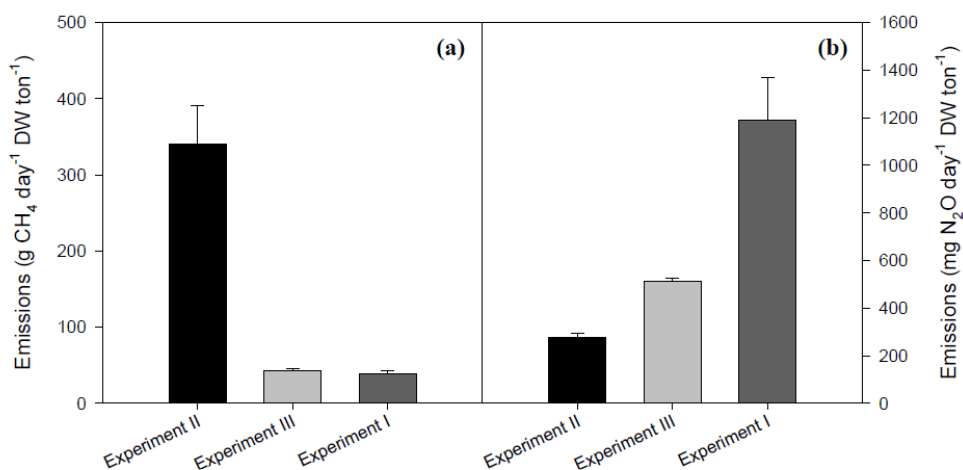


Table 2.2: Calculated grams CO₂ equivalents (\pm expanded uncertainty) day⁻¹ DW tons⁻¹ using the AR5 global warming potentials, 25 for CH₄ and 310 for N₂O. The expanded uncertainty was based on a standard uncertainty multiplied by a coverage factor k = 2, providing a level of confidence of approximately 95%.

	Experiment I	Experiment II	Experiment III
g CO ₂ .eq day ⁻¹ DW tons ⁻¹ for CH ₄	770 \pm 230	8,500 \pm 3,000	1400 \pm 270
g CO ₂ .eq day ⁻¹ DW tons ⁻¹ for N ₂ O	370 \pm 92	75 \pm 14	170 \pm 19
Total g CO ₂ .eq day ⁻¹ DW tons ⁻¹	1100 \pm 250	8,600 \pm 3,000	1600 \pm 270

Discussion

As noted earlier, the DW of the final output of Experiment III has some inclusion of soil that can account for the increase in mass (Table 2.1). This did not affect the emissions values that were based on the input DW. However, if the compost was not well mixed by the time the output analysis samples were taken, there may have been an overestimation in the other values in Table 2.1 that were based on DW of the output. The individual data of the values in Table 2.1 are located in the appendices for reference (Tables A.2.9 - A.2.11). For future experiments, careful management of compost and weighing could allow for a mass balance approach, with the addition that the contributions of ammonia gas (NH₃) and CO are acknowledged.

A trend of low oxygen to low temperature correlation was seen when looking at the average internal concentrations for the center, three-foot depth in the windrows of Experiments I-III (Figure 2.7). The internal temperature trend of the experiment also mirrored air temperature shown in Figure 2.6. The higher the ambient air temperature, the higher the average internal temperature. Experiment II, with the lowest oxygen concentration, also experienced the most rain. Moisture has been known to hinder oxygen transfer and may have an effect on the different GHG emissions (Buyuksonmez, 2011). Experiment III also contained low oxygen levels at the three-foot depths (Figure 2.8) yet had similar moisture content to Experiment I (Figure 2.10). Therefore, moisture alone cannot account for low oxygen levels. Differences in feedstock, porosity, and the microbial activity likely account for this discrepancy.

Internal oxygen concentrations, temperatures, and moisture contents all vary throughout the composting process and have been known to affect GHG emissions. Oxygen concentrations followed a pattern in Experiment II and III: Oxygen levels were higher in the beginning of the process and diminished within the first 10 to 15 days (Figure 2.8). Experiment I does not follow any pattern and maintains a higher overall average oxygen concentration. Internal temperatures for Experiment II and III decrease slightly near the end of the monitoring process; however, this is not clearly shown in Experiment I, which experienced the highest overall internal temperatures (Figure 2.9). Compost internal temperatures were in the thermophilic range (above 45°C) for the three-foot depth for the duration of each experiment. Observations have shown that at these thermophilic temperatures, CH₄ production increased as oxygen concentration decreased (Beck-Friis et al., 2003). Moisture can play a large role in the magnitude of GHG emissions. Although Experiment II started out as the driest of the three piles, rain events contributed to the increase of the moisture toward the completion of the composting process of the pile (Figure 2.10b). The increase in moisture near the end of the pile is accompanied by high emissions of CH₄ (Figure 2.11b); however, this moisture is not significantly higher than those measured in other piles. Internal moisture may actually be higher in between sampling for the second half of Experiment II. Turning was postponed during heavy rain, and, therefore, moisture samples were not taken and a peak of moisture could have been missed. Experiment I has a small increase of CH₄ near the end of monitoring and could be due to the watering of the pile during the final two turns.

Feedstock also impacts the pattern of CH₄ emissions. In a study using two different feedstocks, one of synthetic food materials (dry dog food) and the other digested biosolids, the synthetic food trimmings produced very little CH₄ whereas the biosolids had high emission rates of CH₄, even just within the first 25 hours (VanderGheynst et al., 1998). Biosolids were obtained from anaerobic digestion, and therefore the pre-handling of materials could play a role in the emissions emitted later in the composting process. Variations in yard trimmings alone can influence the emissions of N₂O and CH₄. Leaves and grass clippings are small and flexible when compared to shrubs and cut tree branches, so windrows with a large majority of these smaller materials may experience greater compaction, especially when wet. Experiment II, containing a high

percentage of leaf material, may have experienced this effect, but it is difficult to isolate the variation of the material with the increase in moisture and the decrease in oxygen. Experiments II and III have shown similar oxygen levels and trends throughout the monitoring of the experiments (Figure 2.8), yet have very different levels of CH₄ emissions near the end of monitoring (Figure 2.11). Experiment II emitted a significant amount of CH₄ later in the composting process. That pile also had higher levels of moisture than Experiment III (Figure 2.10) at the time of the significant CH₄ emissions seen in Experiment II. This discrepancy suggests that oxygen alone cannot predict higher emissions in CH₄ but that moisture and feedstock may also be involved in the levels of production.

Methane, known to form under anaerobic conditions (Beck-Friis et al., 2000; Hellebrand, 1998; Beck-Friis et al., 2003), has a pattern of starting with relatively low emissions and then increasing after approximately ten days have passed (Figure 2.11). This trend is also observed in Hellmann et al. (1997) and Hobsen et al. (2005), although Hobsen et al. used in-vessel composting for the first six days. This pattern indicates oxygen depletion occurred over the first few days of composting, which is supported by Figure 2.8 (b and c) where depletion of internal oxygen is shown. Also, the decrease in CH₄ observed after turn events implies that the introduction of oxygen may also lessen CH₄ emissions. Experiment II experienced CH₄ emissions more than ten times that of the other two experiments during the last 15 days of composting. This discrepancy of emissions is most likely caused by the unusual amount of rain experienced during Experiment II and the difference in feedstock. There was a large rain event centering on 12/01/2012, 26 days in pile age (Figure 2.6). Between days 22 and 36, the Experiment II pile was not turned due to the rain (Figure 2.11b). As mentioned earlier, piles are meant to be turned weekly following the intensive initial five-turns in two-weeks period. The lack of turning in addition to the filling of pore space with water could have led to the depletion of oxygen in the pile or hindrance of oxygen transport (Buyuksonmez, 2011). Methane would be expected to increase during these times, as is observed.

The two piles with higher N₂O emissions, Experiments I and III, show a pattern of higher emissions at the start of the pile with emissions tapering off within the first ten days (Figure 2.12). This production of N₂O near the start of the pile is also seen in Hellmann et al. (1997) and Hobsen et al. (2005). Buyuksonmez (2011) suggests that in some cases of nitrification and denitrification, high oxygen levels will lead to higher N₂O production. Because higher N₂O concentrations are seen during periods with suggested higher oxygen concentrations, this indicates that ammonia oxidation (incomplete nitrification) may be a major contributor to the overall N₂O emissions of compost piles. This is due to ammonia oxidation coming solely from aerobic bacteria. However, incomplete denitrification is also a potential contributor to N₂O emissions since it is carried out by both aerobic and anaerobic types of bacteria (Beck-Friis et al., 2000). Oxygen was seen to be at similar concentrations in Experiments II and III for the beginning of the experiment and nearing the end of study (Figure 2.8a and 2.8b). Differences in feedstock or moisture may be the reason for this discrepancy in N₂O

emissions. Further analysis of the nutrient substrates found in the appendices could provide insight into these pathways (Table A.2.10-A.2.12).

The convection process of the windrow is indicated by the highest emissions coming from the top of the pile (Figure 2.13). Methane emissions from the top area (A) of Experiments I-III were 74, 87, and 83 percent of the total emissions for each experiment, respectively. Area A for N₂O accounts for 48, 24, and 51 percent for each experiment. This is fairly consistent to findings in Andersen et al. (2010), where chambers along the top of the pile accounted for 55 percent of the CH₄ flux with just one chamber and 100 percent of the CH₄ flux for three chambers. One chamber accounted for 49 percent of the N₂O flux and 91 percent with all three chambers. It is uncertain why the relative fraction of N₂O fluxes from the top was somewhat lower than that of CH₄ fluxes for our results, compared to those of Andersen et al. (2010).

The greatest CH₄ emissions are correlated with the least amount of N₂O emissions and vice versa (Figure 2.14), when the total emissions (integrated over the pile lifetime, then expressed per day and per unit dry weight) are compared. Experiment II had the lowest internal oxygen concentrations and temperatures, with the highest CH₄ emissions and lowest N₂O emissions, followed by Experiment III, which had median numbers for gas emissions, oxygen concentrations, and temperatures. The highest N₂O emissions and lowest CH₄ emissions occurred in Experiment I when the temperature and oxygen levels were highest (Figure 2.13 and 2.14). For Experiment I, the negative correlation of CH₄ emissions with N₂O emissions was not as strong as with the other experiments, in that the CH₄ emissions were not dramatically lower than Experiment III. Oxygen concentrations are again suggested to be a requirement for significant amounts of N₂O emissions. The apparent variability in the negative correlation between CH₄ fluxes and N₂O fluxes could be due to a complex combination of different material inputs, temperatures, oxygen concentrations, and precipitation, or moisture contents. In Experiment III there was a rain event around 4/01/2013, 39 days into the pile. This could explain the suppression of any N₂O gas near the end of the pile. Buyuksonmez (2011) notes that irrigation of windrow piles may lessen some GHG emissions, such as CH₄.

In comparison to other studies, Beck-Friis et al. (2000) had a range of $1.1 \pm 1.4 \text{ g CH}_4 \text{ m}^{-2} \text{ day}^{-1}$ to $17.8 \pm 24.0 \text{ g CH}_4 \text{ m}^{-2} \text{ day}^{-1}$ and $2 \pm 2 \text{ mg N}_2\text{O-N m}^{-2} \text{ day}^{-1}$ to $270 \pm 160 \text{ mg N}_2\text{O-N m}^{-2} \text{ day}^{-1}$ using a closed chamber technique. Andersen et al. (2010) used a flux chamber method on a 150-day-old compost pile with windrow dimensions of approximately 115 m × 9 m × 4 m, and found an average flux density of $106 \pm 60 \text{ g CH}_4\text{-C g m}^{-2} \text{ day}^{-1}$ and $2.40 \pm 0.96 \text{ g N}_2\text{O-N m}^{-2} \text{ day}^{-1}$ over an eight-day sampling period. These values are comparable to the findings in this study. Methane fluxes per unit area were $4.2 \pm 3.6 \text{ g CH}_4$ ($3.1 \pm 2.7 \text{ g CH}_4\text{-C}$) $\text{m}^{-2} \text{ day}^{-1}$, $34 \pm 52 \text{ g CH}_4$ ($26 \pm 39 \text{ g CH}_4\text{-C}$) $\text{m}^{-2} \text{ day}^{-1}$, and $5.4 \pm 4.6 \text{ g CH}_4$ ($4.1 \pm 3.5 \text{ g CH}_4\text{-C}$) $\text{m}^{-2} \text{ day}^{-1}$ for Experiments I, II, and III, respectively, and N₂O fluxes were $160 \pm 150 \text{ mg N}_2\text{O}$ ($100 \pm 96 \text{ mg N}_2\text{O-N}$) $\text{m}^{-2} \text{ day}^{-1}$, $36 \pm 31 \text{ mg N}_2\text{O}$ ($23 \pm 19 \text{ mg N}_2\text{O-N}$) $\text{m}^{-2} \text{ day}^{-1}$, and $75 \pm 93 \text{ mg N}_2\text{O}$ ($48 \pm 59 \text{ mg N}_2\text{O-N}$) $\text{m}^{-2} \text{ day}^{-1}$ in order of Experiments I-III.

Methane was a greater contributor to the CO₂ equivalents than N₂O, despite N₂O having a higher GWP (Table 2.2). For this reason, oxygen should be introduced into the system as often as possible to mitigate CH₄ emissions. This can be done in a variety of ways, such as changing the feedstock, increasing the porosity of a pile by adding wood chips or branches, carefully managing moisture content, and increasing turning. These changes should be made especially for winter composting, since heavily oxygen-depleted piles such as that seen in Experiment II have larger emissions in comparison to the other two piles. Andersen et al. (2010) reports 81 ± 16 kg CO₂-eq Mg⁻¹ WW per year for CH₄-C and 30 ± 14 kg CO₂-eq Mg⁻¹ WW per year for N₂O-N for the dynamic plume method. Conversion of Table 2.2 to these units gives 160 ± 17 kg CO₂-eq Mg⁻¹ WW per year, $1,300 \pm 200$ kg CO₂-eq Mg⁻¹ WW per year, and 140 ± 11 kg CO₂-eq Mg⁻¹ WW per year for CH₄-C for Experiment I, II, and III, respectively. For N₂O-N the experiments give 49 ± 7 kg CO₂-eq Mg⁻¹ WW per year, 11 ± 1 kg CO₂-eq Mg⁻¹ WW per year, and 17 ± 0.6 kg CO₂-eq Mg⁻¹ WW per year. These values are similar in magnitude but may suggest that piles were better managed for the Anderson et al. (2010) study, with more oxygen provided for the compost.

Some error due to the experimental design or techniques may be present in the measured data. One additional consideration is that the windrow test pile was approximately four times smaller in terms of surface area (caused by reduced pile length) when compared to regular windrows at this site. This smaller size in area compared to the standard piles could lead to an underestimation or overestimation of emissions. In Beck-Friis et al. (2000) small piles on the order of the test pile size in this study have shown a lower flux than larger piles in both CH₄ and N₂O. In contrast, Buyuksonmez (2011) shows the opposite for smaller piles with higher emissions of these GHGs than larger piles. These differences are likely attributable to such factors as management and feedstock.

In addition to the size differences between a normal windrow pile and the test windrow, inconsistent shape was also an issue. With differing amounts and types of material to turn and shape in each experiment, the test windrows were at times slanted or lumpy in spots, in differing ways. Final emissions calculations are based on an estimated surface area, described in detail in the Appendix (see section A.2.1.3- A.2.1.4). In short, the calculated flux density in g m⁻² day⁻¹ is multiplied by the estimated surface area to achieve the total emissions in g day⁻¹. Integration of these values over time provides the total emissions for that pile, which can then be divided by the starting dry weight. Three-dimensional mapping of the windrow surface, as done in Buyuksonmez (2011), would provide a more accurate surface area measurement. Additionally, more sampling days will always be more beneficial to avoid missing peak events or diurnal patterns. The time integration could underestimate emissions if a peak in flux is missed and overestimate if the lowering of flux after a peak is not measured. Turning events could lead to under- or overestimation during integration when discrepancies between the before and after values vary significantly. For example, on day 36 in Experiment II, the CH₄ flux decreased significantly post-turn (Figure 2.11). The length of time that the flux takes to transition back to its pre-turn values affects the outcome of the integration.

According to the single 2.5-hour test during Experiment II, the flux starts to return to the pre-turn levels within a matter of hours (Figure 2.11b and 2.12b). However, more tests should be performed to verify this.

The test pile was located on a different surface than the rest of the windrows on the facility. The soil underneath the test pile was clay-like and became muddy when rain events occurred. As described earlier, this prevented regular turnings, especially in Experiment II. Other piles on the facility grounds could still be turned unless the rain event was especially heavy. This creates a discrepancy between the test windrow and other windrows which may have led to higher recordings of CH₄ in the test pile than would be observed in piles that could be turned. This could have affected the results for the Experiment II winter season pile. Although as noted earlier, Figure 2.11b does show the decrease in emissions for the turn on day 36 of Experiment II; after the turn, the emissions are back to a similar amount four days later. With the amount of moisture contained in the compost, perhaps turning would only account for a small difference if compaction and oxygen depletion returned quickly. According to Rynk et al. (1992), oxygen depletion by microbial consumption can occur in as little as 30 minutes after a turn has taken place.

Another error, although difficult to avoid when using the chamber technique, would be pile disturbance. The necessary act of walking on the pile to place chambers, and the physical act of placing the chambers on the surface of the pile may have some influence. Compaction due to walking could alter oxygen levels leading to a possible overestimation of CH₄. If the surface of compost can be related to soil surface chamber measurement, then the disturbance due to placing the chamber could lead to an overestimation of flux (Norman et al., 1997). However, because flux from compost is usually much greater than flux from soil, this disturbance will have a lesser effect. The eight-minute equilibration time given in this study should have lessened these effects. Upper and lower side location measurements may have an element of introduced error leading to an overestimation of flux because of the technique used to place these chambers on the sloping sides. The rod placed through the chamber and into the surface of the compost to support and stabilize it while taking measurements could create a new pathway for gaseous emissions to reach the chamber. The insertion of the rod could also be another form of surface disturbance, as discussed above. Emissions from the sides of the compost tend to be lower than those at the top of the pile and will therefore contribute less to the error associated in the final emissions calculations.

Conclusions

The data obtained in this chamber study of compost windrows compared favorably with previous research. Performing this experiment with different input materials and during different seasons was a good method to obtain a range of fluxes. The findings suggest that environmental and seasonality influences, and particularly compost management, have a large impact on GHG emissions. Experiment II has shown that a rainy season with cooler temperatures will produce an oxygen-depleted pile that generates more

CH₄. Proper windrow management may be able to lessen these effects through moisture control, feedstock changes to increase porosity, and turning to provide aeration. However, using turning as the only solution to provide oxygen may have diminishing returns due to the reduction in particle size (decrease in porosity), an increase in the GHG contributions from the windrow turner itself, and increased maintenance on the turner. Methane data supports the idea that the gas is produced under anaerobic conditions. Nitrous oxide, however, can only be produced when oxygen is available, and therefore would be inherently associated with ammonia oxidation processes. The highest N₂O emissions occurred in the driest, hottest, and most oxygenated pile.

In the future, more could be done with the data obtained during these experiments but not used in this study, as well as improvements for future experiments of this kind. Analysis of the rest of the oxygen and temperature data taken for Experiments I–III could lead to more insights into the relationship with GHG emissions. Also, further analysis of the moisture content, ammonia, nitrate, DOC, total carbon, and total N₂ could give more information about the inputs of these piles and how they relate and change with the GHG emissions. Future experiments should pay close attention to moisture content because of the great effect on emissions observed here. Comparison with the micrometeorological data taken simultaneously during Experiments I and III will give insight into the patterns of GHG emissions. Better placement of the test pile would have benefited this study so soil would not be incorporated into the compost when turning and so that turning could occur even around rain events. Achieving a more consistent shape of the windrows or obtaining a virtual mapping of the windrow would provide excellent information on surface area and volume. More accurate mass measurement would also have helped this study to confidently compare values with other literature. Time-consuming but more frequent, comprehensive monitoring of the emissions would lead to more information, including any peaks of gas emissions that have been missed or observation of a possible diurnal pattern. To avoid the time consumption, more focus on micrometeorological techniques could achieve similar results and benefit from less compost disturbance. Also, mass balance could be a useful accompaniment to flux measurement. Finally, a way to determine the gas emissions lost during a turning would be an interesting addition to the data. In the end, combining emissions results with a life cycle analysis of compost would be the best way to determine proper management practices and the net effect of composting on the environment.

Chapter 3. Measurements of Greenhouse Gas Fluxes from Composting Green Materials Using Micrometeorological Mass Balance and Comparison to Flow-Through Chambers

Introduction

Micrometeorological techniques provide alternatives that are non-intrusive and may be used to check and/or improve flux estimates obtained from less expensive chamber measurements. Micrometeorological mass balance, and backward Lagrangian stochastic (bLs) techniques are best suited for emissions estimates from small, well-defined source areas and, though there is a distinct lack of studies applying them to composting plant-matter, they have been applied to measuring emissions from small field plots with different fertilizer or chemical treatments, animal manure storage ponds (e.g. Khan et al., 1997, Brown et al., 2002, Wagner-Riddle et al., 2006, Park et al., 2010a,b, VanderZaag et al., 2011), and composting of animal manure (Sommer et al., 2004). The bLs method utilizes a Lagrangian atmospheric dispersion model to estimate the ratio between gas concentration and flux from the source by repeatedly simulating particle trajectory paths backward from the concentration sensor to the source area (Flesch et al., 1995, Denmead, 2008). Geometry of the source and surface roughness information, wind speed, wind direction, frictional velocity, and Monin-Obukhov length (which can be obtained from a sonic anemometer) as well as downwind and upwind gas concentration are needed for this method. Fluxes using this method have been found to compare well with MMB estimates (Flesch et al., 1995).

The MMB technique has been used to estimate emissions from a variety of sources, but there are no studies applying a MMB approach to full-scale open windrows of composting yard trimmings in the literature. Sommer et al. (2004) uses a novel micrometeorological technique to assess emissions from a small pile of composting animal manure, but the scale and substrate are not comparable with the current study. We compared an open flow-through chamber approach with a MMB technique to estimate GHG emissions from a composting yard trimmings windrow system. There is a dearth of information on both of these techniques applied to compost studies in the literature. The current study adopts a flexible MMB approach similar to the one used by Wagner-Riddle et al. (2006) to measure emissions from animal manure storage ponds. This approach is explained in further detail in section 2.2.

Materials and Methods

Experimental Site and Timeline

Measurements of CH₄, N₂O, and CO₂ flux from an individual windrow of compost were carried out at a composting facility in Zamora (38° 46' N, 121° 52' W), Calif. The pile emissions data reported here are from the pile labeled Experiment I in the previous section. No MMB data were collected for Experiment II. MMB data for Experiment III required additional analysis and is not reported here.

As described in chapter 2, the test windrow lay on the western edge of the facility and was approximately 15 to 20 meters long, two to four meters wide, and, one to two meters high (the exact size varied as the pile was turned). The feedstock for the pile was shredded municipal green materials, composed of grass clippings, and shrub and tree trimmings, and subsequently mixed with wood chips to increase porosity. The weight of the starting material, measured by a truck scale operated by the composting facility, was 24.375 tons. Moisture of 40.2% ± 0.7% was measured using a series of grab samples from the mixed pile (Bailey, 2013).

Bare soil lay directly south of the pile (Figure 3.1a), with a large pile of debris (concrete and soil) about 25 meters to the north (Figure 3.1c). There was a farm along the west side of the facility, separated from the windrow by a chain-link fence and scattered trees (Figure 3.1d). To the northeast (Figure 3.1c) lay an equipment trailer housing the gas sampling and analysis system used in the study, and beyond to the east was the rest of the compost facility (Figure 3.1b). Farther to the north were an almond orchard and tomato fields.

Figure 3.1. Relative positions of the compost pile (large rectangle) and the wind and gas sampling towers (numbered 1-4). The smaller rectangle is the equipment enclosure containing the gas sampling and analysis system used in the study. Arrows indicate approximate direction from which the corresponding photographs were taken. Colored angles represent range of wind directions considered upwind for each gas sampling tower. After each turn event, exact positions of the pile and gas sampling towers shifted.

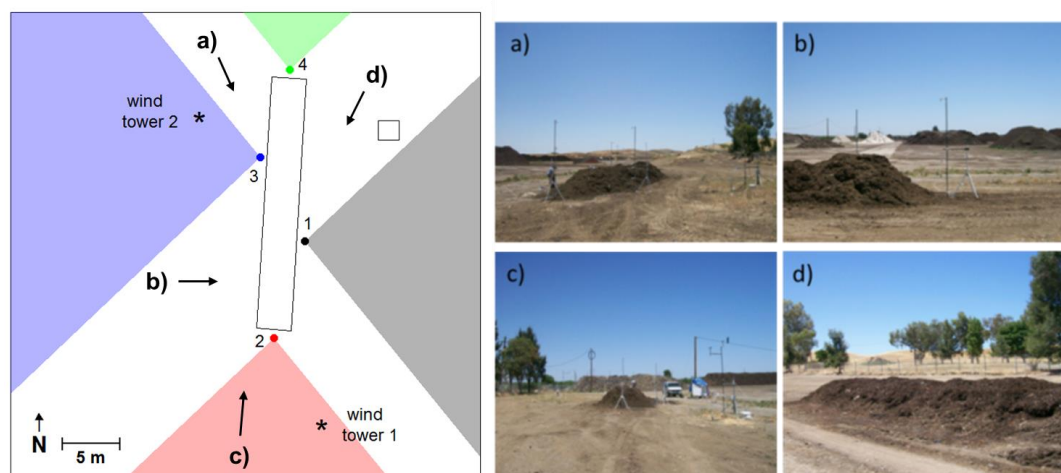
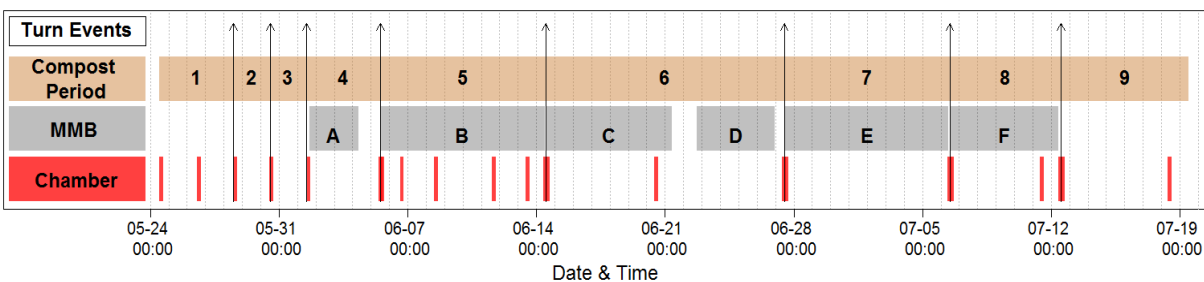


Figure 3.2 presents a timeline of the sampling periods for both the chamber and MMB techniques. Measurements using the open chamber technique were taken in approximately 1.5-hour periods spread out over the complete lifetime of the compost windrow (Bailey, 2013). Sampling often occurred immediately before and after turn events, although some sampling was done at other times. Further details on chamber sampling are given in Section 2.9 and by Bailey (2013). Monitoring using the micrometeorological technique did not span the lifetime of the windrow due to technical difficulties; measurements were taken continuously in six periods (mostly separated by turn events, labeled A-F in Figure 3.2). The compost windrow was turned eight times from 5/24/2012 to 7/19/2012, with watering occurring shortly before turns in most cases (Bailey, 2013). Five of these turn events occurred during the periods when the micrometeorological system was operational, though monitoring did not occur during the turn events themselves and often resumed a few hours after the pile was turned.

Shortly after the compost pile was removed from the site, monitoring was continued for approximately 11 days (8/3/2012 to 8/14/2012). The compost pile was expected to be the only significant source of emissions within the monitoring area; fluxes estimated when a compost pile was not present were expected to be zero. The area previously occupied by the pile was covered by plastic sheeting and a tarp to prevent measurement of any flux coming from the soil itself. This zero-source test allowed us to examine the MMB technique and gauge the noise associated with our experimental set-up. An additional test of the photoacoustic gas analyzer (Innova AirTech Instruments A/S, Ballerup, Denmark, Model 1312) used to measure GHGs in the field was carried out in the lab by taking repeated measurements from a gas cylinder with known concentrations of CO₂, CH₄, and N₂O. These lab results were compared with the zero-source test results, enabling one to gauge noise inherent in the photoacoustic gas analyzer itself against noise introduced by the sampling system and experimental set-up.

Figure 3.2. Experiment timeline. Month, day, and time (in 2012) are given along the horizontal axis. Upper brown rectangle spans the duration that the compost pile was present with numbers labeling periods in between turn events (black vertical lines). Gray rectangles in the middle indicate periods when micrometeorological measurements were taken (with letters labeling each continuous measurement period) and thick vertical red lines at the bottom indicate chamber measurements.



Micrometeorological Mass Balance Method

Emission source strength expressed as a mass flux density (hereafter informally called “flux”) is calculated as the horizontal flux leaving the source minus the flux entering the source, integrated over the measurement profile (Denmead, 1995):

$$Flux = \frac{1}{X} \int_0^Z \overline{u(c_{dw} - c_{uw})} dz + \overline{w\bar{c}} \quad [EQ 3.1]$$

where X is the fetch of the source area over which the wind travels before reaching the sensor locations, z is the height at which emissions from the source area no longer affect gas concentration, and $\overline{u(c_{dw} - c_{uw})}$ is the mean instantaneous flux of the gas, as the product of the horizontal wind speed, u (in $m\ s^{-1}$) and the gas concentrations (in $kg\ m^{-3}$) downwind and upwind of the source area, c_{dw} and c_{uw} , respectively. $\overline{w\bar{c}}$ represents the mean instantaneous flux in the vertical direction, and is not usually considered when using the mass balance technique. One issue with this equation is that it requires the mean of instantaneous fluxes. This requires fast response sensors measuring wind speed and gas concentration at all heights in the profile. These types of sensors, until recently, had not been commercially available and even now are prohibitively expensive, especially when considering multiple profile measurements. A solution is to use Reynolds decomposition and make reasonable assumptions; so Equation 3.1 becomes:

$$Flux = \frac{1}{X} \int_0^Z \left(\overline{u\bar{c}_{dw}} - \overline{u\bar{c}_{uw}} + \overline{u'c'_{dw}} \right) dz + \overline{w\bar{c}} + \overline{w'c'_{dw}} \quad [EQ 3.2]$$

Measurement of mean horizontal wind speed and mean gas concentration profiles is economically and operationally feasible.

The product of the deviations from the mean, $\overline{u'c'_{dw}}$, also called the turbulent horizontal diffusive flux, is often considered small compared to the mean flux term. There have been suggestions that it may be as much as 20 percent of the total flux in some situations (Wilson and Shum, 1992). Studies will sometimes systematically correct their flux estimations by ten to twenty percent to account for it. Park and Paw U (2004) and Kochendorfer et al. (2011) established that this horizontal flux is usually small, and the vertical turbulent flux term is also small when the fetch from an edge is limited, as is the case for this compost windrow. Assuming these terms can be neglected, as is often done when employing this method, Equation 3.1 becomes solely dependent on the product of mean wind speed and gas concentrations, which are more easily measurable:

$$Flux = \frac{1}{X} \int_0^Z (\overline{U\bar{c}_{dw}} - \overline{U\bar{c}_{uw}}) dz \quad [EQ 3.3]$$

The geometry of the source in conjunction with wind direction observations provide the mean distance over the source that the wind travels before reaching the downwind measurement location (\bar{X}).

Micrometeorological Mass Balance Method Set-Up

The MMB technique has traditionally been employed over relatively homogenous surfaces such as soils, grazed pastures (e.g. Beauchamp et al., 1978), and manure ponds (e.g. Wagner-Riddle et al., 2006; Park et al., 2010a, 2010b). Wind speed and direction are assumed constant at their mean values, for the purpose of the MMB flux calculation [Eq. 3.3]. Sommer et al. (2004) used the technique over a small pile of composting animal manure, but measured wind speed only downwind of the pile, and wind direction above the pile. For employment of the mass balance method over horizontally uniform surfaces, wind speed need only be measured in one location at each height (McGinn, 2006). Given the non-homogeneous nature of the experimental site and source area, it was expected that the compost windrow could modify the wind speed and direction, leading to ambiguity as to where wind velocity should be measured for calculation of fetch and fluxes. Two towers measuring profiles of wind speed were therefore deployed to investigate this effect on the MMB technique and flux calculation. Wind speed was measured at 0.7 m, 1.25 m, 2.25 m, and 3.5 m above ground at two different horizontal locations around the compost pile (Figure 3.1). Three-dimensional sonic anemometers (R.M. Young, model 81000 and Campbell Scientific, model CSAT3, respectively) were mounted at the 0.7 m and 1.25 m heights, and cup anemometers (Met One, model 014A) were used at the remaining two heights. The cup anemometers recorded average wind speed over one-minute intervals, while the sonic anemometers sampled at ten hertz, and the raw data as well as one-minute averages were recorded. One-minute average wind directions were also calculated from the wind component measurements from the anemometers mounted at 1.25 m. Wind direction data from these lowest heights were used because airflow was more likely to be disturbed by the compost pile, yielding different wind directions at the two wind tower locations. The one-minute average wind speeds measured by the cup anemometers were averaged over 15-minute intervals, and a cross-calibration correction was applied. This correction was based on a linear regression equation developed from data recorded by the cup anemometers and a sonic anemometer over a period prior to the experiment (Kent, 2012).

Ambient air was sampled through intake tubes at 0.7 m, 1.25 m, 2.25 m, and 3.5 m above ground at four different horizontal locations around the compost pile (Figure 3.1). This ensured an upwind and downwind tower for any wind direction. The exact position of the sampling locations shifted throughout the study as the compost pile was turned. Locations of the gas sampling towers were triangulated with a theodolite after each turn event.

According to McGinn (2006), five or more gas measurement heights are needed to ensure accurate definition of the vertical gas concentration profile in fluctuating atmospheric stability. However, because of instrument limitations, studies using MMB

methods often define the concentration profiles using measurements at four heights (e.g. Park et al., 2010; Wagner-Riddle et al., 2006). Four measurement heights were employed in this study because a single gas analyzer was being used to sample all intake lines sequentially. Given the time required to perform a single gas analysis, adding additional intake lines for added measurement heights would reduce the number of samples per intake line per 30-minute interval from two to one.

The highest sampling height needed is determined by the size of the source area. In neutral conditions, emitted gas reaches about one tenth the distance the wind travels over the source area (Denmead, 1995; Denmead, 2008; Fowler et al., 2001). It may reach one-third the distance in highly unstable conditions (Denmead, 2008). Given the dimensions of the compost piles in our study (approximately 3 m x 15 m x 2 m), the rule would necessitate a maximum height of five meters when the wind was blowing along the length of the pile in unstable conditions. The highest measurement height in this study was 3.5 meters above ground, which should be adequate for most wind directions in unstable conditions and all wind directions in neutral and stable conditions.

Gas sample tubing (three-millimeter inner diameter polytetrafluoroethylene (PTFE)) was mounted on four towers at each sampling height and had a uniform tubing length of 30 meters back to an equipment trailer where it was connected to a valve manifold system. Each of the 16 intake tubes was connected to a different three-way solenoid valve. The “on” position of the valves connected the intake tubes to a series of “T” connectors that combined the 16 lines into a single line that was connected to a pump. This pump ran continuously, constantly pulling air from the sampling locations. The “off” position of solenoid valves combined the 16 lines into a single line, which was connected to another series of two valves before running to a photoacoustic gas analyzer. The two intermediate valves acted to control the flushing of the dead common space in the “T” manifold between the 16 intake valves and the gas analyzer.

All solenoid valves were controlled by relays via a controller connected to a desktop PC. The gas analyzer was set to run continuously. After the analyzer finished analysis on a sample, the result would be output to a computer file and would also activate the relay controller to switch valves. In this manner, a single line through a single relay was feeding to the analyzer while the remaining 15 were being flushed by the pump. Analysis occurred sequentially through the 16 intake lines. In the period while the gas analyzer was performing an analysis and not drawing in a sample, the two-valve system operated to allow flushing of the common dead space of the manifold, so that air being analyzed was representative of a single intake line, and not a mix of air from the current and preceding intake lines. The analyzer drew in a sample and analyzed it in about 56 seconds. This translates to air from each of the 16 intake lines being analyzed once in a 15-minute period (twice in a 30-minute period).

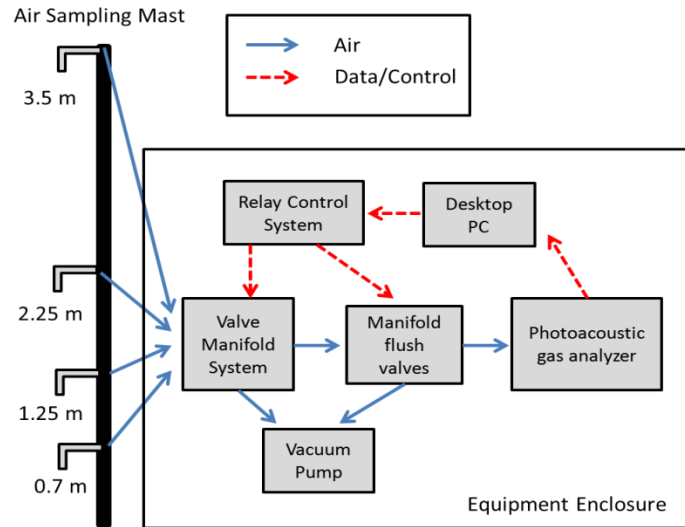
The ideal gas law was used (standard pressure, normalization temperature of 25° C) to convert gas concentrations (parts per million by volume; ppmv) into units of mass per volume (milligrams per cubic meter; mg m⁻³). This assumes gas samples reach an equilibrium temperature as they pass through the tubing and valve system en route to

the gas analyzer inside the air-conditioned equipment enclosure. Analysis was also carried out to test sensitivity of the fluxes and patterns to this assumption. An average sonic temperature for each half-hour period was calculated from ultrasonic anemometer measurements and was used as the temperature in the ideal gas law for the units conversion. This calculation makes the assumption that gas samples kept the same ambient air temperature as they passed through the sampling system until they reached the gas analyzer. The actual values are likely somewhere in between the two aforementioned assumptions. In any case, the differences in concentrations and fluxes due to the absolute temperature differences present were expected to be small, though the possibility of an effect on diurnal patterns was considered.

Fetch Calculation

Relative positions of all measurement towers were triangulated using angle measurements taken with a theodolite. Gas towers were removed from around the pile before each turning of the compost pile to allow access to the pile by the compost turning machine. The turning of the pile shifted the pile location so that replacing the gas measurement towers in exactly the same location every time was neither possible nor desirable. Gas towers were replaced in approximately the same position relative to the pile (using spacers with length 67.3 cm) after each turn (Figure 3.1), and new angle measurements were taken to calculate the new positions of each tower. Given the constant spacing, the location of the pile could be determined from the locations of the gas sampling towers. These positions were used to calculate the distance over the pile that the wind traveled before reaching each of the four gas sampling towers (fetch). A fetch value for each gas tower for each one-minute average wind direction observation was calculated. These values were averaged to obtain an average fetch for each 30-minute interval.

Figure 3.3. Schematic of gas sampling and analysis system. Air is drawn from the intake tubes (4 of 16 shown) through the valve manifold system by the vacuum pump. The photoacoustic analyzer draws air from a single line through the flush valves. When it is not drawing air (during analysis), the flush valves connect the common manifold space (and the next line to be analyzed) to the vacuum pump. When the photoacoustic analyzer finishes analysis the data are saved on the desktop PC and the relay control system is activated to switch valves.



Upwind/Downwind Gas Sampling Tower Classification

The mean one-minute horizontal wind components measured with the sonic anemometers mounted at 0.7 m above ground were averaged for each 30-minute interval. The resultant average wind directions for the 30-minute interval were used to determine the upwind and downwind gas sampling towers for the interval. If the wind direction fell in a specified angle range for each gas sampling tower, it was classified as upwind or downwind for the interval. Upwind angle ranges were defined relative to the sides of the compost pile. The ranges were exclusive; if one gas sampling tower was considered upwind, all others were not considered upwind.

Downwind classification was based solely on the upwind classification; the towers were paired so that if one was classified as upwind, the tower on the opposite side of the pile would be considered downwind. Gas sampling tower 1 (east of the pile) was paired with tower 3 (west), while tower 2 (south) was paired with tower 4 (north). For every 30-minute interval, one of these pairs was considered the upwind-downwind pair and the measurements from the other pair of towers were not used.

Flux Calculations

Two methods were used to calculate fluxes in this study. The first utilized only observations; horizontal fluxes were calculated only from measured wind speed and upwind and downwind gas concentrations. The horizontal fluxes were then integrated over the measurement profile using the trapezoidal rule:

$$Flux = \frac{1}{X} \sum_{i=2}^n (z_i - z_{i-1}) \left(\frac{\overline{u_i \Delta c_i} + \overline{u_{i-1} \Delta c_{i-1}}}{2} \right) \quad [EQ 3.4]$$

Where n is the number of sampling heights, \bar{X} is the mean half-hourly fetch, z is the sampling height, \bar{u} is the mean half-hourly wind speed, and $\overline{\Delta c}$ is the mean half-hourly difference in gas concentration between the downwind and upwind sampling locations. This method was used as a baseline minimum flux because it was defined only by the observations and did not span down to ground level. It was also used as a diagnostic to check that the fundamental patterns in fluxes did not change by the extrapolation to ground level as described in the second method below.

In the second method for calculating fluxes, profiles of wind speed and gas concentration from 0 to 3.5 meters were defined, and these were numerically integrated using:

$$Flux = \frac{1}{\bar{X}} \sum_{i=1}^n \bar{u}_i \overline{\Delta c}_i \overline{\Delta z}_i \quad [EQ 3.5]$$

To apply the integration, approximations must be used to define a continuous profile from discrete measurements and wind speeds, and gas concentrations below the lowest measurement level must be estimated. Wagner-Riddle et al. (2006) calculated fluxes using Equation 3.5 and several integration methods and found the spline interpolation method the most accurate. In the present study, the *splinefun* function in R (R Development Core Team, 2010) was used to interpolate gas concentrations between measurement heights as well as extrapolate down to surface level (linearly). This gave gas concentration profiles from 0 m to 3.5 m that corresponded with the measured values at 0.7 m, 1.25 m, 2.25 m, and 3.5 m levels.

Wind speed for the same profile was defined by fitting a logarithmic equation to the four wind speed measurements. Although the profiles did not correspond exactly with the measured values, they succeeded in mimicking realistic wind speed profiles down to the surface better than the spline-interpolation with linear extrapolation used for the gas profiles. The spline and logarithmic fit profiles were used to predict gas concentration and wind speed respectively in 0.01 m layers from the surface to 3.5 m, and fluxes were then calculated using Equation 3.5.

Data Filtering

An initial quality control filtering was performed before further analysis of the data. Both sonic and cup anemometers were used in this study, and this was taken into account by adjusting wind speeds measured by the sonic anemometers to a cup-speed equivalent (Kent, 2012). Despite this adjustment, additional caution had to be used when measuring low wind speeds. Cup anemometers must overcome a frictional force to start spinning, resulting in a minimum threshold speed needed for the anemometers to start registering the wind speed. If wind speeds are below this threshold for a given period of time, the wind speed for that period will be recorded as 0 m s⁻¹ by the cup anemometer even though the sonic anemometer records a greater than zero wind speed. Given that wind speed generally increases with height, and that the cup anemometers were placed at the highest heights, one way to identify mean wind speeds that are likely affected by

the cup threshold issue is to look for a decrease in wind speed with height. Data from half-hour intervals were omitted when wind speed measured at 3.5 m (with a cup anemometer) was below the speed measured at 0.7 m (with a sonic anemometer). It was considered very likely that such intervals did not give a true picture of the wind profile, and thus were not considered in further calculations and analysis.

Further data-filtering criteria similar to those used by Wagner-Riddle et al. (2006) were tested. A restricted half-hour mean upwind angle range was used. The original angle range of 90° was further restricted by 15° and 30° less on each side, resulting in angle ranges of 60° and 30°. These were intended to reduce the number of periods where wind directions were close to the border between the upwind range of one gas sampling tower and another, and it was hoped that these restricted angle ranges would ensure that the sampling tower selected as upwind is truly the most upwind tower.

The next set of filtering criteria was based on the range of one-minute mean wind directions within each half-hour period. Changes in the wind direction had potential to change which tower pair was considered upwind or downwind, even within the half-hour mean screening described in the preceding paragraph. Half-hour periods were filtered based on the ranges of the one-minute means being less than 30°, 60°, and 90°.

Finally, the data were filtered based on the 30-minute mean wind speed at 3.5 m being less than 1.5 m s⁻¹. Higher wind speeds should have minimized back-diffusion and plume meandering effects. With lower wind speeds, emissions from the top of the compost pile could have escaped above the tallest measurement height before being advected across the measurement point. The wind speed filter was intended to remove half-hour periods when this would be more likely to occur.

Open Flux Chamber Measurements

Open flow-through flux chambers were employed over the compost pile's lifetime, starting on 5/24/12 and ending on 7/19/12. The open chambers consisted of a large, cylindrical main chamber with a small, cylindrical chimney that is open to the atmosphere. Compared to closed chambers, which use the build-up of concentration over time to estimate a flux, open chambers use a sweep gas in order to calculate a flux. This is thought to be more appropriate in the convective environment of actively composting material (Sommer et al., 2004). Nitrogen gas was used as a sweep gas in this study at a rate of approximately 8 L min⁻¹. The nitrogen gas was introduced into the chamber containing a fan for mixing the headspace. Chamber measurements were performed on nine different locations during each sampling event, which lasted approximately 1.5 hours.

The sampling locations were split into three different sections by visually dividing the pile into a north, middle, and south area. These areas were then sampled in three different locations: the center top of the pile, the upper side of the pile, and the lower side of the pile (Bailey, 2013). Chambers are placed directly on the surface of the compost pile, sometimes using a small rod to support the chambers placed on the sides of the pile. A homogeneous mixture and bilateral symmetry was assumed, and therefore

samples were only taken on the east side of the compost pile. Equilibration was performed for eight minutes with the nitrogen gas flowing before samples were removed from the chamber. A septa located on the chimney of the chamber was the sampling port from which gas samples were taken. A 20 mL syringe was used to remove the gas and was injected into a previously evacuated 12 mL Exetainer vial (Labco International Inc., Houston, TX).

Each chamber was placed individually to take a sample and subsequently moved to the next location to allow for equilibration. In many cases, chamber sampling events would be performed both before and after a turn event. The GHG samples contained in the Exetainer vials were run within three weeks of collection in tandem with GHG standards on a gas chromatograph (GC-2014, Shimadzu) to measure CH₄, N₂O, and CO₂. Flux was calculated using the following formula (Playa Vista Dev. Regional Geochemical Assessment, 2001):

$$E \approx \frac{Q_{\text{Sweep}}(1/(1 - C_{\text{Sample}})) Y_{\text{Sample}}}{A} \quad [\text{EQ 3.6}]$$

Where E is the flux density or emission of a GHG of interest in $\text{g m}^{-2}\text{s}^{-1}$, Q_{sweep} is the flow rate of the sweep gas (N₂) going into the chamber in L min^{-1} , Y_{sample} is the concentration of the gas sampled from the chamber mg L^{-1} , C_{sample} is the concentration of the gas sampled from the chamber in vol/vol, and A is the surface emission area of the bottom of the chamber in m^2 . Fluxes were calculated from each individual chamber measurement and then combined by averaging fluxes from the three sections (north, middle, and south) delineated by location (top, upper side, and lower side). Therefore, all of the fluxes from the top of the pile were averaged together separately from all the upper side fluxes that were averaged together and so on. These fluxes were then multiplied by a calculated ratio of the surface area contributing to that location (top, upper side, and lower side). These fluxes were then added together to obtain an estimated flux for the surface area of the whole compost pile (Bailey, 2013).

Resulting fluxes are expressed per unit total surface area of the compost pile, while the micrometeorological method expresses them in terms of the compost pile's "footprint" area on the ground. Fluxes obtained from the chambers are converted into terms of footprint area for comparison with the micrometeorological fluxes by multiplying by the ratio of total surface area to footprint area of the pile. Footprint areas were calculated using pile dimensions obtained with the theodolite measurements taken when the pile was turned (starting with the turn event on 6/1 and continuing for as long as micrometeorological measurements were taken). Additional measurements and estimations of pile dimensions were carried out over the entire compost windrow lifetime (Bailey, 2013), and when the theodolite-based pile dimensions were not available, these were used.

Results and Discussion

Temperature Dependence of Gas Concentration Conversion

Individual half-hour fluxes were less than seven percent different using average sonic temperatures compared to assuming equilibrium temperature of 25°C. There was a diurnal pattern to these differences with highest differences occurring as sonic temperatures departed from 25°C. Given the long pathway through tubing and multiple valves, as well as the fact that the equipment enclosure was air-conditioned, we consider the equilibrium temperature scenario reasonable, and further results and discussion are based on the 25°C normalization temperature calculation.

Mean Concentration Profiles

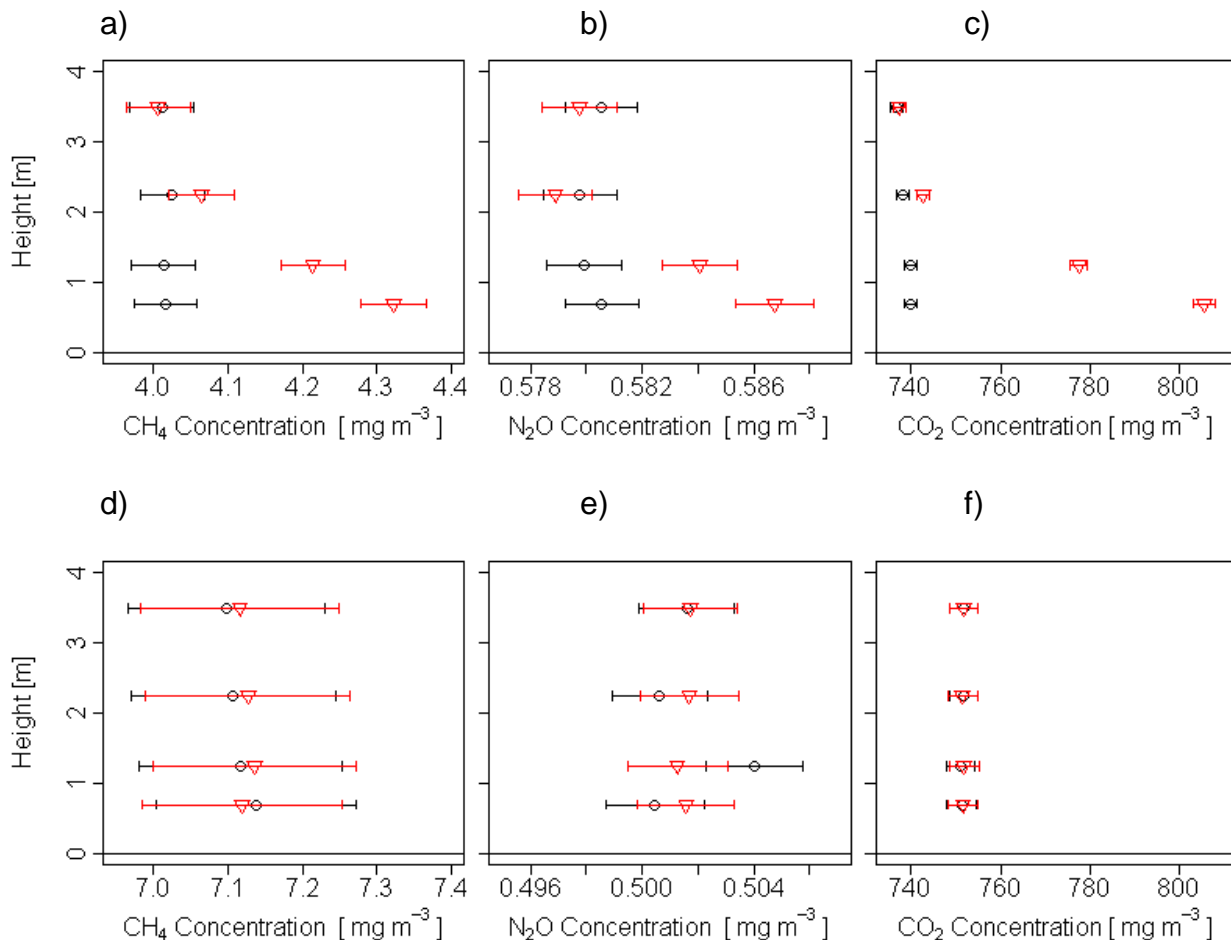
Mean upwind and downwind concentrations of CH₄, N₂O, and CO₂ at each height were calculated for the period in between each turn event (not shown), for these periods as a whole (Figure 3.4 a-c), and for the zero-source test period (Figure 3.4 d-f). Differences between the mean half-hourly upwind and downwind concentrations at each height were tested for significance at the 0.05 level using a Welch's *t* test (Table 3.1). Differences in the upwind and downwind mean concentrations for all three species were significant at the 0.7 m and 1.25 m sampling heights over the experiment as a whole, showing clear enrichment of the air downwind of the compost pile at these levels. Significance of mean concentration differences for any individual measurement period varied. At the 2.25 m level, the difference was only statistically significant for CO₂. No significant mean difference in concentration was found at 3.5 m for any period or species indicating that on average the pile did not modify the air at this height. Additionally, no significant mean difference in upwind and downwind concentrations were observed during the zero-source test period (Figure 3.4 d-f), as expected.

Additional t-tests were carried out to test whether the concentration differences measured during the experiment period were greater than those measured during the zero-source test period (Table 3.1). Significance is assessed at the 0.05 level. For the periods when the compost pile was present (taken as a whole), CO₂ concentration differences were significantly greater than during the zero-source period for the lowest three sampling heights (0.7 m, 1.25 m, 2.25 m). No significant difference was found for the 3.5 m sampling height, which supports the evidence that the pile does not on average modify CO₂ concentrations at this height. CH₄ and N₂O concentration differences were significantly greater than during the zero-source test at the lowest two sampling heights.

One final set of t-tests comparing the mean concentration difference at each height during the zero-source test period with the difference between subsequent measurements from a constant, known source in the lab also showed no significant difference in means for all heights and species (not shown). F-tests (not shown) were performed to test if the variances of zero-source test differences were less than or equal to the variance of the lab test differences. Variances of CH₄ differences during the zero-source test were found to be significantly greater than during the lab test, indicating

greater noise with the gas analyzer in combination with the sampling system and experimental set-up than with the analyzer alone. The variances of CO₂ and N₂O differences were not greater for the zero-source test versus the lab test. One possible explanation for the increased variance in CH₄ is plumes of that species from other sources in the field (possibly larger piles of stored compost).

Figure 3.4. Mean upwind (black circles) and downwind (red triangles) profiles of CH₄, N₂O, and CO₂ concentration as measured using the micrometeorological technique for a-c when the compost was present and d-f during the zero source test when the compost pile was not present. Bars indicate standard error of the mean (1,664 and 435 half-hourly means were used in calculating the mean concentration differences over the experiment period and zero-source test period respectively).



Mean upwind gas concentration at each height was calculated for the entire field experiment and profiles were grouped according to which gas tower they were sampled from. There were 527, 648, 283, and 641 half-hour periods considered upwind for gas

sampling towers 1-4 respectively. Most upwind concentration profiles were approximately constant with height, indicating the gases were well mixed upwind of the pile (not shown). Another noticeable feature is the difference in concentration at all heights for the different towers. The differences in mean concentrations for different wind directions indicate variable background sources of CH₄, N₂O, and CO₂. Given the pile's diverse surroundings, this is not surprising and demonstrates the need to measure background gas concentration for use in the micrometeorological mass balance method when surroundings are not homogeneous (Wagner-Riddle et al., 2006).

Table 3.1. Mean downwind-upwind concentration differences at each height and p values from t-test testing if mean upwind and downwind concentrations are significantly different from one another a) while the compost pile was in place and b) during the zero source test period. P-values from t-tests conducted to test if concentration differences when the compost was present are significantly greater than during the zero source test period are given in c).

Height	Compost Periods (a)						Zero Source Test Period (b)						Compost Periods vs. Zero Source Test Period Difference in Mean Concentration Differences (c)		
	CO ₂		CH ₄		N ₂ O		CO ₂		CH ₄		N ₂ O		CO ₂	CH ₄	N ₂ O
	\bar{dC} [mg/m ³]	ν	\bar{dC} [mg/m ³]	ν	\bar{dC} [mg/m ³]	ν	\bar{dC} [mg/m ³]	ν	\bar{dC} [mg/m ³]	ν	\bar{dC} [mg/m ³]	ν	ν	ν	ν
h4 3.5m	0.480	0.805	-0.005	0.932	-0.001	0.67 1	-0.019	0.997	0.018	0.923	0.000	0.957	0.177	0.704	0.713
h3 2.25m	4.587	0.023	0.039	0.527	-0.001	0.63 6	-0.233	0.960	0.020	0.917	0.001	0.668	0.000	0.341	0.885
h2 1.25m	37.792	0.000	0.201	0.001	0.004	0.02 8	0.768	0.869	0.018	0.924	-0.003	0.267	0.000	0.000	0.000
h1 0.7m	65.778	0.000	0.306	0.000	0.006	0.00 1	0.346	0.940	-0.020	0.917	0.001	0.648	0.000	0.000	0.001

Effects of Filtering Criteria

Air sampled from locations upwind should have gas concentrations lower than air sampled from locations downwind of a source (compost windrow). Upwind and downwind concentrations could be about equal for some periods if the source is weak or varies temporally. Concentrations of gases measured at downwind locations should not be lower than concentrations measured at upwind locations, as sink activities by the compost pile are assumed not to occur. When negative concentration differences are observed, there could be several explanations: Upwind and downwind gas sampling locations selected may be changing due to changes in wind direction on short time scales; wind direction could be modified by the pile itself so that upwind air is diverted and does not travel over the pile to the opposite downwind location; or backward diffusion or random noise associated with the experimental set-up (including the sampling system and photo-acoustic gas analyzer) could be responsible. Negative concentration differences may also lead to calculated negative fluxes; what should be a source may appear to be a sink. For all periods when the compost was present combined (1,664 half-hour periods), 40, 46, and 27 percent of downwind-upwind

concentration differences (any height) were negative, with 30, 46, and seven percent half-hourly flux values being negative for CH₄, N₂O, and CO₂ respectively. The pairs of percentages do not necessarily match because the fluxes are integrated over the full profile; negative differences at one height may be offset by positive differences at other heights.

Marginal reductions in both the number of negative concentration differences and flux values are seen after applying various filtering criteria (see above). Negative CO₂ fluxes could be reduced from about seven percent to less than one percent when applying a couple of the filtering schemes, while the percentage of negative concentration differences dropped from 27 to 20 percent. For N₂O, none of the filtering schemes decreased the percentage of negative fluxes by more than about three percent and in many cases filtering slightly increased the percentage of fluxes that were negative. CH₄ showed up to ten percent drops in negative values with filtering, although this left 20 percent of the half-hour fluxes negative. The large number of negative concentration differences and fluxes for N₂O and CH₄, even after the most restrictive filtering was applied in conjunction with the lower number of negative values for CO₂, points to random instrument noise as the cause. Unfiltered data (only the quality control filter described above are applied) are used in the remaining analysis because filtering only marginally reduced the percentage of periods with negative fluxes but significantly reduced the number half-hour observations. Given that the main issue seems to be separation of instrument signal and noise, more observations are valuable.

Wind Velocity

The degree to which wind velocity measurements at the two sampling towers differed and changed upwind/downwind classification and calculated fetches and fluxes was examined. Due to instrumentation and data-logging issues, wind measurements at both locations were not continuous. A sonic anemometer used at wind tower 1 malfunctioned for three of the periods (Figure 3.2 B, E, F), and a data-logger problem caused measurements from the entire second wind tower (all heights) to not be recorded for one period (C). Of the six continuous measurement periods (Figure 3.2 A-F) in the study, periods A and D were the only full periods when all anemometers and data-loggers were functioning properly, thus, the remainder of this section will focus on these two periods.

The two measurement periods considered contained a total of 335 half-hour periods with 21 of these excluded by the quality control filtering. 9.5 percent (30) of the remaining 314 half-hour periods saw changes in which gas sampling tower was classified as upwind depending on which wind measurement tower was used. For these periods, concentration differences, and thus fluxes, were different depending on which wind tower was used. Differences could be substantial if, for instance, concentration differences were high between one gas sampling pair and close to zero (or even negative) between the other gas sampling tower pair.

For the remaining periods, concentration differences were identical, and analysis was carried out to determine how differences in wind direction and speed influenced fluxes.

The wind speeds measured at each tower and each height were plotted against each other, stratified by which gas sampling tower was classified as upwind at the time. Some evidence of pile blockage of airflow was seen in periods with westerly wind in which wind tower 2 was downwind of the pile; wind speeds were generally lower for wind tower 2 than tower 1.

Fluxes were calculated based on each wind tower in three ways to gauge the importance of differences in wind directions versus differences in wind speeds on the fluxes. First, each tower was treated independently: only wind speed and wind direction from each tower were used to calculate a flux from that tower. This represents the resulting fluxes had only one of the towers been employed. Second, wind speed at each height was averaged, and used in the flux calculation for each tower; each tower's wind direction remained independent. Third, wind direction from both towers were broken into horizontal components, averaged, and recombined to yield an average wind direction used in the flux calculation for both towers; wind speeds for each tower remained independent. The resulting fluxes from each tower were then plotted against each other for each method of calculation and a line was fit to each plot (not shown). In all cases, slopes of the best-fit line indicate larger fluxes calculated based on wind tower 1 than based on wind tower 2. Plots for the case when average wind speed was used (and wind direction was independent for each tower) yield a best-fit line with slope closer to one than do plots for the case when fluxes were calculated completely separately for each tower and plots when average wind direction (wind speeds were independent). This indicates that differences in wind speed play a more important role than differences in wind direction in explaining differences in fluxes calculated from each tower. This becomes more pronounced when only half-hour periods where the same concentration gradients are considered. Lastly, the fluxes from the two towers were averaged together for each method and compared. In all cases, slopes were very close to one.

Temporal Patterns

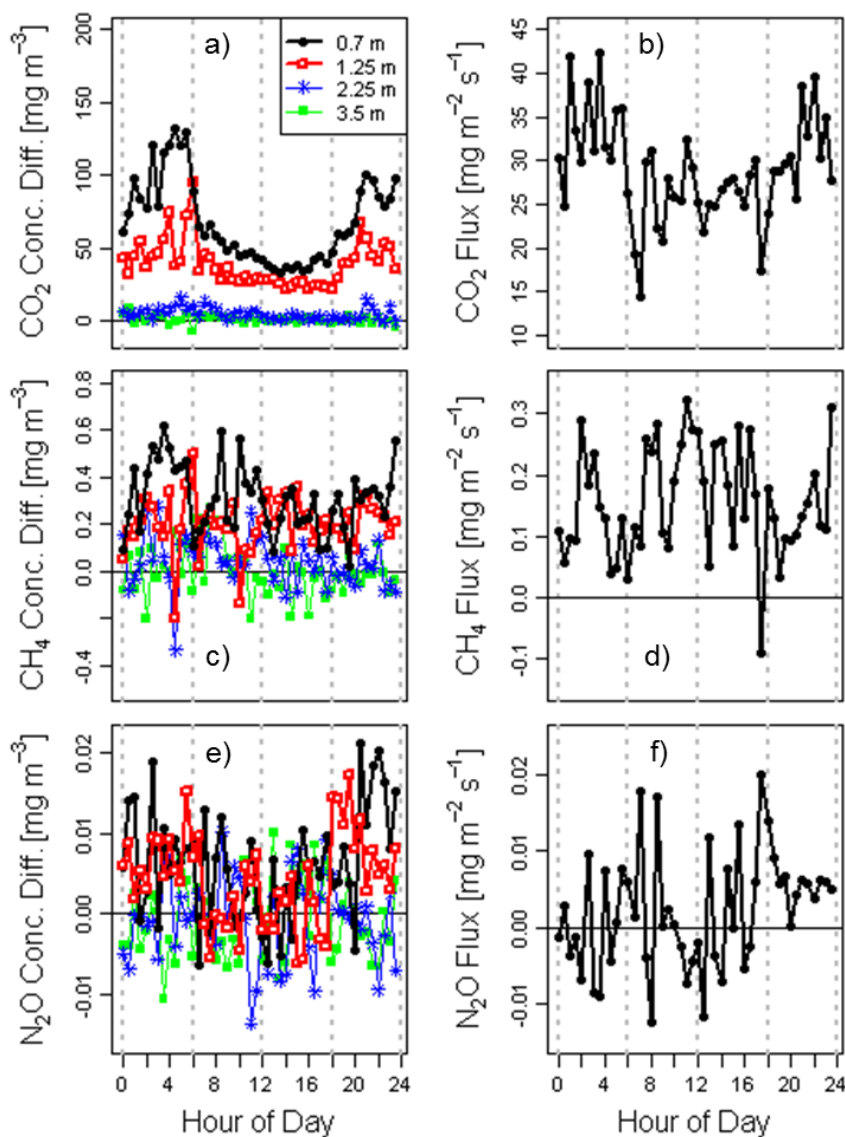
Temporal patterns were analyzed on time scales including over the diurnal cycle and in between turn events. Wind speed, fetch, concentration differences, and fluxes were averaged hourly to look for consistent diurnal patterns. There are clear diurnal patterns in several of these variables that are used in the flux calculation. Wind speed showed a typical pattern with building speeds in the morning, highest speeds during the afternoon and lower speeds at night (not shown). Fetch, a function of the wind direction and pile geometry, peaked mid-morning, slowly decreased until evening, and then sharply dropped off at night, only to sharply rise again in the morning. This likely reflects the diurnal shift in wind direction (not shown). Little variation throughout the day was seen in the concentration differences of all of the gases at the highest two levels, pointing to the pile's small influence at these levels (Figure 3.5). CO₂ concentration difference patterns at the lower two heights were very pronounced, with differences generally being much higher at night than during the day. The higher temperature gradients likely present between the warm compost pile and cold air at night could explain this enhancement at night, as it would tend to induce more convection, although it is not clear why this is not reflected in the differences in the other two gases. The diurnal pattern is muted in the

CO₂ flux because while the concentration gradient is high at night, the wind speed is low. There is no clear diurnal pattern in the concentration differences or fluxes of either CH₄ or N₂O. It is possible that emission of these gases by the pile was too weak and/or intermittent to exhibit the diurnal pattern as CO₂ does.

The periods between turn events were also examined. There were five turn events after which micrometeorological measurements were taken, with the period after each event containing between 130 and 491 half-hour observations. Several features show up in the averages of concentration differences and fluxes taken over all turn periods. First, the diurnal patterns (or lack thereof) discussed in the previous section show up again. Peaks in CO₂ concentration differences (at the lower heights) and fluxes are apparent shortly after midnight, and decay in the height of these peaks is also seen as time passes since the turn event. A diurnal pattern is not seen in the concentration differences or fluxes of CH₄ or N₂O.

The second feature is a rapid initial rise observed in the time series of CO₂ and possibly N₂O concentration differences and fluxes in the hours after the turn event. For CO₂ this rapid rise peaks near 13 hours after the turn event, whereas for N₂O, the peak is seen closer to 10 hours after the turn, although it is difficult to distinguish from the noise. The rapid rise is not as clear with CH₄. The concentration difference and flux do start out negative in the 30-minute period immediately following the turn, but observations were only available for this 30-minute period during turn period 5 so it is unclear how representative this point is of the overall trend. By one hour after the turn event, concentration difference and flux have risen to a peak. If the first 30-minute interval is considered unreliable (because there is only data from one turn period for it), CH₄ does not show the initial rise; it starts out high. One explanation for the difference between methane and the two other gases is that methane is not soluble whereas the other two gases are. Disturbing the pile by turning could expose regions of the pile that are supersaturated, leading to off-gassing of CO₂ and N₂O. CH₄ on the other hand is constantly trying to escape the polar environment of the pile. Another possibility (somewhat opposite of the first) is that pockets of CH₄ released during and subsequent to the turn lead to high initial fluxes, whereas the other gases start low and rise. Yet another hypothesis is that release/production of methane is able to pick up much more quickly than CO₂ and N₂O, within an hour of the turn event. Additional experiments are needed to test this. Measuring emissions during (as opposed to shortly after) turn events is also one gap in our study. Given physical constraints on placement of sampling towers while the compost turning equipment is operating, a different sampling strategy may need to be developed. Monitoring of integrated emissions for windrows with different turning frequencies is another possibility for future work. Future research could also benefit from comprehensive windrow temperature measurements that are a dominant controller of compost microbial activity (Hellmann et al., 1997).

Figure 3.5. Hourly averages of concentration differences at each height and flux of CO₂ (a, b), CH₄ (c, d), N₂O (e, f).



A third characteristic seen in the plots of all three gases is a decrease in concentration differences and fluxes with increasing time since the turn event. The patterns show up best in the upwind-downwind concentration differences that are driving the fluxes and are more muted in the actual fluxes themselves due to the effects of other variables in the calculation (wind speed, fetch, and integration of other concentration differences). The decaying sinusoidal diurnal pattern is superimposed on top of this exponential decay in the case of CO₂ concentration differences, but is not picked up well in the CO₂

fluxes or in the concentration differences or fluxes of the other two species. The three predominant features described were incorporated into a non-linear least squares fit for each concentration difference (lowest height) and flux (Table 3.2).

The rapid initial rise can be modeled as an exponential function,

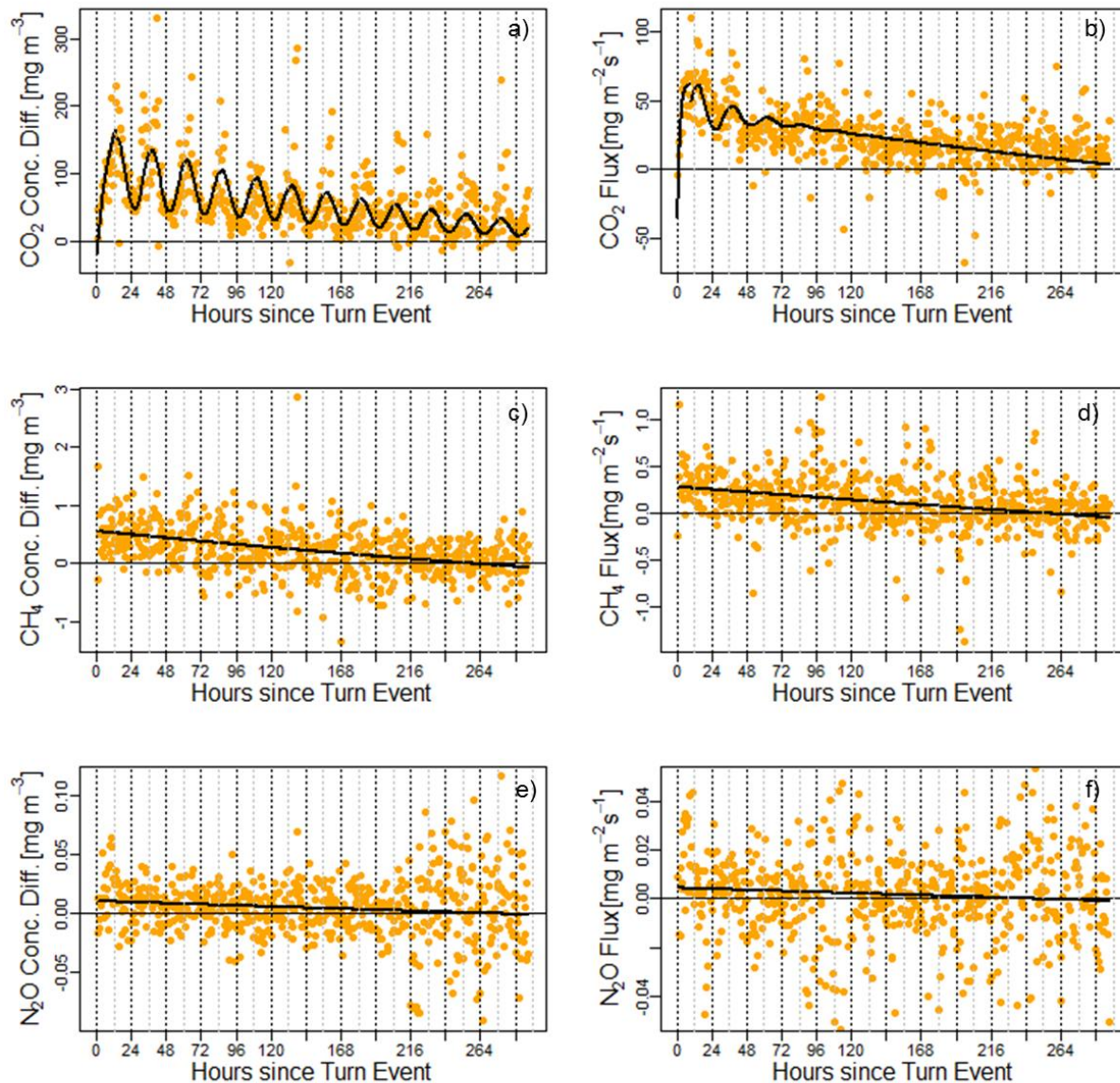
$$Y = A_1(1 - e^{k_1 * X}) \quad [\text{EQ 3.7}]$$

Where Y is the flux (or concentration difference), X is the number of hours since the turn event, A_1 is the coefficient representing the final amplitude of the rise, and k_1 represents the degree of curvature of the exponential function and also is the inverse of the time constant. This was applied to the concentration differences and fluxes of CO_2 , but not N_2O or CH_4 . The fluxes after the initial rise are modeled as an exponential decay, with the addition of a sine wave with exponentially decaying amplitude in the case of CO_2 ,

$$Y = A_2 e^{(k_2 X)} + A_3 e^{(k_3 X)} \sin(\omega X + \varphi) \quad [\text{EQ 3.8}]$$

where Y is the flux (or concentration difference), X is the number of hours since the turn event, A_2 and A_3 are coefficients representing the initial amplitudes of the overall decay and the decay of the sin wave amplitude respectively, k_2 and k_3 two are coefficients representing the degree of curvature (and inverse time constants) of the exponential functions, ω is the frequency of the sine wave (set as $2\pi/24$ radians hr^{-1} for the diurnal cycle), and φ is the phase shift in the sine wave. The second term on the right hand of equation 3.7 representing the diurnal variation was applied to CO_2 but not N_2O or CH_4 .

Figure 3.6. Half-hourly concentration differences (left) and fluxes (right) of CO₂, CH₄, and N₂O averaged across periods in between turn events. Each point represents an average of half-hour periods a certain time after a turn event for between 2 and 5 turn periods. Thick black lines give the best fit curve obtained using the nls function in R in combination with equations 3.7 and 3.8. The y-axis in the N₂O flux plot has been truncated so that the best fit line can be seen.



Given negative values of concentration difference and flux measured, an offset was added before the best fit curve was calculated and subtracted to get the final curve, because the curve fitting routines were sensitive to the negative values. In some instances the curve values were negative. This tended to occur at the start or end of the

turn period. Where these negative values occur, the curves are likely unrealistic (if the pile is assumed to be a source).

Table 3.2. Coefficients of the piecewise nonlinear weighted least squares curves fit to the concentration differences (at 0.7m) and fluxes of the CO₂, CH₄, and N₂O averaged across periods in between turn events. The break point is when the piecewise curve switches from being represented by Equation 3.7 to Equation 3.8.

	GHG	A ₁ [mg m ⁻³]	k ₁ [hr ⁻¹]	Break point [hr]	A ₂ [mg m ⁻³]	k ₂ [hr ⁻¹]	A ₃ [mg m ⁻³]	K ₃ [hr ⁻¹]	Φ [radians]
Concentration Difference (0.7 m) [mg m ⁻³]	CO ₂	251.5401	-0.1151	13.5	140.4576	- 0.0035	55.2377	- 0.0054	-2.1802
	CH ₄	-	-	-	1.9018	- 0.0013	-	-	-
	N ₂ O	-	-	-	0.1018	- 0.0004	-	-	-
Flux [mg m ⁻² s ⁻¹]	CO ₂	130.2625	-0.5893	10.0	112.4349	- 0.0016	33.0148	- 0.0391	-2.3410
	CH ₄	-	-	-	1.6548	- 0.0007	-	-	-
	N ₂ O	-	-	-	0.1514	- 0.0001	-	-	-

Comparison with Chamber Technique

Average fluxes per unit ground area were calculated for each chamber sampling period. When both theodolite and other measurements (Bailey, 2013) were available, fluxes were calculated with each separately and compared. Maximum percentage differences in the average flux for a sampling event of each gas using the different pile dimensions were 3.9, 1.6, and 5.4 percent for CO₂, CH₄, and N₂O respectively. Remaining analysis uses the theodolite measurements when available (16 sampling events) and the dimensions used in Bailey 2013 for the remainder (6 sampling events).

Maximum fluxes observed over the windrow lifetime with the open chambers were 42.1 mg CO₂ m⁻² s⁻¹, 0.201 mg CH₄ m⁻² s⁻¹, and 0.0110 mg N₂O m⁻² s⁻¹. The chamber CO₂ flux was close to the maximum reported by Anderson et al. (2010) using closed chambers (34 mg CO₂ m⁻² s⁻¹), although the maximum CH₄ and N₂O seen in the present study were much lower than what they observed (2.6 mg CH₄ m⁻² s⁻¹ and 0.09 mg N₂O m⁻² s⁻¹). This supports their suggestion that smaller windrows and more frequent turn events (such as in the present study) may decrease emissions compared to the larger, less intensively managed windrows in their study. Beck-Friis et al. (2000) also reported CH₄ flux (using closed chambers, 1.4 mg CH₄ m⁻² s⁻¹) an order of magnitude greater than that seen in the present study (open chambers) and also observed higher fluxes

with larger pile dimensions. N₂O flux reported by Beck-Friis et al. (2000) (0.017 mg N₂O m⁻² s⁻¹) agreed well with the maximum flux observed using the chambers in the present study. Maximum observed fluxes using the micrometeorological mass balance technique for individual 30-minute periods were much higher, but these were balanced by lower, sometimes negative fluxes, making block-averaged fluxes more representative of the overall picture given by the MMB technique. Maximum 3.5-hour mean fluxes were 156.1 mg CO₂ m⁻² s⁻¹, 0.923 mg CH₄ m⁻² s⁻¹, and 0.122 mg N₂O m⁻² s⁻¹.

The windrow remained in place for a total of 2,689 30-minute periods. MMB measurements were taken and passed the quality control filter (Section 2.8) for 1,664 of these periods (62 percent). The average flux calculated for each 30-minute period was multiplied by 1,800 s to give an average emission per area for each period. These 1,664 average emissions were summed to give a total integrated emission per area of 86.04 kg CO₂ m⁻², 472.23 g CH₄ m⁻², and 7.14 g N₂O m⁻², representing the integrated emission per area over the 62 percent of the time the windrow was in place, monitoring occurred, and measurements passed the quality control filter. The 22 chamber-measured average fluxes were linearly interpolated onto a 30-minute time grid so that integrated emissions per area could be directly compared with emissions calculated with the MMB technique. Integrated emissions per area calculated in this way were 54.02 kg CO₂ m⁻², 191.17 g CH₄ m⁻², and 4.45 g N₂O m⁻². These total emissions per area calculated using chamber data differ by 37, 60, and 38 percent from the emissions calculated using the MMB technique for CO₂, CH₄, and N₂O respectively.

Although chamber measurements were less frequent than the MMB measurements, they were spread out over most of the windrow lifetime, with 98 percent of the 2,689 30-minute periods between the first and last chamber sampling event. Integrating over this span, total emissions per area were 89.37 kg CO₂ m⁻², 306.20 g CH₄ m⁻², and 9.81 g N₂O m⁻². This can be extrapolated to emissions per area over the entire compost windrow lifetime by assuming proportionality to the 98 percent of the time that the chamber measurements did span. This estimates total emissions per area based on the chamber measurements of 91.24 kg CO₂ m⁻², 312.60 g CH₄ m⁻², and 10.01 g N₂O m⁻².

Two different methods were used to estimate an integrated emissions per area over the same time span with the MMB measurements. Interpolation and extrapolation via the proportionality assumption gives MMB-based estimated emissions per area over the windrow lifetime of 139.05 kg CO₂ m⁻², 763.12 g CH₄ m⁻², and 11.54 g N₂O m⁻². The second method utilized an average ratio between the MMB and chamber estimated fluxes. Over the 62 percent of the windrow lifetime that measurements overlapped, the average ratios of MMB to chamber fluxes were 1.64, 4.48, and 1.53 for CO₂, CH₄, and N₂O, respectively. These ratios were multiplied by the interpolated chamber fluxes outside the MMB measurement periods to yield estimates MMB fluxes for these periods. The integrated emissions per area calculated in this way were 144.11 kg CO₂ m⁻², 987.84 g CH₄ m⁻², and 15.36 g N₂O m⁻² (147.12 kg CO₂ m⁻², 1008.46 g CH₄ m⁻², and 15.68 g N₂O m⁻² assuming proportionality for the additional two percent of the windrow lifetime that chamber measurements did not span). The two different methods for

extrapolating MMB fluxes were 5, 24, and 26 percent different for CO₂, CH₄, and N₂O, respectively. Both these estimates are gross extrapolations given the lack of MMB during 38 percent of the windrow lifetime.

While estimates of integrated emissions per area are given above for the open chamber and MMB techniques, there is some difficulty in assessing the differences due to differences in sampling time, duration, and frequency. Chamber measurements tended to be taken directly before and after turn events with few measurements taken in between, whereas the micrometeorological sampling system would sometimes take up to several hours after a turn event to start operating (actually after data-downloading, which usually occurred shortly before each turn event). This meant that for some chamber sampling events, there were very few or no micrometeorological observations to compare. During turn period 5 however, there was relatively high temporal resolution in the chamber sampling (six sampling events in the nine-day turn period) and micrometeorological measurements began very shortly after the turning event, with seven 30-minute micrometeorological fluxes in the window around the chamber sampling for five out of six of the samples in this period. Figure 3.7 presents the fluxes calculated using the chamber compared to MMB fluxes averaged around the chamber sampling events. Individual fluxes calculated using the micrometeorological techniques are compared with those calculated using the chamber technique by averaging over the 1.5-hour duration of the chamber sampling period. This gives a maximum of three 30-minute periods of fluxes obtained with the micrometeorological method that are averaged and compared with the average of chamber measurements. Two additional 30-minute periods before and after each chamber sampling period extended this window to help average out noise in the MMB fluxes. Thirty-minute MMB fluxes were used only if they were within this window and also within the same turn period as the chamber measurements. This ensured measurements before a turn were not averaged with those after a turn event.

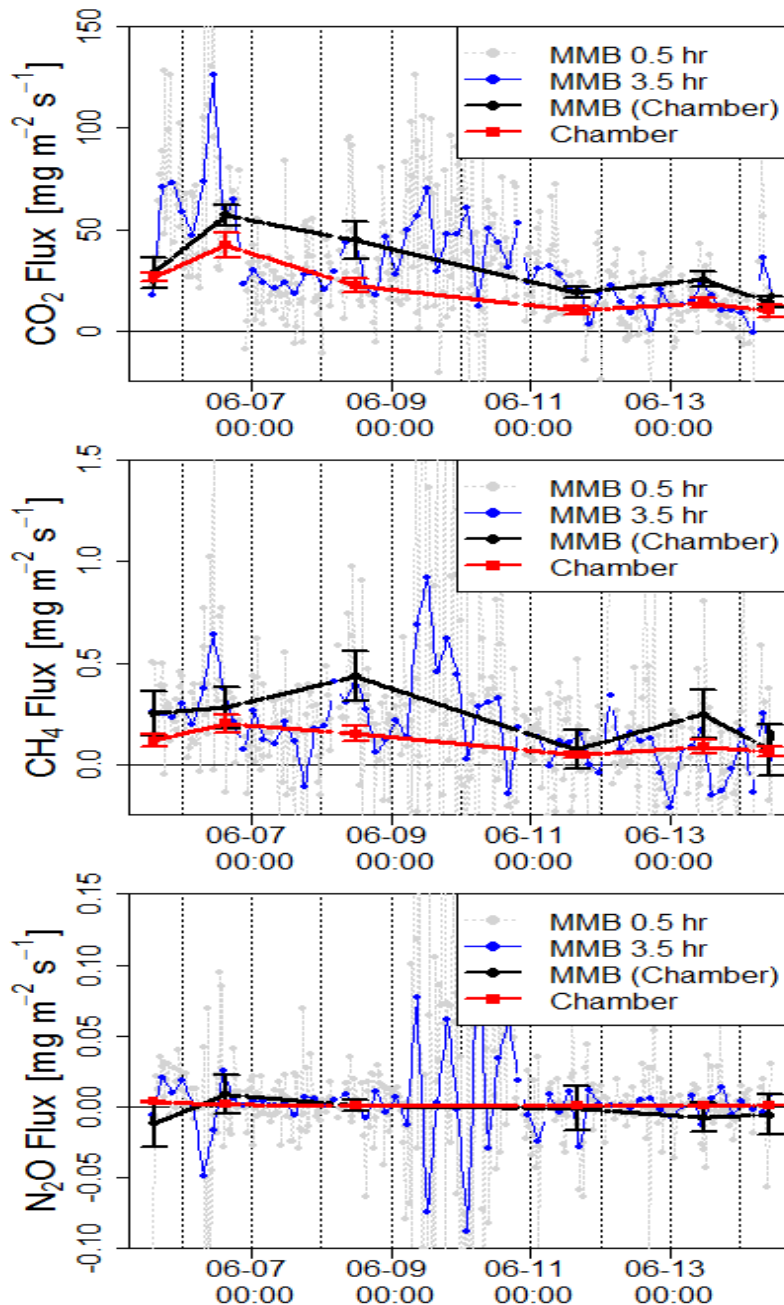
In this period, fluxes calculated using the two techniques agreed reasonably well in terms of the temporal pattern, but the absolute magnitude of the fluxes could differ substantially (Figure 3.7). Chamber fluxes tended to underestimate MMB fluxes, though this was not always the case for all three gases and for all chamber sampling events. In period 5, total emissions calculated from integrating the chamber measurements (Table 3.3) were 40, 54, and 243 percent different from the emissions calculated using the 3.5-hour average MMB measurements centered on the chamber sampling events.

Table 3.3. Integrated emissions of CO₂, CH₄, and N₂O during period 5 using chamber fluxes, MMB fluxes, MMB fluxes averaged around chamber sampling events, and MMB fluxes averaged into 3.5-hour periods. All fluxes were interpolated into 30-minute intervals and block-integrated.

	Chamber	MMB (Chamber)	MMB (3.5 hr)	MMB
CO ₂ (kg m ⁻²)	14.55	24.13	23.60	23.69
CH ₄ (g m ⁻²)	81.00	177.73	134.96	135.76
N ₂ O (g m ⁻²)	0.88	-0.61	2.51	2.30

The much larger disagreement in the case of N₂O is due to the relatively high noise levels and low measured flux of N₂O, although individual mean fluxes calculated during this period using the two techniques all agreed within one standard error of the mean. Even using the relatively higher-frequency chamber measurements in turn period 5, it is clear from the individual 30-minute fluxes, and 3.5-hour-average fluxes also presented in Figure 3.7, that discrete sampling with the chamber misses important features in the fluxes over time, including peaks. This is compounded when chamber measurements are only taken a few hours before and after turn events. Lack of nighttime and early morning chamber measurements may also bias the samples if there are diurnal patterns in the fluxes, as is the case with CO₂. Frequency of sampling can substantially change the total emission measured. For instance, total emissions during turn period 5 calculated from integrating the micrometeorological measurements centered on the chamber sampling events (3.5 h averages) were 2, 24, and 509 percent different than fluxes calculated integrating 3.5 h MMB observations over the whole period for CO₂, CH₄, and N₂O, respectively.

Figure 3.7. Fluxes of CO₂, CH₄, and N₂O calculated with the chamber and micrometeorological mass balance method during turn period 5 (see Figure 3.2). Micrometeorological fluxes are presented as the raw 30-minute averages (gray), 3.5-hour averages (blue), and 3.5-hour averages centered on the window spanning the duration of the chamber sampling event as well as an hour before and after that window (black). Bars represent one standard error of the mean.



Conclusions

This study quantified GHG fluxes from composting of green materials using both MMB and open flow-through chamber techniques. Mean concentration profiles of CO₂, CH₄, and N₂O using the MMB approach indicate that on average the pile was a source of all three gases; however, a significant number of data pairs showed lower readings downwind from the pile than from upwind. The wind speeds and directions measured in separate locations sometimes differed, and evidence was observed of airflow blockage by the pile itself. A diurnal pattern was seen in the downwind-upwind CO₂ concentration differences closer to the ground, as well as in the fluxes. Turn-related patterns were evident for all three gases, with the pattern in CO₂ being most clear.

Fluxes obtained with the MMB technique were compared with those obtained using the open chambers. The present study tends to agree with Anderson et al.'s (2010) conclusion that accurately estimating GHG emissions from composting windrows of green materials with chamber techniques is difficult and problematic. The finer-grained (albeit noisy) observations of GHG fluxes obtained using the MMB technique suggest peaks and troughs not detected by the limited chamber-sampling periods, including a potential diurnal emissions pattern. In addition to the issue of sampling frequency, estimates of fluxes obtained with the chamber were sometimes substantially different from estimates obtained with the MMB approach, leading to substantial differences in the overall GHG emissions calculated. However, the large amount of samples where the downwind concentrations and fluxes of the target gases were smaller than the upwind samples, and the large periods of time when wind patterns were unstable, also highlight the difficulty of obtaining accurate measurements using the MMB method.

Several improvements for future work are suggested. A more precise and higher frequency gas analyzer could help reduce noise in the micrometeorological mass balance technique and further help elucidate temporal patterns in compost gas emissions, especially for CH₄ and N₂O. Sampling closer to the ground would reduce the need to extrapolate and associated uncertainty. Measurements over multiple piles, during different seasons, and with different feedstock would also help quantify uncertainties. Increasing frequency of chamber sampling would allow more assessment of the differences between the two methods. For a more process-based analysis of compost emissions, quasi-continuous measurements of temperature, oxygen, CO₂, and the other trace gases, within the pile itself would be useful.

Chapter 4. A Study on Biofilter Efficiency and Flux Emissions from Composting

Introduction

Biofilters are a proven technology for removing gases and odorous emissions from various systems such as landfills (Dever et al., 2007), waste management/treatment, agricultural practices including animal waste management (Nicolai and Janni, 2001), and even leaking underground gasoline tank contaminated sites (Namkoong et al., 2003). This literature review is not intended to be exhaustively comprehensive; the reader is referred to Swanson et al. (1997) and Chen and Hoff (2009) for more complete literature surveys and general descriptions of the many forms of biofiltration. High removal efficiency, low cost, and low energy requirements are advantages of biofiltration (Akdeniz and Janni, 2012). A biofilter is made up of a biologically active bed of filter material through which the contaminated air is passed. Treatment of the contaminated air occurs by absorption, diffusion, and biodegradation (Dixit et al., 2012). The gas transfers from the air into the biofilm, an aqueous biologically active layer surrounding the organic material, and then into the solid phase in the filter material where the gases are biodegraded (McNevin and Barford, 2000; Hong, 2005). The magnitude of pollutant biodegradation depends on many factors. Some key factors are the characteristics of the pollutant, its concentration, the gas flow rate through the biofilter, the microbial ecology, and biofilter media properties (Dixit et al., 2012). Gases targeted for filtration include VOCs (McNevin and Barford, 2000; Dixit et al., 2012), CH₄ (Dever et al., 2007; Huang et al., 2011), hydrogen sulfide (McNevin and Barford, 2000), and N₂O (Martinec et al., 2001).

Biofilters are classified in multiple ways depending on the layout. How air circulates in the biofilter defines whether it is an open or closed system. In closed systems, air is supplied by a forced ventilation system into the biofilter media, whereas in open systems the air flows upward through the filter media by passive transfer (Huang et al., 2011). The majority of biofilters are closed systems. Closed-system biofilters are used to treat air from livestock barns, covered manure storage or treatment, meat meal factories, and many other practices. Open systems are most commonly found at landfills.

Biofiltration has come into use with commercial composting in the last 20 years, mostly for the removal of odors and VOCs. As laws regarding landfilling of organic waste, and local waste reduction goals, become more common, necessitating the composting of more complicated waste streams, it is expected that composting sites will be a growth area for biofiltration technology. Negative aeration refers to composting systems where air is sucked from the piles of composting material using blowers or fans, and then routed into a dedicated, engineered biofilter. Positive aeration refers to systems where ambient air is pumped into the pile to provide oxygen and then filters up through the pile using the natural convection action of the pile. In positive aeration systems, a biofilter “cap” consisting of 6 to 12 inches of unscreened, composted materials is often placed

on top of the pile to provide the filtration. In this study, we tested the efficacy of a negatively aerated system.

Whether a biofilter is horizontal or vertical is another classification. In a horizontal biofilter, the polluted air is spread evenly under the biofilter and air flows up through the filter media, while in a vertical biofilter, the filter media is piled in an enclosure where air passes either horizontally through the sides or through the top (Air Quality, 2011). Vertical biofilters generally require less area and have lower pressure drops than horizontal biofilters, but the media settles and compacts at the bottom reducing the airflow at the bottom over time (Sadaka et al., 2002).

Biofilter media needs to be porous, supply a surface for microorganisms to live on, provide nutrients, and provide a structure that makes moisture available to the microorganisms. Commonly used materials include peat, soil, green materials, manure, coconut peels, wood chips, and straw. (Hong and Park, 2005). In some cases, inorganic material such as ceramic media (Park et al., 2001) and rockwool packing materials (Yasuda et al., 2009) are inoculated with activated biomaterials. Important media characteristics are water absorption, density, porosity, particle size distribution, and pressure drop across the media (Chen and Hoff, 2009). Biofilter media needs to have a large amount of void space for air to flow through easily. Porosities for organic media range from 40 to 50 percent for soils and 50 to 80 percent for compost (Bohn, 1992). This quality makes compost and wood chips the most commonly used filter media.

Media moisture content is one of the most important parameters for biofilter viability. Inadequate moisture content reduces filtering efficiency through media drying out, creating cracks in airflow, and deactivating microbial activity (Air Quality, 2011). Excess moisture can fill up void spaces, restricting airflow through the media and creating anaerobic zones where oxygen required for bio-degradation is depleted (McNevin and Barford, 2000). When the moisture content is too high, the capacity of the filter media to remove pollutants noticeably drops. Optimal moisture content depends on media selection and the gas to be removed, but the recommended optimal range is 40 to 70 percent (Chen and Hoff, 2009). For CH₄, Huang et al. (2011) reported lower optimum moisture contents for various soils, landfill cover soil, and woodland soil (11 to 35 percent moisture by weight) compared to filter media made from compost and meadow soil (25 to 50 percent moisture).

Another important parameter for biofilter capability is temperature of the media. Microorganisms can function in a wide range of temperatures. Optimal temperatures can enhance microbial activity while extreme temperatures can slow or kill the microbes (Bohn, 1992). The suggested operating range for temperature is 20°C to 40°C, with 35°C being the optimal temperature (Leson and Winer, 1991). Optimum temperature also depends on which gas is targeted for removal; for CH₄, the best temperature is 30°C within a range from 10°C to 45°C (Huang et al., 2011).

Nutrients needed by microbes may be added as fertilized water; for example, copper, nitrogen, and phosphorus may be needed (Trotsenko and Khmelenina, 2002; Nikiema et al., 2005; Huang et al., 2011).

Filtration effectiveness has been defined in multiple fashions, with the definitions tailored to the particular applications appropriate to each study. Rene et al. (2005) define an elimination capacity as the mass of the target gas that is removed per volume of the filter per unit time ($\text{g m}^{-3} \text{h}^{-1}$) and the removal efficiency, also known as reduction efficiency (Akdeniz and Janni, 2012), as fraction of the gas flux removed expressed as a percentage; this works out to be, for the sealed vertical filter system used, the concentration difference between the filter inlet and outlet, divided by the gas concentration at the inlet. A similar definition for removal efficiency was used by McNevin and Barford (2000) and Huang et al. (2011). Rene et al. (2005) also found that the elimination capacity was a function of the gaseous inlet load expressed as the $\text{g m}^{-3} \text{hr}^{-1}$. Removal efficiencies ranged from 0.964 to 0.999 for ammonia and hydrogen sulfide, and from 0.40 to 1.00 for VOC's (McNevin and Barford, 2000). Filter composition included compost, oyster shell, peat, perlite, bark mulch, and wood chips. For toluene and *n*-propanol, measured removal efficiencies ranged from 0.43 to 0.98, with differential equation-based modeling predicting removal efficiencies of 0.54 to 0.94 (Dixit et al., 2011). VOCs were removed at about a 0.5 removal efficiency in a vertical column biofilter, based on the concentration data reported in Pagans et al. (2006), but rates even lower than 0.3 were also reported (Pagans et al., 2007).

McNevin and Barford (2000) developed expressions relating filtration with biochemical degradation constants from microbiological action within the biofilter. They used a removal or elimination rate closely related to Rene et al.'s (2005) elimination capacity, but in this case McNevin and Barford (2000) used a mass specific measure of the gaseous removal, in mass of gas removed per mass filter per hour: $\text{g kg}^{-1} \text{hr}^{-1}$. The biochemical focus meant McNevin and Barford (2000) identified residency time of the gas within the filter (and therefore the flow rate and physical dimensions/mass of the filter) as a key factor related to the ability of the biochemical kinetics of removal. The empty bed residence time (EBRT) is a common way to assess the time needed for sufficient bioactive removal, with a typical value of 25 seconds, but for CH_4 , which is insoluble, can range from five minutes to five hours (Huang et al., 2011). The EBRT can be related to the pressure drop and flow rates (Schmidt et al., 2004), and removal efficiencies are proportional to the EBRT, with the longer the EBRT, the higher the removal capacity (Morgan-Sagastume and Noyola, 2006). Differential equations for convective and diffusive transfer within the biofilter coupled with the bioremoval of gases have been developed and tested successfully for filtration of toluene and *n*-propanol (Dixit et al., 2012). Mathematical models can also be used to obtain the relationship between flow rates and the design variables (permeability, height, temperature, density, etc.) in a system. An example of this was done with passively aerated static piles in Lynch and Cherry (1996).

Engineering issues such as the pressure drop and flow rate are especially important for the design and implementation of biofilters in association with animal facilities (Nicolai and Janni, 2001; Schmidt et al., 2004), but also for other applications (Park et al., 2001) because fan and pump requirements imply energy usage and operating costs.

Odors and GHG emissions from composting facilities can also be controlled by directing effluent gases to a biofilter (Park et al., 2001), such as an ASP with exhaust gases directed through an “odor-absorbing filter” (Rynk et al., 1992), with various design criteria ranging from covered compost with filtration material contained in flow-through tanks to open piles of material through which the gases are pumped. Covered-compost piles with open biofilter systems are described in Mueller (1988), Marsh (1992), and Rynk et al. (1992).

Materials and Methods

Experimental Site

Greenhouse gas emissions were monitored at the Northern Recycling LLC compost facility (11220 County Road 94; latitude 38.77564°N, longitude 121.88007°W) in Zamora, Calif. In this study a closed ASP with filtration through a biofilter was tested for GHG emissions emitted from the biofilter bed. The system is an AC Composter™ designed and manufactured by Engineered Compost Systems (ECS). The AC Composter™ system is a covered ASP using negative aeration for removing VOCs and reducing odor. The covering is made out of a UV resistant, water-impermeable fabric containing multiple half-circle flaps in the fabric to allow for air to be pulled through by the negative aeration system (Engineered Compost Systems, 2011). The ECS system measures compost temperature and allows for control over the aeration rates using user-defined temperature set-points (Engineered Compost Systems, 2011). There are two temperature probes in the compost pile measuring 48 inches (1.2 m) deep. The probes are located along the centerline of the length of the compost pile, one at approximately 20 feet (6.1 m) and the other approximately 40 feet (12.2 m) from the aeration pipe edge of the pile (northern end). The biofilter designed for Northern Recycling is capable of obtaining effluent gases from four simultaneous piles of composting material.

At the time of this study, only one compost pile of a total of four possible piles was being used as an emissions source to the biofilter system. Composting material producing the effluent gases being pumped to the biofilter weighed approximately 225 metric tons and was comprised of 15 percent food trimmings and the rest green materials. The material is estimated to contain 50 percent moisture, the average moisture of the open windrow piles in this study. The study occurred over a three-week period (05/21/13 to 06/07/13) for a total of nine sampling days. The compost pile was laid out over a pipe-less aeration floor system, called a CompDog™ by ECS. This was comprised of two large tubes that were inflated and then subsequently removed to leave behind aeration vaults from which gas could travel (Engineered Compost Systems, 2011). The compost pile was approximately 61.4 feet long, 22 feet wide and seven feet high (18.7 m x 6.7 m x 2.1 m).

Over the course of this study the emission source compost pile was not turned. Turnings were scheduled to occur after 21 days had passed with the compost pile temperature reaching above 131°F (55°C), called “process to further remove pathogen” (PFRP) days. Per the facility manager, the compost pile under observation underwent

the state-mandated pathogen reduction process for 15 days, before and during sampling (i.e., temperatures above 131°F). Facility network problems led to loss of compost temperature data storage, and therefore data are not available in this study. The AC Composter™ system can regulate aeration, allowing more or less oxygen into the system depending on a set temperature. Negative aeration is used to pull air continuously through the compost pile (and then pipe it into the biofilter) and can be increased when temperatures reach a given set-point. The set-point temperature for the compost pile used in the study was 150°F (65.6°C); when temperatures reached this point, aeration was increased.

Figure 4.1. Compost pile laid out over the CompDog™ by ECS and covered by the ECS tarp.



Wood overs were used as the media for the biofilter. Wood overs consist of the large woody material used for increasing porosity during windrow composting. The wood overs are screened out of the mature compost to obtain pieces greater than 3/8 inch (0.95 cm) and less than four inches (10.2 cm). These wood chips and sticks contain a coating of the mature compost which served as an inoculum for microorganisms. This media is then watered in order to activate the microorganisms and raise the temperature of the biofilter. The media for this biofilter was constructed on 5/2/13. There were 19 rows of tubing containing misters on top of the biofilter. Although moisture content of the biofilter media is an important factor in filtration efficiency, it was not measured in this study to avoid disturbance of the biofilter. The moisture content was maintained by the facility to operate at optimal scrubbing efficiency. The composting gases were routed to the biofilter and released through a system of tubing underneath the wood chips. The biofilter was in the shape of a trapezoidal prism, with dimensions of

approximately five feet high (H), 69 feet long on the bottom (L1; 60 feet long on the top (L2), 26 feet wide on the bottom (W1), and 17 feet wide on the top (W2). Figure 4.2 displays a visual representation of the biofilter with 19 black sprinkler lines on top of the pile. A large green pipe on the west side of the pile has tubes underneath the biofilter bed which distribute the exhaust gas from the compost pile into the media for filtration. Black arrows represent the hypothetical air flow from the negative aeration system to the emission of exhaust gases from the biofilter bed. Figure 4.3 contains photographs of the biofilter.

Figure 4.2. Biofilter layout containing 19 lines of misting sprinklers on top and an inflated tube that releases the gases underneath the biofilter. Pink flags and lines represent the four north-south sampling directions. Black arrows represent hypothetical air flow.

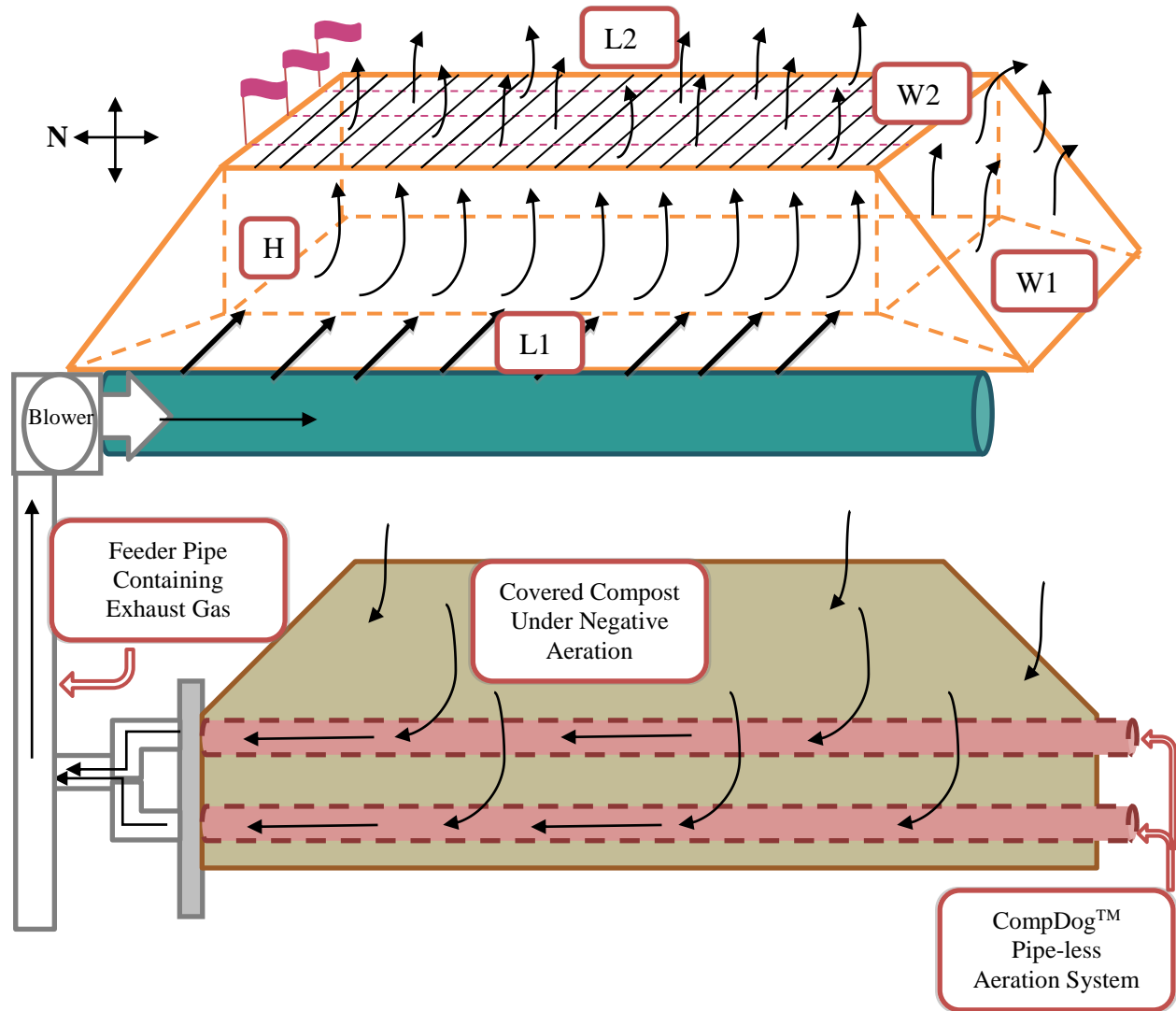


Figure 4.3. Photographs of the biofilter. In the photo on the left, the tube is not inflated. During the sampling period, the tube was inflated and feeding gases. Photo of the tube as it is normally inflated (right).



Greenhouse Gas Measurements – Mass and Flow Balance Theory

A set of formulae based on the principles of mass and flow balance was developed for the calculation of the biofilter efficiency. The idea of a trace gas was used to derive some of the formulae used in this study. The production or consumption of components in the gas phase are considered to have a negligible effect on the overall flow of the air from the compost pile effluent into the biofilter as well as the flow coming out of the biofilter; this is especially justified for trace gases because of the very low percentage (generally appreciably less than one percent) they represent in the overall composition of the air. In the case described here, the term “trace gas” can be used to describe the GHG of interest because their concentrations represent trace amounts in the composition of the air. This theory can be expressed by the following equations.

$$F = vAC \quad \text{[EQ 4.1]}$$

$$F_{b_i} = v_b A_b C_{b_i} \quad \text{[EQ 4.1a]}$$

$$F_{1_i} = v_1 A_1 C_{1_i} \quad \text{[EQ 4.1b]}$$

$$RE_i \equiv 1 - f_i ; f_i = \frac{F_{b_i}}{F_{1_i}} \quad \text{[EQ 4.2]}$$

$$f_i \times (v_1 A_1 C_{1_i}) = v_b A_b C_{b_i} \quad \text{[EQ 4.3]}$$

$$v_1 A_1 C_{1_i} + (f_i - 1)(v_1 A_1 C_{1_i}) = v_b A_b C_{b_i} \quad \text{[EQ 4.3a]}$$

$$\underbrace{\quad\quad\quad} \quad \underbrace{\quad\quad\quad} \quad \underbrace{\quad\quad\quad}$$

Where F is mass flow rate in g min^{-1} , v is velocity in m min^{-1} , A is the area in m^2 , C is the GHG concentration in g m^{-3} . Equation 4.1 [EQ 4.1] is a general equation for any mass flow rate defined by a velocity, area, and concentration. Subscript “ i ” indicates the variable can be applied to multiple GHGs, each indicated by the value of subscript “ i ,” in trace concentrations in the atmosphere, subscript “1” indicates the values associated with the pipe before the biofilter (in the feeder pipe), F_{1_i} (mass flow rate of the GHG of interest in the pipe), v_1 (velocity inside the pipe), A_1 (cross-sectional area of the pipe), and C_{1_i} (concentration of a gas of interest in the pipe), and subscript “b” indicates values associated with the biofilter surface, F_{b_i} (mass flow rate of the GHG of interest coming out of the biofilter, originating from the compost pile), v_b (velocity of air flow from the biofilter, originating from the compost pile), A_b (area over which gas from the biofilter is emitting), and C_{b_i} (concentration of a gas of interest from the surface of the biofilter bed, originating from the compost pile). EQ 4.1a and EQ 4.1b describe the mass flow rates directly defined by the variables associated with the biofilter in equation 1a and the feeder pipe in 1b. Filter efficiency, f_i , is always defined as the mass flow rate output of a biofilter divided by the mass flow rate input into a biofilter. EQ 4.2 defines f_i as the filter efficiency for the GHG of interest, a unit-less ratio of the mass flow rate of the GHG of interest at the biofilter surface divided by the mass flow rate of the GHG of interest from the pipe. An f_i value of one would indicate no filtration, and an f_i value of zero would indicate complete filtration. Thus, the filter efficiency (expressed as a fraction) defined here is one minus the “removal efficiency” (RE, expressed as a fraction also) defined in much of the previous research (McNevin and Barford, 2000; Pagans et al., 2007; Dixit et al. 2011), and is used here for convenience to the equation derivations and calculations. EQ 4.3, based on the definition in EQ 4.2, shows that the mass flow rate of the GHG of interest exiting the biofilter equals the mass flow rate of the GHG of interest from the pipe multiplied by the filter efficiency of the biofilter. This is related to the formal mass balance equation shown in EQ 4.3a (an expanded version of EQ 4.3) where an input, output, and generation/consumption term are defined. This mass balance assumes a steady state where the accumulation term is equal to zero and f_i determines the net consumption (if $f_i < 1$) or generation (if $f_i > 1$). It is also assumed that temperature and moisture changes from the pipe to the biofilter surface do not significantly change the gas density, thus introducing some error into this approach.

Because the biofilter is open to the atmosphere and consists of porous material, some possibility of entrainment (also called infiltration) from ambient air could add to the flow and mass of the biofilter through the actions of ambient wind. Therefore, EQ 4.4 can be modified to include an additional term of flow input, defined as the entrainment mass flow rate ($v_e A_e C_{e_i}$). The definition of filtration efficiency, f_i , used in equation 4.4 is still defined as the mass flow output of the biofilter divided by the mass flow input into the biofilter as shown in EQ 4.2, but now entrainment is included in both the output and the input into the biofilter.

$$f_i \times (v_1 A_1 C_{1_i} + v_e A_e C_{e_i}) = v_{be} A_b C_{be_i} \quad [\text{EQ 4.4}]$$

Subscript “e” indicates the entrainment related variables, v_e (velocity of air flow of the entrainment), A_e (area over which entrainment takes place), and C_{e_i} (concentration of a gas of interest from the entrainment source). Variables with the subscript “be” indicate variables that include both biofilter and entrainment sources. In the field, C_{be_i} is the concentration of the GHG of interest in the air coming directly from the biofilter, measured using a chamber. In this case C_{e_i} is equal to the ambient concentration taken near the biofilter; ambient samples were not taken off site. For simplification, the following ratio in EQ 4.5 will be defined. It represents the relative amount of entrained flow compared to the pipe flow, referred to as the entrainment factor (R).

$$R \equiv \frac{v_e A_e}{v_1 A_1}, v_e A_e \equiv R(v_1 A_1) \quad [\text{EQ 4.5}]$$

The idea of total mass flow conservation can be used to generate EQ 4.6. This again assumes the generation or consumption of the components in the gas phase are negligible compared to the overall flow of the system and no accumulation is occurring as well as again assuming negligible changes in gas density from temperature and humidity variation. EQ 4.7 is found by substituting $v_e A_e$ in EQ 4.5 into EQ 4.6.

$$v_1 A_1 + v_e A_e = v_{be} A_b \quad [\text{EQ 4.6}]$$

$$v_{be} A_b = v_1 A_1(1 + R) \quad [\text{EQ 4.7}]$$

The product of $v_e A_e$ from EQ 4.5 and $v_{be} A_b$ from EQ 4.7 can be substituted into EQ 4.4 to obtain EQ 4.8. This can be rearranged into EQ 4.9 to define the filter efficiency for a specific GHG of interest in terms that can be measured directly when R can be determined.

$$f_i(C_{1_i} + RC_{e_i}) = C_{be_i} + RC_{be_i} \quad [\text{EQ 4.8}]$$

$$f_i = \frac{C_{be_i} + RC_{be_i}}{C_{1_i} + RC_{e_i}} \quad [\text{EQ 4.9}]$$

$$F_{b_i} = \left(\frac{C_{be_i} + RC_{be_i}}{C_{1_i} + RC_{e_i}} \right) \times v_1 A_1 C_{1_i} \quad [\text{EQ 4.10}]$$

The final calculation of the GHG mass flow rate from the biofilter originating from the compost emissions and corrected for entrainment is then defined as EQ 4.10 by substituting f_i from EQ 4.9 into EQ 4.3. The emissions contributed by entrainment are not explicitly included for the purpose of obtaining the emissions mass flow rate from the biofilter for GHGs originating only from the compost source. This will allow for comparison with other studies on biofilters that did have the possibility for entrainment.

This equation can apply to any trace gas, “i”, however in this case it is the GHGs of interest, CH₄ and N₂O. Subscript “i” has been replaced with “CH₄” to indicate concentrations of methane and subscript “N₂O” to indicate concentrations of nitrous oxide.

$$F_{bCH_4} = \left(\frac{C_{beCH_4} + RC_{beCH_4}}{C_{1CH_4} + RC_{eCH_4}} \right) \times v_1 A_1 C_{1CH_4} \quad [\text{EQ 4.10a}]$$

$$F_{bN_2O} = \left(\frac{C_{beN_2O} + RC_{beN_2O}}{C_{1N_2O} + RC_{eN_2O}} \right) \times v_1 A_1 C_{1N_2O} \quad [\text{EQ 4.10b}]$$

One way to measure R is to use an inert tracer gas that will not be filtered by the system. If one considers the equation defining f_i above, when an inert gas is not filtered then f_t is equal to 1 and R is equal to a ratio of measurable concentrations. The subscript “t” is used to indicate the concentrations are associated with the inert tracer gas.

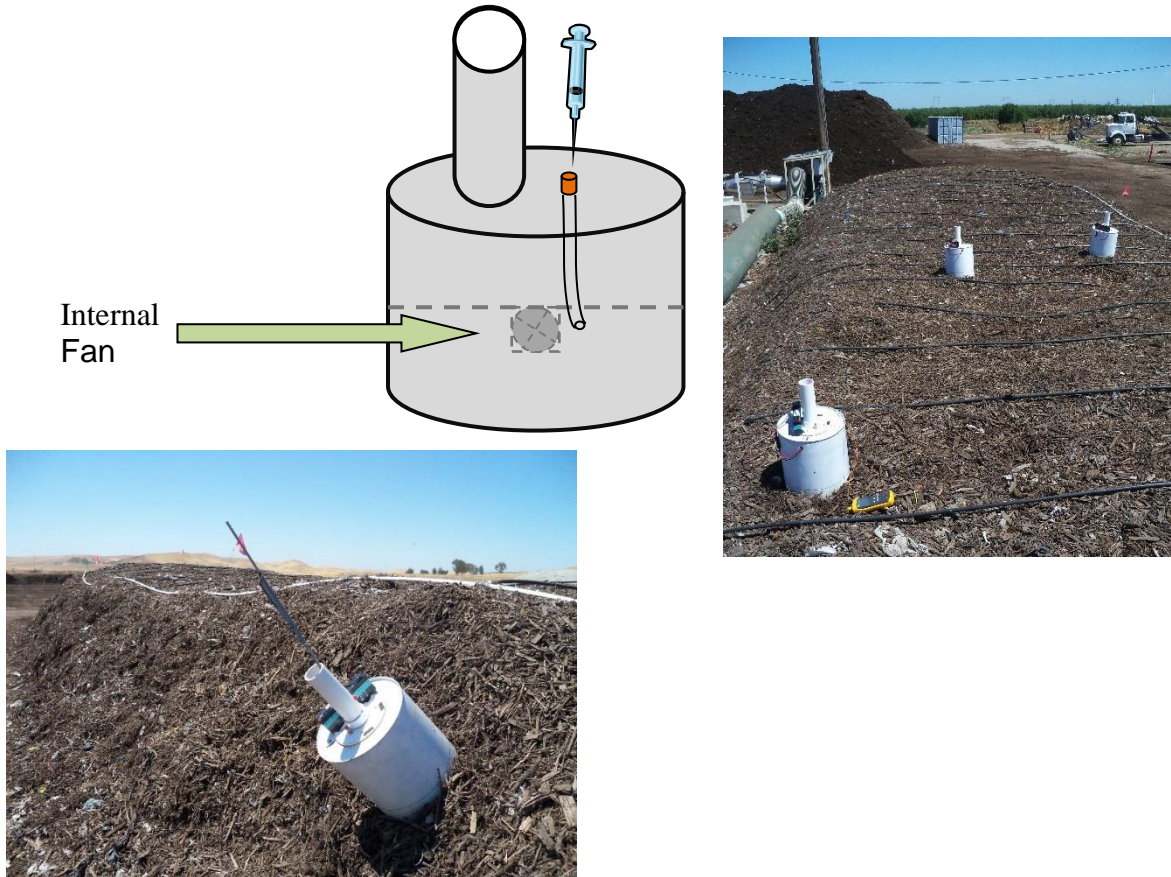
$$R = \frac{C_{1t} - C_{bet}}{C_{bet} - C_{et}} \quad [\text{EQ 4.11}]$$

In this study, CO₂ was used as the inert gas as it has been shown to encounter minimal filtration in biofilter media as seen in Martinec et al. (2001). Therefore a concentration for CO₂ in the pipe, biofilter and ambient air is easily used to calculate R. Carbon dioxide is not the ideal choice for the inert gas because CO₂ will be produced as a product of microbial respiration and oxidation of CH₄. If significant production within the biofilter is detectable, it will have an effect on the entrainment factor (R) calculation. The advantage to using CO₂ is that concentrations can be easily measured with the other gases of interest, CH₄ and N₂O, without the need to spike in a separate gas or send samples to a specialty lab for measurement. In the future argon, a truly inert gas, will be used. R from [EQ 4.11] is used to calculate the mass flow rate (F_{bi}) of GHGs in EQ 4.10 and used for both CH₄ and N₂O in EQ 4.10a and b.

Mass and Flow Balance Measurement Methodology

Open chambers were used in this study on top of the biofilter to obtain a concentration for the surface of the biofilter (C_{be_i}). These chambers were modified versions of the open flow chambers used for windrow gas measurements in Chapter 2. The chamber design is composed of a main, large cylindrical chamber with a small cylindrical chimney that is open to the atmosphere (Figure 4.4). The large chamber has a diameter of 28.5 cm and a height of 31.7 cm, and the chimney has a diameter of 5.25 cm and a height of 20.5 cm. Inside the large chamber there is a small fan for circulation.

Figure 4.4. Photographs of flux chamber on compost pile. Left: Representation of sampling from the chamber. Right: Photograph of chamber being used on the top of the biofilter. Bottom: Photograph of chamber being used on the side of the biofilter.



The sampling port is located on the main section of the chamber and contained a tube to the center of the chamber. The feeder pipe leading into the biofilter (diameter of 41.3 cm) contained a sampling port located in its side, from which concentration and velocity samples could be taken (v_1 and C_{1_i}), as shown in Figure 4.5.

Figure 4.5. Photograph of the pipes bringing the compost gases into the main feeder pipe and finally to the biofilter. The arrow points to the pipe segment with the sampling port used to measure the concentration and velocity of the gases feeding into the biofilter.



Mass and Flow Balance Experimental Sampling Design

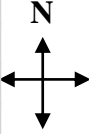
A three-week sampling plan was designed for biofilter testing three days a week for the period from 05/21/13 to 06/07/13. The biofilter, as described and pictured above, has a large surface area on the top as well as appreciable surface area exposed on the sides. Some testing was done with smoke candles to determine from which areas the exhaust air flow may be released. From the test we observed the south side of the compost pile

emitting more smoke than the north side. It was also apparent that the air may escape from the sides as well. From this information, a sampling design was created to sample three different sections: north (N) and south top (S) and the sides (Side), for a total of nine sampling locations.

A semi-randomized sampling plan was used to determine the location of the chambers so the biofilter could be better characterized over a larger area. The biofilter surface was delineated into a grid, based upon the 19 lines of the watering system, which were used to divide the sections in the east-west direction (Figure 4.2). In the north-south direction the biofilter was divided evenly into four sections on the top, marked by flags. The sides were divided in the east-west direction by visually extending the water lines, and the lines defined by the flags, to create sections. Side sampling occurred on the east side and the south side, as the north side was used for access to the top section, and the feeder pipe system entered the biofilter on the west side. Emission symmetry was assumed for the sides. The first two rows of the biofilter were not sampled, as advised by ECS personnel at the beginning of the experiment, because the feeder tube beneath the pile at that point was tied off and not functioning. Therefore, sampling was performed on the remaining 17 rows and the side sections of the biofilter, for a total of 89 sections. To allow for some repetition of sampling location over the three-week period, 27 locations were chosen for sampling, nine from each of the three sections (N, S, and Side). Figure 4.6 is a diagram of the layout.

Figure 4.6. Blueprint of the biofilter semi-randomized sampling locations (numbered 1 to 89). The first two rows were not sampled. Red represents the north, blue represents the south and brown represents the side areas. All purple locations were chamber sampling locations. Each of the three sections contains nine sampling locations.

1	1	19	37	55	73	
2	2	20	38	56	74	
3	3	21	39	57	75	
4	4	22	40	58	76	
5	5	23	41	59	77	
6	6	24	42	60	78	
7	7	25	43	61	79	
8	8	26	44	62	80	
9	9	27	45	63	81	
10	10	28	46	64	82	
11	11	29	47	65	83	
12	12	30	48	66	84	
13	13	31	49	67	85	
14	14	32	50	68	86	
15	15	33	51	69	87	
16	16	34	52	70	88	
17	17	35	53	71	89	
	18	36	54	72		



These nine locations from each section were further broken down so that three of these locations were sampled from each section for each day’s sampling event. For the first day of sampling during a week, the chamber locations were decided by a random selection. For the second day of the week, a random selection of the remaining chamber locations was sampled. The last sampling day of every week included the nine remaining chamber locations.

Chambers were placed on the three locations quasi-simultaneously in one section. When chambers were placed on the side positions, a small metal rod was inserted through the chamber into the biofilter to secure the chambers to the sloping surface. The fans were turned on, and a timer was set for 15 minutes to allow for equilibration of the exhaust air into the chambers. Samples were taken out of a small rubber septa located on the main chamber containing tubing that reached to the middle of the chamber near the fan. A 20 mL syringe was used to expel stagnant air from the sample tube of the chamber. A second 20 mL sample from the chamber was then injected into a previously evacuated Exetainer vial. Chamber temperature measurements were taken at the time of sampling, 36 cm (downward) from the top of the chimney with a Fluke 51II

Thermometer using a type K thermocouple. On the first sampling day, three samples were taken consecutively from each chamber to estimate the average sampling error. The relative standard deviation for samples taken from a chamber is 33 percent ($n = 3$). For the following days, only one sample per chamber was taken.

Measurements of the pipe center line air velocity and gas concentrations were taken three times a day: once before chambers were put on the biofilter, once midway through, and once after the biofilter sampling had ended (except for 5/21/13, when only two samples were taken). The pipe velocity was measured with a TSI Velocicalc Model 9555 hotwire anemometer in ft min^{-1} (later converted to $\text{m}^3 \text{min}^{-1}$ using the pipe area) at the midsection of the pipe, and on the last sampling day using a Test Products International model 575C1 hotwire anemometer. Velocity profiles were taken on 5/21/13 and 7/5/13 to allow calculation of the average velocity of the pipe. A correction factor was determined using the average of the calculated velocity determined from the velocity profile for each of the days. The following formula was used:

$$\frac{u_{avg}}{u_{amax}} = \int_0^1 (1-r')^{n_a} r' dr' + \frac{1}{u_{amax}} \left(\frac{m}{24} + \frac{b}{8} \right) + \frac{u_{bmax}}{u_{amax}} \int_0^1 (1-r')^{n_b} r' dr' \quad [\text{EQ 4.12}]$$

where u_{avg} is the radially (integral) averaged pipe air velocity, u_{amax} is the relative maximum pipe velocity measured at the center line of the pipe, r' is the radial position normalized to the radius of the pipe, n_a is a pipe velocity profile shape coefficient determined from two detailed velocity profiles taken in the distal (to the sampling port) half of the pipe (from the center line to the distal pipe wall), m and b are the linear slope and intercept obtained from the detailed velocity profiles for the velocity profile from the center line to the proximal $\frac{1}{2}$ radius, u_{amax} is the relative maximum velocity occurring approximately $\frac{1}{2}$ the radial distance on the proximal side of the pipe, and n_b is a pipe velocity profile shape coefficient determined from two detailed velocity profiles taken in the proximal (to the sampling port) quarter of the pipe (from $\frac{1}{2}$ the radius from the center line to the proximal wall to the distal pipe wall). This somewhat complicated formula was needed because the two detailed velocity profiles confirmed an unusual profile shape occurred in the feeder pipe, where velocity maximum occurred at approximately half the radius distance from the proximal wall, and then from the center line to the distal wall, making the profile look more like conventional turbulent pipe flow. This equation allowed taking only mid-section (center pipe) readings for each daily sampling event to obtain the average pipe flow velocity (see Appendix A.4.1.1. for additional information).

Gas samples were removed from the feeder pipe using a septa attached to stiff tubing through a rubber stopper that was inserted into the port. The tubing was located 17 cm into the pipe. Again the first 20 mL of gas was expelled before injecting the next 20 mL into a sample vial. Five gas samples were taken during each pipe sampling time point. Internal flow temperature was also taken 19 cm from the wall of the pipe with a Fluke 51II Thermometer using a type K thermocouple.

Five samples of ambient concentrations were taken at ground level while standing (approximately ½ meter to 1 meter height) on the north side of the biofilter during each experiment.

Gas Analysis

The Exetainer vials from the biofilter GHG testing were stored at a temperature range of 19°C to 25°C for three and a half weeks and then placed in a gas chromatograph (GC). This GC was fitted with an electron capture detector (ECD) for N₂O measurement, a thermal conductivity detector (TCD) for CO₂ measurement, and a flame ionization detector (FID) for CH₄ measurement (GC-2014, Shimadzu). Calibration gases (AirGas Inc., Sacramento) were run in tandem with the samples to act as standards with a known concentration. These standards were treated in the same manner as the samples, by injecting 20 mL of gas into an evacuated Exetainer vial. The GC gives an output of peak area for each standard and sample run on the instrument. Using the known concentration of the standard (independent variable) and the peak area of the result (dependent variable), we calibrated the machine using a known standard concentration and analyzed a total of 275 samples in this fashion over the experimental period.

Results

Greenhouse Gas Concentrations

As noted in the materials and methods section, GHG concentrations were measured at three main locations: the pipe leading into the biofilter, in chambers placed in nine locations on the biofilter, and an ambient concentration near the biofilter. Each of the nine chamber samples were divided into the north, south, and side areas to be analyzed separately to determine any bias for that area. Figure 4.7 shows the concentration values of CH₄ measured in this study from 5/21/13 to 6/7/13. In Figure 4.7a the values are broken down into the average of the north, south and side, along with the average pipe and ambient concentrations. In Figure 4.7b the north, south and side surface measurements are averaged for comparison with the average pipe and ambient concentrations, which remain the same. The highest pipe concentration is seen on the first day at $2.32 \times 10^{-4} \pm 0.23 \times 10^{-4}$ g CH₄ L⁻¹. However the surface concentration output of the biofilter on the first day is only slightly higher than the rest of the days with lower pipe concentrations. The total biofilter surface concentration average is $7.12 \times 10^{-6} \pm 1.0 \times 10^{-6}$ g CH₄ L⁻¹.

Figure 4.8 shows similar results to Figure 4.7 but for N₂O concentrations; all values were fairly consistent, as no day had a dramatically greater concentration in the pipe than in the chambers. The N₂O concentration in the pipe, which started at $7.59 \times 10^{-4} \pm 0.26 \times 10^{-4}$ mg N₂O L⁻¹ on 5/21/13, did climb in the last three sampling days to a high of $14.2 \times 10^{-4} \pm 0.38 \times 10^{-4}$ mg N₂O L⁻¹ on 6/7/13. The surface concentration of N₂O from the biofilter appears to be consistent regardless of concentration in the pipe. This biofilter does not have a much greater surface concentration than the ambient concentration of N₂O. The overall average of the biofilter surface concentration was $6.16 \times 10^{-4} \pm 0.28 \times 10^{-4}$ mg N₂O L⁻¹ and the average ambient concentration was $4.98 \times 10^{-4} \pm 0.15 \times 10^{-4}$ mg N₂O L⁻¹.

Figure 4.7. The average CH₄ concentrations in g L⁻¹ for the pipe, the biofilter surface concentrations of the north, south, side, and the ambient concentrations (a). The average CH₄ concentrations in g L⁻¹ for the pipe, the total daily average of the biofilter surface, and the ambient concentrations (b). Error bars represent standard error.

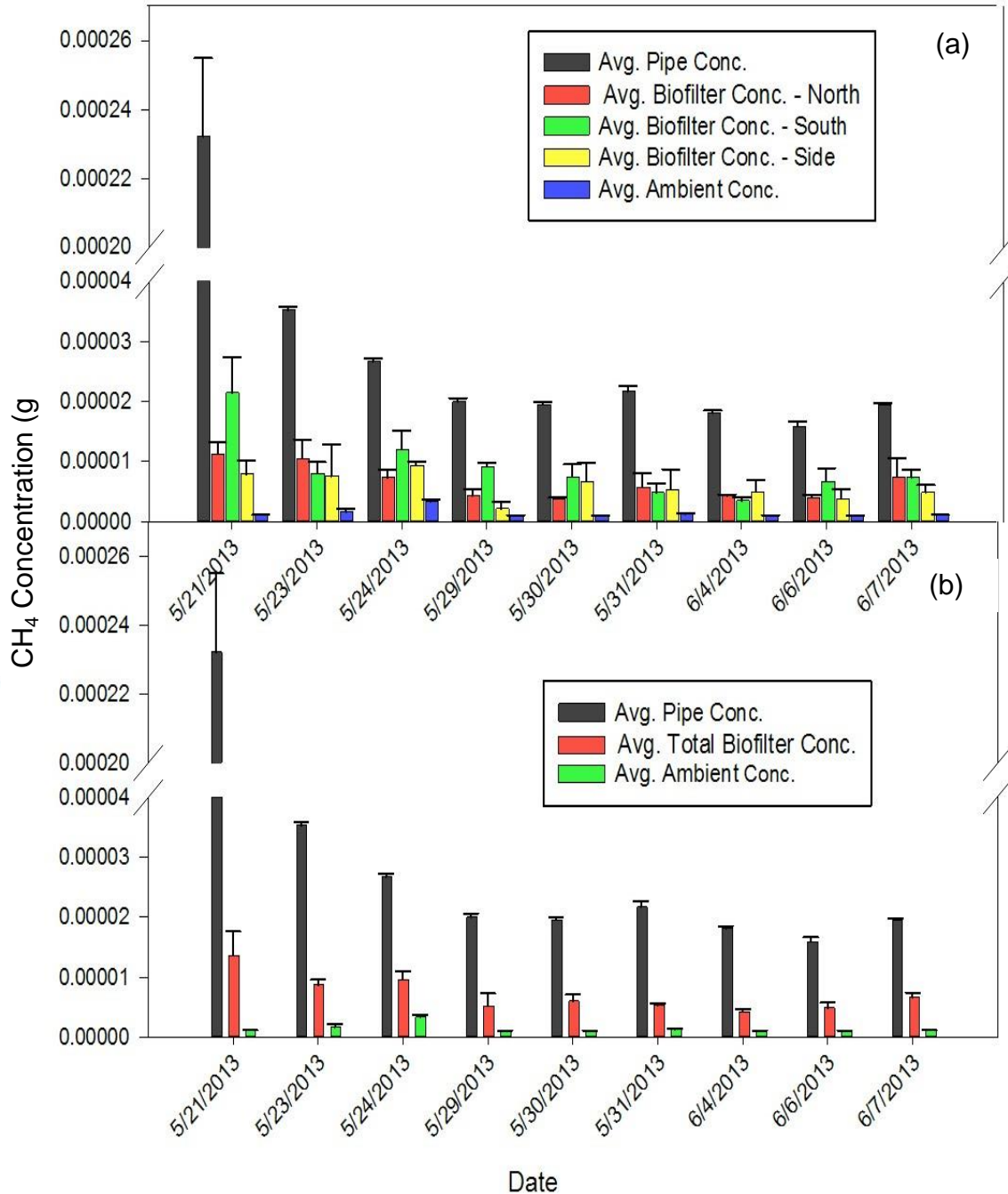
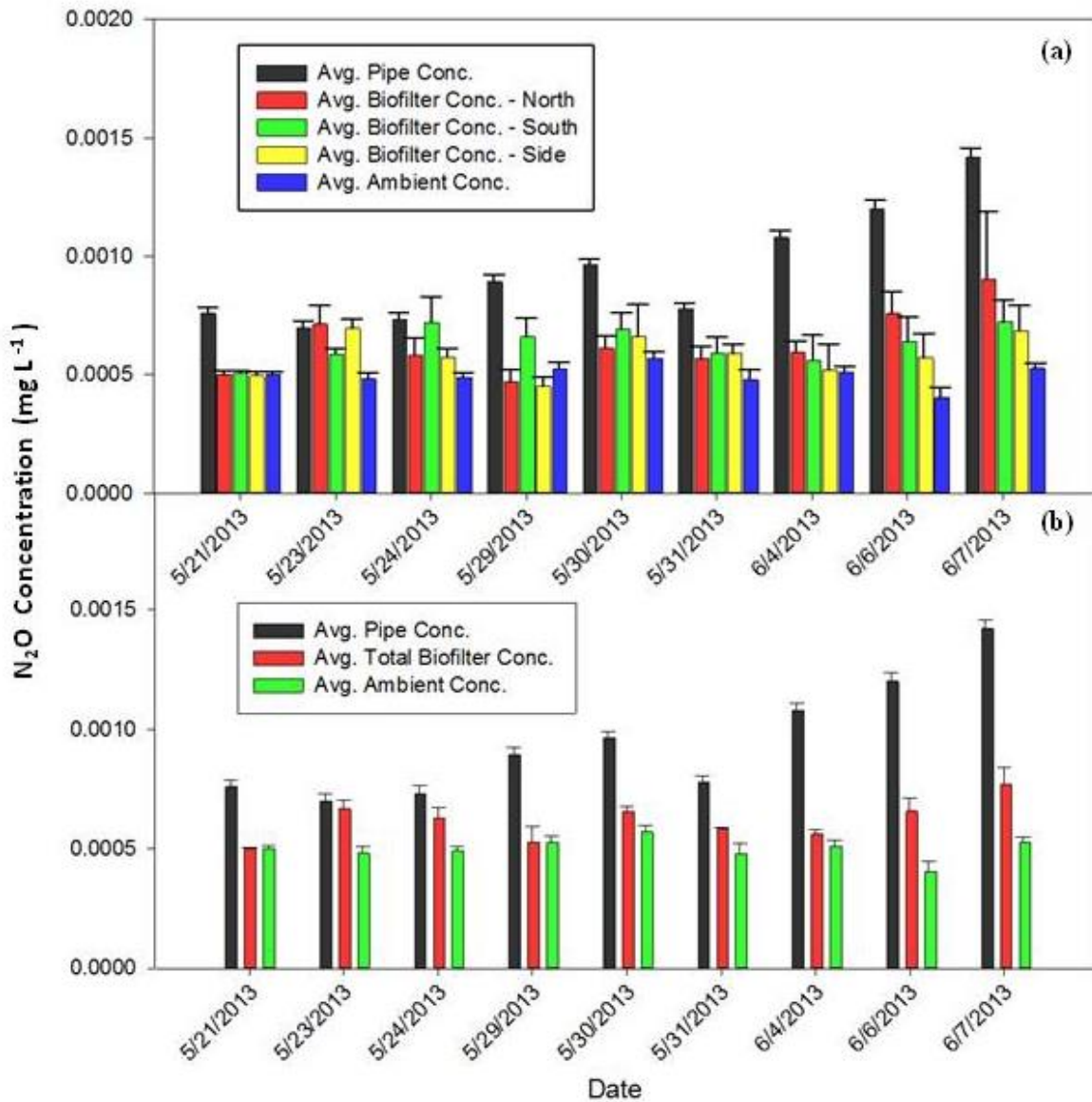
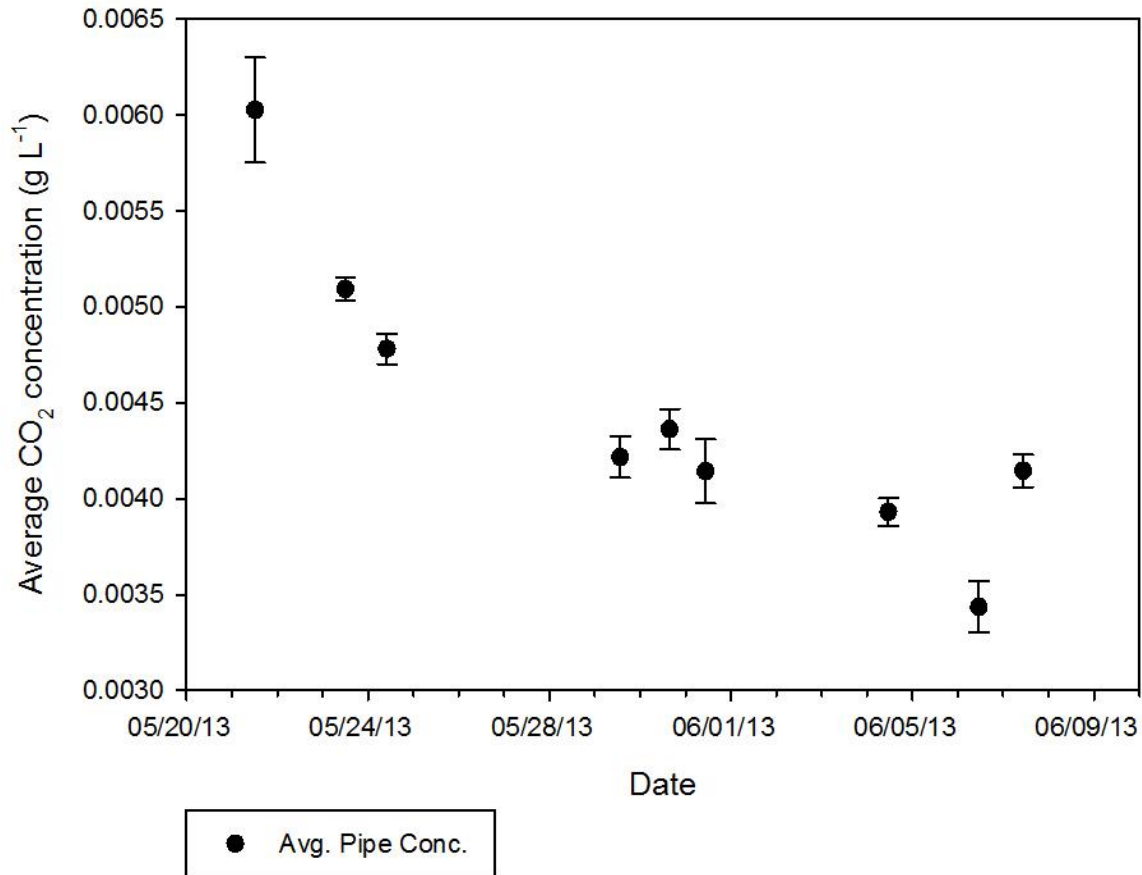


Figure 4.8. The average N_2O concentrations in $mg L^{-1}$ for the pipe, the biofilter surface concentrations of the north, south, side, and the ambient concentrations (a). The average N_2O concentrations in $mg L^{-1}$ for the pipe, the total daily average of the biofilter surface and the ambient concentration (b). Error bars represent standard error.



The daily average CO_2 concentration from the pipe is presented in Figure 4.9. This follows a similar trend to the CH_4 concentration shown in Figure 4.7.

Figure 4.9. The average CO₂ concentration (g L⁻¹) in the pipe vs. time. Error bars represent standard error.



CO₂ Calculated Entrainment Factor

Carbon dioxide was measured in every sample along with the CH₄ and N₂O, so the degree of air entrained into the biofilter could be estimated, as described in the materials and methods section. This daily entrainment factor was determined for the north, south, and side sections, using the average biofilter concentrations for each section and the average pipe and ambient concentrations. R was postulated to have some dependence on wind speed, with higher wind speeds linked to greater entrainment of air. Daily averages of R plotted against the daily averaged wind speed taken at the nearby Esparto California Irrigation Management Information System (CIMIS) site support the postulate with an R² value of 0.63 (Figure 4.10). The full table of R values is found in the Appendix Table A.4.8. Figure 4.11 displays R versus time delineated by location. The first sampling day had the highest average R value. Also, the sides of the biofilter tended to have the highest R values, but all positions averaged below five.

Figure 4.10. Averaged daily CO₂ calculated entrainment factor (R) vs. daily averaged wind speed in m s⁻¹ from the Esparto, California CIMIS site.

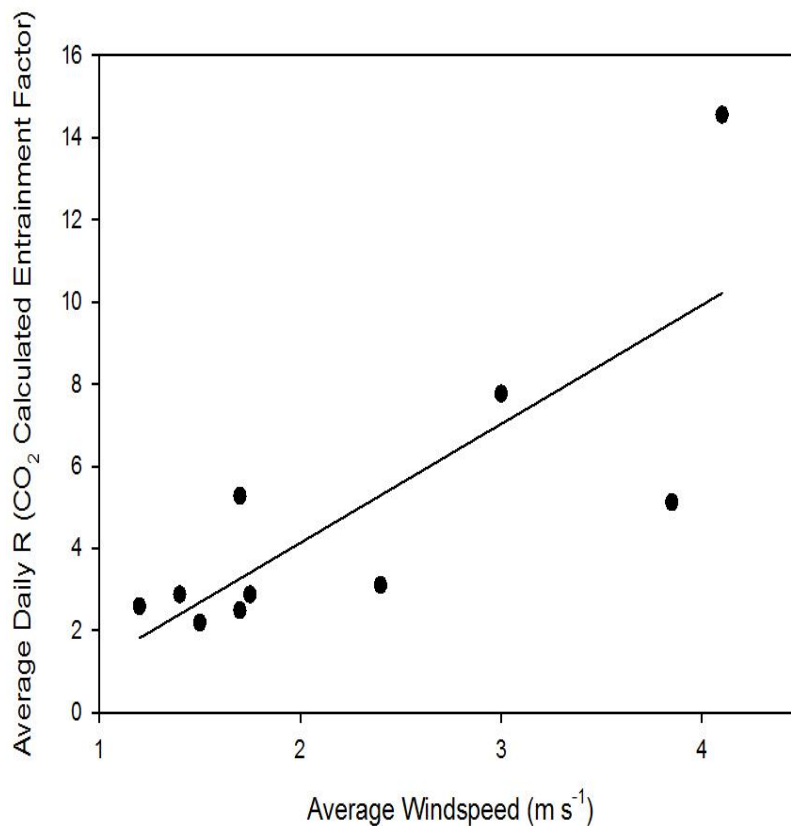
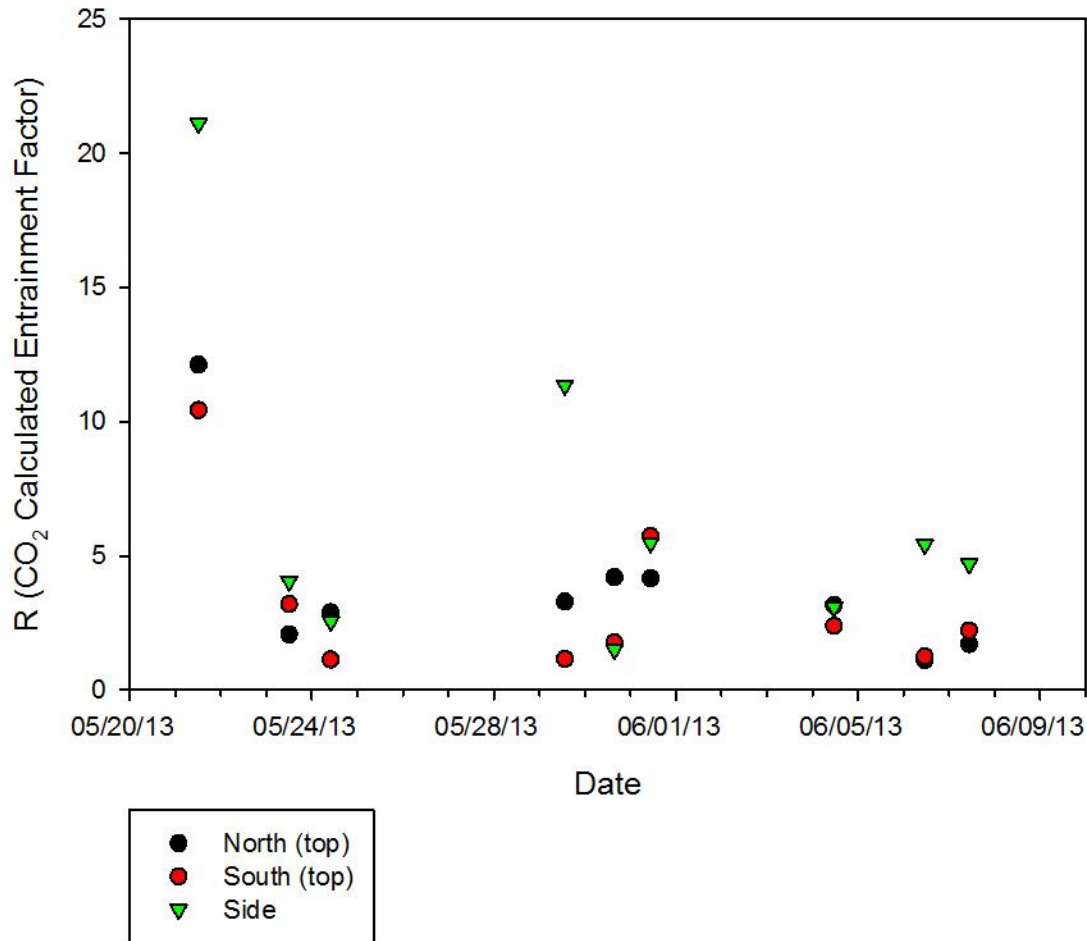


Figure 4.11. CO₂ calculated entrainment factor (R) vs. time, delineated by location (north, south, and side).



Removal Efficiency

The main purpose of a biofilter is to provide filtration of GHGs and VOCs in an inexpensive and efficient way. The filter efficiency, f_i , a ratio that describes how well the system is doing at filtering a certain substance, designated by subscript “ i ”, is calculated by EQ 4.9 and includes the effects of infiltration/entrainment. The higher the f_i ratio, the lower the filtration of the substance; a value of 1 indicates no filtration at all. Removal efficiency is defined as $(1 - f_i)$, with gas “ i ” explicitly identified for the removal efficiency term. To separate the removal efficiency (RE) calculated in this study, which contains an additional correction for entrainment, from other studies such as McNevin and Barford (2000), Huang et al. (2011) and Rene et al. (2005), RE calculated from $(1 - f_i$

(of EQ 4.9) will be referred to as RE_e (subscript “e” to represent entrainment). The RE calculated in previous studies using the concentration difference between the filter inlet and outlet, divided by the gas concentration at the inlet, will be referred to as RE_c (subscript “c” representing the concentration only). Figure 4.12 shows RE_e for both CH_4 (Figure 4.12a) and N_2O (Figure 4.12b) for each sampling day. The solid line is the average of all the sampling days with the standard error shown in the dotted lines. The average RE_e for CH_4 is 0.11 ± 0.04 and for N_2O is 0.50 ± 0.04 . On two occasions the calculated RE_e is less than one for CH_4 , 5/31/13 and 6/7/13. Table 4.1 shows the average RE_e from $(1 - f_i)$ (of EQ 4.9) and the average RE_c that can be calculated from the measured concentrations of GHG in this study. These methods provide significantly different results.

Figure 4.12. Removal efficiency (RE_e) of CH_4 vs. date of sampling. (a) Removal efficiency (RE_e) of N_2O vs. date of sampling. (b) Solid line represents the average of all days, and dotted lines represent the standard error of that average.

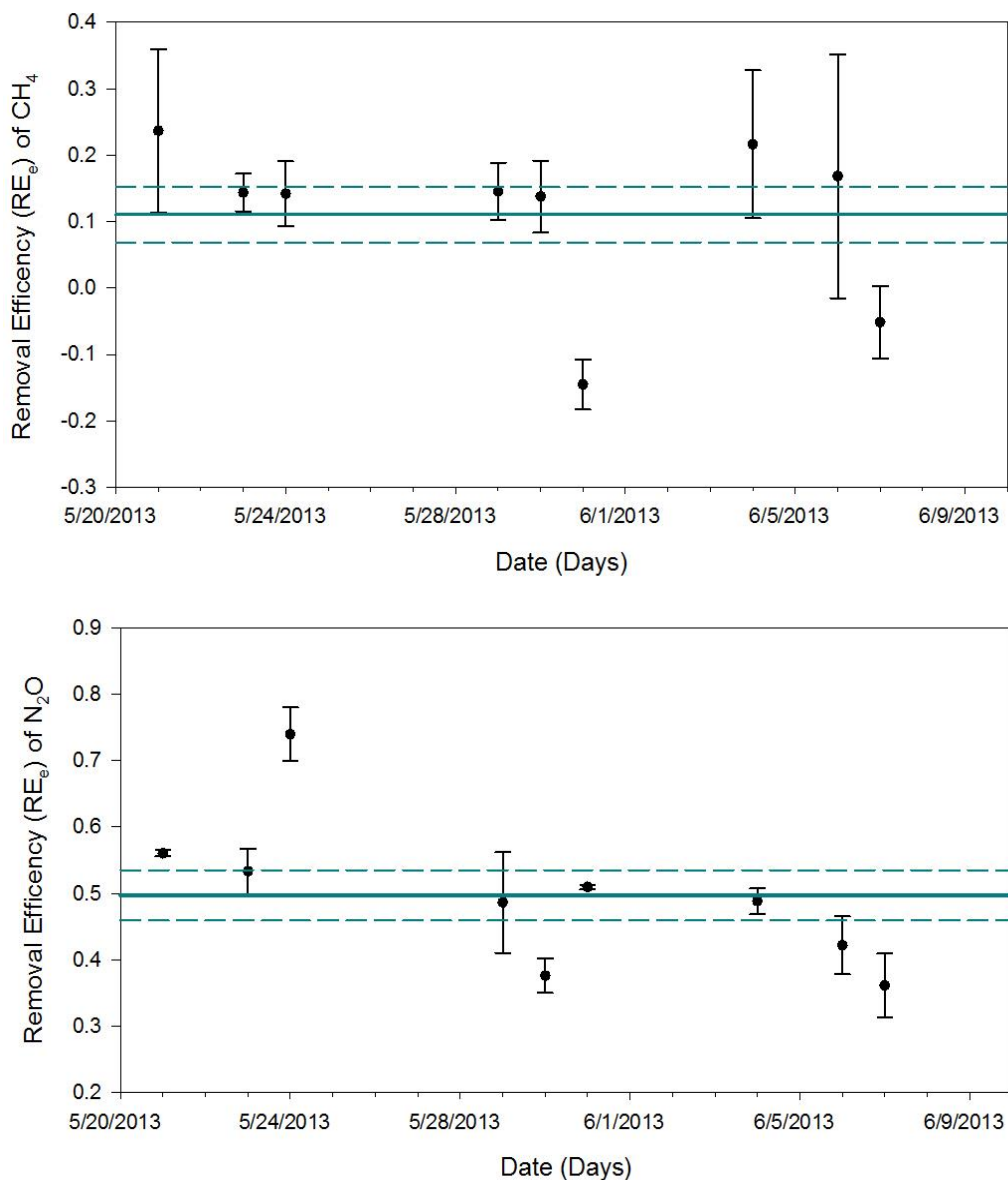


Table 4.1: Calculated grams removal efficiency, expressed as a fraction. RE_c is based on the concentration changes alone, RE_e is the new method of analysis used in this study to include a correction for entrainment.

	Average RE_c	Average RE_e
CH_4 Removal Efficiency	0.73 ± 0.03	0.11 ± 0.04
N_2O Removal Efficiency	0.32 ± 0.05	0.50 ± 0.04

Greenhouse Gas Emissions

Greenhouse gas emissions (mass flow rates) from the biofilter originating from the compost pile can be calculated with EQ 4.10 inputting the measured pipe air velocity into the biofilter, the GHG concentration in the pipe, the GHG biofilter surface concentrations gathered during the sampling, and the entrainment factor (R). EQs 4.10a and 4.10b give explicit formulas for CH₄ and N₂O respectively, for emissions coming from the compost pile filtered through the biofilter. All GHG emissions in the following section include only emissions from the biofilter that are coming from the compost pile and omit emissions contributed by entrainment. The average velocities in the pipe are given in the Appendix Table A.4.7 along with the value calculated from EQ 4.12, expressed as a volumetric flow rate in m³ min⁻¹. Figure 4.13 displays the calculated daily emissions of CH₄ (top) and N₂O (bottom) from the biofilter. Again, the solid line represents the average of all the daily emissions with dotted lines indicating the standard error. The trends in the emissions mirror the concentrations of the pipe shown in Figures 4.7 and 4.8. The highest CH₄ emission of 5611 ± 906 g CH₄ day⁻¹ is on 5/21/13, the first sampling day, but is consistent for the rest of the days, leading to an average of 1400 ± 540 g CH₄ day⁻¹. The N₂O emissions are fairly consistent but do increase toward the end with the highest value being 36.4 ± 2.7 g N₂O day⁻¹ on 6/7/13 and the average coming out to be 19.8 ± 2.8 g N₂O day⁻¹.

Figure 4.13. Daily emissions of CH₄ from the biofilter vs. date of sampling. (a) Daily emissions of N₂O from the biofilter vs. date of sampling. (b) All emissions are from contributions only made from the compost pile and omit contributions from the entrainment. The solid line represents the average of all days, and dotted lines represent the standard error of that average.

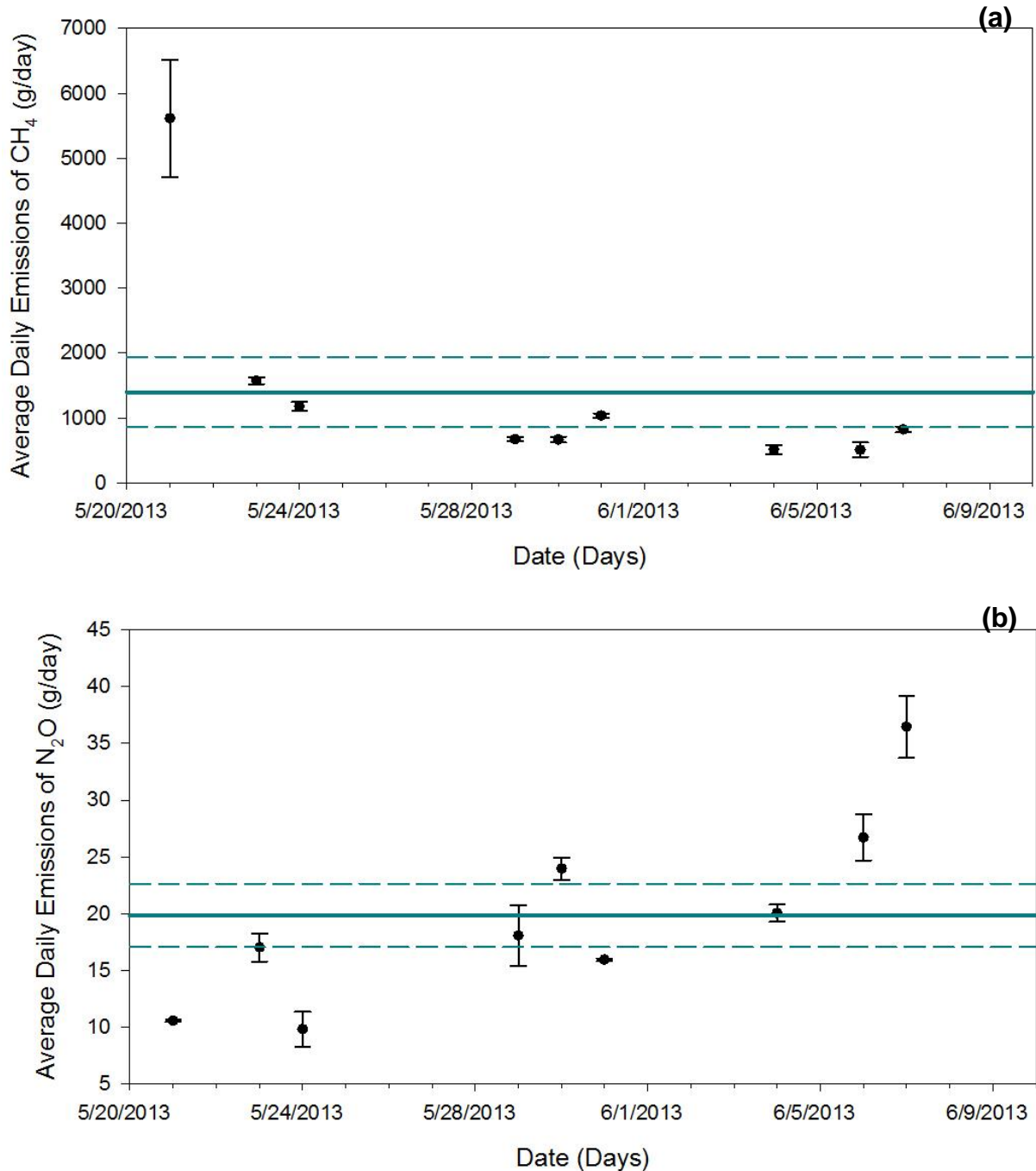


Table 4.2 contains the carbon dioxide equivalents (CO₂-eq) of the biofilter emissions using the GWPs from Fourth IPCC assessment report (AR4) (Solomon et al., 2007) and the approximate mass for the source compost.

Table 4.2: Calculated grams CO₂ equivalents day⁻¹ DW tons⁻¹ for the ASP using the AR4 GWPs equaling 25 for CH₄ and 298 for N₂O.

	Compost GHG emissions from the feeder pipe	Emissions from biofilter bed (omitting entrainment contributions)
g CO ₂ -eq day ⁻¹ DW tons ⁻¹ for CH ₄	335 ± 144	280 ± 108
g CO ₂ -eq day ⁻¹ DW tons ⁻¹ for N ₂ O	91.9 ± 7.2	47.3 ± 6.6
Total g CO ₂ -eq day ⁻¹ DW tons ⁻¹	427 ± 145	327 ± 108

Discussion

This study was to determine the GHG emissions from a biofilter being used to mitigate CH₄ and N₂O emissions from composting in an ASP. The biofilter has other benefits such as odor and VOC reductions that were not measured here. The concentrations of CH₄ and N₂O at the biofilter surface, inside the feeder pipe, and the ambient concentrations are shown in Figures 4.7 and 4.8. Any decrease in GHG concentrations from the feeder pipe to the surface of the biofilter can be attributed to either reduction by the biofilter or entrainment. It is apparent the biofilter significantly reduces CH₄ emissions (Figure 4.7b). Nitrous oxide is also reduced but not as dramatically due to its lower input concentration (Figure 4.8b). When entrainment is high, a decrease in GHG emissions may not be indicative of a biofilter with high removal efficiency. A high entrainment would dilute biofilter output, making it look like a higher efficiency.

For comparison with previous studies, RE_c can be calculated using the daily average surface GHG concentration in this study's biofilter, and the daily average GHG concentrations in the feeder pipe, although this RE_c can be expected to have large errors due to possible entrainment from ambient air into the filter. RE_e calculated from (1 - f_i) (from EQ 4.9) will be different than the RE_c calculated directly from the concentrations; the results from RE_e are discussed later. The biofilter in the current study, excluding any entrainment factor has a RE_c of 0.73 ± 0.03 for CH₄ and 0.32 ± 0.05 for N₂O (Table 4.1). Chen and Hoff (2009) summarize many studies, mostly containing VOC or odor related REs, however one reference by Martinec et al. (2001) reports RE_c for CH₄ in two different studies range from 0.102 to 0.248 and -0.021 to 0.099. Martinec et al. (2001) also reports N₂O RE_c for two studies to range from -0.85 to 0.10 and -0.29 to -0.16. The ranges for each of the two studies included a variety of different biofilter media. The findings from Martinec et al. (2001) for RE_c's do not compare well with this study when using the concentration-based calculation of removal

efficiency (RE_c). This discrepancy is expected if entrainment is occurring. Their study also included many negative values indicating the biofilter was not reducing the concentration of these gases but contributing to or producing more of the gases.

In a review by Nikiema et al. (2007) RE_c was found to be as high as 0.9 for CH_4 in some studies. Another report in Chen and Hoff (2009) shows CH_4 had a RE_c up to 0.85, closer to the RE_c calculated for this study (Table 4.2). Biofilter media and source material used in this study may have been different than those used in these and other comparison studies. Also, most of the other studies in the literature pertained to closed biofilters that are walled-off on all the sides, so entrainment would not be significant.

This study did not focus on measuring the compost source emissions from the pile but rather on the emissions from the biofilter bed and how they differ from the input given from the feeder pipe. Thus, the possibility of GHG flux from the covered ASP pile was not considered. However, in order to compare emissions from the biofilter to emissions from windrows, biological activity should be compared as well. In order to approximate the biological activity CO_2 concentration is plotted against time for the biofilter study (Figure 4.9). The concentration started at 0.0060 g L^{-1} and then decreased slightly over time. Carbon dioxide is an indicator of microbial respiration. This could mean that biological activity decreased over time but did not become completely inactive. One reason for this decrease could be due to a decrease in moisture in the source compost pile. Decreasing pile moisture would reduce microbial activity. The cover of the compost is impermeable to water and designed to keep in moisture; however, there were no additional watering periods during the study. Also, higher levels of aeration, like that of an ASP, can lead to lower moisture content due to drying (VanderGheynst et al., 1998).

Despite this possible slight decrease in activity over time from the source material of the biofilter, overall activity of the biofilter may still compare to that of the windrow. Concentrations of GHGs are approximately the same order of magnitude across the windrow and ASP studies, however this is a rough comparison due to the different methods used to take these measurements and different techniques of composting (windrow vs. ASP). Standard deviations are high because of the variability in the GHG concentrations, especially over the long time periods measured in Chapter 2. These similar GHG concentration averages do not necessarily indicate that emissions of windrows and ASPs will be similar, but it does help indicate that comparable biological activity is taking place in the ASP.

The entrainment factor (R) for the biofilter in the current study was calculated using the change in CO_2 concentrations from the source pipe to concentrations exiting the biofilter bed. Figure 4.10 suggests a linear relationship between the R factor and wind speed, with higher wind speeds correlating with higher R values. This is logical because the entrainment assumed in this study is ambient air infiltrating the biofilter, causing a dilution, so higher wind speed would contribute to higher flow through the biofilter. The porous media is necessary for biofiltration (Chen and Hoff, 2009) but can lead to exposure from other sources when the biofilter media is not walled off. The change in R over time is displayed in Figure 4.11. Day 1 (5/21/2013) has the highest R values and

subsequently begins to decrease and stabilize. This difference in R indicates higher entrainment on that day. Another possibility could be a difference in CO₂ for reasons other than entrainment, such as CO₂ evolution from biological activity. An increase of CO₂ concentration in the gas emitted from the biofilter would increase C_b, and according to EQ 4.11, this would likely cause a decrease in R. Therefore there is a possibility that the decrease in R from day 1 may be due to an increase in CO₂ respiration. The side tends to have a higher R when compared to the top of the biofilter bed. This indicates that more entrainment is occurring on these sides than compared to the top, which can be expected due to horizontal wind. Other reasons for this occurrence could be uneven distribution of air flow, or as mentioned before, a difference in CO₂ from microbial production. To explain this increase in R on the sides there would have to be a lower level of CO₂ production on the sides than on the top of the biofilter media. Possible errors in the calculation of R are discussed below.

Filter efficiency is calculated using EQ 4.9, then converted to removal efficiency (RE_e) by $1 - f_i$. Figure 4.12 displays the RE_e of CH₄ and N₂O. Methane has lower RE_e values than N₂O. At times a negative RE_e is observed, indicating the production of CH₄ within the biofilter. Anaerobic pockets could be formed when channeling of flow occurs. Channeling can increase when the biofilter bed becomes too dry (Chen and Hoff, 2009). The average RE_e for CH₄ is 0.11 ± 0.04 and for N₂O is 0.50 ± 0.04 . It is apparent R significantly impacts the interpretation of the efficiency of the biofilter, because the RE_e containing the entrainment correction differs greatly from the RE_c based only on the concentration measurements (Table 4.1). The RE_e for CH₄ removal (RE_e = 0.11) is consistent with the values of RE_c reported by Martinec et al. (2001) (RE_c ranges from -0.021 to 0.248); but for N₂O, the RE_e from this study (RE_e = 0.50) differs from the corresponding literature RE_c values reported by Martinec et al. (2001) (RE_c ranges from -0.85 to 0.10).

Many possible errors may be involved in the R factor. It was assumed that CO₂ would not be filtered and therefore $f_t (f_{CO_2})$ s equal to 1. CO₂ may actually be produced within a biofilter due to methanogens oxidizing CH₄ (Huang et al., 2011) and microbial respiration. Therefore $f_t (f_{CO_2})$ would be greater than one and affect the calculation of R. However it has been reported by Martinec et al. (2001) that CO₂ had an RE of -0.01 to 0.0 and -0.006 to 0.007 in two different studies, translating to $f_t (f_{CO_2})$ values of 0.99 to 1.0 and 1.006 to 0.993, consistent with our assumption of an f of 1.0. Martinec et al. (2001) included ten different types of biofilters (five in each study) using a variety of material including biochips, coconut fiber, fiber peat, compost and mixed bark and chopped wood. In one set of studies all the biofilters were an up-flow air-supply biofilter and in the second study up- and down-flow air supply was used. Therefore, CO₂ filtration or production is not a likely source of error. Using argon in a future study to compare with the results obtained from the CO₂ would be a way to check the results from this study. Argon is advantageous because it is known to be inert. The disadvantages are the cost of argon gas, cost of measurement, and additional sample preparation that would prevent use of argon for every sampling day.

It was also assumed entrainment was the only reason for reduction in CO₂, and, therefore, all other GHGs. Other possibilities included a leak in the system prior to the biofilter, non-uniform distribution of flow from the feeder pipe to the biofilter, or wind interference in surface measurements by the open chambers. Leaks in the system were addressed by the smoke test performed prior to the study. Found leaks were corrected prior to sampling, but any leaks formed after the smoke test could affect the system. The smoke test did indicate non-uniform distribution of smoke, and therefore the assumption of uniform mass flow balance may be the largest source of error. This test was performed on the previous biofilter media as well as the freshly constructed media used in this study. The concentrations were sampled in three separate areas to minimize the effects of non-uniform distribution. In the end, the average concentrations from the three areas were not significantly different (Figures 4.7 and 4.8). However the R factors using CO₂ concentration did vary for the different areas (Figure 4.11, and Appendix Table A.4.8). Interference from ambient air for the surface chamber concentration measurements of the biofilter could have great effect as well. The surface concentration could be lowered by ambient air infiltrating into the chamber, to cause an artificially low measurement of GHGs. This is different from entrainment into the biofilter because the dilution of the concentration would not be from the addition of flow into the biofilter. The sampling of chambers was variable based on the relative standard deviation of 33 percent noted in the materials and methods; however, this could be due to the chamber or from ebbs in flow of the emissions from the biofilter unrelated to chamber design. A new chamber design might be required to measure the concentration at the surface of the biofilter to determine if a steady reading can be made. This chamber would still have to be open to the outside to prevent concentration build up.

Emissions from the biofilter originating from the compost source are displayed in Figure 4.13. Assuming mass and flow conservation, the emissions from the biofilter is the filter efficiency (f_i) of the particular gas multiplied by the mass flow rate in the feeder pipe of the same gas EQ 4.10. The same errors as discussed above are involved with the mass flow rate calculation because of the reliance on the filter efficiency. Values were relatively constant for CH₄, except for the first day, which had higher emissions due to the higher concentrations of CH₄ coming from the feeder pipe that day. The average emissions for CH₄ were 1400 ± 540 g CH₄ day⁻¹. The average N₂O emissions were 19.8 ± 2.8 g N₂O day⁻¹. The literature does not normally present mass flow rates from biofilters used to mitigate compost pile emissions, and therefore there are not any overall values to compare to. Also, the emissions output would depend on the source compost material producing the gases in addition to the biofilter efficiency. Many biofilters are used for animal and landfill waste, which is why the literature focuses on the removal efficiency of these types of filters.

This study's biofilter emissions originating from the compost source can be compared to the windrow emissions from Chapter 2 where CH₄ emissions ranged from 38.6 to 340 g CH₄ day⁻¹ ton DW⁻¹ and 277 to 1,189 mg N₂O day⁻¹ ton DW⁻¹. The emissions from this biofilter study in units per ton of dry weight compost can be calculated using the

approximate mass and moisture of the source compost. Due to these approximations, these values will have additional error associated with them. Biofilter emissions are 11.2 ± 4.3 g CH₄ day⁻¹ ton DW⁻¹ and 159 ± 22 mg N₂O day⁻¹ ton DW⁻¹. These windrows were monitored over a period of six to nine weeks, only in the early stages of composting. To improve the research of the biofilter, both the emissions and biofilter efficiency should be monitored over a longer period, and compare adding new source piles into the system. There could be a change in efficiency with a higher GHG load on the biofilter, and, of course, emissions would be expected to increase with greater amounts of source material.

Carbon dioxide equivalents for the emissions from the ASP are presented in Table 4.2. The emissions for the feeder pipe are given to compare the reduction in emissions that occurred for both CH₄ and N₂O from filtration by directing exhaust gas to the biofilter media bed. Table 4.2 can be compared with Table 2.2 for the windrow experiments in Chapter 2. The difference between the grams of CO₂ equivalents day⁻¹ ton DW⁻¹ from a windrow to that of this ASP is significant. The range of total CO₂ equivalents for the windrow experiments are 1,210 to 8,587 g CO₂-eq day⁻¹ DW tons⁻¹ compared to the 427 ± 145 g CO₂-eq day⁻¹ DW tons⁻¹ from the pipe, even before entrainment or filtration. This difference in emissions from the ASP could be attributed to a variety of differences between the two composting methods. Aeration, porosity, moisture, oxygen availability, feedstock, and temperature could be some of the many factors affecting emissions. The shorter monitoring period may also influence these results. A pile of a larger mass compared to that of the windrows, with less frequent turning could potentially take a longer time to compost and therefore should be monitored over a longer time period. This would also determine if emissions from the ASP will change over time, as is observed with windrow composting.

It is important to note many variables affect the efficiency of the biofilter. The three most important to performance are the packing media, media moisture content, and EBRT (Chen and Hoff, 2009). Compost and wood chips are one of the most common types of media because they make a porous bed and do not usually require additional nutrients or inoculation (Chen and Hoff, 2009). In this study, moisture and EBRT were not monitored. Even though the biofilter was fitted with irrigation, media moisture likely decreased throughout the sampling because no additional water was added after the initial activation of the microbes. Ideal moisture content is between 40 and 60 percent. When the biofilter media becomes too dry, microbes may become deactivated and increased medium cracking can reduce EBRT, leading to channeling and decreased absorption capacity (Chen and Hoff, 2009). For CH₄ reduction, 25 to 50 percent moisture in the compost residual is ideal. The need for less water is due to methane's low water solubility that can restrict delivery to methanotrophs (Huang et al., 2011). Compaction of material, which leads to a decrease in porosity and oxygen, can often be a problem for biofilters. However, the material for the biofilter bed in this study was constructed within a month of sampling and should not be an issue.

Conclusions

The biofilter used in this study is specific for compost applications and is different from many seen in previous studies due to the lack of retaining walls on the sides, which may potentially allow greater entrainment of ambient air. Though biofilters are used routinely to reduce the emission of VOCs from composting sites, little information exists on their efficacy to reduce composting GHG emissions at the same time. This preliminary biofilter study relied on a new method for deriving GHG emissions and for determining the efficiency of the biofilter. It was difficult to compare our results with values from the literature for multiple reasons.

1. There are many types of media used for biofilters, and each type affects the efficiency.
2. Most studies are more interested in VOC reduction and do not focus on GHG reduction.
3. Biofilters mentioned in the literature contain media that does not have the possibility for entrainment as hypothesized in our system.

In this study, the biofilter reduced CH₄ and N₂O emissions from the compost pile by 11 and 50 percent respectively when adjusted for entrainment. The estimate for biofilter efficacy without the novel entrainment calculation is 73 percent for CH₄ and 32 percent for N₂O. For studies where there are CH₄ and N₂O data, our comparisons show mixed results. This could be due to any of the reasons listed above as well as issues with the techniques or theory of the mass and flow balance method used in this study. Of particular importance is that the media used in this study is intended to mitigate VOC emissions and was not intended to address GHGs. Also, it was not known if the actual residence time of air in the biofilter matched the system manufacturer's specifications.

More validation tests are needed on this method to determine if the assumptions made in the calculations are reasonable with the media used. The entrainment factor is an important aspect of the theory and can be tested in a few ways. One could be to contain the biofilter media by blocking off possible entrainment and testing the system again. Using argon as the inert gas in combination with physically blocking the entrainment pathways could help to verify if CO₂ was a viable choice for calculating the entrainment factor. We did use argon gas, but the results were uninterpretable, likely because of the uncontrollable entrainment in the current system design. Chamber design could be improved to obtain a better surface concentration measurement from the biofilter. The media used in this study was not suitable to use the chamber approach effectively due to the coarseness of the media material. To be effective, the chambers would have had to be inserted to a greater depth. However, in this current biofilter design, this would have introduced unacceptable disturbance to the biofilter, possibly affecting its performance. A longer and more intensive study would be necessary to do a fully comprehensive test of the use of biofiltration on compost. In this study, the goal was to use existing methodology to assess biofilter performance on GHG emission reduction. It was not the intent of this study to assess or modify the current biofilter design.

Characterizing different biofilter media (size of wood chips, mixing of different size wood chips, including some finished compost to reduce large pore spaces in the media) would greatly help to compare values in the literature, such as EBRT, moisture, temperature, pressure drop, pH, and porosity. Also, characterization of the input compost source material with data such as moisture content, ammonia, nitrate, DOC, total carbon, and total nitrogen would provide additional information to analyze relationships to the potential amount of emissions from the biofilter. Our final recommendation is to conduct a study to assess a biofilter design that is intended to mitigate the emissions of both VOCs and GHGs.

Chapter 5. Monitoring N₂O Emissions Following Yard Trimmings Compost Amendment in Tomato Fields and Almond Orchards

Introduction

In this part of the study, we examined the effects of yard trimmings compost as a soil amendment on N₂O emissions. Agricultural soils are estimated to account for 68 percent of total N₂O emissions nationally, and in California N₂O may contribute as much as 50 percent to the total net agricultural GHG emissions (California Energy Commission, 2005). With the passage of the Global Climate Change Solution Act (AB 32), quantifying N₂O emission is essential to determine the magnitude of the impact of California agriculture on GHG emissions.

Denitrification is often considered to be the main source of N₂O emitted from agricultural soils, as emissions derived from fertilizer N application tend to increase with increasing soil water content (Abbasi and Adams, 2000; Bateman and Baggs, 2005). Ammonia oxidation-derived N₂O, measured in the laboratory, also has been observed to increase with increasing soil moisture (Bremner and Blackmer, 1979). These divergent processes have made it difficult to predict N₂O emissions based on soil properties and agricultural management practices.

The effect of yard trimmings compost on GHG emissions from soils ranges from decreasing N₂O emissions (Dalal et al., 2009) to increasing emissions (Mondini et al., 2007). When organic amendments such as compost reduce N₂O emissions (Dalal et al., 2010), it is most likely due to a reduction in mineral N through microbial immobilization and growth (Wright et al., 2008). In contrast, increases in N₂O emissions after compost application (Mondini et al., 2007) can occur due to increases in available soil N and DOC (Wright et al., 2008), which could stimulate microbial activity and lead to increased oxygen consumption resulting in N₂O production via denitrification and nitrifier denitrification (Zhu et al., 2013). In addition, compost application to soils may maintain optimal soil moisture conditions longer, which could favor denitrification. In contrast, improving soil moisture status often maintains lower soil temperatures, prolonging N₂O solubility, leading to greater reduction to dinitrogen (N₂) from denitrification and nitrifier denitrification. However, there is a dearth of information to test these hypotheses or generalize the effects of compost application to soils.

The effect of field compost applications on N₂O emissions was monitored at four locations as applied to two specialty crops, tomato and almond. Growers often only apply compost on high-value crops. In lower-value row crops such corn or forages, the added expense of the compost amendment and additional costs of application and management make it an infeasible agronomic approach. Growers who apply yard

trimmings compost remark that good-quality compost has soil-improving properties that include nutrient addition and increases in water-holding capacity. Farmers may view this as an increase in irrigation efficiency (Horwath, personal communication). The nutrient source is mainly for all nutrients, but yard trimmings compost is not an especially good source of N (Churchill et al., 1995). However, improvement in soil properties may improve nutrient uptake by providing better soil water status and soil physical conditions. Better soil water status is reflected in maintaining soil moisture through increased infiltration, water-holding capacity, and extended duration of favorable soil moisture status. In essence, improving soil properties through compost addition likely increases the capacity to take up fertilizer and soil nutrients, and increase the resilience of a crop. The increased resilience of crops and crop rotation was observed in previous studies at UC Davis where composted poultry manure and bedding was applied (Poudel et al., 2001; Poudel et al., 2002; Krammer et al., 2002). The compost treatments in these studies provided crop and cropping system resilience under water and temperature stress (excessive rainfall during the growing season and in years with periods of prolonged high temperatures). In the future, as climate becomes more variable due to climate change, managing soil properties with organic amendments such as yard trimmings compost could be a good strategy for growers to increase crop resilience to stress.

The objective of this subtask was to evaluate the effect of compost on N₂O emissions in tomato row crop rotations and almond orchards. We also intended to determine whether compost affects the ability of soils to oxidize atmospheric CH₄. Soils are the largest sinks for CH₄ through the ability of the microbial community to oxidize it (Horwath, 2007). No change in CH₄ oxidation potential was observed in preliminary observations in both the lab and field components of this study; therefore, no further monitoring was done and no results are reported. An additional intent was to determine N₂O emission factors for compost-amended soils compared to soils to which no compost was applied. However, no emission factors could be calculated because yard trimmings compost had no significant effect on N₂O emissions under standard fertilization practices (see Results and Discussion section). Therefore the use of compost as a soil amendment may not mitigate N₂O emissions, but a more beneficial use of yard trimmings compost is to improve soil properties, such as promoting favorable soil water status, and possibly increasing crop resilience to climate change.

Methods and Materials

Field investigations to monitor emissions of N₂O from applications of compost were done at four locations. On-site characterization of soil parameters was conducted prior to final selection of monitoring sites. Critical variables that were determined included soil C and N content, soil texture, bulk density, and pH. The areas selected reflect typical soil conditions and agronomic management for the crops examined. Soil texture influences N₂O emissions mainly through its effects in controlling the duration of water-filled pore space after soil-wetting events. Overall, the site selection process was based on a variety of information, such as management practices, site management histories, and soil characteristics.

A site located at Russell Ranch Sustainable Agricultural Facility (RRSAF) at UC Davis was chosen to represent a tomato-based row-crop rotation. The UC Davis site represents a 20-year study comparing conventional, cover cropping, and organic agricultural systems. The long-term study is designed to elucidate the linkage of soil C content, irrigation practices, and other factors (soil moisture, temperature, soil nitrate content, etc.) on soil sustainability. The plots at the RRSAF were complemented with additional sites on farm to reflect more applied agronomic management. Two farmer fields, one in Esparto and one in Woodland, were selected to represent California tomato growers. An almond orchard located on the Leslie J. Nickels Soil Laboratory (NSL) in Arbuckle, Calif., a research and educational facility administered jointly by the Colusa County Water District and the University of California, was chosen to determine the effect of surface compost application in almonds.

Russell Ranch Sustainable Agricultural Facility

The tomato system experiments were conducted at the UC Davis Russell Ranch Sustainable Agriculture research site (38°32'30"N, 121°52'30"W). The soils are classified as mixture of Yolo silt loam, a fine-silty, mixed, non-acid, thermic Typic Xerorthent and Rincon silty clay loam, a fine monmorillonitic, thermic Typic Haploxeralf (Table 5.1). We examined two rotations containing tomatoes, one termed conventional—which was left fallow during the winter—and another on which a leguminous cover crop was planted in the winter.

Table 5.1. Soil characteristics (0–30 cm) tomato cropping system.

Sand (%)	21.83
Silt (%)	47.00
Clay (%)	31.17
pH (H ₂ O 1:1)	6.8
Bulk density (Mg m ⁻³):	
Beds 5-15 cm	1.37
Furrows	1.52
Organic C (g kg ⁻¹)	10.3
Organic N (g kg ⁻¹)	1.0

In the conventional treatment 8 and 16 Mg compost ha⁻¹ was applied in microplots of 4.6 x 4.6 meters in an existing rotation of tomato/winter fallow/tomato/winter wheat in the winter of 2010. The rotation covered a two-year period. The treatments had three replicates, with each replicate located on a separate experimental field (each replicate is a separate one-acre field randomly assigned). A set of plots within the wheat-tomato rotation replicated fields was fertilized on April 10, 2010, with NPK-15-15-15 starter fertilizer (8.7 percent ammonium (NH₄⁺), 6.3 percent nitrate (NO₃⁻)) in granular form at the rate of 50 kg N ha⁻¹, banded at a depth of about 16 cm, and urea ammonium nitrate (UAN32) was used as side dress (applied May 30) to bring the total N application to 162

kg N ha⁻¹. Tomato seedlings were transplanted May 3, 2010. Harvest was Sept. 1, 2010. The plots were then left fallow through the winter.

The same treatments and fertilizer rates were used in 2011-12 on a new set of previously fallow plots using the same rates of compost applied. This gave us two site years of observations. The fertilization regime was the same as in the previous year (NPK applied April 12; UAN32 application May 13). Planting occurred April 21, 2011, and harvest was on Sept 14, 2011. Plots were left fallow, and N₂O emissions were monitored throughout the winter and into spring 2011 (see section on N₂O monitoring for details). A picture of a typical tomato rotation is shown in Figure 5.1.

In the winter cover crops (a mixture of oats, vetch, and bell beans) rotation, planting of the cover crop occurred Nov. 18, 2010. The rotation was winter cover crop/tomato/winter wheat covering a period just under two years. Prior to planting the cover crop, compost (8 Mg compost ha⁻¹) was applied in 4.6 x 4.6 meter microplots within each of three replicates (each replicate is a separate one-acre field). The cover crops were mowed on April 5, 2011, and subsequently the plots were tilled. Fertilizers were applied as in the conventional plots (above), and tomato planting and harvesting occurred at the same time as in the conventional plots. Wheat was planted on Nov. 3, 2011, and N₂O was monitored in the same plots up to harvest in late June 2012. Nitrous oxide fluxes were monitored in these plots for a total one and a half years, representing three crops. In addition, soil samples were taken at each sampling in all treatments for soil moisture and nitrate determination to a depth of 15 centimeters (six inch) depth.

Figure 5.1. A picture of tomato plots at the RRSF site.



Leslie J. Nickels Soil Laboratory

The NSL is a private research center supported by Colusa County and the Colusa Irrigation District. Soil properties are shown in Table 5.2. The facility has 22 acres with four varieties of almonds. For this study we monitored the Nonpareil variety since it is the most widely planted variety throughout the state. The experimental setup consisted of four treatments: 1) control (no compost), 2) three tons compost ha⁻¹ rate, 3) six tons compost ha⁻¹ rate, and 4) road (no treatment) (Figure 5.2 and 5.3). The treatments were randomly assigned in a mature orchard into main plots replicated three times. The replicate plots measured 4 feet wide by 16 feet long with each plot containing four trees with one tree assigned treatment. The “road” treatment was located outside each main plot. The fertilizer N applied is shown in Table 5.3. After the first year of monitoring following harvest, the compost was blown off the plots from the harvesting activity one year after its application. This necessitated reestablishing the plots for the second year of monitoring. The plots were established in new areas to avoid first-year residual effects from any remaining compost. Nitrous oxide monitoring occurred frequently with more intense sampling done following fertilization, irrigation, and rain events (see section on N₂O monitoring below). In addition, soil samples were taken at each sampling event for soil moisture and nitrate determination to a 15 centimeter (6 inch) depth.

Figure 5.2. Randomly assigned replicate plots containing 4 trees. Within each plot, treatments were assigned randomly. The “road treatment” was assigned outside each main plot.

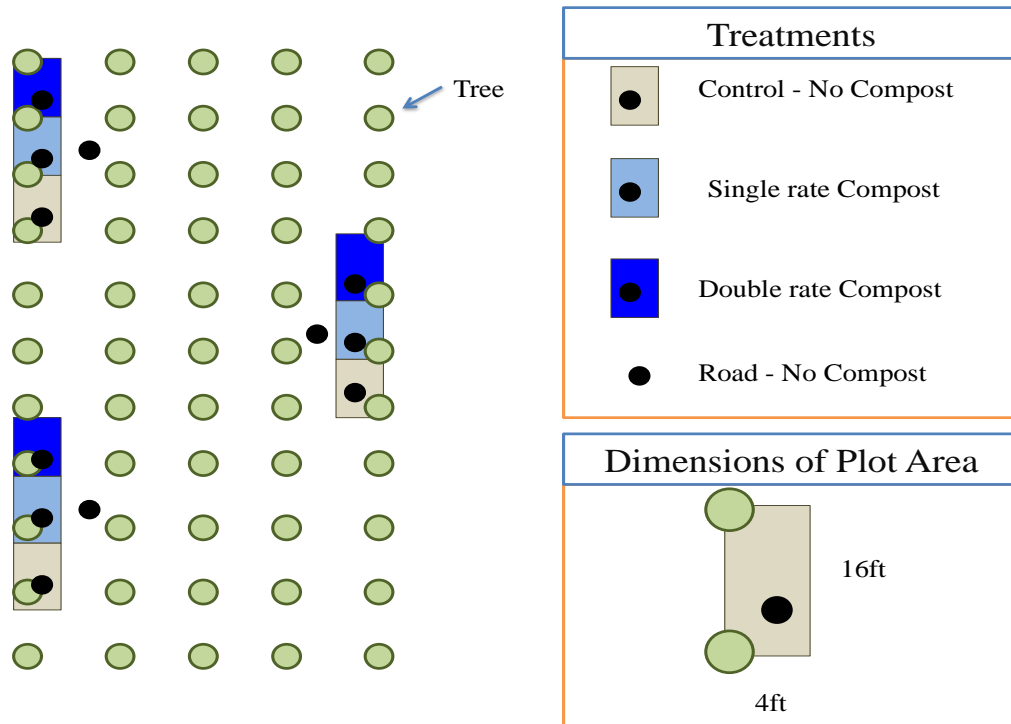


Table 5.2. Soil characteristics (0–30 cm) almond system.

Sand (%)	66.8
Silt (%)	19.2
Clay (%)	14.0
pH (H ₂ O 1:1)	7.3
Bulk density 0-20 cm (Mg m ⁻³)	1.68
Organic C (g kg ⁻¹)	7.1
Organic N (g kg ⁻¹)	0.6

Figure 5.3. Picture of the various compost treatments at the Nickels Soil Laboratory.

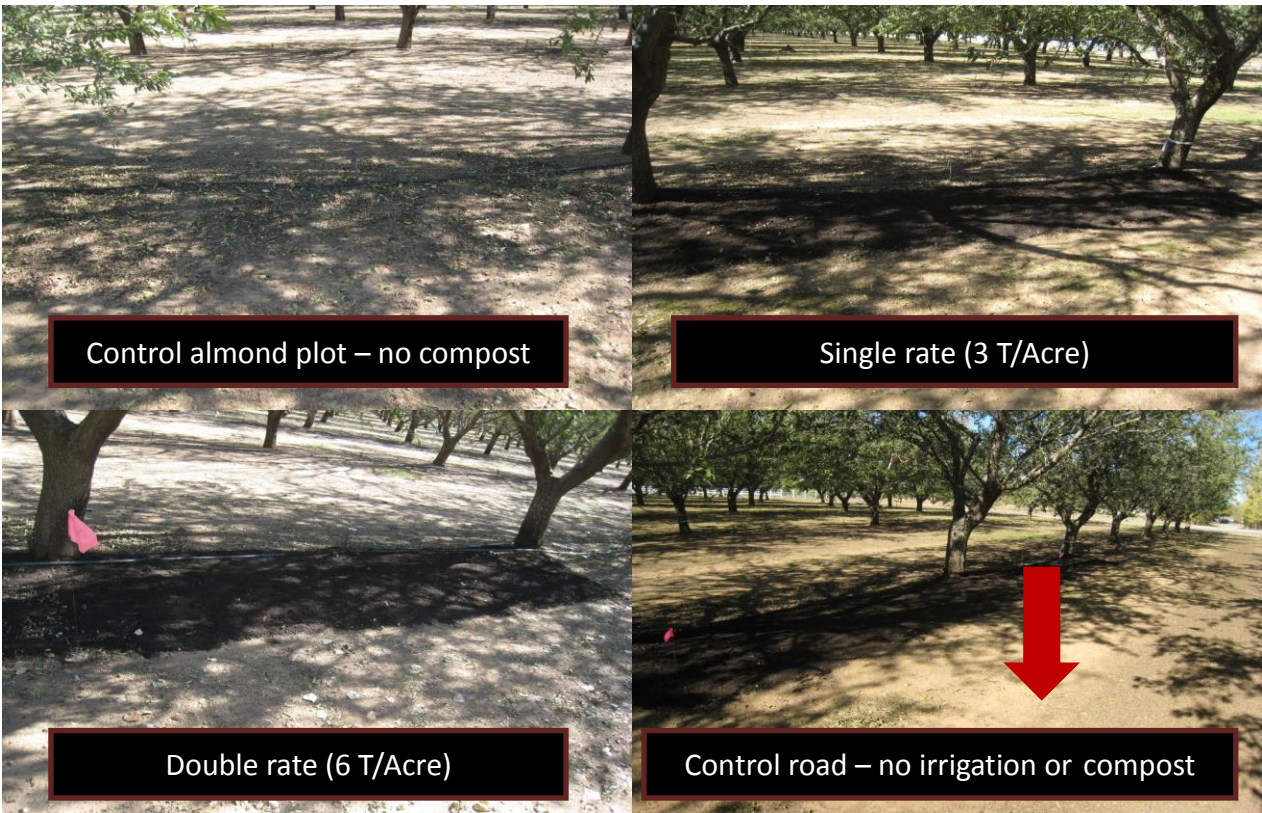


Table 5.3. Timing, quantities, and types of fertilizer applied in the almond experiment.

Year and date of fertilizer application	Fertilizer amount applied (lbs. ac-1 N)	Fertilizer Type
2012		
April 9	50	CAN-17
May 5	75	UN32
June 7	75	UN32
2013		
April 13	45	UN32
May 8	90	UN32
June 12	90	UN32

Farmer Sites

Two farmers' fields were selected for the study, one near Esparto and one near Woodland. The grower site near Esparto was on two fields in a tomato-sunflower rotation. The soil type was Marvin silty clay loam, classified as "fine, montmorillonitic, thermic Aquic Haploxeralfs" with soil properties shown in Table 5.4. The grower applied compost in October 2010 on one of two adjacent fields at a rate of six megagrams per hectare (Mg ha^{-1}) that were previously in sunflower. Both fields were fallow during the rainy season. Three chamber bases were installed about ten meters from the edge of each field. In spring, one field was planted to tomato, the other to sunflower, so the experiment was terminated. Originally the grower was to plant tomatoes on both fields so we could make the comparison of no compost versus compost addition, but he decided not to. The preliminary data for the winter following compost application is shown in the Results and Discussion section.

The Woodland site was also a furrow-irrigated tomato-sunflower rotation. The soil type was a Brentwood silty clay, classified as "fine, montmorillonitic, thermic, Typic Xerochrepts" with soil properties shown in Table 5.5. The 2011 crop was sunflower. Compost was applied following the sunflower crop at the rate of ten Mg ha^{-1} in three separate areas in three by one meter sections on the beds and worked in with a shovel to simulate disking. The N_2O emissions were monitored in each of these microplots and in the areas without compost adjacent to the treatment plots. The field was left fallow in the winter. In mid-April, a starter N-P-K fertilizer (8-24-6) was applied at a rate of 14 kg N ha^{-1} . Tomato seedlings were transplanted at the end of April 2012, and a few weeks later, an additional 166 kg N ha^{-1} in the form of urea ammonium nitrate was applied. Chamber bases for N_2O monitoring were removed for bed preparation, transplanting, and fertilizer applications.

Table 5.4. Soil characteristics (0-30 cm) at the Esparto site.

Sand (%)	20.0
Silt (%)	50.0
Clay (%)	30.0
pH (H ₂ O 1:1)	7.1
Bulk density 0-20 cm (Mg m ⁻³)	1.68
Organic C (g kg ⁻¹)	10.3
Organic N (g kg ⁻¹)	1.3

Table 5.5. Soil characteristics (0-30 cm) at the Woodland site.

Sand (%)	20.0
Silt (%)	48.0
Clay (%)	32.0
pH (H ₂ O 1:1)	7.2
Bulk density 0-20 cm (Mg m ⁻³)	1.68
Organic C (g kg ⁻¹)	10.1
Organic N (g kg ⁻¹)	1.1

Nitrous Oxide Monitoring

In each system and site, data were collected for two years with the exceptions noted in the site and management sections above. We measured N₂O flux intensively immediately before and after N fertilization and irrigation or rainfall events to capture the extent of elevated N₂O fluxes until the fluxes subsided to background levels, usually for two weeks every two to three days following its application. After N₂O flux receded and soils were relatively dry, measurements were taken less frequently.

Nitrous oxide flux was measured using a static chamber technique (Hutchinson and Livingston, 1993). Round PVC chambers (25.4 cm diameter) were used in the wheat systems. In tomato systems, rectangular thin-wall stainless steel chambers, 50 centimeters x 30 centimeters, were used on beds, and ten centimeter-diameter PVC chambers were used in the furrows. The chamber dimensions in the almond systems were 15 centimeters by 14 centimeters. The height of all chambers was ten centimeters. In tomato systems, the chamber bases had a two-centimeters-wide horizontal flange at the top end and were inserted eight centimeters deep into the soil, so that the flange was resting on the soil surface (Figure 5.4).

Figure 5.4. Picture of a typical sampling event in tomatoes showing the vented chamber.



During sampling, the vented and insulated chambers (4.8 mm diameter, 10 cm long tubes) were fitted onto the bases previously inserted into the soil. Headspace air was removed from a sampling port via syringe at 0, 20, and 40 minutes after deploying the chamber tops onto the bases. To collect a gas sample from the chamber, headspace air was removed by inserting the needle of a polypropylene syringe (Monoject) through the septum of the sampling port and slowly withdrawing 20 mL gas. The gas in the syringes was immediately transferred into evacuated 12-mL glass vials with gray butyl rubber septa (Exetainer, Labco Ltd., Buckinghamshire, UK). When N₂O fluxes were expected to be high, samples were taken from the chamber at shorter intervals (0, 15, and 30 min.).

The gas samples were analyzed on a Shimadzu gas chromatograph (Model GC-2014) with a ⁶³Ni electron capture detector (ECD) linked to a Shimadzu auto sampler (Model AOC-5000). The autosampler uses a gas-tight syringe to remove 2 mL gas from the sample vials and inject it into the GC port. The GC uses as carrier gas a mixture of helium and P5 (mixture of 95 percent argon and five percent CH₄). The CO₂ and N₂O are separated by a Haysep Q column at 80° C. The ECD is set at 320° C and the pressure of the carrier gas flowing into the ECD is 60 kPa. The minimum quantity of N₂O detected by this GC system is 0.1 pg s⁻¹.

The GC system was calibrated daily using analytical grade N₂O standards (Airgas Inc., Sacramento, Calif.). Quality assurance of the N₂O values generated by the GC and its software was obtained by processing N₂O standards after taking them to the field and treating them the same way as field samples. The two standard preparation approaches ensured quality assurance of the lab and field protocols used in this study. Samples

were analyzed within two weeks of collection, and their quality was ensured by ascertaining that the field N₂O standards were not compromised as a result of storage. During one period in fall 2010, samples were stored up to five weeks because of a bottleneck due to autosampler problems. However, during this time, the most critical samples (the ones with presumably high N₂O concentrations) were processed on another GC within the usual two-week time frame.

Gas fluxes were calculated from the rate of change in chamber concentration, chamber volume, and soil surface area (Hutchinson and Mosier, 1981). Chamber gas concentrations determined by GC (volumetric parts per million) were converted to mass per volume units assuming ideal gas relations using chamber air temperature values, which were measured by a thermocouple thermometer during each sampling event. Two separate flux calculations were made. The first used an algorithm appropriate for curvilinear concentration data with time when N₂O concentration in the chamber increased at a decreasing rate (Hutchinson and Mosier, 1981; Hutchinson and Livingston, 1993), and linear regression at all other times. All the emission estimates presented in this report are based on this widely accepted method to calculate soil-to-atmosphere gas flux when at least three data points (N₂O concentration at three time intervals) are available. The calculation compensates for the diffusion constraints imposed by the rapid increase in the partial pressure of certain gas species (e.g., N₂O) within the chamber when the flux is high. The second method used assumed a linear increase in N₂O concentration in the chamber at all times.

Statistics

The annual N₂O emissions were calculated by trapezoidal integration of daily fluxes under the assumption that the measured fluxes represented mean daily fluxes, and that mean daily fluxes changed linearly between measurements. Differences in time-integrated annual N₂O emissions between N fertilization treatments were assessed using analysis of variance (ANOVA) and standard mean separation procedures.

Results and Discussion

Background

Many factors influence the emission of N₂O from soils. In addition to fertilizer N, soil mineralization, soil moisture and carbon (substrate) availability affect N₂O emissions. Irrigation and rainfall events stimulate microbial activity, including nitrification and denitrification, resulting in N₂O production. Denitrification occurs under oxygen (O₂) limitation, typically when diffusion of O₂ from the atmosphere into the soil is limited at high soil-water content, for most soils at a water-filled pore space (WFPS) greater than 60 percent (Linn and Doran 1984). The highest N₂O fluxes occur at WFPS 60 to 90 percent (Dobbie et al., 1999; Simojoki and Jaakkola, 2000; Linn and Doran, 1984). Nitrous oxide is also produced during nitrification, although the exact mechanisms are not as well understood as those of denitrification (Bremner and Blackmer, 1979; Wrage

et al., 2001; Zhu et al., 2013). The main driver for the production of N₂O during nitrification is NH₄⁺ availability. The application of compost to soils can alter soil properties and conditions that could influence N₂O emissions, particularly from fertilizer N.

The reports of N₂O emissions from California cropping systems have been limited mainly due to the immense diversity and complexity of crops and crop rotations in comparison to other agricultural regions (Kong et al., 2009; Burger, 2005; Garland et al., 2011; Kallenbach et al., 2010; Lee et al., 2009; Steenwerth et al., 2008). The huge variety of crops—in excess of 400—in California agriculture compared to other regions such as the Midwest has resulted in fewer observations for particular crops compared to the numerous studies on corn and soybeans.

Numerous studies have shown N₂O emissions increase in response to N inputs, particularly when inputs exceed crop N requirements or economic N yield (Edis et al., 2008; McSwiney and Robertson, 2005). Thus, fertilizer N is a primary determinant of N₂O emissions in most agronomic situations. Crop N uptake, timing and placement of the N application, and fertilizer type all influence the magnitude of the N₂O emissions (Burger and Venterea, 2011). Reducing fertilizer N inputs has been suggested as the best strategy to mitigate N₂O emissions; however, this could compromise yield potential, negatively affecting the economic viability of growers and efforts to achieve food security. An underfertilized crop will not reach yield potential and will leave residual N in the soil, leading to potential N₂O emissions or to nitrate leaching into ground water. Therefore, other strategies or practices to reduce N₂O emissions would support efforts to reduce GHG emissions from agriculture.

In this project, we examined the effect of yard trimmings compost emission on N₂O emissions in the California specialty crops of tomatoes and almond. They represent high-value crops in the top ten commodities produced in California. In 2012, almonds ranked third at a value of \$4.3 billion, and tomatoes ranked tenth at \$1.2 billion (<http://www.cdfa.ca.gov/statistics/>).

Tomatoes at RRSFAF

We monitored N₂O emissions from long-term research plots at the RRSFAF and in farmers' fields in Yolo County. Though the farmer fields had different N application rates, the applications are considered standard practice for their conditions and soils. The same compost source from the Zamora facility was used in all experiments. The RRSFAF represents a long-term effort to examine the efficacy of different cropping systems at addressing future issues confronting agriculture as well as defining the components of cropping system sustainability. At RRSFAF, we examined conventional tomatoes (tomato/winter fallow/tomato/wheat; two-year rotation) and those grown with a winter cover crop (cover crop/tomato/winter wheat; part of a two-year rotation) under three rates of compost (none, 8 ton, and 16 ton ac⁻¹; dry weight). The cover crop containing rotation received only 8 t ac⁻¹ since the cover crop was considered an additional soil amendment and to more closely simulate how growers manage compost

applications when growing cover crops. The conventional tomatoes represented a typical farmer tomato/wheat rotation practiced widely in the Sacramento Valley.

The tomato/winter fallow treatment had overall N₂O emissions similar to those observed in a previous CARB study to determine N₂O emissions factors for major crops in California (CARB, 2011). Summer emissions in this system averaged between 2 and 2.5 kg N₂O ha⁻¹ (Figure 5.5 and 5.6.; N₂O emission factor of 1.2). Daily emissions for the conventional rotation during the summer tomato crop are shown in Figures 5.7 and 5.8. There were no significant differences among compost treatments showing no effect of compost on N₂O emissions across treatments and years.

Figure 5.5. Emissions of N₂O during the summer and winter from the tomato/winter fallow/tomato/winter wheat system from 2010 to 2011.

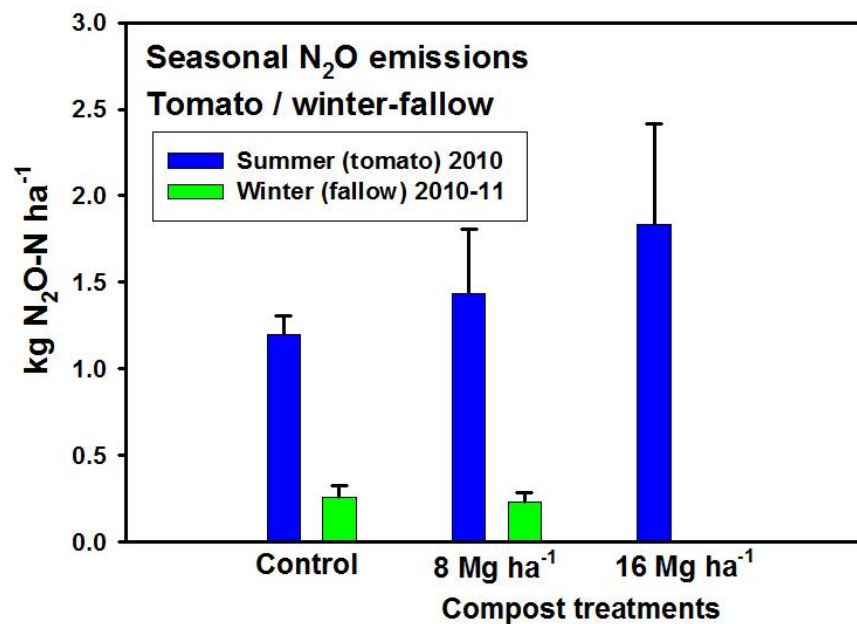


Figure 5.6. Emissions of N₂O during the summer and winter from the tomato/winter fallow/tomato/winter wheat system from 2011 to 2012.

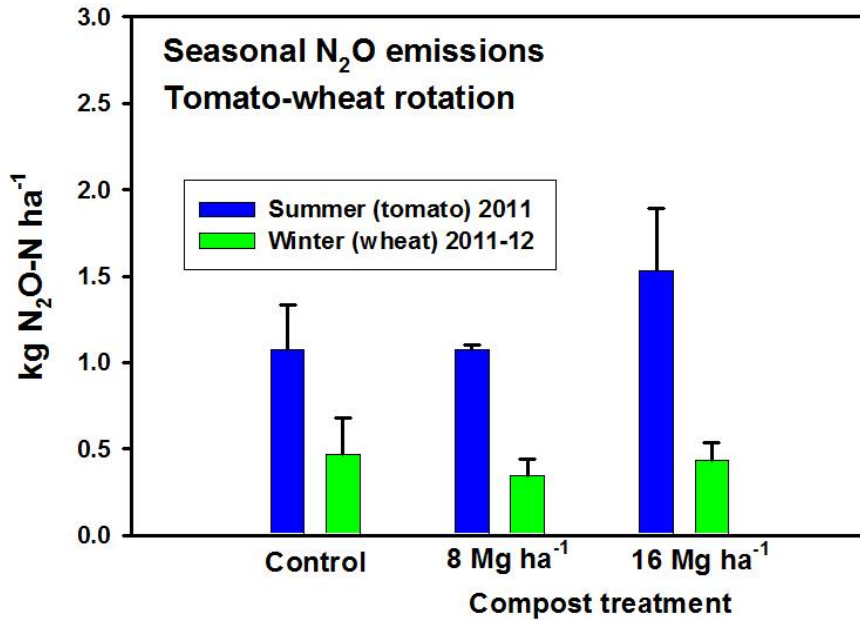


Figure 5.7. The daily N₂O flux in the conventional tomato plot during the summer of 2010. Error bars represent standard error (SE), N = 3.

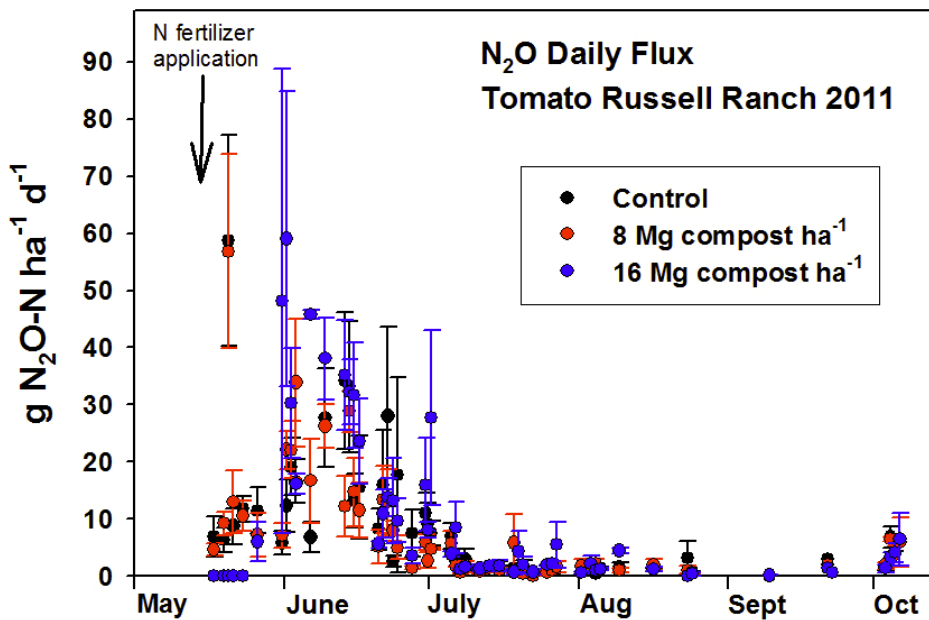
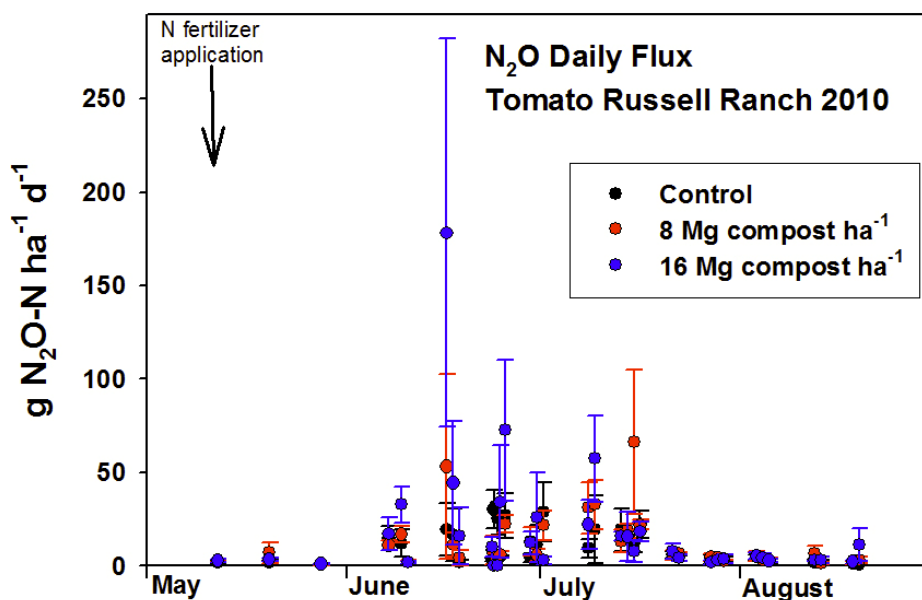


Figure 5.8. The daily N₂O flux in the conventional tomato plot during the summer of 2011. Error bars represent SE, N=3.



In the cover-crop-containing tomato plots, only one rate of compost application was examined (8 Mg compost ha⁻¹). This rate represented the typical application rate done by tomato growers in the area, particularly if compost is also applied with a cover crop. The use of cover crops under furrow irrigation in tomatoes can increase N₂O emissions (Kallenbach et al., 2010). In this study, the emission of N₂O (N₂O emission factor of 1.2 to 1.7) was slightly higher compared to the conventional tomato rotation (Figure 5.9). Again, no significant differences were found among treatments over the monitoring period. Daily emissions for the cover crop rotation in the tomato and wheat entry point are shown in Figures 5.10 and 5.11.

Tomato Grower Fields

We monitored N₂O emissions in tomato grower fields to compare to the results obtained at RRSAF. The grower used a standard compost application rate of 10 Mg ha⁻¹. The N₂O emissions in the grower field (Esparto and Woodland) were comparable to the RRSAF conventional tomato rotation, having slightly lower N₂O emissions with an N₂O emission factor of 1.0 (Figure 5.12). There was no significant effect of compost on winter or summer N₂O emissions. Daily N₂O emissions for the Esparto and Woodland sites during the winter are shown in Figures 5.13 and 5.14. Daily N₂O emissions for the Woodland site during the summer tomato crop are shown in Figure 5.15.

Figure 5.9. Emissions of N₂O during the summer and winter from the cover crop/tomato/winter wheat two-year rotation system from 2010 to 2012.

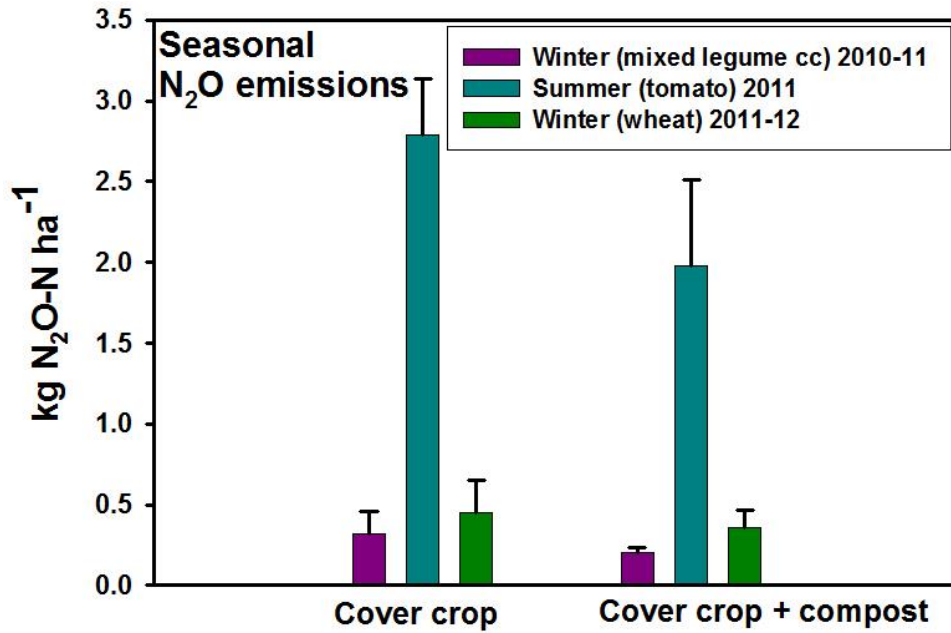


Figure 5.10. The daily N₂O flux in the cover crop tomato rotation during summer 2011. Fertilizer N applied the end of May. Error bars represent SE, N = 3.

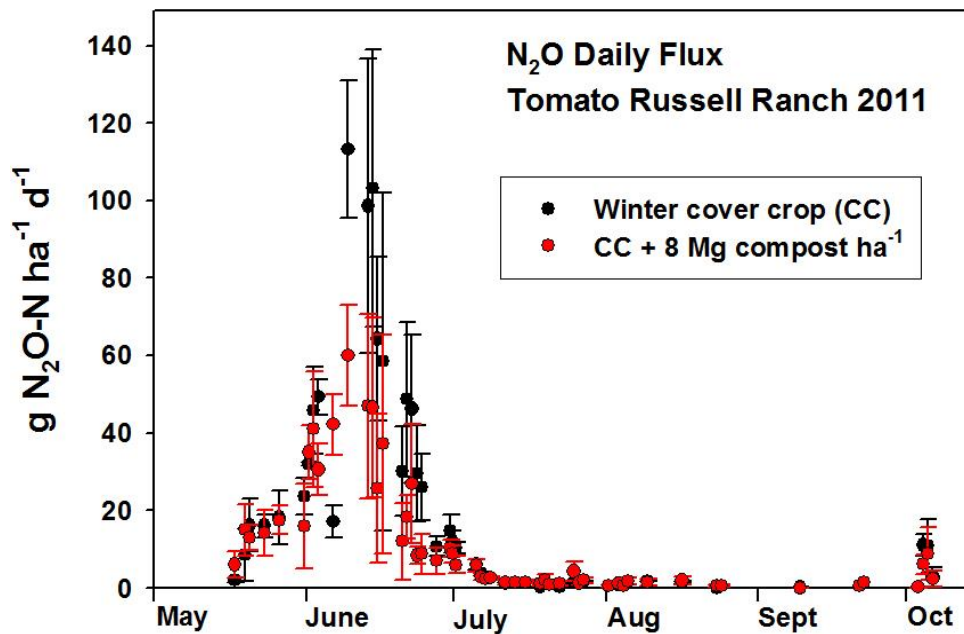


Figure 5.11. The daily N₂O flux in the cover crop tomato rotation during winter 2011-2012. Error bars represent SE, N = 3.

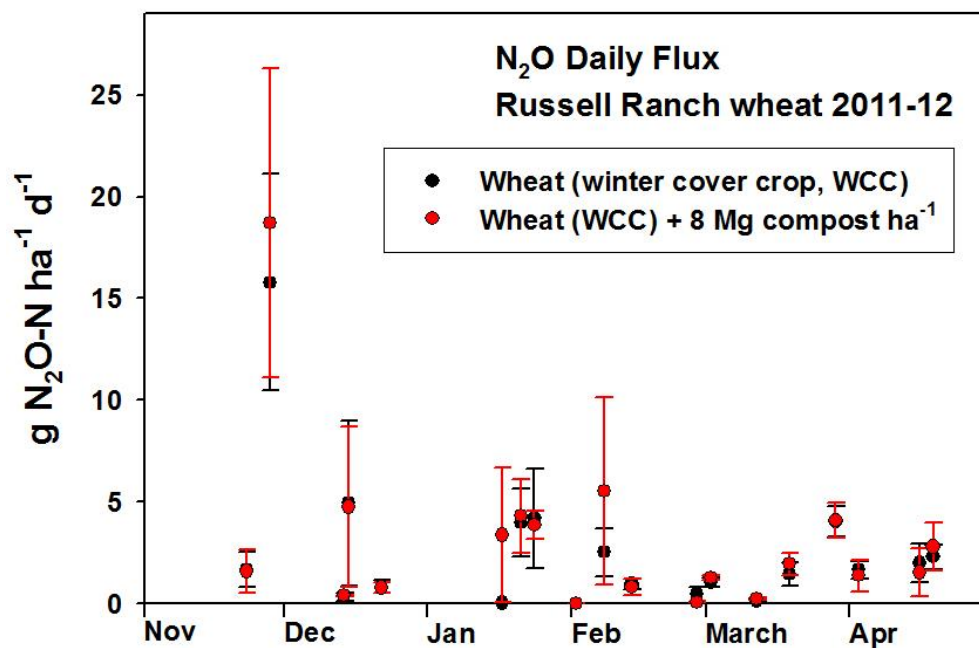


Figure 5.12. Total N₂O emissions for winter and summer (Esparto winter only; no tomato) at both grower sites. Error bars represent SE, N = 3.

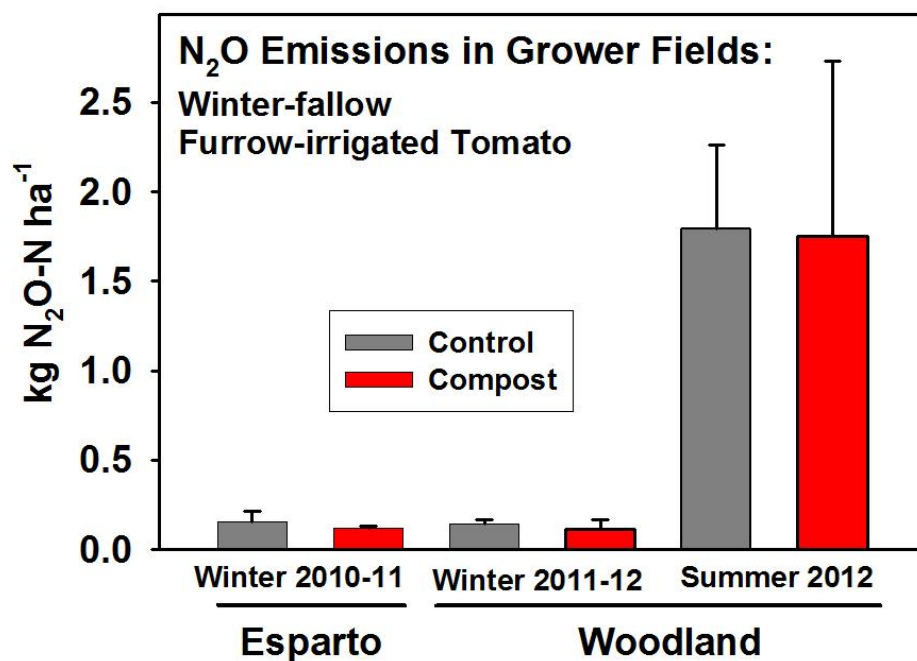


Figure 5.13. The daily N₂O emissions over the winter of 2010-2011 at the Esparto site. Error bars represent SE, N=3.

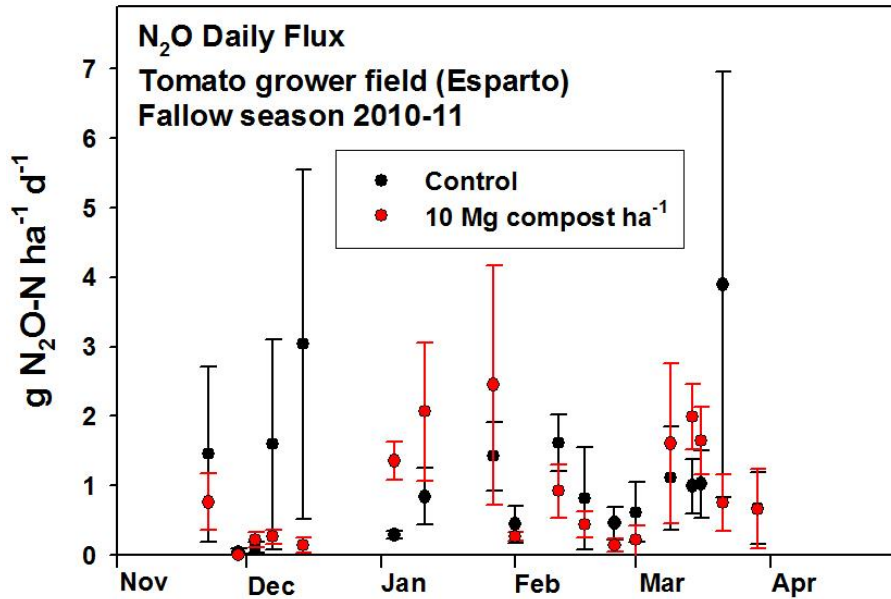


Figure 5.14. The daily N₂O emissions over the winter of 2010-2011 at the Woodland site. Error bars represent SE, N = 3.

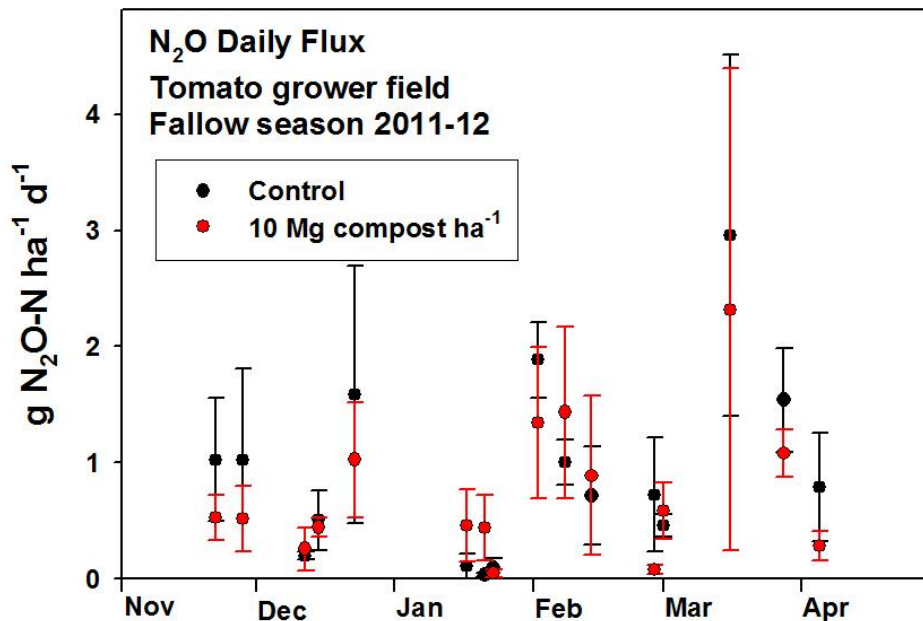
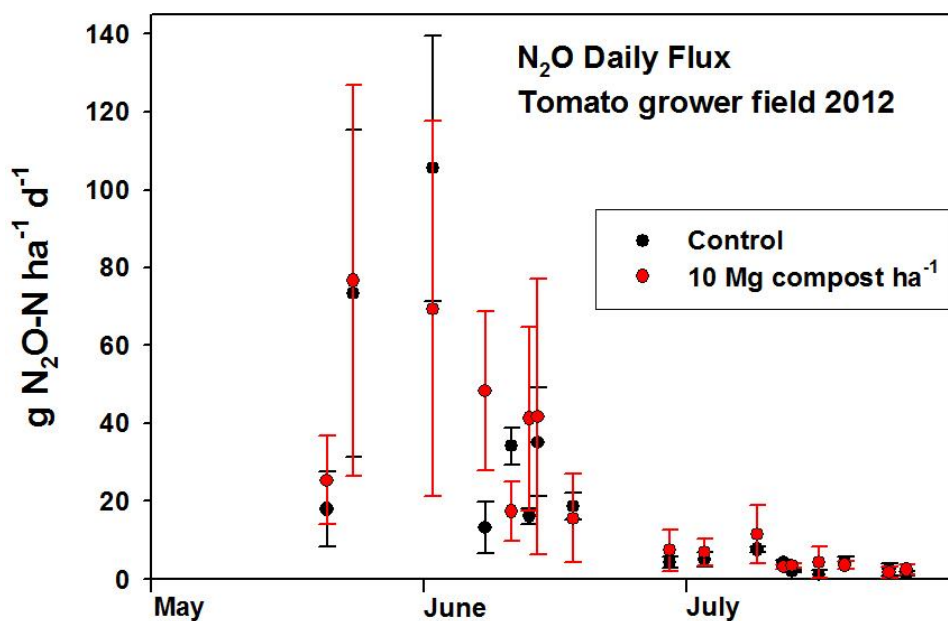


Figure 5.15. The daily N₂O emissions over the summer tomato crop of 2012 at the Woodland site. Error bars represent SE, N = 3.



To our knowledge, there has only been one field study that has examined N₂O emissions with organic amendments previous to this study in California. Burger et al. (2005) examined emissions in tomatoes under an organic system (cover crops and poultry manure bedding compost) and under a conventional system (inorganic fertilizer). They found the highest emission fluxes occurred after fertilizer incorporation, in both organic (0.94 mg N₂O-N m⁻² h⁻¹) and conventionally managed soils (2.12 mg N₂O-N m⁻² h⁻¹) as was seen in this study. However, the number of sampling periods was too infrequent to estimate seasonal or annual emission rates. A long-term cropping system N-use-efficiency study showed an organically managed four-year rotation lost only 4.5 percent of the N applied as poultry manure and bedding compost over a 10-year period in northern California (Poudel et al., 2001). In contrast, a long-term cropping system N use efficiency study showed that an organically managed two-year rotation lost 65 percent of the N applied as poultry manure and bedding compost over a ten-year period in Northern California (Horwath, unpublished). The intensity (every year versus every two years in the four-year rotation) of poultry manure and bedding compost application in the two-year rotation resulted in substantial N losses through leaching and likely denitrification. The poultry manure and bedding compost had a significantly higher content of available N, which likely leads to N losses if applied too frequently. There was no interaction of cover crop and manure compost additions on N losses compared to conventional tillage, as was also seen in this study.

Almonds

There are only a handful of published studies on N₂O emissions in almond orchards (Alsina et al., 2013; Schellenberg et al., 2012; Suddick et al., 2011; Smart et al., 2011). In general, N₂O emissions from almonds are about half that produced in tomato systems. The N₂O emission factor is also about half that found in tomatoes, averaging approximately 0.5 percent of the applied fertilizer. The low emission factor is despite the larger amount of fertilizer N added, often exceeding 200kg N ha⁻¹. We monitored N₂O emissions in a typical mature almond orchard and confirmed the results of the above studies. Figures 5.16 and 5.17 show the annual emissions over the two-year period from 2011 to 2013. The lower emissions rate is likely due to the increased N use efficiency in almonds compared to tomatoes. The comparatively high emissions in the tractor row in the second year are likely due to soil compaction, which reduces aeration and promotes denitrification activity.

There was no significant effect of the compost treatments on N₂O emissions. There seemed to be a trend to reduce N₂O emissions during the first year that corresponded to increasing compost addition; however, this can be explained by a high reading in the daily emissions in one of the replicates of the control treatment following fertilization (Figure 5.18). During the second year, variability in the daily emissions in the other treatments accounted for the lack of significant difference among treatments (Figure 5.19). The variable N₂O emissions readings are common for chamber analysis and are one of the problems with the approach. Unfortunately, this is a limitation to this research that could be overcome by additional sampling, but it would make the approach not feasible due to resource limitations.

Very few studies conducted in California have examined N₂O emissions from perennial and orchard cropping systems. Smart et al. (2011) and Alsina et al. (2013) measured N₂O emissions from a California almond orchard that was fertigated using either a surface drip irrigation system or a stationary microsprinkler system. Notably, Alsina et al. (2013) reported that cumulative annual N₂O emissions were significantly higher in the drip-irrigated system (1.6 kg N₂O-N ha⁻¹ yr⁻¹) than in the microsprinkler-irrigated system (0.6 kg N₂O-N ha⁻¹ yr⁻¹). In this study, the almonds were microsprinkler irrigated. Emissions of N₂O in the drip irrigated system, where water and N fertilizer applied in a more concentrated spatial pattern, were positively correlated with water-filled pore space but not with soil mineral-N concentrations. This is a common conclusion for GHG measurements in agricultural systems. However, as stated above, overall emissions are lower than for row crops and have a corresponding lower N₂O emission factor.

Figure 5.16. Total N₂O emissions in the four treatments (control/no compost, 3 Mg ha⁻¹, 6 Mg ha⁻¹ and the tractor row) in 2011 to 2012. Error bars represent SE, N=3.

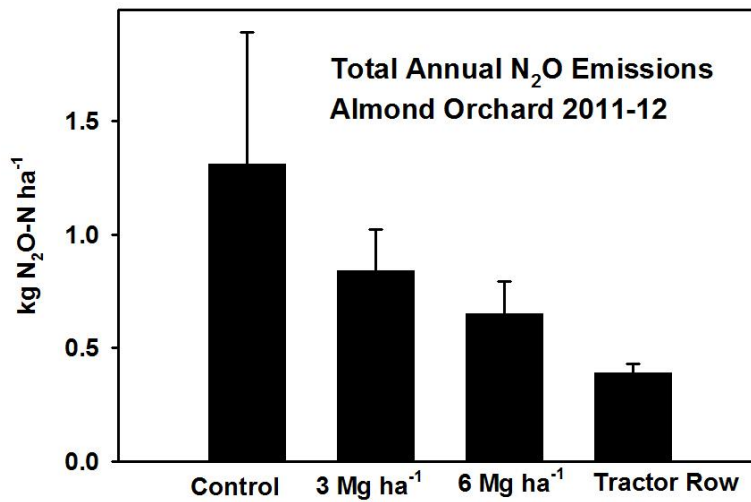


Figure 5.17. Total N₂O emissions in the four treatments (control/no compost, 3 Mg ha⁻¹, 6 Mg ha⁻¹ and the tractor row) in 2012 to 2013. Error bars represent SE, N=3.

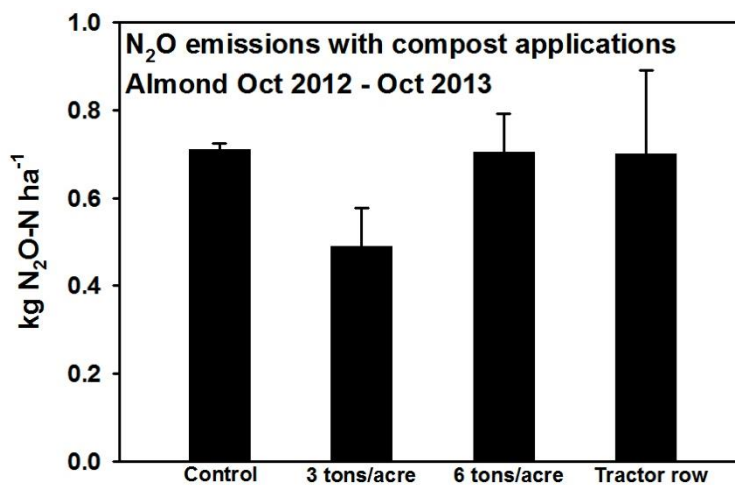


Figure 5.18. Daily N₂O emissions from all treatments during the first year (2011-2012) of the almond trial. Error bars represent SE, N=3.

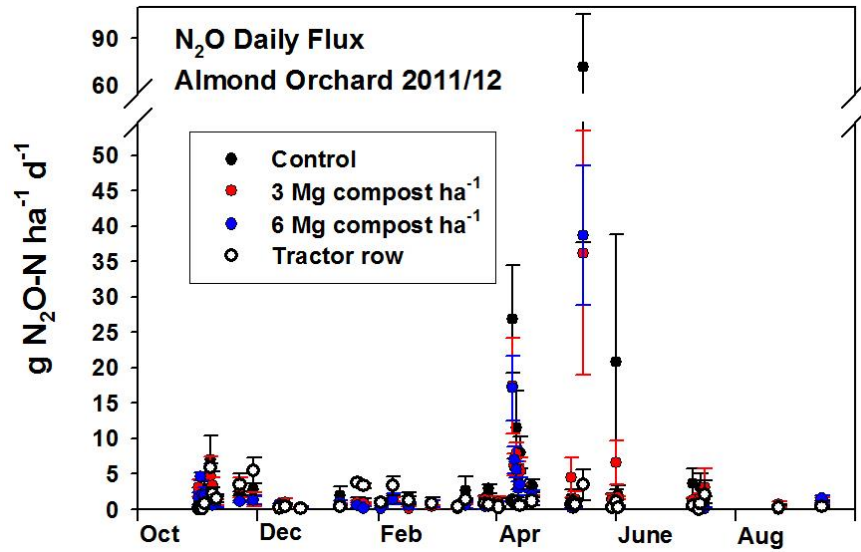
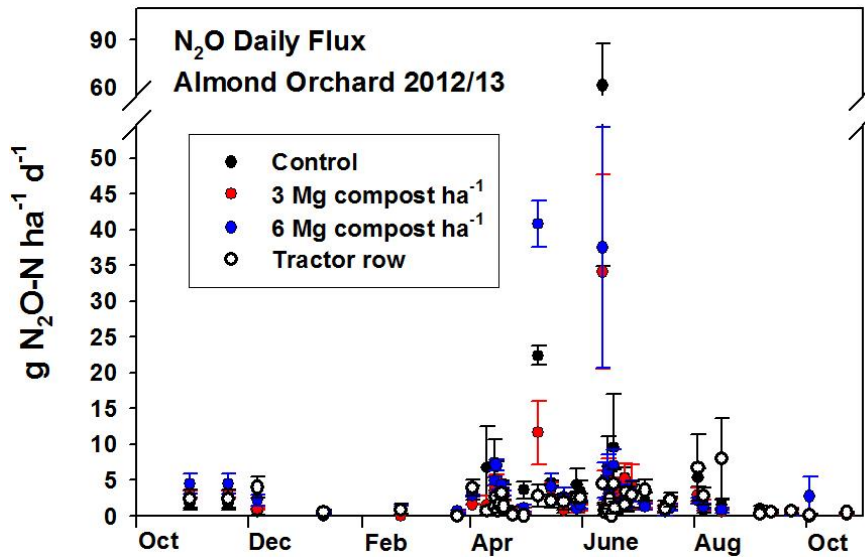


Figure 5.19. Daily N₂O emissions from all treatments during the second year (2012-2013) of the almond trial. Error bars represent SE, N = 3.



Conclusions

Overall, compost application to soils had no effect on N₂O emissions in tomato or almond systems. In tomatoes, a number of management practices were monitored including cover cropping and various cropping sequences (rotations) both at the RRSAF and farmer fields. None of the effects of these practices on soil processes on N₂O emissions was significantly influenced by compost addition. The observed annual N₂O emissions in tomato fields were similar to observed measurements in previous studies, validating the observation done in this study. In the almond orchard, overall emissions were lower than in the tomato field, also validating the results of previous studies. During the first year of the almond study, the results suggested a trend of decreasing N₂O emissions with increasing compost application. The high variability in N₂O emissions across compost treatments, particularly following fertilization, resulted in no significant treatment effect during the two years of the study. Chamber studies to assess N₂O emissions from soils are generally characterized by high variability (Hutchinson and Mosier, 1978). Since no differences in emissions occurred when compost was applied, no N₂O emission factors from the effect of compost application could be calculated. Though compost had no effect on N₂O emissions in the crops examined in this study, growers remarked they use compost for a variety of reasons, namely to improve soil properties. The most notable improvement in soil properties after compost application was said to be a more even infiltration of irrigation water and greater soil water-holding capacity, which was perceived to increase irrigation efficiency. Growers also remarked that crop growth was generally improved after compost applications, likely from the addition of nutrients and the build-up of soil organic matter, which positively affected soil properties. The application of compost may help to promote crop resilience to variable climatic conditions of excessive growing season rainfall and prolonged periods of high temperatures that will likely occur as the climate changes.

Chapter 6. Using Laboratory Incubations to Assess N₂O Emissions from Yard Trimmings Compost Application to California Agricultural Soils

Introduction

Laboratory incubations were designed to provide additional information to expand the interpretation of the limited results of the field trials done in the almond orchards and tomato fields. The main goal of this study was to determine the effect of compost amendments on a range of soils and influence of management practices. The lab incubations covered a range of soil not possible to observe in the field component of this project. The incubations incorporated various rates of fertilizer additions, different fertilizer types, various compost application rates (none and standard amendment), and various soil moisture contents. Most importantly, they used a variety of soils ranging in textures from sandy to silty clay typical for agricultural production in California.

The production of N₂O in soils occurs through denitrification and ammonium oxidation (nitrifier nitrification, nitrifier denitrification, and nitrification-coupled denitrification) (Wrage et al., 2001). Many soil properties have influence on N₂O produced through these pathways in soils, such as soil texture, organic carbon, pH, N form and availability, and concentration of certain metals, including iron (Bouwman et al., 2002a; Bremner et al., 1980; Stehfest and Bouwman, 2006). Most of these properties are affected by agricultural management such as compost application, irrigation, and fertilization (Mulvaney et al., 1997; Wright et al., 2008).

Results from the literature vary widely as to the effect of yard trimmings compost on GHG emission from soils ranging from decreasing N₂O emissions (Dalal et al., 2009) to increasing emissions (Mondini et al., 2007). When the use of organic amendments such as compost reduce N₂O emissions from soils (Dalal et al., 2010), it is most likely due to a reduction in mineral N (Wright et al., 2008), which is the substrate of denitrification and nitrification. In contrast, it can also increase N₂O emission after compost application (Mondini et al., 2007) by increasing the available N and dissolved organic carbon (DOC) (Wright et al., 2008), which could stimulate microbial activity and lead to increased oxygen consumption resulting in N₂O production via denitrification and nitrifier denitrification. In addition, compost application to soils may help to maintain optimal soil moisture conditions longer, which could favor denitrification. In contrast, improving soil moisture status may maintain lower soil temperatures and prolong N₂O solubility, leading to greater reduction potential to dinitrogen (N₂) from denitrification and nitrifier denitrification. However, little data exist to substantiate these hypotheses or generalize

the effects of composts. For this reason, generalizing the effects of green material compost on soil N₂O emissions from previous studies is difficult.

Denitrification is often considered to be the main source of N₂O emitted from soils, as emissions derived from N application tend to increase with increasing soil water content (Abbasi and Adams, 2000; Bateman and Baggs, 2005), although ammonia oxidation-derived N₂O measured in the laboratory also has been observed to increase with increasing soil moisture (Bremner and Blackmer, 1979). These divergent processes and pathways make it difficult for modelers to predict N₂O emissions based on a combination of soil properties and agricultural management activities. A better understanding of how these multiple controls affect edaphic properties and drive N₂O production is needed to guide management practices with the goal of mitigating emissions, particularly with the use of soil amendments. These factors were the primary considerations in designing and interpreting the Task 3 lab incubation experiments.

The objective of Task 3 was to develop a quantitative understanding of the complexities that occur among multiple controls of N₂O production and the main factors affecting its production in highly productive agricultural soils following application of green material compost. Using ten different soils, a series of laboratory incubations were performed to test the effect of compost application, soil water content, N fertilizer amount and form, and their interactions on N₂O emissions. The soils were selected to represent different textures from sandy loam to loam to silty clay across a range of row and specialty crops in California (Table 6.1). The lab incubations were used to determine whether compost additions increase/decrease the denitrification of fertilizer N and whether compost N serves as a substrate for denitrification. For the latter, we used isotopically labeled ¹⁵N fertilizer in the form of NH₄⁺, NO₃⁻ and urea-N to determine the source of N contributing to denitrification. Using a broader range of soil types and moisture contents allowed us to generalize the data obtained from field studies and extrapolate them to a broader level. In addition, the comparison of labeled and unlabeled fertilizer N treatments allowed us to estimate the contribution of different sources of N (fertilizer, soil, compost) to N₂O production. Finally, we examined soil characteristics and simulated management practices (fertilization and irrigation) known to influence N₂O production.

Materials and Methods

This study was comprised of two sub-studies to determine the role of compost application to soil on influencing the production of N₂O across a range of fertilizer and soil moisture manipulations. Study 1 examined the effect of compost, fertilizer N additions, and soil moisture in ten agricultural soils sampled from various regions across California (Table 6.1). In addition, soil characteristics known to influence N₂O production were examined in Study 1. Study 2 elucidated the source of N (compost versus soil versus fertilizer N) contributing to N₂O production in a subset of four soils using stable N isotope methods following the application of compost to soils.

Soil and Compost Sampling

Soil samples were collected from ten agricultural fields, chosen to provide a diverse set of soils from the main agricultural production areas in California. All soil samples were collected before fertilizer application. The location, previous crop, and soil properties at each site are summarized in Table 6.1. Composite soil samples from numerous auger borings from 0 to 15 cm in depth were sieved to two millimeters and refrigerated (4° C) until the experiments began (sample storage time less than seven days). Compost samples were collected from green material compost windrows from Northern Recycling Compost in Zamora, Calif. The material had been composted for more than eight weeks and met the mandated PFRP (process to further reduce pathogens) requirement for soil application (CalRecycle, 2012). The respiration of compost was 2.8 mg CO₂-C g⁻¹ OM day⁻¹, and the relative seedling vigor averaged 100 percent of control, indicating that the compost was stable and mature (CalRecycle, 2012).

Table 6.1. Soil characteristics used in lab incubation.

Soil	Location	Classification	Previous crop	Soil texture	Sand %	Clay %	Silt %	pH †	I N mg kg ⁻¹	DOC mg kg ⁻¹	Total C g-kg ⁻¹	Total I N g-kg ⁻¹	Fe ‡ mg-kg ⁻¹
S1	Sanger	CL, mixed, nonacid, thermic Typic X	Grape	Sandy	61	7	32	4.2	3.6	28	3	0.3	260
S2	Modesto	FL, mixed, super-active, thermic Typic A	Grape	Sandy	72	10	18	6.9	129.9	164	9.7	1.1	240
S3	Salinas	Fine, MM, thermic Pachic A	Lettuce	Sandy	64	13	23	7.2	5.3	44.0	6.6	0.7	150
S4	Castroville	Fine, MM, thermic Ultic Palexerol	Tomato	Sandy	72	13	15	6.4	31.8	88.3	7.5	0.8	550
L1	Spence	FL, mixed, thermic Typic Argixeroll	Artichoke	Loam	50	21	29	6.6	18.1	63.2	12.8	1.1	270
L2	Davis	Fine, MM, thermic Mollic Haploxeralfs	Tomato	Loam	30	24	42	5.4	2.2	16.8	8.5	0.9	170
CL1	Dixon	FS, mixed, nonacid, thermic Typic X	Wheat	Clay loam	23	28	49	5.6	10.7	30.4	16	1.4	290
CL2	Five Points	FL, mixed, super-active, thermic Typic H	Tomato	Clay loam	36	32	32	6.8	3.7	57.2	6.7	0.8	60
C1	Salinas	Clear Lake clay: fine, MM, thermic Typic P	Broccoli	Clay	22	42	36	7.4	27.7	87.7	17.8	1.6	240
SC 1	Dixon	FS, mixed, nonacid, thermic Typic X	Radish	Silty clay	15	44	41	5.5	4.6	19.3	11.8	1.1	210
-	-	CV%	-	-	49	56	34	16	141	77	46	38	52
-	-	Compost	-	-				8.1	324	270	227	15	1700

CL = coarse-loamy; FL = fine-loamy; FS = fine-silty; I = inorganic; MM = montmorillonitic; X = Xerorthents; A = Argixeroll; H = Haplocambid; P = Pelloxerert; †pH measured in KCl 1:1. ‡pyrophosphate extractable iron.

Soil Extraction and Analysis

To determine the inorganic N of soils and composts, they were extracted with 0.5 M K_2SO_4 (one to ten ratio w:v). The extracts were filtered, and the filtrate was stored at 4°C. The NH_4^+ and NO_3^- content of the extracts was determined using colorimetric methods (Doane and Horwath, 2003; Verdouw et al., 1978). Dissolved organic carbon levels were determined by UV-persulfate oxidation (Teledyne-Tekmar Phoenix 8000). Soil pH was determined in 1M KCl extracts (1:1 w:v), which gives a lower pH value than in water but reveals potential soil acidity. Total C and N content were determined using an elemental analyzer (Costech EAS 4010, Valencia, Calif.) following sample ball milling preparation. Percent clay, silt, and sand were determined by a modified pipet method (USDA, 1992). Iron (Fe) was determined by shaking 1 g soil with 100 mL 0.1 M sodium pyrophosphate for 16 hours, followed by centrifuging for 30 minutes at 15,600 × G; further centrifugation did not result in any difference in measured Fe concentration, indicating that all fine Fe colloids had been removed, an important consideration when using this extraction (Loveland and Digby, 1984).

Study 1: Effect of Compost Additions on N_2O Production

The incubation conditions used in these experiments were done under standard laboratory conditions (22°C). Soils were weighed (50 g dry mass) into standard 120 mL specimen cups (Fisher Scientific) and placed in 1 L Mason jars containing septum for gas sampling and 2 mL of water to maintain sample soil moisture throughout incubations. To simulate management practices typically performed in the field, 1.2 g (dry mass) of ground compost was mixed with soil and incubated at 40 percent of water holding capacity (WHC) for seven days. The amount of compost added represented 16 tons dry weight per acre. Identical non-compost soil samples were incubated under the same conditions. For each soil/compost treatment (compost and non-compost), three N fertilization treatments were applied: no fertilizer, ammonium sulfate [$(NH_4)_2SO_4$], and potassium nitrate (KNO_3). Fertilizer N treatments received 100 mg N kg^{-1} of soil, representing 150 kg N per hectare or 150 lbs. N per acre. To assure uniform distribution of fertilizer into the soil, the N treatments were applied in water solution and sprayed onto the different soils and mixed to obtain a final moisture content of 50 percent or 100 percent of soil WHC. The “no fertilizer” N treatment received deionized water to reproduce moisture contents of the treated samples. The experimental design and treatment application were set up as completely randomized blocks, with three replicates per treatment (total experimental units of 360), and incubated for 14 days at 22°C. Soil moisture remained constant throughout the entire incubation period.

Study 2: Determining Sources of N Contributing to N_2O Production

In order to determine the sources of soil, fertilizer, or compost N contributing to N_2O production, the different sources of N present needed to be differentiated. The contribution of soil N was determined by labeling it with ^{15}N , a heavy isotope of N. The pre-labeling of soil was achieved by adding ^{15}N labeled ammonium sulfate [$(^{15}NH_4)_2SO_4$] together with a carbon substrate to force its immobilization into the

microbial biomass (Horwath and Elliott, 1996; Hood et al., 2000). A subset of four of the ten soils used in Study 1 was used to represent soil texture from sand to clay loam, representing the most common soils in California agriculture. For each of the four soils used (soils used were S1, S4, CL1 and CL2; see Table 6.1 for details), $50 \mu\text{g N kg}^{-1}$ $(\text{NH}_4)_2\text{SO}_4$ and $500 \mu\text{g C kg}^{-1}$ glucose (C: N ratio = 10:1) were added to the soils. A subset of the soils (one half) was labeled with isotopically enriched $(^{15}\text{NH}_4)_2\text{SO}_4$ (50 atom% ^{15}N excess), and the other with unlabeled $(\text{NH}_4)_2\text{SO}_4$. To assure uniform distribution, the added N source and glucose were applied in water solutions as done in Study 1 to obtain a final moisture content of 55 percent soil WHC. All treated soils were further incubated and monitored for inorganic N to assure complete immobilization of the added N source into the microbial biomass. The soils were then incubated for up to 50 days. During this period, the microbial biomass turnover resulted in labeling the soil organic fractions with the ^{15}N isotope. These soils were used to determine the soil N contribution to N_2O production as described in the next section.

The labeled and unlabeled soils were weighed (50 g dry mass) into standard 120 mL specimen cups and placed in Mason jars (1 L), each containing a septum for gas sampling and 2 mL of water to maintain soil moisture throughout the incubation. To simulate management practices typically performed in the field, 1.2 g (dry mass) of ground compost (16 t per acre rate) was mixed with soil and incubated at 40 percent of WHC for seven days. Identical non-compost soil samples were incubated under the same conditions. For the unlabeled-soil compost treatment (compost and non-compost), two N fertilization treatments, namely ^{15}N enriched $(\text{NH}_4)_2\text{SO}_4$ (10 atom% excess) and ^{15}N enriched KNO_3 (10 atom% excess), were applied. For the labeled-soil compost treatment (only compost), unlabeled $(\text{NH}_4)_2\text{SO}_4$ and KNO_3 were applied. The overall treatments are as follows:

- [1] ^{15}N -soil + Compost + $(\text{NH}_4)_2\text{SO}_4$
- [2] ^{15}N -soil + Compost+ KNO_3
- [3] Soil + Compost + ^{15}N - $(\text{NH}_4)_2\text{SO}_4$
- [4] Soil + Compost + ^{15}N - KNO_3
- [5] Soil + ^{15}N - $(\text{NH}_4)_2\text{SO}_4$
- [6] Soil + ^{15}N - KNO_3
- [7] Control-I (Soil + Compost + $(\text{NH}_4)_2\text{SO}_4$)
- [8] Control-II (Soil + Compost + KNO_3)
- [9] Control-III (Soil + $(\text{NH}_4)_2\text{SO}_4$)
- [10] Control-IV (Soil + KNO_3)

All fertilizer N treatments received a dose equivalent to 100 mg kg^{-1} of soil (150 kg Ha^{-1} or $150 \text{ lbs. N ac}^{-1}$). To assure uniform distribution, fertilization treatments were applied in

water solution and sprayed onto the different soils and mixed to obtain a final moisture content of 60 percent of soil WHC. The experimental design and treatment application was a completely randomized block design and incubated for 14 days at 22°C. Each treatment was replicated four times. In treatments 3, 4, 5, and 6, an additional four samplings occurred for each soil for a total of seven sampling events. There were a total of 280 samples.

The fraction of N₂O produced (see Section 3.1.6. for N₂O analysis details) from soil, fertilizer, and compost N was based on the ¹⁵N isotopic enrichment of the N₂O, and NH₄⁺ and NO₃⁻ in treatments 1, 2, 3, and 4 (Equations 6.1, 6.2, and 6.3). The contribution of denitrification and ammonia oxidation to N₂O production was calculated based on ¹⁵N data in treatments 3, 4, 5, and 6, following a modified method reported by Steven et al. (1997), and Senbayram et al. (2009).

$$P_{\text{soil}} = \frac{^{15}\text{N}_{2\text{Oatom}}\% \text{intrt1orrt2} - \text{controlIatom}\%}{^{15}\text{N}_{\text{soilatom}}\% - \text{controlIatom}\%} \quad [\text{EQ 6.1}]$$

$$P_{\text{fertilizer}} = \frac{^{15}\text{N}_{2\text{Oexcessatom}}\% \text{intrt3orrt4}}{^{15}\text{N}_{\text{fertilizerexcessatom}}\% \text{intrt3orrt4}} \quad [\text{EQ 6.2}]$$

$$P_{\text{compost}} = 1 - P_{\text{soil}} - P_{\text{fertilizer}} \quad [\text{EQ 6.3}]$$

The gross mineralization rates were calculated using the results of the remaining control treatments and an ¹⁵N isotope pool dilution method (Barraclough, 1995). The net nitrification rates were calculated from the net increase of the NO₃⁻ in these treatments during the incubation period.

Determining the Role of Soil Properties on N₂O Production in Compost Amended Soils

The following soil properties were examined to provide insight on factors affecting N₂O emissions in Studies 1 and 2. The properties are the most commonly believed to control emissions of N₂O from agricultural soil and include texture, pH, organic matter content, Fe, and the inherent ability of the soil to release inorganic nitrogen or mineralization potential. These are intrinsic properties, which are not abruptly altered by environmental conditions. In contrast, treatments were designed to manipulate the most common temporary changes that influence N₂O production: water content, fertilization, and organic amendments. Fertilizer and compost were either withheld or added at a rate typical of agriculture in California, and two water contents were chosen according to the range expected in agricultural soils. Field capacity, the amount of water a soil can retain against gravity, was chosen as the upper reference point. This is not uncommon, as soil moisture can temporarily exceed field capacity following irrigation or rainfall events. In practice, WHC was used to represent field capacity. As a contrasting treatment, 50 percent WHC was also used. This is near the permanent wilting point of most soils, and it is not likely that soil moisture will fall below this in the field except during fallow periods. Although many intermediate values could have been selected as treatments,

the selected treatments represent both ends of a typical spectrum of values in order to present a broad yet concise study.

In order to create contrasting indices to characterize soil Fe composition, two extraction compounds were used: acid hydroxylamine (FeA), an index of reactive Fe(III) minerals (Lovley and Phillips, 1987); and pyrophosphate (FeP), representing Fe complexed with soil organic matter (Bremner et al., 1946; Schuppli et al., 1983; Loveland and Digby, 1984). FeA was extracted by shaking 0.8 g soil for one hour with 40 ml 0.25 M hydroxylamine hydrochloride in 0.25 M HCl, followed by centrifuging for 30 minutes at 15,600 x G. FeP was extracted by shaking 1 g soil with 100 ml 0.1 M tetrasodium pyrophosphate for 16 hours, followed by centrifuging for 30 minutes at 15,600 x G; further centrifugation did not result in any difference in measured Fe concentration, indicating that all fine Fe colloids had been removed, an important consideration when using this extractant (Schuppli et al., 1983; Loveland and Digby, 1984). The concentration of Fe in all extracts was determined colorimetrically (Dominik and Kuapenjohan, 2000); pyrophosphate extracts were neutralized by a small addition of HCl prior to this determination. There was no interference from pyrophosphate in the colorimetric analysis. All analyses of soil properties were performed in duplicate. These properties are reported in Table 6.1.

N₂O Sampling and Analysis

Gas samples for N₂O were taken from the Mason jars for both studies 1 and 2 on days 0, 1, 2, 3, 5, 9, and 14 following preincubation. Jars were closed with septum-equipped lids for 60 minutes, and 20 mL gas samples were removed from each jar headspace at 0, 30, and 60 minutes after jar closure, and transferred to 12 mL evacuated vials. The flux was determined by linear interpolation between samples. Cumulative N₂O-N was calculated using total (daily) estimates of N₂O flux, with an assumption that N₂O flux measured on a sampling date was representative of the average daily flux (Williams et al., 1992). Gas samples were analyzed using a GC with an ECD (Model 2014, Shimadzu Scientific Instruments, Pleasanton, Calif.).

Statistical Analyses

Ten different soils with variable properties shown in Table 6.1 were analyzed to illustrate differences based on the original soil conditions affecting N₂O production. The coefficient of variation (CV) was calculated by dividing standard deviations by means across all soils. The effect of treatments (compost application, water content, and N fertilization) as well as their interactions with soils on the cumulative N₂O emissions were analyzed by full factorial analysis of variance and Partial Least Square (PLS) multivariate analysis, using log-transformed data to improve variance homogeneity. Post hoc Tukey's Honestly Significant Difference (HSD) multiple comparisons of means or paired t tests were used when appropriate to verify significant differences (P<0.05) between treatments within a given soil type. The objective of this analysis was to identify the most important drivers of N₂O emissions while accounting for variability found across soil. Background N₂O emissions, measured in control treatments in each soil type, were also included in this analysis as an integrated measure of intrinsic

emission potential. Data standardization and statistical analyses were performed using JMP 10 software (Sall et al., 2005).

Results and Discussion

The results and discussion will be presented by study. A summary conclusion for each study will be presented following the discussion of both Studies 1 and 2.

Statistical Analysis of Soil Properties

To illustrate intrinsic differences based on the original condition of these soils, mean values of all measured properties and the CV were calculated by dividing standard deviations by means across all soils (Table 6.2). The effect of treatments (compost application, water content, and N fertilization) as well as their interactions with soils on the cumulative N₂O emissions was analyzed by full factorial analysis of variance (Table 6.3), using log-transformed data to improve variance homogeneity. To convert the effect of treatments (categorical variables) into continuous numeric responses, the calculated change (Δ), comparing measurements from before and after the treatment, and the following variables [pH, DOC, and inorganic N (IN)] were used to assess their impact on N₂O emission. These measures of change were used in PLS multivariate analysis, which also incorporated nine other continuous numeric variables (soil original pH (OpH), soil original DOC (ODOC), soil original IN (OIN), soil original Fe (OFe), clay, sand, silt, soil original total N (OTN), and soil original total C (OTC)) representing original edaphic traits that could also affect the N₂O emission potentials of soils. The objective of this analysis was to identify the most important drivers of N₂O emissions while accounting for variability found across soils. Background N₂O emissions, measured in control treatments in each soil type, were also included in this analysis as an integrated measure of intrinsic emission potential.

Table 6.2. Correlation matrix of the soil properties evaluated in this study.

Soil Property	FeA ^a	FeP ^b	DOC ^c	Inorganic N	Total N	Total C	Sand	Silt	Clay	pH
FeA	-	-0.07	-0.41	-0.37	0.68	0.70	-0.91	0.84	0.79	-0.15
FeP	-0.07	-	0.25	0.05	0.04	0.08	0.38	-0.37	-0.31	-0.10
DOC	-0.41	0.25	-	0.93	0.25	0.12	0.53	-0.68	-0.29	0.59
Inorganic N	-0.37	0.05	0.93	-	0.18	0.02	0.45	-0.54	-0.28	0.43
Total N	0.68	0.04	0.25	0.18	-	0.98	-0.57	0.37	0.66	0.47
Total C	0.70	0.08	0.12	0.02	0.98	-	-0.61	0.46	0.66	0.36
Sand	-0.91	0.38	0.53	0.45	-0.57	-0.61	-	-0.89	-0.91	0.13
Silt	0.84	-0.37	-0.68	-0.54	0.37	0.46	-0.89	-	0.63	-0.44
Clay	0.79	-0.31	-0.29	-0.28	0.66	0.66	-0.91	0.63	-	0.17
pH	-0.15	-0.10	0.59	0.43	0.47	0.36	0.13	-0.44	0.17	-

^a acid hydroxylamine-extractable iron, ^b pyrophosphate-extractable iron, ^c dissolved organic carbon

PLS analysis bears some relation to principal component analysis (PCA), representing a form of structural equation modeling, distinguished from the PCA method by being component-based rather than covariance-based (Esposito Vinzi, 2010; Tenenhaus et al., 2005). The essential output of the analysis ranks the most important components (independent variables) based on linear regression models that project the predicted variables and the observable variables to a new multivariate space. PLS analysis is particularly suited when the matrix of predictors (here represented by original soil properties, or Δ following treatments) has more variables than resulting observations (here represented by N₂O emissions), and when multi-collinearity is expected among predictors (Tenenhaus et al., 2005), which is the case here. PLS is also generally preferable in circumstances in which assumptions of multivariate normality cannot be made but data can be standardized (Esposito Vinzi, 2010). In our analysis, both predictors and response were standardized (centered and scaled to have mean 0 and standard deviation 1) prior to PLS analysis, to ensure that the criterion for choosing the most important factors driving N₂O emissions is based on how much variation they explain when having the same weight.

Table 6.3. Results of simple linear regression of cumulative N₂O emissions (as ng N₂O-N g⁻¹ soil) against iron, across ten soils and under 12 different conditions. The first value given is that of r², and the second value is the slope of the regression. NS = regression was not significant for either iron index. WHC = water holding capacity; FeA = acid hydroxylamine-extractable iron; FeP = pyrophosphate-extractable iron.

	50% WHC	50% WHC + compost	100% WHC	100% WHC + compost
No fertilizer	NS	FeP: 0.37, 0.38	FeA: 0.12, -0.09	NS
Ammonium	NS	FeA: 0.28, -0.20	FeP: 0.62, 11.9	FeA: 0.23, -0.62
Nitrate	FeP: 0.19, 0.46	NS	FeP: 0.16, 2.1	NS

Study 1: Effect of Compost on N₂O Emissions Across a Range of Agriculture Soils

Table 6.4 shows that compost application, water content, and N fertilization significantly affected N₂O emissions, with no interactions observed among the applied treatments. However, significant interactions occurred between treatments and soils. In Figure 6.1, the results indicate how treatments affected cumulative N₂O emissions in each soil studied. Compost application statistically significantly increased N₂O emissions in soils S1, S3, CL2, and SC1. In these soils, the increase in N₂O emissions due to the compost application was equivalent to 0.05, 0.26, 0.41, and 0.12 percent conversion of the OIN present at the start of the incubation, respectively. In soils S2, S4, and CL1, compost application decreased N₂O emissions, and the decrease in N₂O emissions was equivalent to 0.52, 1.4, and 0.61 percent of the total OIN present at the start of the incubation, respectively (Figure 6.1a). With exception of soils S1, L1, and C1, much higher N₂O emissions were observed with increased water availability (100 percent versus 50 percent WHC; Figure 6.1b). In all soils except in L1 and CL1, the application of (NH₄)₂SO₄ significantly increased N₂O emissions while no significant effects of KNO₃ application were observed compared to non-fertilized soil (Figure 6.1c). The highest N₂O emissions occurred in soil fertilized with (NH₄)₂SO₄ under high moisture content (100 percent WHC) (Figure 6.1a and b).

The results show that compost application promoted N₂O emissions in soils S1, S3 (sandy loam), CL2 (clay loam) and SC1 (silty clay), suggesting that in soil with low OIN (<6 µg g⁻¹) and low background N₂O emissions (< 79 ng g⁻¹), compost application promotes N₂O emissions. N₂O emissions from soil are mainly the result of ammonium oxidation (nitrifier nitrification, nitrifier denitrification, and nitrification coupled denitrification) and denitrification (Wrage et al., 2001). Increased N₂O emissions in soils with low OIN likely occurred as a result of the compost eliminating the N and C substrate limitation for ammonium oxidation and denitrification. Decreased N₂O emissions by compost application compared to no compost application were observed in soils S2, S4 (sandy), and CL1 (clay loam). The decrease in N₂O was significantly larger than the increase in N₂O due to compost addition in S1, S3, CL2, and SC1 soil (Figure 6.1a), indicating that it is not possible to draw general conclusions based solely

on soil texture. Compost application is known to have a substantial effect on N₂O production pathways (Alluvione et al., 2010; Dalal et al., 2010). The application of compost influences several edaphic factors that control N₂O emission pathways, such as soil organic C availability, N availability, microbial activity, soil pH, and metal (i.e., Fe) content (Inubushi, 2000; Wright et al., 2008). In this study, the application of compost increased soil organic C availability (DOC), which could stimulate soil respiration and consume O₂ in soil (Contreras-Ramos et al., 2009), promoting N₂O emissions from nitrifier denitrification and denitrification (Bollmann and Conrad, 1998; Wrage et al., 2001). However, it is well known that reductions in soil O₂ also favor reduction of N₂O to N₂ (Firestone et al., 1980) and that increasing soil C availability stimulates IN immobilization by soil microorganisms. As a result, less N₂O might be emitted from some soils amended with compost, despite increased nitrifier denitrification. The results show that depending on the interplay of these controlling factors, divergent effects can be expected from compost application on N₂O emissions.

Table 6.4. Effects of soil, compost, water content, and nitrogen (N) fertilization on cumulative N₂O emissions.

Source	DF	Sum of Squares	F Ratio	Prob > F
Soil	9	70.85	9.46	<.0001*
Compost	1	9.35	11.24	0.0009*
Water Content	1	14.18	17.05	<.0001*
N Fertilization	2	98.34	59.11	<.0001*
Soil-Compost	9	6.08	0.81	0.605
Soil-Water Content	9	27.33	3.65	0.0003*
Soil-N Fertilization	18	23.8	1.59	0.063
Soil-Compost-Water Content	9	11.64	1.56	0.130
Soil-Compost-N Fertilization	18	25.45	1.70	0.040*
Soil-Water-N Fertilization	18	12.61	0.84	0.649
Compost-Water Content	1	1.15	1.39	0.240
Compost-N Fertilization	2	2.12	1.28	0.281
Water content-N Fertilization	2	1.67	1.01	0.368
Compost-Water Content-N Fertilization	2	1.28	0.77	0.466
Soil-Compost-Water Content-N Fertilization	18	14.35	0.96	0.509

* Significant at the 0.05 probability level.

Contrasting with compost application, the significant increase in N₂O emissions with increased soil moisture are consistent across soils, suggesting that the process of N₂O emissions is controlled by O₂ diffusion in soil and availability of substrates for microbial activity (Stark and Firestone, 1995). Traditionally, it has been assumed that with

increasing soil moisture and restricted O₂ diffusion into the soil, anoxic microbial activity is increased (Renault and Sierra, 1994) and as a result, emissions of N₂O derive mostly (or exclusively) from microbial-driven denitrification (Abbasi and Adams, 2000). However, we observed consistent and significantly greater N₂O emissions in soils fertilized with (NH₄)₂SO₄ than in those fertilized with KNO₃, even under high moisture content (100 percent WHC) (ranging from a three-fold to 44-fold increase, Figures 6.1a and b). These results indicate that ammonium oxidation, rather than denitrification, is the predominant process of N₂O production in soil with limited O₂ availability. This notion has been previously supported by Bremner (1979) and could be explained by nitrifier denitrification, a process promoted by ammonia-oxidizing bacteria, which uses nitrite (NO₂⁻) instead of O₂ as a terminal electron acceptor, reducing NO₂⁻ to N₂O (Goreau et al., 1980; Poth and Focht, 1985).

The original edaphic (pre-treatment) properties vary widely with soil as shown in Table 6.1. The most variable soil properties include clay, IN, and DOC. Among the soil variables, pH, DOC, and IN could change by an unknown amount following application of treatments; therefore, these variables were measured again after the incubation. Changes in these variables during the incubation could, in turn, influence N₂O emissions. A full factorial analysis testing the effect of compost application, water content, N fertilization, and the interactions among them, on soil pH, DOC, and IN, shows that all treatments significantly affected these variables, but no significant interactions (with the exception of water*compost effect on DOC) were observed among treatments (Table 6.5). The application of compost significantly increased soil pH and DOC across all soils, but soil pH decreased following (NH₄)₂SO₄ application, and lower pH was observed in 50 percent WHC compared to 100 percent WHC. Applied N fertilizer, regardless of its form, significantly increased levels of IN in soils. A larger increase in IN was found under drier conditions (50 percent WHC), but compost application significantly decreased total IN concentration.

Fig. 6.1. Quantifying the effects of compost application, water content, and nitrogen fertilization on nitrous oxide emissions in ten agricultural soils.

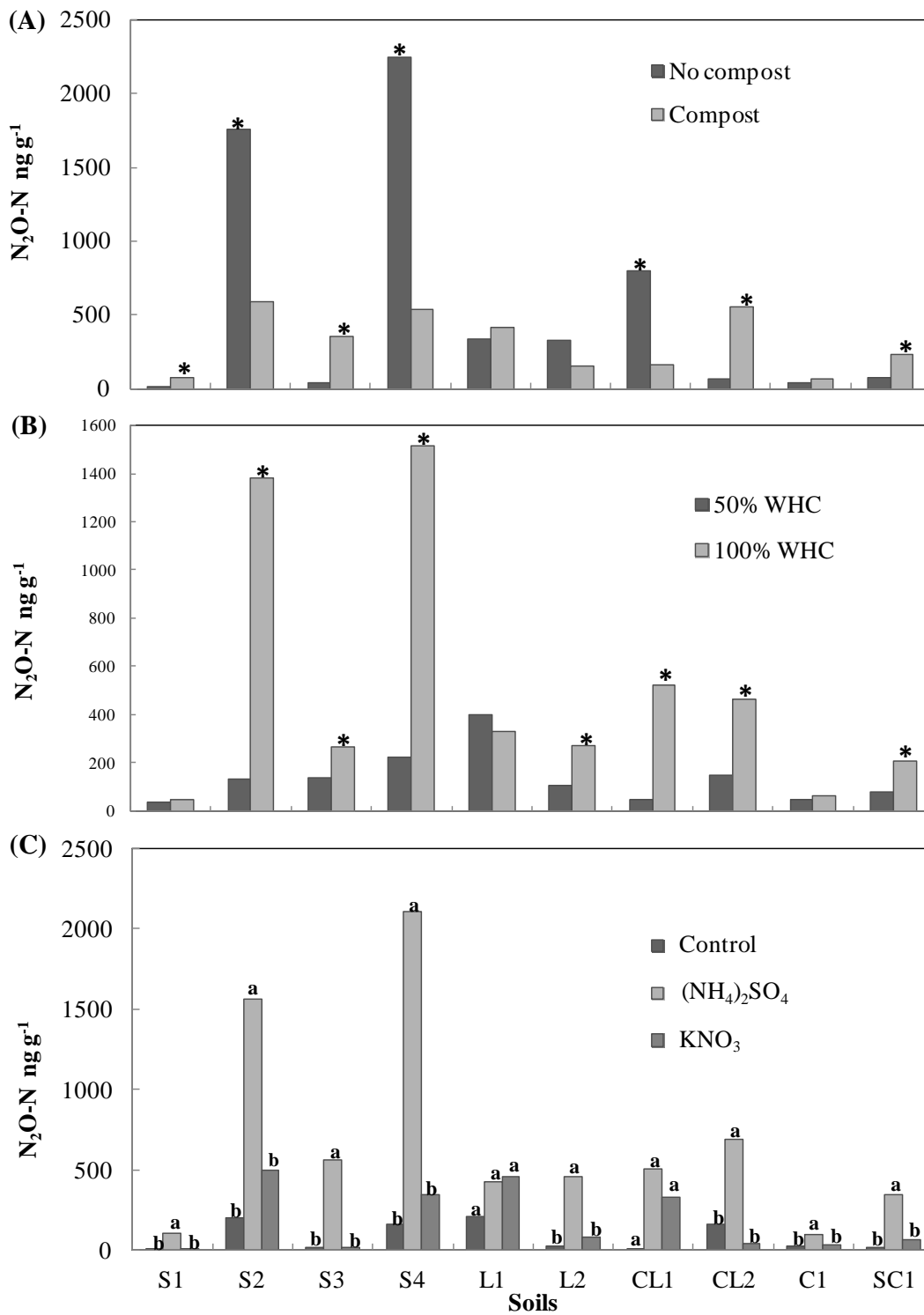


Table 6.5. The effect of compost, water content, and N fertilization and their interaction on soil pH, DOC, and IN. Effects are shown as NS=Not Significant, * P<0.05, ** P<0.01 and * P<0.001.**

Treatment	Level	ΔpH^a	$\Delta\text{DOC } \mu\text{g g}^{-1}$	$\Delta\text{IN } \mu\text{g g}^{-1}$
Compost	No compost	-0.08±0.00	0.41±0.24	58.09±0.26
	Compost	0.47±0.00	74.24±0.14	49.68±0.26
Water content	50% WHC	0.10±0.00	29.49±0.24	62.07±0.26
	100% WHC	0.22±0.00	41.84±0.14	50.33±0.26
N fertilization	Control	0.32±0.00	38.17±0.09	-2.31±0.08
	(NH ₄) ₂ SO ₄	-0.16±0.00	32.35±0.14	79.81±0.14
	KNO ₃	0.33±0.00	36.47±0.10	91.09±0.13
Compost		***	***	***
Water content		**	***	***
N fertilization		***	NS	***
Compost*Water content		NS	*	NS
Compost*N fertilization		NS	NS	NS
Water content*N fertilization		NS	NS	NS
Compost*Water content*N fertilization		NS	NS	NS

^a Δ measured as the difference between values obtained post-treatment and measured original soil conditions (Table 6.1).

Original Soil Properties and Change in Response to Applied Treatments

The soils used in this study were collected from different agricultural areas under different climatic and geomorphological conditions. Therefore, intrinsic properties related to soil genesis and development, such as texture, Fe content, and levels of DOC and IN vary widely with soil type. Lower soil pH was observed in 50 percent WHC compared to the soil pH in 100 percent WHC treatment, which suggests that nitrification is stronger in drier conditions, as nitrification contributes to increases in soil acidity (reduces pH) (Mulvaney et al., 1997). Soil IN and DOC were also significantly influenced by compost application, water content, and N fertilization. The application of compost not only added DOC but also added IN to soils (Table 6.1). However, IN content at the end of incubation was lower in compost treatments compared to no compost treatments. This could be explained by two factors. First, the application of compost promoted N gas loss due to rapid consumption of oxygen by microbial respiration (Vaughan et al., 2011), as well as an increase in soil pH (Venterea, 2007).

Second, more added IN was immobilized by microbial biomass as more DOC was available (Hood et al., 2000; Seligman et al., 1986). Less IN was found after incubation at 100 percent WHC compared to 50 percent WHC, probably because greater N gas loss happened in wet soil than in dry soil (Figure 6.1b).

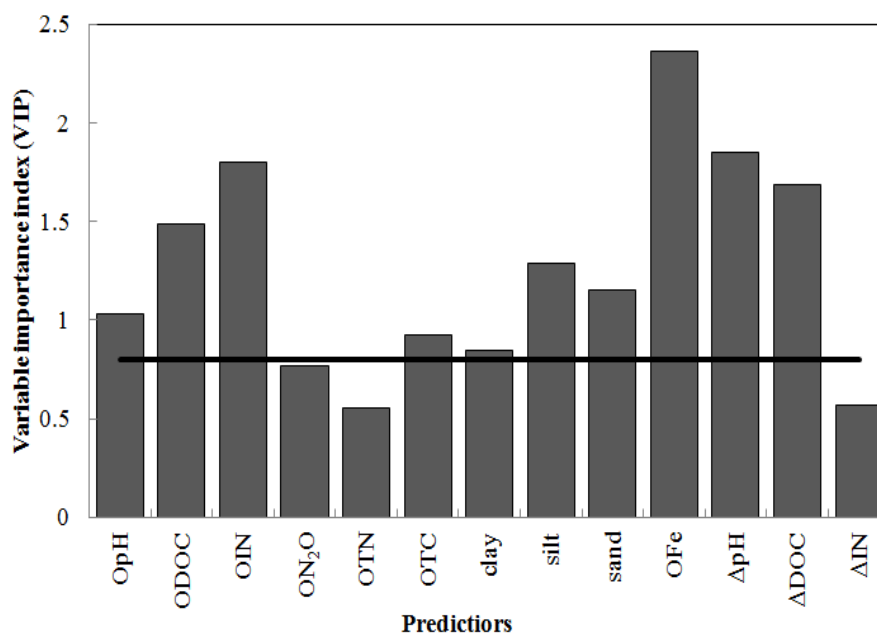
Key Soil Properties Driving N₂O Emissions

The PLS multivariate analysis generated a variable importance plot (VIP), which describes the relative importance of each measured variable in explaining total N₂O emissions across all studied soils. The contribution of each variable is compared with a significance coefficient (0.8) (Wold, 1995) represented by the black line in Figure 6.2. Any variable in which the explanatory power represented by the VIP value goes above the black line is considered significant in the multivariate PLS model. In the analysis, background N₂O emissions (ON₂O), levels of OTN, and Δ IN were not considered significant in explaining emissions. All other variables [OpH, ODOC, OIN, OTC, OFe, clay, silt, sand, Δ pH and Δ DOC] were significant. Five variables—namely OFe, Δ pH, OIN, Δ DOC, and ODOC—collectively explain more than 75 percent of the variation in N₂O emissions across soils.

The results show that the influence of treatments on total N₂O emissions varied in different soils. Inherent soil properties, combined with the properties that changed following treatments, contributed to these results. Following the dynamics of certain key variables can aid in explaining mechanisms of N₂O generation under a variety of conditions. Rather than use a traditional time course of measurements, which would involve many data points, an approach to “follow the dynamics” of certain variables was used to quantify how these variables changed during the experiment as an indicator of a soil’s response to specific conditions. The measured values of these responses were included as variables alongside initial soil properties in the analysis of relative predictive ability. Some of these incubation-induced changes in properties turned out to be important in explaining N₂O emissions (Figure 6.2). From all measured parameters integrated across all soils, the main variables affecting N₂O emissions were, in increasing order of importance, ODOC < Δ DOC < OIN < Δ pH < OFe. Typically, the variables described as major regulators in N₂O emissions from soils are soil texture, soil organic C, soil pH, and N form and availability (Bouwman et al., 2002b; Stehfest and Bouwman, 2006). While these results support that these variables significantly affect N₂O emissions, rather surprisingly, OFe (traditionally omitted from analysis of N₂O emissions in agricultural soils) appears as the most important soil variable affecting N₂O emissions. The result from linear regression analysis shows that the amount of OFe was significantly positively correlated with N₂O emissions (slope = 0.53, F ratio = 4.60, P = 0.03). The impact of Fe (as pyrophosphate-extractable Fe, which represents iron complexed with soil organic matter) can be explained by abiotic and biotic potential mechanisms. On the abiotic aspect: (i) the reaction of ferric iron (Fe³⁺) with reactive nitrification intermediates such as hydroxylamine can yield N₂O or N₂ as the oxidation product depending on the relative concentration of Fe³⁺ to hydroxylamine (Bengtsson et al., 2002); (ii) chemical nitrite reduction by ferrous iron (Fe²⁺) can also yield N₂O (Kampschreur et al., 2011). On the biotic aspect, it is widely known that Fe is contained

in metalloenzymes involved in N₂O production (Glass and Orphan, 2012). The ability of microorganisms to acquire Fe consequently influences the amount of N₂O produced. The application of compost increased soil pH, which could have the potential to decrease the availability of Fe. However, compost also brought Fe into soil (34 μg g⁻¹ dry soil), even though the same amount was added across all soils. In either case, the OFe content of the soils studied here appears to be a more important regulator of N₂O emissions than other properties traditionally considered as the main regulators of N₂O production in soil (e.g. pH, DOC, texture), and thus the role of Fe should be further investigated in future studies.

Fig. 6.2. Quantifying the effects of compost application, water content, and nitrogen fertilization on nitrous oxide emissions in ten agricultural soils. The contribution of each variable is compared with a significance coefficient (0.8) represented by the solid line (Wold, 1995).



Regarding the other most important variables, DOC, which here was increased by compost application and water content in all soils, could increase N₂O emissions by stimulating microbial activity (Fortuna et al., 2012), limiting O₂ availability for nitrifiers and denitrifiers (Coyne and Tiedje, 1990; Goreau et al., 1980), decreasing N₂O emissions by promoting IN immobilization by microbial biomass (Hood et al., 2000; Seligman et al., 1986), or by increasing the reduction rate of N₂O to N₂ (Firestone et al., 1980). Indigenous IN was a more important factor driving N₂O emissions than the increase in total IN caused by fertilization treatments. At the end of the incubation, there was no significant difference in soil IN between (NH₄)₂SO₄ and KNO₃ treatments, whereas N₂O emissions were significantly increased by the application of (NH₄)₂SO₄ compared to KNO₃.

Study 2: The Source of N for Production of N₂O in Compost-Amended Soils

In Study 2, the influence of green material compost application and N fertilizer types on the sources of N₂O production in four types of agricultural soils was investigated. To estimate the contribution of soil, fertilizer, and compost N to N₂O production, a stable isotope (¹⁵N) method was used combined with lab incubations. Based on ¹⁵N-labeling method, the study also addressed the relative importance of heterotrophic denitrification and ammonia oxidation to total N₂O production as affected by the green material compost soil amendment. It was hypothesized that green material compost amendment would promote N₂O emissions and that compost N could be a significant source for its production. Furthermore, it was hypothesized that the application of green material compost would promote N₂O production from both heterotrophic denitrification and ammonia oxidation, while ammonia oxidation will be the major pathway of N₂O production in the soil amended with ammonia-based fertilizer. The overall purpose of this study was to improve the understanding of how N₂O production is regulated by green material compost application. Such information could be used in designing agricultural and waste management strategies with the goal of mitigating N₂O emissions.

Inorganic N Concentrations, Net Nitrification, and Gross N Mineralization

The dynamics of the soil inorganic N concentration during the 14-day incubation are shown in Figure 6.3. In S1 (sandy soil), the NH₄⁺ concentration remained almost constant in the (NH₄)₂SO₄ treatment, whereas it significantly decreased when compost was applied to the soil. In S4 (sandy soil) and all the clay loam soils (CL1 and CL2), the NH₄⁺ concentration decreased in both compost + (NH₄)₂SO₄ and (NH₄)₂SO₄ only treatments. The NO₃⁻ concentrations showed a significant increase in all the compost + (NH₄)₂SO₄ and (NH₄)₂SO₄ treatments, except in the S1 soil amended with (NH₄)₂SO₄ treatment.

Gross mineralization and net nitrification rates were significantly higher in the compost-amended soils than in the non-compost-amended sandy soils, whereas this significant difference was not found in the clay loam soils (Table 6.6). In the non-compost treatment, the net nitrification rate remained almost constant or increased in all the soils until day 3 after the onset of incubation, and then sharply decreased. In the compost treatment, however, this sharp decrease was only found in the clay loam soils. The gross N mineralization rate was 50 percent lower in S1 sandy soil compared to that in the other soils (average 2.41 μg g⁻¹ d⁻¹). The net nitrification rate in CL2 clay loam soil was at least twice as large as, and significantly greater than, that in any of the other soils, while the S1 soil had a significantly lower net nitrification rate than that in S4 and CL1 soils.

In the sandy soils (S1 and S4), the compost significantly increased soil pH, which can lead to increased nitrification rates (Goodroad and Keeney, 1984). Moreover, the application of compost added Fe into soil (200 ug Fe g⁻¹soil), an essential co-factor for

the transfer of electrons in enzymes participating in nitrification (Davidson, 2011; Glass and Orphan, 2012; Meiklejohn, 1953). The net nitrification rate was significantly greater in the clay loam soils (CL1 and CL2) than in the sandy soils, likely due to the soil clay content, which can affect soil nitrifier populations

Figure 6.3 Change in NH_4^+ and NO_3^- concentrations over incubation time in different soils incubated with or without compost, and with different N fertilizer type. As observed, concentrations after addition of labeled or unlabeled N were equivalent; results were grouped. Vertical bars represent standards error.

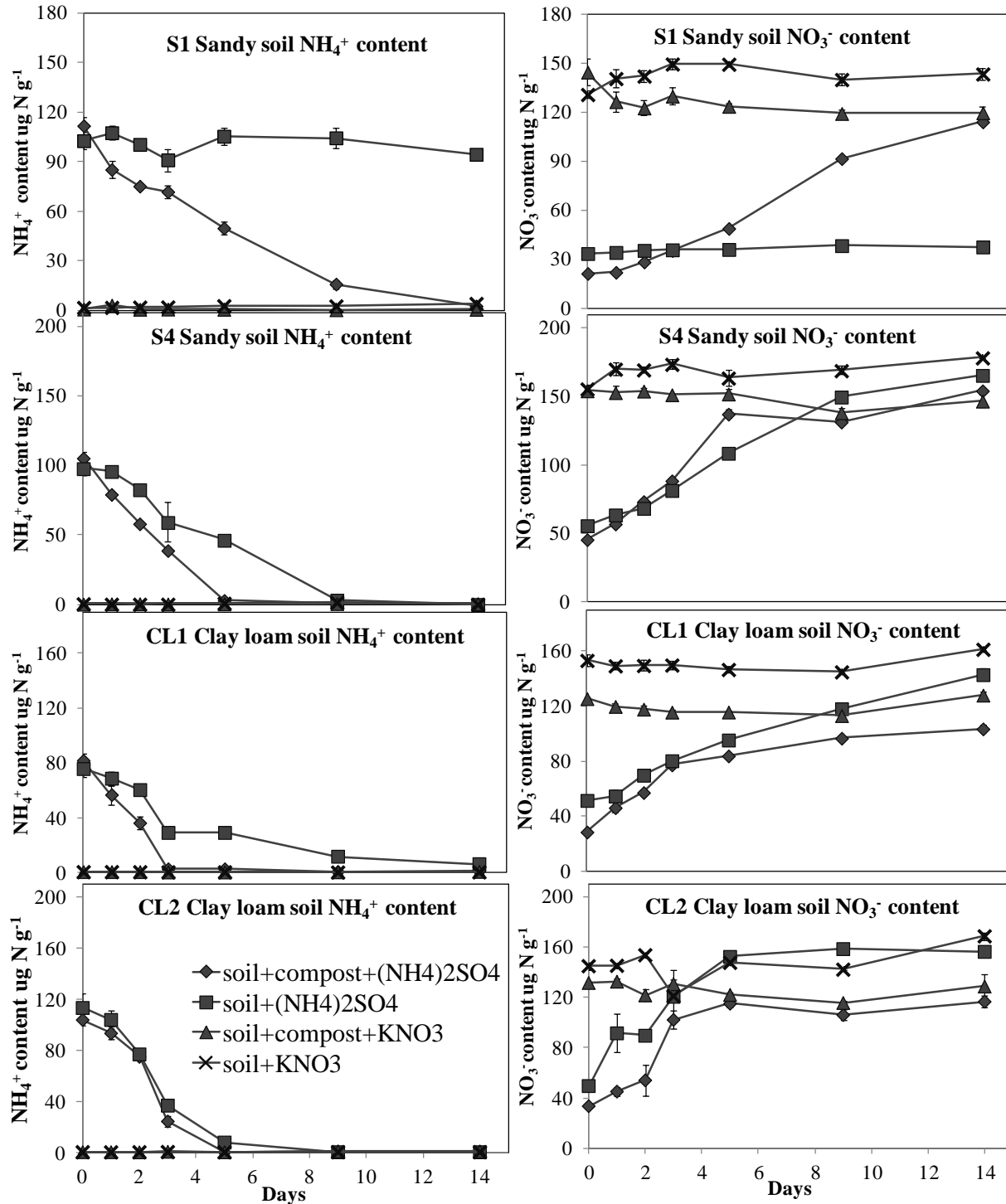


Table 6.6. Soil gross mineralization and net nitrification rates in soils during the incubation period. For each N transformation variable in each soil, different uppercase letters indicate a significant difference between compost treatments within each incubation period, whereas different lowercase letters indicate significant differences among incubation periods (P <0.05); n = 4.

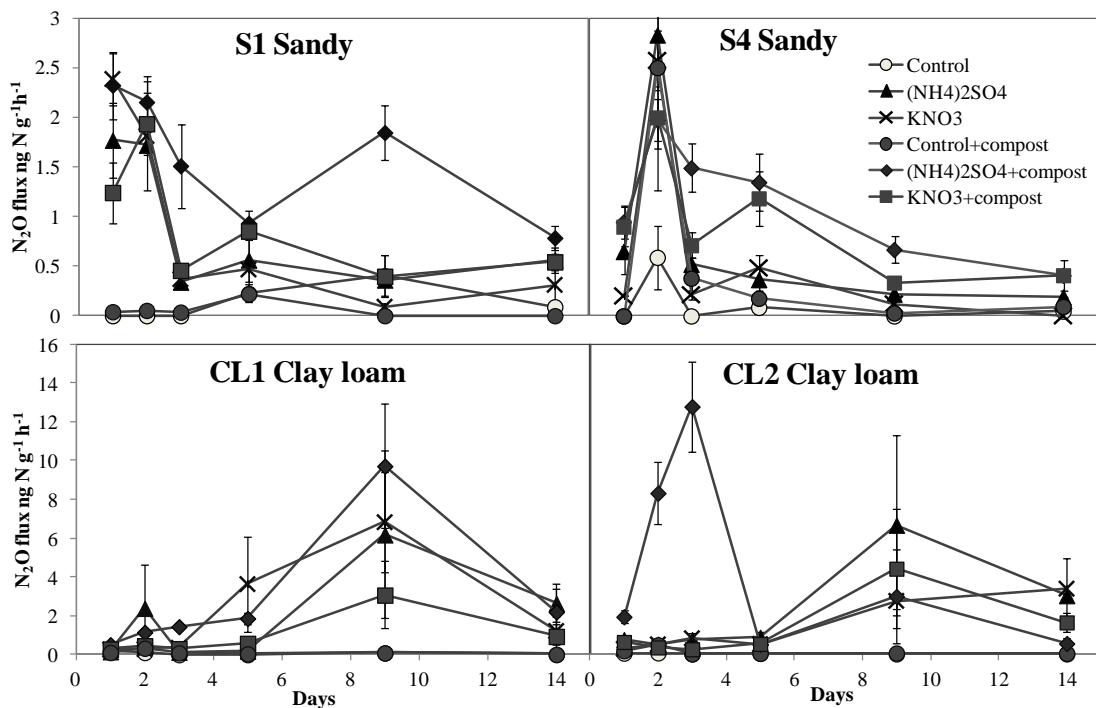
Soil type	Period (Days)	Gross mineralization rate (ug/g-d)						Net nitrification rate (ug/g-d)					
		Non-compost			Compost			Non-compost			Compost		
S1 Sandy	0-1	0.45	±	0.16Bb	3.67	±	0.64Aa	1.46	±	0.39Ba	4.55	±	0.60Aab
	1-2	0.53	±	0.23Bb	3.67	±	1.00Aa	1.27	±	0.45Ba	6.32	±	0.91Aa
	2-3	0.93	±	0.09Ba	1.81	±	0.11Ab	1.63	±	0.86Ba	6.63	±	0.74Aa
	3-5	0.62	±	0.01Bb	2.24	±	0.35Aab	0.34	±	0.17Bb	5.59	±	1.26Aab
	5-9	0.56	±	0.01Bb	1.32	±	0.20Ab	0.15	±	0.07Bb	2.67	±	0.06Abc
	9-14	0.33	±	0.04Bb	1.59	±	0.52Ab	0.07	±	0.01Bb	0.90	±	0.11Ac
S4 Sandy	0-1	0.38	±	0.15Bb	3.87	±	1.03Ab	7.83	±	1.36Ab	11.44	±	2.07Aa
	1-2	0.36	±	0.15Bb	3.19	±	0.60Ab	4.82	±	0.89Bc	16.40	±	1.41Aa
	2-3	0.42	±	0.09Bb	1.89	±	0.11Ac	13.09	±	0.64Aa	15.15	±	3.24Aa
	3-5	0.45	±	0.11Bb	14.43	±	1.64Aa	6.80	±	0.72Bb	12.19	±	1.10Aa
	5-9	5.79	±	0.66Aa	3.21	±	0.71Ab	2.57	±	0.16Bc	0.09	±	0.02Ab
	9-14	0.50	±	0.12b	ND			0.63	±	0.19Ad	0.91	±	0.05Ab
CL1 Clay loam	0-1	2.63	±	1.27Aa	4.44	±	1.27Aa	11.51	±	2.53Aa	17.70	±	2.53Aab
	1-2	1.78	±	0.06Aab	5.36	±	3.18Aa	15.11	±	4.49Aa	15.74	±	1.93Ab
	2-3	0.78	±	0.13Ab	3.19	±	1.16Aa	10.52	±	1.24Aa	20.10	±	3.43Aa
	3-5	0.68	±	0.21Ab	1.10	±	0.40Ab	3.77	±	0.77Ab	1.64	±	0.69Ac
	5-9	1.47	±	0.32Aab	1.58	±	0.42Ab	1.42	±	0.29Ab	0.81	±	0.02Ac
	9-14	0.57	±	0.17b	ND			0.99	±	0.24Ab	0.27	±	0.18Ac
CL2 Clay loam	0-1	2.24	±	1.40Aa	3.44	±	0.85Aab	17.10	±	0.73Ac	15.00	±	0.53Ab
	1-2	2.02	±	0.60Aa	1.41	±	0.46Ab	25.94	±	2.05Ab	26.54	±	0.75Aa
	2-3	3.18	±	0.55Aa	5.95	±	3.31Aa	30.95	±	1.61Aa	48.02	±	12.32Aa
	3-5	1.08	±	0.61Aa	2.54	±	1.31Aab	7.91	±	0.79Ad	4.55	±	1.69Ac
	5-9	0.32	±	0.11Ab	0.86	±	0.42Ab	0.62	±	0.35Ae	1.23	±	0.30Ac
	9-14	ND			ND			0.26	±	0.05Ae	0.68	±	0.20Ac

(Fortuna et al., 2012). Nitrifier populations inhabit surfaces of clays to protect themselves from, and minimize the effects of, H⁺ produced by ammonia oxidation (Powell and Prosser, 1991).

Production of N₂O

Addition of compost and N fertilizer to soil had a substantial effect on N₂O emissions (Fig. 3.4, Table 6.7), in agreement with previous studies (Alluvione et al., 2010; Dalal et al., 2010). Nitrous oxide emitted from the different treatments fluctuated significantly. In the S1 and S4 soils, the N₂O flux from the (NH₄)₂SO₄ + compost-amended treatments was an average four times higher than that from all other treatments on days 3 and 9 (P<0.05). In the S4 soil, the N₂O from all treatments reached their maximum fluxes on day 2 and began to decrease. However, in the CL1 and CL2 soils, the greatest N₂O fluxes from all treatments were measured on day 9, except that the N₂O flux from the (NH₄)₂SO₄ + compost treatment in the CL2 soil occurred on day 3. By day 14, the N₂O flux in all soils was relatively low from all treatments.

Figure 6.4. Dynamics of soil N₂O emissions under various compost and fertilizer treatments.



The cumulative N₂O emissions during the 14 days of incubation are shown in Table 6.7. The application of fertilizer significantly promoted N₂O emissions from all soils, with the total N₂O emitted from the (NH₄)₂SO₄ treatment averaging 1.8, 1.3, 2.2, and 2.0 times greater than that emitted from the KNO₃ treatment in S1, S4, CL1, and CL2 soil, respectively. The total N₂O emissions from the compost treatment was 1.9 times higher than that from the non-compost treatment in both S1 and S2 sandy soils, whereas no significant difference was found between compost and non-compost treatments in CL1 and CL2 clay loam soils (Table 6.7).

Table 6.7. Cumulative N₂O emissions from different treatment during incubation period. For each soil, different uppercase letters indicate a significant difference in total N₂O emission between fertilizer treatments for the same compost level. Different lowercase letters indicate a significant difference in total N₂O emissions between compost treatments for the same fertilizer type.

Soils	Treatment	No compost			Compost		
S1 Sandy	Control	0.01	±	0.00Ca	0.00	±	0.00Ca
	(NH ₄) ₂ SO ₄	0.19	±	0.02Ab	0.45	±	0.05Aa
	KNO ₃	0.15	±	0.02Bb	0.21	±	0.01Ba
S4 Sandy	Control	0.07	±	0.04Bb	0.20	±	0.05Ba
	(NH ₄) ₂ SO ₄	0.16	±	0.01Ab	0.31	±	0.03Aa
	KNO ₃	0.12	±	0.01Bb	0.23	±	0.02Ba
CL1 Clay Loam	Control	0.01	±	0.00Ba	0.01	±	0.01Ca
	(NH ₄) ₂ SO ₄	0.90	±	0.55Aa	1.40	±	0.10Aa
	KNO ₃	1.10	±	0.35Aa	0.46	±	0.17Ba
CL2 Clay Loam	Control	0.02	±	0.01Ca	0.04	±	0.02Ca
	(NH ₄) ₂ SO ₄	1.01	±	0.12Aa	1.21	±	0.28Aa
	KNO ₃	0.58	±	0.08Ba	0.55	±	0.13Ba

Sources of N₂O from Heterotrophic Denitrification and Ammonia Oxidation

The fractional contributions of heterotrophic denitrification and ammonia oxidation to N₂O production were determined for all treatments (Figure 6.8). The 14-day incubation was selected since allowing more time would risk recycling N out of the microbial biomass due to turnover, resulting in a misinterpretation of the results. In the S1 soil, ammonia oxidation was the dominant source of N₂O. In the S4 soil, the fraction of the N₂O production due to ammonia oxidation was significantly higher than that from heterotrophic denitrification on days 3 and 4 in the compost treatments; in the non-compost treatment, this significant difference was observed on days 9 and 15. In the CL1 soil, the fraction of heterotrophic denitrification derived N₂O increased for the first nine days in the compost treatment and for the first three days in the non-compost treatment. In the CL2 soil, ammonia oxidation was the dominant source of N₂O, except on day 1 in the compost treatment and days 1, 3, and 14 in the non-compost treatment.

Cumulative N₂O emissions from heterotrophic denitrification and ammonia oxidation are shown in Figure 6.9. The application of compost significantly promoted N₂O from heterotrophic denitrification in sandy soils ($P < 0.05$), while this significant difference was not shown in the clay loam soils ($P > 0.05$). In the sandy soils amended with (NH₄)₂SO₄, the total N₂O emitted from ammonia oxidation was significantly increased by compost addition, which averaged 190 percent higher ammonia oxidation derived N₂O than that in the non-compost treatments. Greater N₂O emissions, derived from ammonia oxidation, were found in all the soils amended with (NH₄)₂SO₄ than in soils amended

with KNO_3 treatments, except in the C1 clay loam soil without compost application. The results showed that in most fertilizer treatments, more than 50 percent of total N_2O emissions were derived from ammonia oxidation (Figure 6.8 and 6.9).

Previous studies on N_2O soil emissions have identified soil moisture, oxygen content, and fertilizer types as main factors affecting the pathways for N_2O production (Bateman and Baggs, 2005; Bouwman et al., 2002; Zhu et al., 2013a). In this study, the soil water content was 60 percent of WHC, which may have resulted in less opportunity for heterotrophic denitrifiers to produce N_2O than nitrifiers (Bateman and Baggs, 2005; Davidson, 1991; Dobbie et al., 1999; Venterea et al., 2010; Zhu et al., 2013a), even under the soil conditions with sufficient NO_3^- and organic C for denitrification (Weier et al., 1993). Nevertheless, in the S4 soil without compost and the CL1 soil with compost, ammonia oxidation produced only 28 percent and 31 percent of all N_2O emissions, respectively (Figures 3.9 and 3.10). Besides soil moisture, other soil edaphic factors, such as soil DOC content and denitrifier or nitrifier populations, can also significantly affect the importance of which N_2O production pathway is active (Fortuna et al., 2012; Weier et al., 1993).

In summary, the application of compost significantly promoted N_2O derived from both heterotrophic denitrification and ammonia oxidation in sandy soils, whereas no significant effect was found in clay loam soils. In the sandy soil with compost treatments, the total N_2O derived from heterotrophic denitrification and ammonia oxidation was 2.2 and 3.2 times that in the non-compost treatments. Generally, nitrification is the main process under aerobic conditions, usually ≤ 60 percent WFPS, and denitrification is the dominant process under anaerobic conditions, usually > 80 percent WFPS (Linn and Doran, 1984). However, even under aerobic conditions, N_2O can be produced via the denitrification pathway due to the anaerobic microsites within soil aggregate (Renault and Sierra, 1994; Renault and Stengel, 1994) or fungi (Laughlin and Stevens, 2002; Zhang et al., 2011). In this study, the application of compost increased soil organic C availability, likely depleting soil O_2 due to biological O_2 demand (Contreras-Ramos et al., 2009) and consequently promoting both heterotrophic denitrification and ammonia oxidation (Bollmann and Conrad, 1998; Zhu et al., 2013a). The concentration of O_2 that evokes N_2O production via heterotrophic denitrification is relatively low (≤ 0.5 percent), while N_2O derived by ammonia oxidation significantly increases once the O_2 concentration goes lower than 21 percent (Khalil et al., 2004; Zhu et al., 2013a). Higher ammonia oxidation compared to heterotrophic denitrification was promoted by compost application. In contrast, more N_2O was derived from ammonia oxidation in the $(\text{NH}_4)_2\text{SO}_4$ treatment than in the KNO_3 treatment, whereas no difference in heterotrophic denitrification derived N_2O was found between these treatments, indicating that the increased NO_3^- concentration did not affect heterotrophic denitrification, probably because the soil conditions did not promote this N_2O production pathway (Thauer et al., 1977; Zhu et al., 2013a).

Figure 6.8. Fraction of the N₂O flux derived from denitrification and ammonia oxidation.

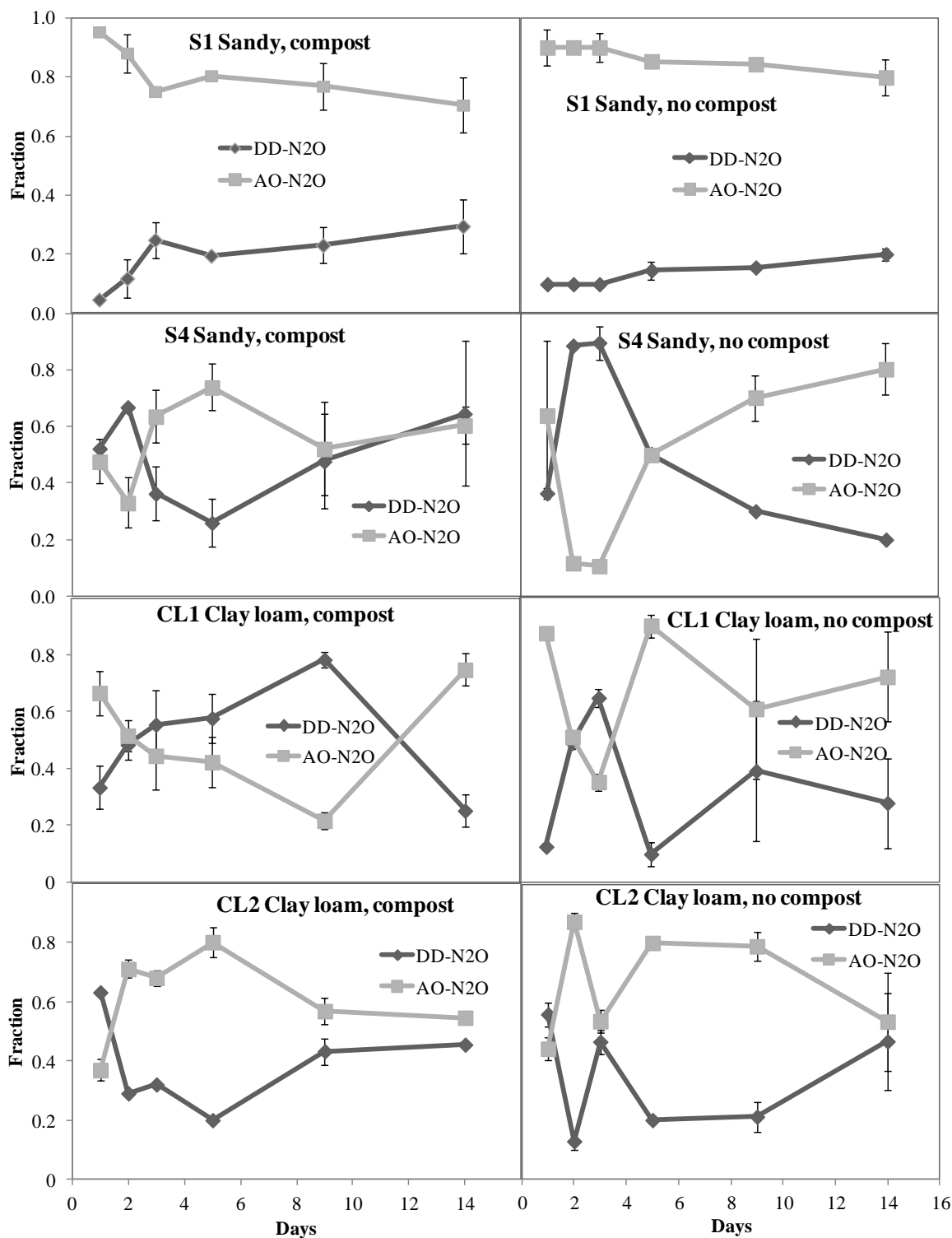
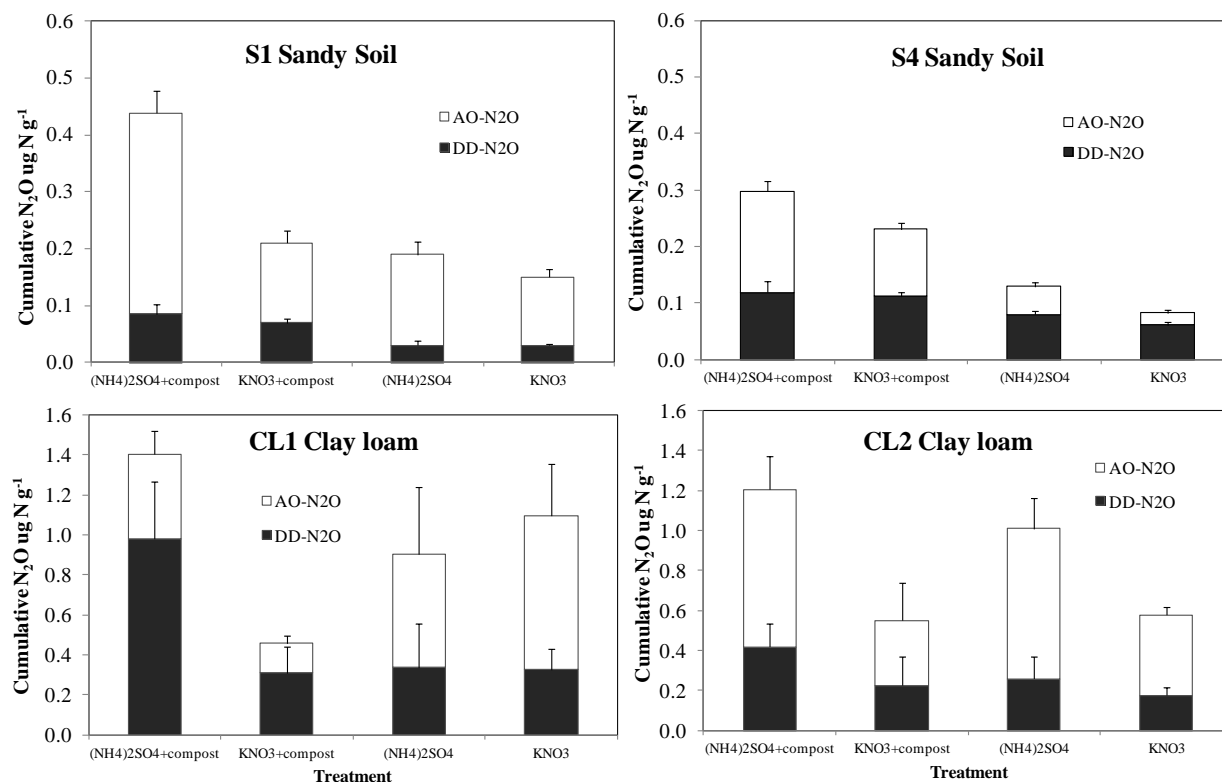


Figure 6.10. Total N₂O emissions from denitrification and ammonia oxidation in different soil types and treatments.



Quantifying the N₂O Emitted from the Soil, Fertilizer, and Compost Pools

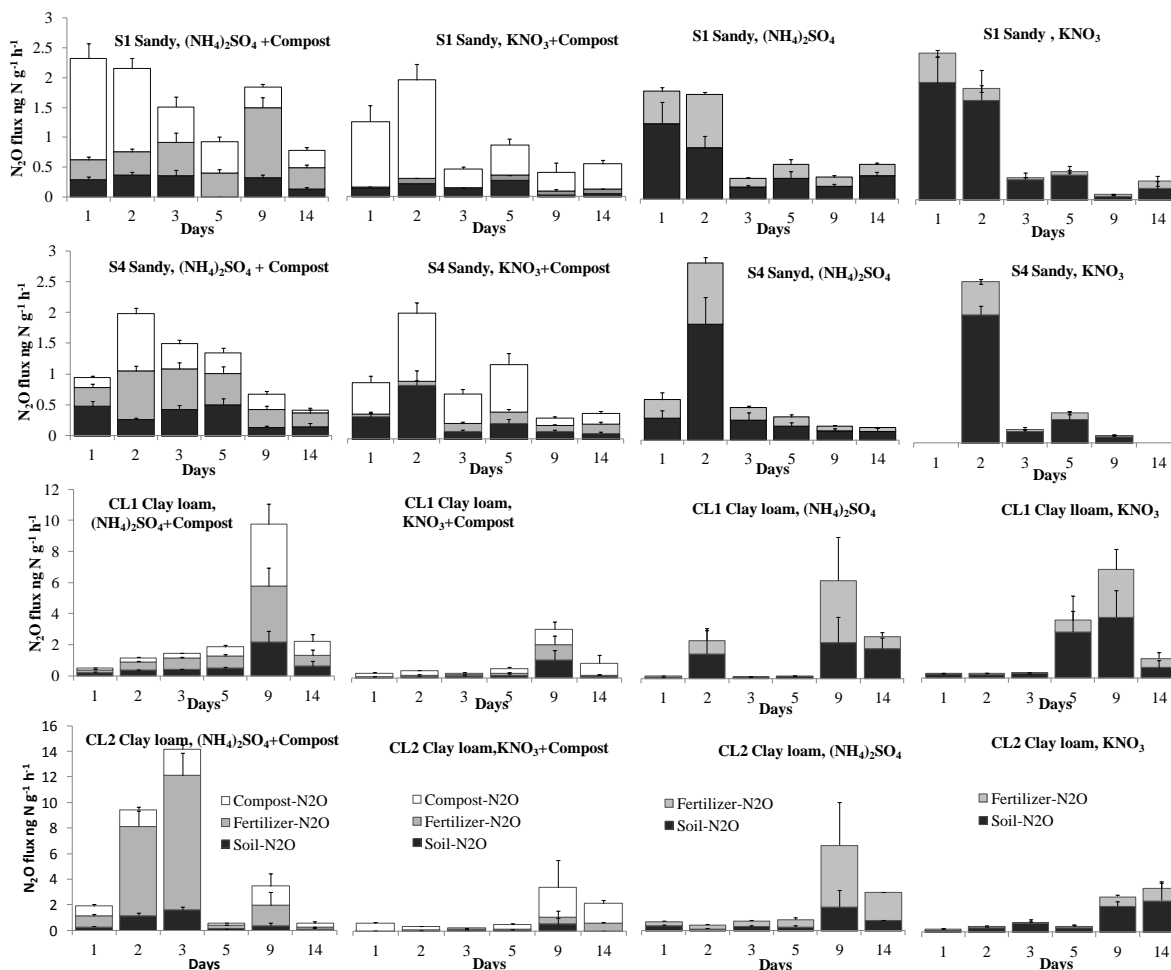
The contribution of soil, fertilizer, and compost N to N₂O flux were quantified for all treatments (Fig. 6.11). In the S1 soil, compost N was the dominant source of N₂O for the first five days in the (NH₄)₂SO₄ + compost treatment, while fertilizer N became the dominant source for the remainder of the incubation. In the S4 soil, more N₂O was produced from fertilizer N than from compost N on days 1, 3, 5, and 14 (*P*<0.05). In the CL1 soil, N₂O was mainly produced from fertilizer N in the (NH₄)₂SO₄ + compost treatment on days 2 and 3, while compost N was the dominant source on day 14. In the CL2 soil, fertilizer N was the dominant source of N₂O for the first five days, and then compost N became the dominant source on day 14. In all KNO₃ + compost treatment soils, compost N was the main source of N₂O emissions for the entire incubation, except on day 3 in clay loam soils. In the treatments without compost application, N₂O was only emitted from fertilizer and soil N. The dominant source of N₂O was soil N in sandy soils for the entire incubation, while fertilizer N was the main source of N₂O production in CL2 soil amended with (NH₄)₂SO₄.

Cumulative N₂O emissions from soil, fertilizer, and compost N are shown in Figure 6.12. In both the sandy and clay loam soils, compost N was a significant source of N₂O emissions. In the S1 and S2 soils amended with (NH₄)₂SO₄, the N₂O produced from fertilizer N were 2.6 and 2.2 times higher in the compost than in the non-compost treatment, while no significant effect was found in the sandy soils amended with KNO₃.

Meanwhile, 30 percent and 75 percent higher cumulative N₂O was found in the sandy soils amended with (NH₄)₂SO₄ than with KNO₃ in the non-compost and compost treatments, respectively. In clay loam soils, there was no significant effect of compost application on N₂O emitted from fertilizer N. In contrast, N₂O emitted from soil N decreased an average 59 percent after compost application. Fertilizer N was the main source of N₂O emissions in the CL2 soil amended with (NH₄)₂SO₄.

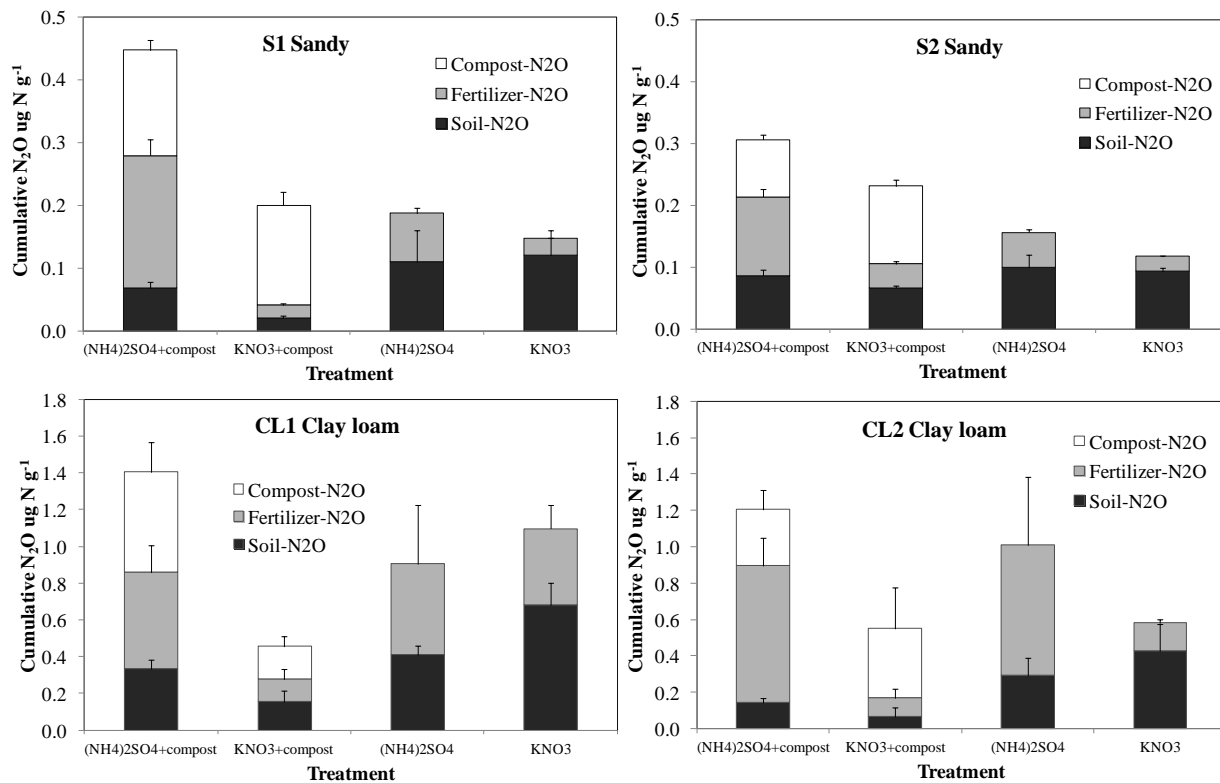
The application of compost introduced IN into soil (Table 6.1) and was a significant source of N for N₂O emissions, which contributed 26 to 76 percent to total N₂O emissions (Figure 6.12). The influence of compost application affects several edaphic factors that control N₂O emissions, such as soil organic C availability, N availability, microbial activity, and soil pH (Inubushi, 2000; Wright et al., 2008; Zhu et al., 2013c). In addition, these factors affecting N₂O emissions respond to soil conditions such as soil texture, soil moisture content, and soil IN form (Dalal et al., 2010; Inubushi, 2000; Mondini et al., 2007; Zhu et al., 2013c).

Figure 6.11. N₂O emissions from soil, fertilizer, and compost N in different soils and treatments.



In this study, 2.4 times higher N₂O emissions was derived from fertilizer N in the (NH₄)₂SO₄ + compost treatment than that in the (NH₄)₂SO₄ treatment in sandy soils. As discussed above, the application of compost could stimulate soil respiration and consume O₂ in soil (Contreras-Ramos et al., 2009), promoting N₂O emissions from NH₄⁺ based fertilizer via nitrifier denitrification (Zhu et al., 2013a). In addition, increased soil pH can result from compost application, which can increase NO₂⁻ accumulation from nitrification, which promotes N₂O production from NH₄⁺ fertilizer via nitrifier denitrification (Poth and Focht, 1985; Zhu et al., 2013a) or/and chemodenitrification (VanCleemput and Samater, 1996; Venterea, 2007; Venterea and Rolston, 2000). However, the application of compost had no effect on fertilizer-N derived N₂O when KNO₃ was applied. In the clay loam soils, the high clay content (Table 6.1), which relates to the buffer capacity of soil, may explain why there were no differences in N₂O derived from fertilizer N between compost and non-compost treatments. Nevertheless, less N₂O was derived from soil N in the compost treatments than in the non-compost treatments, suggesting that the microbes prefer to use N from compost instead of soil N.

Figure 6.12. Total N₂O emissions from soil, fertilizer, and compost N in different soil types and treatments.



Conclusions

The results of Study 1 show that compost application, water content, and N fertilization have important effects on N₂O emissions from agricultural soils. The application of compost increased N₂O emissions in soils with low N availability and low background N₂O emissions. For those soils in which the compost application caused a decrease in N₂O emissions, this decrease was larger than any of the increases caused by compost application. In soils fertilized with (NH₄)₂SO₄, N₂O emissions were greater than in soils fertilized with KNO₃, even under 100 percent WHC (from a three-fold to 44-fold increase). This indicates that ammonium oxidation is the main pathway of N₂O production under limited O₂ availability. Soil pH and DOC were increased whereas available N was decreased by compost application at the end of incubation. Among all studied variables, extractable Fe proved to be the most important factor regulating soil N₂O emissions, followed by ΔpH, available N, ΔDOC, and original DOC. These results indicate that to mitigate N₂O emissions, compost application should be avoided in high soil moisture conditions and in combination with NH₄⁺ fertilization events in soils with low background N₂O emissions, primarily sandy soils. The role of Fe as a regulator of N₂O production in soils should be further investigated.

In Study 2, the complex relationships between green material compost, N fertilizer type, and N₂O emissions were examined. In addition, the heterotrophic denitrification/ammonia oxidation pathways for N₂O production were examined. The results demonstrated that the application of compost increased nitrification rates and N₂O emissions from sandy soils while no significant effect was found in clay loam soils, confirming the results of Study 1. Greater N₂O emissions were observed in fertilizer treatments that received fertilizer in the form of NH₄⁺ compared to NO₃⁻ in sandy soils. Nitrous oxide production was mainly attributable to ammonia oxidation in sandy soils. In sandy soils, compost N was a significant source of N₂O emissions. In addition, the application of compost increased N₂O emitted from fertilizer N in the form of (NH₄)₂SO₄ in sandy soils whereas N₂O emitted from soil N was decreased by compost application. These results indicate that the source of N₂O emissions in sandy soils with compost applied is mainly from the compost itself. The application of green material compost in sandy soils should be avoided to reduce the environmental impact of green material compost and mitigate N₂O emissions from agricultural soil. This is especially true if the finished compost has a high level of ammonium. Further experiments over a longer period to investigate the potential of other soil types, different application rates of green material compost, and N fertilizer to N₂O emissions would be useful to extend this research.

Conclusions and Recommendations

The following are the major conclusions of the study:

1. The bulk of the data obtained in the chamber study of compost windrows falls within the range of previous emissions studies of these materials. Performing this experiment with different feedstock materials and during different seasons allowed the research team to obtain three seasonal fluxes. The findings suggest that environmental and seasonal influences, as well as composting process management, have a large impact on GHG emissions.
2. We used a modified chamber using a sweep gas to estimate CH₄ emissions from compost piles. Daily methane emissions ranged from about 30 ± 10 to 340 ± 120 grams CH₄ per day per dry weight ton of composted material depending on the season in which composting occurred. The low estimate represents emissions for the non-winter time periods of the year. The high estimate represents composting during the winter (wetter) pile where appropriate turning of the pile did not occur throughout the composting period and emissions spiked as a result of this situation. The winter pile was turned less frequently than the other seasonal piles due to lack of equipment accessibility for the compost windrow turner (scarab), resulting in a prolonged CH₄ emissions profile compared to the other seasonal piles and other published results. Therefore, two scenarios of CH₄ emissions are presented that reflect the results as collected, and one is presented that reflects the emissions profile expected to occur (a gradual decline or level response) during the latter stages of the composting in windrows (see details in table footnote below). Assuming approximately 150 compost facilities receive about 5.0 Mt of yard waste (wet wt.; 45% avg. moisture) per year currently, the total yearly emissions range from about 10,000 ± 1,400 Mg CH₄ per year (extrapolating assuming the winter pile was able to be turned appropriately) to 20,000 ± 6,100 Mg CH₄ per year (extrapolating using the raw winter pile data, which was not appropriately turned during the late stages of composting). The 2012 California Air Resources Board (CARB) estimate for CH₄ emissions from composting approximately 4.4 Mt green waste in California is 16,000 Mg per year (http://www.arb.ca.gov/cc/inventory/doc/docs4/4b_solidwastetreatment_composting_feedstockprocessed_ch4_2012.htm); the results reported in this study are comparable to CARB estimates. The average emissions factor for CH₄ in this study is 4.5 ± 0.12 grams per kilogram of material (wet weight). This compares favorably to 4.1 grams per kilogram from organic wastes (wet weight) reported by CARB (2012).
3. The same modified chamber with which we monitored CH₄ emissions was used to estimate N₂O emissions from three compost piles. Daily nitrous oxide emissions estimates ranged from about 240 ± 47 to 1,100 ± 300 mg N₂O per

dry weight of composted material. Assuming approximately 150 compost facilities in the state receive 5.0 Mt green waste (wet weight) per year, total annual N₂O emissions from composting of organic waste in this study were about 120 ± 20 tons per year, while the 2012 CARB estimates for N₂O emissions from composting organic waste in California are 362 tons per year (http://www.arb.ca.gov/cc/inventory/doc/docs4/4b_solidwastetreatment_composting_feedstockprocessed_n2o_2012.htm). The average emissions factor for N₂O in this study is 0.02 ± 0.0004 grams per kilogram of material (wet weight). This compares to 0.09 grams per kilogram from organic wastes (wet weight) reported by CARB (2012). For comparison, the total annual N₂O emission represents 0.25 ± 0.04 % of total N₂O agricultural soil management emissions annually in California.

4. The MMB approach results are only reported for Experiment I. Difficulties with equipment and data analysis prevented comparison for Experiment II. Data for Experiment III requires further analysis. Experiment 1 data are highly variable and dependent on consistent wind. In many data pairings, upwind N₂O measurements were higher than those downwind of the pile. Although overall MMB estimates for CH₄ and N₂O are 163 percent (62.9 kg t⁻¹ vs. 40 kg t⁻¹) and 261 percent (3,103 mg t⁻¹ vs. 1,189 mg t⁻¹) higher than estimates obtained using the chamber technique, direct comparison of the approaches is not validated here or anywhere in the literature. This approach requires further validation, particularly in order to measure N₂O emissions, before any conclusions may be drawn.
5. The ASP system produced similar CH₄ and N₂O emissions when compared to mechanically turned windrow composting. The ASP biofilter removal efficiency for CH₄ and N₂O was 73 ± 0.03 percent and 32 ± 0.05 percent, respectively, based on measured concentrations before and after biofiltration. This biofilter had open sides, however, and was subject to entrainment of ambient air, which could dilute emissions exiting the biofilter, leading to a potential overestimation of biofilter efficiency. In addition, the difficulty in sealing the bottom of the chamber on the coarse biofilter likely resulted in additional air from the top of the biofilter being drawn into the sampling chamber. Novel calculations, based in part on wind data and emissions measurements of ambient air, were devised to correct the biofilter exit GHG concentrations for entrainment of ambient air from both sources. These calculations revised the removal efficiency of the biofilter to 11 percent for CH₄ and 50 percent for N₂O. These calculations have not been validated, but suggest that as a GHG mitigation practice, biofilters may be more effective to reduce N₂O emissions than CH₄. Another consideration is that the biofilter examined was composed of wood chips designed originally to reduce VOC emissions. Additional research on biofilter substrates and system design could lead to further reductions of CH₄ and N₂O. However, since the emissions of N₂O and CH₄ from all composting sources are 0.2 to 1 percent or less of total statewide emissions, respectively, a greater implementation of

potentially improved ASP type systems would have a small overall effect on reducing both CH₄ and N₂O emissions statewide.

6. Suggested practices to reduce GHG emissions during composting in mechanically turned windrows and windrow systems would focus on improved aeration. Though ASPs theoretically should aerate piles more effectively than static windrows, preferential flow through the pile could occur, causing areas within the piles to become oxygen-deprived. Smaller piles (height by width) may produce fewer emissions. Some studies show the opposite suggesting this is an area where additional research is needed. In windrows, a smaller cross section would reduce the path length of fresh air moving through as a result of convective processes produced by the self-heating composting process. However, smaller piles may produce less total heat, retarding the convective flow process when compared to larger piles. Alternatively, aeration could be improved in negatively aerated static piles by running a perforated pipe through the pile and pumping in fresh air to combine with the existing convective flow. The additional aeration would likely reduce both CH₄ and N₂O emissions.
7. The application of finished yard trimmings compost as a soil amendment to agricultural lands was studied in tomato fields and almond orchards to determine whether it affected soil N₂O emissions. Overall, compost application to soils had no significant effect on N₂O emissions in tomato or almond systems. Though compost had no effect on N₂O emissions in the crops examined in this study, growers remarked they use compost for a variety of reasons, namely to improve soil properties. The most notable improvement after compost application was said to be a more even infiltration of irrigation water and greater soil water-holding capacity, which was perceived to increase irrigation efficiency. Second, growers remarked that crop growth was generally improved following compost applications, likely from the addition of a wide variety of macro- and micro-nutrients and the buildup of soil organic matter, which positively affects soil properties. The application of compost may help to promote crop resilience to variable climatic conditions of excessive growing season rainfall, and prolonged periods of high temperatures that will likely occur as California's climate changes.
8. Lab studies using ten different agricultural soils to assess the effect of compost applications on CH₄ and N₂O emissions were done to broaden the results of the field compost application studies. Two studies (1 and 2) were conducted to examine the interaction of compost with fertilizer nitrogen (N) and to determine the sources (fertilizer versus compost N) contributing to CH₄ and N₂O emissions. Methane was examined to determine whether compost-amended soils became a greater sink. Compost appeared to have no effect on CH₄ consumption. The results of Study 1 show compost application, water content, and N fertilization have important effects on N₂O emissions from

agricultural soils. The application of compost increased N₂O emission in soils with low N availability and low background N₂O emissions. These soils generally had higher sand contents. For soils in which the compost application caused a decrease (more clay fraction) in N₂O emissions, this decrease was larger than any of the increases caused by compost application across all soils. In soils fertilized with ammonium sulfate ((NH₄)₂SO₄), N₂O emissions were greater than in soils fertilized with potassium nitrate (KNO₃), even under 100 percent water-holding capacity (WHC; the maximum amount of water a soil can retain), resulting in a three-fold to 44-fold increase, indicating ammonium oxidation is the main pathway of N₂O production. Among all studied variables, extractable iron proved to be the most important factor regulating soil N₂O emissions, followed by changes in pH, available N, changes in dissolved organic carbon (DOC), and original DOC.

In Study 2, the complex relationships between green material compost, N fertilizer type, and N₂O emissions were examined. The results suggested the application of compost increased nitrification rates and N₂O emissions from sandy soils, while no significant effect was found in clay loam soils, confirming the results of Study 1. Greater N₂O emissions were observed in fertilizer treatments receiving fertilizer in the form of ammonium (NH₄; NH₄⁺) compared to nitrate (NO₃; NO₃⁻) in sandy soils, suggesting N₂O production was mainly attributable to ammonia oxidation in these soils. In sandy soils, compost N was a significant source of N₂O production. In addition, the application of compost increased N₂O emitted from fertilizer N in the form of (NH₄)₂SO₄ in sandy soils, whereas N₂O emitted from soil N was decreased by compost application. These results indicate that the source of N₂O emissions in sandy soils with compost applied is mainly from the compost itself. The results of the lab studies indicate that to mitigate N₂O emissions, if compost application is to be paired with fertilizer application, nitrate fertilizers are a better choice than ammonium. This is particularly true for sandy soils. In soils where there is an elevated background concentration of NH₄, compost application may elevate N₂O emissions due to ammonia oxidation during the nitrification process.

Overall, this study confirms that composting of green materials produces both CH₄ and N₂O. The results are comparable to other studies, though in general the number of total studies is limited. From the perspective of statewide emissions, the total estimated CH₄ and N₂O contributions from green material processing facilities is small, contributing less than 0.01 to 0.1 percent of total emissions for N₂O and CH₄, respectively. Although there were technical difficulties using the MMB approach in this application, this may be a method worth further study to capture a more complete profile of emissions in comparison to the standard chamber approach. The use of the finished compost as a soil amendment proved to have no effect on N₂O production at standard application rates in both research and farmer fields for tomato and almond crops. Lab studies indicated that sandy soils could be prone to increased N₂O emissions following the addition of compost compared to finer

textured loam and clay soils. In summary, composting of green materials and its use as a soil amendment are recommended to reduce waste and improve soil productivity.

Abbreviations and Acronyms

Δ	Calculated change
ASP	Aerated static pile
bLs	Backward Lagrangian stochastic technique
C	Carbon
CARB	California Air Resources Board
CH ₄	Methane
CO ₂	Carbon dioxide
CO ₂ -eq	Carbon dioxide equivalent
CV	Coefficient of variance
DOC	Dissolved organic carbon
DW; dry wt.	Dry weight
EBRT	Empty bed residence time
ECD	Electron capture detector
ECS	Engineered Compost Systems
Fe	Iron
FeA	Acid hydroxylamine-extractable iron
FeP	Pyrophosphate-extractable iron
FID	Flame ionization detector
GC	Gas chromatograph
GHG	Greenhouse gas
GWP	Global warming potential
HCl	Hydrochloric acid
HSD	Tukey's honestly significant difference
IN	Inorganic nitrogen
KNO ₃	Potassium nitrate
MMB; micro-met	Micrometeorological mass balance

N	Nitrogen
N ₂	Dinitrogen
NH ₃	Ammonia gas
NH ₄ ; NH ₄ ⁺	Ammonium
(NH ₄) ₂ SO ₄	Ammonium sulfate
NO ₃ ; NO ₃ ⁻	Nitrate
NO ₂ ⁻	Nitrite
N ₂ O	Nitrous oxide
NSL	Leslie J. Nickels Soil Laboratory
O ₂	Oxygen
ODOC	Soil original dissolved organic carbon
OFe	Soil original iron
OIN	Soil original inorganic nitrogen
ON ₂ O	Background N ₂ O emissions
OpH	Soil original pH
OTN	Soil original total nitrogen
OTC	Soil original total carbon
PCA	Principal component analysis
PLS	Partial least square
PFRP days	Process to further remove pathogen days
RE	Removal efficiency
RRSAF	Russell Ranch Sustainable Agricultural Facility
TCD	Thermal conductivity detector
VOC	Volatile organic compounds
UC	University of California
UV	Ultraviolet
VIP	Variable importance plot
WHC	Water-holding capacity

Appendices

A.2.1 Materials and Methods Supplemental Information

A.2.1.1 Flux Calculations

All GHG concentration data were converted into flux using EQ 2.4. The north, middle, and south replicate fluxes were averaged for each of the three differing locations: top, upper side, and lower side. The standard error for this average was also calculated as standard deviation divided by the square root of three for all cases except 6/13/12 (in which one lower side chamber was missing). Contribution ratios were then applied to the system as described below.

A.2.1.2 Contribution Ratios

Flux density calculations are in the units of $\text{g m}^{-2} \text{day}^{-1}$, where the m^2 are referring to the surface area. According to work by Andersen et al. (2010), the majority of the flux is observed from the top of the pile and less so on the sides of the pile. For this reason it was important that all three locations for which chamber flux measurements were taken not be averaged together. Because the method of chamber measurements are based on surface area, the surface area of each the top, upper side, and lower side surface area was determined. Using these surface area estimations, a ratio for contribution to the area could be determined and multiplied by the flux found for that chamber location.

$$\text{Top Contribution Ratio} = \frac{\text{Total top surface area}}{\text{Total surface area}} \quad [\text{EQ A.2.1}]$$

$$\begin{aligned} \text{Upper Side Contribution Ratio} \\ = \frac{\text{Total Upper Side surface area}}{\text{Total surface area}} \end{aligned} \quad [\text{EQ A.2.2}]$$

$$\begin{aligned} \text{Lower Side Contribution Ratio} \\ = \frac{\text{Total Lower Side surface area}}{\text{Total surface area}} \end{aligned} \quad [\text{EQ A.2.3}]$$

A.2.1.3 Details of the Pile Size

As the experiments progressed, it became clear that measurements of the pile would be vital in data analysis. With each experiment, more measurements of the size of the pile were taken after turning to improve calculations of the contribution ratios.

Experiment I: Only length 1 (L1) (See Figure A.2.1a) of the pile was measured on a regular basis after turning. The height was estimated based on the results of the depth at which the OxyTemp probe could reach the bottom of the pile and a few measurements of height noted throughout the process. Width 1 of the pile was estimated based on its beginning and ending width by evenly distributing the change in

width over the turning days. Using these rough estimations of height, length, and width, estimations for length 2 (L2) and width 2 (W2) were determined by the following formulas:

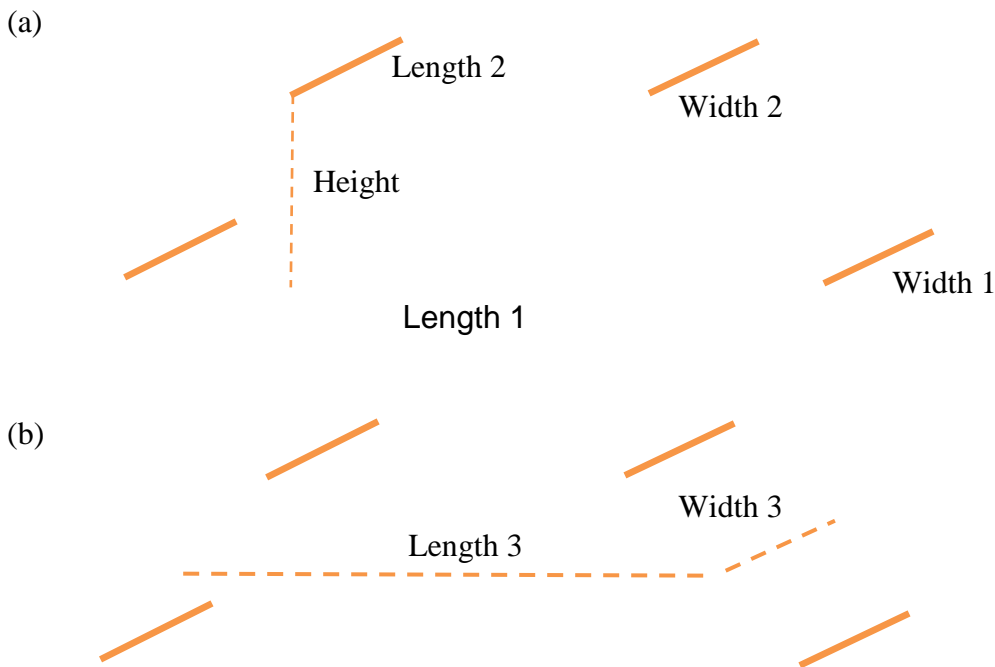
$$L2 = \frac{L1}{4} * 3 \quad \text{[EQ A.2.4]}$$

$$W2 = \frac{W1}{3} \quad \text{[EQ A.2.5]}$$

Experiment II: Length 1 and 2 (L1 and L2), width 1 and 2 (W1 and W2), and height (H) were taken for Experiment II after each turn.

Experiment III: All of the measurements in Experiment II were taken in addition to length 3 (L3) and width 3 (W3) (shown in Figure A.2.1b). These are the mid-lengths between the upper side chambers and the lower side chambers. With all of these measurements the surface area is most accurately determined for each section.

Figure A.2.1: (a) All possible measurements taken in Experiment I and II. (b) The additional measurements taken in Experiment III.



A.2.1.4 Surface Area Calculations

The following formulas were used for all piles to obtain lengths of different aspects of the pile using geometry and the previously described measurements in Appendix section A.2.1.3. See Figure A.2.2a-c for definitions of these values.

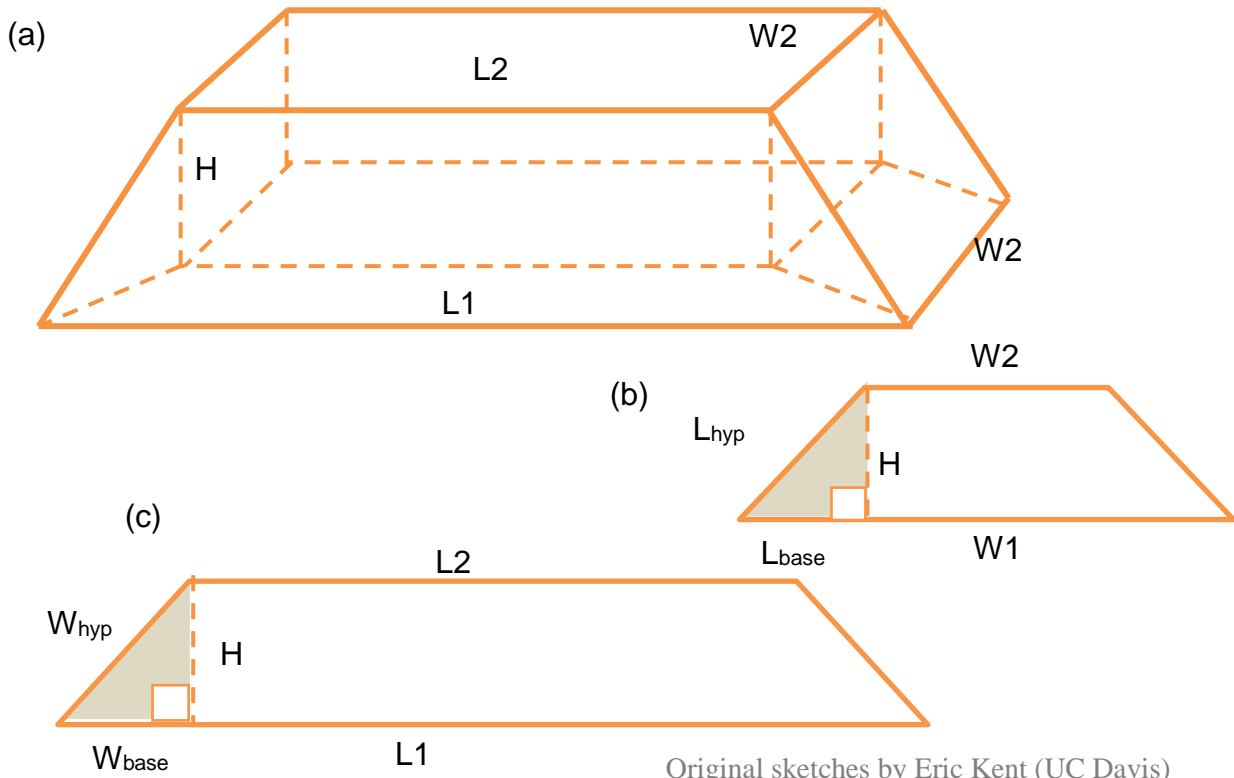
$$W_{base} = \frac{L1 - L2}{2} \quad [\text{EQ A.2.6}]$$

$$L_{base} = \frac{W1 - W2}{2} \quad [\text{EQ A.2.7}]$$

$$W_{hyp} = \sqrt{H^2 + W_{base}^2} \quad [\text{EQ A.2.8}]$$

$$L_{hyp} = \sqrt{H^2 + L_{base}^2} \quad [\text{EQ A.2.9}]$$

Figure A.2.2: Compost pile measurements diagram. (a) Full visualization of the compost pile with measurements taken or estimated for all piles. (b) A side view of the short side of the windrow to show geometrically, L_{base} , the triangle base for the short side of the pile and L_{hyp} , the height of the long side of the pile. (c) A side view of the long side of the windrow to show geometrically W_{base} , the triangle base for the long side of the pile and W_{hyp} , the height of the short side of the pile.



Original sketches by Eric Kent (UC Davis)

Lacking L3 and W3 as shown in Figure A.2.1b, Experiment I and II have a slightly different surface area calculation than Experiment III and requires more geometry. The following formulas were used to calculate the surface area for Experiment I and II (see Figure A.2.3 for visualization of these surface areas).

$$\text{Top surface area} = L2 \times W2 \quad \text{[EQ A.2.10]}$$

$$\text{Upper Side surface area} = \left(L2 \times L_{hyp} + \frac{1}{2} W_{base} L_{hyp} \right) + \left(W2 \times W_{hyp} + \frac{1}{2} L_{base} W_{hyp} \right) \quad \text{[EQ A.2.11]}$$

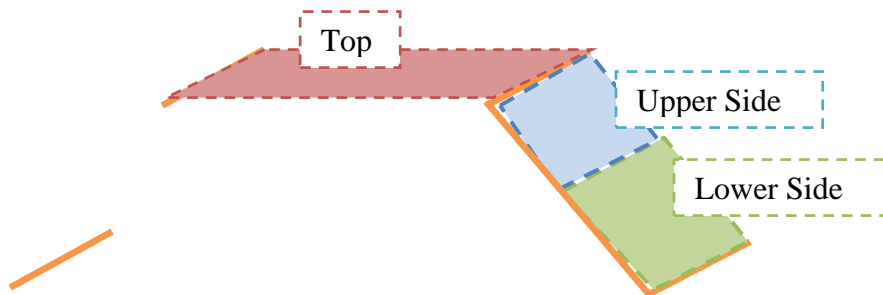
$$\text{Lower Side surface area} = \left(L2 \times L_{hyp} + \frac{3}{2} W_{base} L_{hyp} \right) + \left(W2 \times W_{hyp} + \frac{3}{2} L_{base} W_{hyp} \right) \quad \text{[EQ A.2.12]}$$

$$\begin{aligned} \text{Upper Side surface area} \\ = \left(\frac{L3 + L1}{2} \times L_{hyp} \right) + \left(\frac{W3 + W1}{2} \times W_{hyp} \right) \end{aligned} \quad \begin{array}{l} \text{[EQ} \\ \text{A.2.13]} \end{array}$$

$$\text{Lower Side surface area} = \left(\frac{L3 + L2}{2} \times L_{hyp} \right) + \left(\frac{W3 + W2}{2} \times W_{hyp} \right) \quad \begin{array}{l} \text{[EQ} \\ \text{A.2.14]} \end{array}$$

Experiment III contains the same formula for top surface area EQ A.2.10, however it contains different formulas for upper and lower sides. The formulas are given below.

Figure A.2.3: Visualization of the surface areas that the previous formulas are calculating.



A.2.1.5 Integration

Trapezoidal integration using Sigma Plot. The formula is shown below.

$$\int_0^{n-1} f(x) \approx y_i (x_{i+1} - x_i) + \frac{1}{2} (y_{i+1} - y_i) (x_{i+1} - x_i) \quad \begin{array}{l} \text{[EQ} \\ \text{A.2.15]} \end{array}$$

A.2.2 Supplemental Data

All data presented throughout the report is done with standard error as (\pm SE) unless otherwise noted.

Table A.2.1: CH₄ flux data from Experiment I for each sampling day. These values have been adjusted by the fraction of the total surface area that they contain (contribution ratio). The total flux is the sum of each of these fluxes in g CH₄/ m² day. The total emissions in g/day is the total flux multiplied by the total calculated surface area for that day.

Experiment I – Methane Flux Densities and Emissions								
Date and Time	Pile Age (Days)	Turning Mark*	Daily Flux-Control (g CH ₄ / m ² day)**	Daily Flux-Top (A) (g CH ₄ / m ² day)	Daily Flux-Upper Side (B) (g CH ₄ / m ² day)	Daily Flux-Lower side (C) (g CH ₄ / m ² day)	Total Daily Flux (g CH ₄ / m ² day)	Total Emissions (g CH ₄ / day)
5/24/12 12:00	2	1	0.165	0.020 \pm 0.004	0.047 \pm 0.012	0.060 \pm 0.010	0.126 \pm 0.016	11.6 \pm 1.5
5/26/12 13:00	4	0	0.074	0.082 \pm 0.023	0.078 \pm 0.007	0.101 \pm 0.015	0.261 \pm 0.029	24.3 \pm 2.7
5/28/12 12:20	6	1	0.159	0.988 \pm 0.637	0.068 \pm 0.015	0.092 \pm 0.018	1.15 \pm 0.64	118 \pm 66
5/30/12 11:30	8	1	0.126	1.73 \pm 0.53	0.245 \pm 0.069	0.419 \pm 0.228	2.39 \pm 0.58	226 \pm 55
6/1/12 12:00	10	1	0.081	2.21 \pm 1.13	0.337 \pm 0.144	0.122 \pm 0.038	2.66 \pm 1.14	268 \pm 115
6/5/12 10:30	14	0	0.247	4.12 \pm 1.34	0.927 \pm 0.756	0.436 \pm 0.103	5.48 \pm 1.54	552 \pm 155
6/5/12 13:00	14	1	0.133	5.69 \pm 1.66	0.634 \pm 0.214	0.903 \pm 0.382	7.23 \pm 1.72	762 \pm 182
6/6/12 14:00	15	0	0.164	4.90 \pm 0.90	4.51 \pm 2.52	3.28 \pm 0.45	12.7 \pm 2.7	1308 \pm 280
6/8/12 10:30	17	0	0.190	4.17 \pm 1.04	2.77 \pm 1.99	2.66 \pm 1.04	9.60 \pm 2.47	989 \pm 255
6/11/12 14:30	20	0	0.126	2.19 \pm 1.02	0.408 \pm 0.277	0.397 \pm 0.080	3.00 \pm 1.06	3012 \pm 107
6/13/12 10:00	22	0	0.075	2.67 \pm 1.08	2.29 \pm 1.85	0.566 \pm 0.222	5.52 \pm 2.16	555 \pm 217
6/14/12 9:00	23	0	0.068	1.53 \pm 0.45	1.31 \pm 1.03	1.234 \pm 0.799	4.08 \pm 1.38	410 \pm 138

6/14/12 12:15	23	1	0.063	1.99 ± 0.31	0.160 ± 0.080	0.298 ± 0.146	2.44 ± 0.35	248 ± 35
6/20/12 10:00	29	0	0.199	7.79 ± 3.56	0.181 ± 0.091	0.346 ± 0.222	8.32 ± 3.57	824 ± 353
6/27/12 8:45	36	0	0.088	1.13 ± 0.27	0.161 ± 0.072	0.127 ± 0.007	1.41 ± 0.28	137 ± 27
6/27/12 11:45	36	1	0.109	0.445 ± 0.188	0.071 ± 0.002	0.081 ± 0.007	0.597 ± 0.188	58.6 ± 18.5
7/6/12 9:00	45	0	0.089	0.956 ± 0.042	0.190 ± 0.049	0.122 ± 0.019	1.27 ± 0.07	122 ± 6
7/6/12 12:00	45	1	0.088	0.349 ± 0.147	0.060 ± 0.006	0.091 ± 0.019	0.500 ± 0.148	47.3 ± 14.0
7/11/12 9:30	50	0	0.126	3.23 ± 1.50	1.11 ± 0.55	0.598 ± 0.466	4.94 ± 1.66	468 ± 157
7/12/12 9:30	51	0	0.071	4.08 ± 1.89	0.119 ± 0.032	0.112 ± 0.012	4.31 ± 1.89	399 ± 175
7/12/12 13:30	51	1	0.071	3.38 ± 1.57	0.125 ± 0.034	0.117 ± 0.012	3.62 ± 1.57	276 ± 119
7/18/12 8:45	57	1	0.124	10.4 ± 1.5	0.196 ± 0.052	0.124 ± 0.034	10.726 ± 1.456	816 ± 111

*0: no turn or pre turn, 1: post-turn, 2: 2.5hrs post-turn

**Controls for Experiment II and III are the same for both before the turn and after the turn when they occur on the same day.

Table A.2.2: CH₄ flux data from Experiment II for each sampling day. These values have been adjusted by the fraction of the total surface area that they contain (contribution ratio). The total flux is the sum of each of these fluxes in g CH₄/ m² day. The total emissions in g/day are the total flux multiplied by the total calculated surface area for that day.

Experiment II – Methane Flux Densities and Emissions								
Date and Time	Age of Pile in Days	Turning Mark *	Daily Flux-Control (g CH ₄ /m ² day)**	Daily Flux - Top (A) (g CH ₄ /m ² day)	Daily Flux- Upper Side (B) (g CH ₄ /m ² day)	Daily Flux- Lower side (C) (g CH ₄ /m ² day)	Total Daily Flux- (g CH ₄ /m ² day)	Total Emissions (g CH ₄ /day)
11/5/12 11:45	0	1	0.0624	0.039 ± 0.011	0.043 ± 0.010	0.060 ± 0.013	0.142 ± 0.020	13.1 ± 1.9
11/7/12 10:00	2	0	0.1963	0.441 ± 0.103	0.209 ± 0.066	0.089 ± 0.008	0.740 ± 0.122	67.2 ± 11.1
11/7/12 13:20	2	1	0.1963	0.219 ± 0.082	0.083 ± 0.033	0.091 ± 0.043	0.392 ± 0.098	32.7 ± 8.2
11/9/12 9:50	4	0	0.0687	2.97 ± 0.827	2.41 ± 0.56	0.134 ± 0.027	5.51 ± 1.00	459 ± 83
11/9/12 15:30	4	1	0.0687	0.610 ± 0.124	0.081 ± 0.040	0.042 ± 0.008	0.733 ± 0.131	65 ± 12
11/12/12 9:30	7	0	0.0472	6.07 ± 1.66	2.19 ± 0.93	0.251 ± 0.073	8.51 ± 1.91	750 ± 168
11/12/12 14:30	7	1	0.0472	1.94 ± 0.30	0.471 ± 0.248	0.103 ± 0.027	2.51 ± 0.39	215 ± 33
11/14/12 12:50	9	1	0.0084	1.51 ± 0.33	0.586 ± 0.403	0.106 ± 0.031	2.21 ± 0.52	181 ± 43
11/19/12 10:45	14	0	0.0762	32.9 ± 4.6	1.94 ± 0.90	3.88 ± 1.28	38.7 ± 4.9	3074 ± 388
11/19/12 13:45	14	1	0.0762	7.81 ± 1.35	2.49 ± 1.26	11.0 ± 3.7	21.3 ± 4.1	1902 ± 370

11/23/ 12 15:45	18	0	0.1587	7.83 ± 2.82	3.19 ± 2.57	0.495 ± 0.055	11.5 ± 3.8	1029 ± 342
11/27/ 12 11:00	22	0	0.0396	14.5 ± 1.9	9.57 ± 5.69	0.454 ± 0.247	24.6 ± 6.0	2195 ± 536
11/27/ 12 13:40	22	1	0.0396	7.28 ± 0.91	0.685 ± 0.532	0.253 ± 0.121	8.22 ± 1.06	659 ± 85
11/27/ 12 15:30	22	2	0.0396	14.0 ± 2.7	0.366 ± 0.150	0.078 ± 0.011	14.4 ± 2.7	1157± 215
12/3/1 2 9:55	28	0	-0.0024	49.3 ± 11.4	20.1 ± 4.8	3.09 ± 0.85	72.6 ± 12.4	5769 ± 989
12/7/1 2 10:12	32	0	0.0836	68.2 ± 25.0	7.82 ± 3.63	0.590 ± 0.189	76.6 ± 25.2	6033 ± 1986
12/11/ 12 11:25	36	0	0.1460	53.9 ± 16.9	4.39 ± 3.43	2.15 ± 1.89	60.5 ± 17.4	4719 ± 1357
12/11/ 12 14:10	36	1	0.1460	10.3 ± 5.4	1.41 ± 0.65	0.360 ± 0.096	12.1 ± 5.4	1012 ± 454
12/14/ 12 11:30	39	0	0.0960	204 ± 34	2.46 ± 0.60	0.350 ± 0.100	207 ± 34	17296 ± 2870
12/18/ 12 12:00	43	0	0.0900	112 ± 63	4.08 ± 1.52	0.766 ± 0.070	117 ± 63	9754 ± 5286

*0: no turn or pre turn, 1: post-turn, 2: 2.5hrs post-turn

**Controls for Experiment II and III are the same for both before the turn and after the turn when they occur on the same day.

Table A.2.3: Methane flux data from Experiment III for each sampling day. These values have been adjusted by the fraction of the total surface area that they contain (contribution ratio). The total flux is the sum of each of these fluxes in (g CH₄ m⁻² day⁻¹). The total emissions in g/day is the total flux multiplied by the total calculated surface area for that day.

Experiment III – Methane Flux Densities and Emissions								
Date and Time	Age of Pile in Days	Turning Mark *	Daily Flux-Control (g CH ₄ m ⁻² day ⁻¹)**	Daily Flux-Top (A) (g CH ₄ m ⁻² day ⁻¹)	Daily Flux-Upper Side (B) (g CH ₄ m ⁻² day ⁻¹)	Daily Flux-Lower side (C) (g CH ₄ m ⁻² day ⁻¹)	Total Daily Flux (g CH ₄ m ⁻² day ⁻¹)	Total Emissions (g CH ₄ day ⁻¹)
2/21/13 12:00	0	1	0.117	0.069 ± 0.017	0.088 ± 0.002	0.088 ± 0.001	0.245 ± 0.017	25.1 ± 1.8
2/22/13 15:25	1	1	0.140	0.109 ± 0.024	0.091 ± 0.007	0.101 ± 0.006	0.301 ± 0.026	32.7 ± 2.8
2/26/13 12:15	5	1	0.141	1.10 ± 0.54	0.612 ± 0.273	0.154 ± 0.057	1.87 ± 0.61	178 ± 58
2/28/13 11:22	7	1	0.070	9.02 ± 2.97	0.467 ± 0.255	0.083 ± 0.007	9.58 ± 2.98	838 ± 261
3/5/13 12:15	12	0	0.242	7.57 ± 2.26	0.528 ± 0.190	0.628 ± 0.228	8.72 ± 2.28	761 ± 199
3/7/13 11:20	14	1	0.141	4.46 ± 1.31	2.49 ± 1.24	0.179 ± 0.047	7.12 ± 1.80	662 ± 168
3/12/13 11:03	19	0	0.132	7.01 ± 1.70	0.963 ± 0.440	0.179 ± 0.031	8.16 ± 1.76	759 ± 163
3/12/13 14:03	19	1	0.132	3.43 ± 0.15	0.094 ± 0.027	0.083 ± 0.009	3.60 ± 0.15	296 ± 13
3/14/13 11:40	21	0	0.131	9.85 ± 1.12	0.602 ± 0.185	0.213 ± 0.047	10.7 ± 1.1	874 ± 93
3/15/13 13:08	22	0	0.172	18.5 ± 1.0	2.42 ± 0.41	0.263 ± 0.108	21.1 ± 1.1	1733 ± 90

3/19/ 13 11:17	26	0	0.148	4.79 ± 1.28	0.511 ± 0.204	0.129 ± 0.009	5.43 ± 1.30	445 ± 106
3/21/ 13 12:50	28	0	0.166	3.19 ± 0.80	2.54 ± 2.12	0.250 ± 0.026	5.97 ± 2.27	496 ± 188
3/26/ 13 9:55	33	0	0.097	5.89 ± 1.81	2.15 ± 1.70	0.140 ± 0.013	8.18 ± 2.48	679 ± 206
3/26/ 13 13:05	33	1	0.097	3.29 ± 1.43	0.305 ± 0.085	0.063 ± 0.011	3.66 ± 1.43	262 ± 102
3/28/ 13 12:05	35	0	0.097	2.36 ± 1.29	1.10 ± 0.41	0.094 ± 0.006	3.56 ± 1.35	255 ± 97
4/2/1 3 10:32	40	0	-0.008	2.83 ± 1.39	1.06 ± 0.74	0.073 ± 0.018	3.96 ± 1.58	284 ± 113
4/2/1 3 14:20	40	1	-0.008	0.312 ± 0.234	0.113 ± 0.081	-0.001 ± 0.001	0.424 ± 0.248	30.4 ± 17.7
4/5/1 3 13:15	43	0	0.015	1.57 ± 1.21	0.503 ± 0.006	0.032 ± 0.013	2.10 ± 1.21	151 ± 87
4/9/1 3 13:40	47	0	0.060	1.79 ± 0.85	0.756 ± 0.302	0.107 ± 0.018	2.65 ± 0.90	190 ± 65
4/11/ 13 9:43	49	0	1.401	0.357 ± 0.146	1.242 ± 0.315	0.716 ± 0.337	2.32 ± 0.48	166 ± 35
4/11/ 13 12:19	49	1	1.401	0.807 ± 0.435	1.440 ± 0.491	1.61 ± 0.51	3.86 ± 0.83	240 ± 52
4/16/ 13 10:15	54	0	0.061	3.82 ± 2.62	1.826 ± 0.888	0.104 ± 0.032	5.75 ± 2.77	358 ± 172

*0: no turn or pre turn, 1: post-turn, 2: 2.5hrs post-turn

**Controls for Experiment II and III are the same for both before the turn and after the turn when they occur on the same day.

Table A.2.4: N₂O Flux Data from Experiment I for each sampling day. These values have been adjusted by the fraction of the total surface area that they contain (contribution ratio). The total flux is the sum of each of these fluxes in (mg N₂O m⁻² day⁻¹). The total emissions in g/day is the total flux multiplied by the total calculated surface area for that day.

Experiment I – Nitrous Oxide Flux Densities and Emissions								
Date and Time	Age of Pile in Days	Turn-ing Mark *	Daily Flux-Control- (mg N ₂ O m ⁻² day ⁻¹)**	Daily Flux-Top (A) (mg N ₂ O m ⁻² day ⁻¹)	Daily Flux-Upper Side (B) (mg N ₂ O m ⁻² day ⁻¹)	Daily Flux-Lower Side (C) (mg N ₂ O m ⁻² day ⁻¹)	Total Daily Flux (mg N ₂ O m ⁻² day ⁻¹)	Total Emissions (g N ₂ O day ⁻¹)
5/24/12 12:00	2	1	31.03	511 ± 248	40.1 ± 3.8	74.8 ± 37.3	625 ± 250	57.2 ± 22.9
5/26/12 13:00	4	0	15.59	34.1 ± 6.1	35.6 ± 7.7	36.2 ± 2.4	106 ± 10	9.83 ± 0.94
5/28/12 12:20	6	1	74.49	133 ± 78	55.1 ± 16.1	51.2 ± 9.4	239 ± 80	24.7 ± 8.2
5/30/12 11:30	8	1	57.42	48.5 ± 10.1	111 ± 29	77.9 ± 20.2	238 ± 37	22.5 ± 3.5
6/1/12 12:00	10	1	50.36	20.6 ± 10.5	52.8 ± 35.8	22.6 ± 6.2	96.0 ± 37.8	9.67 ± 3.81
6/5/12 10:30	14	0	45.87	24.9 ± 2.5	20.9 ± 1.2	23.0 ± 1.9	68.8 ± 3.4	6.93 ± 0.34
6/5/12 13:00	14	1	-49.10	140 ± 40	42.7 ± 10.9	32.7 ± 11.2	215 ± 43	22.7 ± 4.5
6/6/12 14:00	15	0	33.24	51.6 ± 12.4	27.7 ± 12.1	20.9 ± 5.1	100 ± 18	10.3 ± 1.9
6/8/12 10:30	17	0	36.21	25.2 ± 2.7	27.8 ± 5.7	22.9 ± 3.6	75.8 ± 7.3	7.81 ± 0.75
6/11/12 14:30	20	0	-19.97	19.3 ± 7.8	13.1 ± 1.7	19.5 ± 3.3	51.9 ± 8.6	5.22 ± 0.87
6/13/12 10:00	22	0	-7.16	18.4 ± 6.5	19.6 ± 4.6	21.0 ± 1.4	59.0 ± 8.1	5.93 ± 0.81
6/14/12 9:00	23	0	-15.86	9.90 ± 5.62	15.4 ± 3.2	17.1 ± 2.8	42.4 ± 7.0	4.26 ± 0.71
6/14/12 12:15	23	1	-13.92	129 ± 69	19.8 ± 4.4	35.8 ± 8.8	184 ± 70	18.7 ± 7.1
6/20/12 10:00	29	0	36.37	21.5 ± 7.1	15.3 ± 2.4	26.3 ± 2.5	63.0 ± 7.9	6.24 ± 0.78
6/27/12 8:45	36	0	-39.06	19.6 ± 11.1	20.2 ± 11.2	28.4 ± 3.6	68.2 ± 16.2	6.60 ± 1.57

6/27/12 11:45	36	1	-27.88	88.8 ± 39.4	15.1 ± 6.2	10.8 ± 7.7	114.6 ± 40.7	11.2 ± 4.0
7/6/12 9:00	45	0	-45.47	9.22 ± 4.75	11.8 ± 3.3	9.42 ± 2.42	30.4 ± 6.3	2.92 ± 0.60
7/6/12 12:00	45	1	-44.87	202 ± 93	6.06 ± 2.39	64.7 ± 48.8	272 ± 105	25.8 ± 9.9
7/11/12 9:30	50	0	11.48	9.76 ± 8.39	25.6 ± 3.4	27.2 ± 8.7	62.5 ± 12.6	5.9 ± 1.2
7/12/12 9:30	51	0	-14.87	140 ± 71	150 ± 106	100 ± 47	390 ± 135	36.1 ± 12.6
7/12/12 13:30	51	1	-14.87	116 ± 59	157 ± 110	104 ± 49	377 ± 134	28.7 ± 10.2
7/18/12 8:45	57	1	-49.34	-0.99 ± 2.43	9.47 ± 1.60	15.9 ± 3.8	24.4 ± 4.8	1.86 ± 0.36

*0: no turn or pre turn, 1: post-turn, 2: 2.5hrs post-turn

**Controls for Experiment II and III are the same for both before the turn and after the turn when they occur on the same day.

Table A.2.5: N₂O Flux Data from Experiment II for each sampling day. These values have been adjusted by the fraction of the total surface area that they contain (contribution ratio). The total flux is the sum of each of these fluxes in (mg N₂O m⁻² day⁻¹). The total emissions in g/day is the total flux multiplied by the total calculated surface area for that day.

Experiment II - Nitrous Oxide Flux Densities and Emissions								
Date and Time	Age of Pile in Days	Turning Mark*	Daily Flux-Control (mg N ₂ O m ⁻² day ⁻¹)**	Daily Flux-Top (A) (mg N ₂ O m ⁻² day ⁻¹)	Daily Flux-Upper Side (B) (mg N ₂ O m ⁻² day ⁻¹)	Daily Flux-Lower Side (C) (mg N ₂ O m ⁻² day ⁻¹)	Total Daily Flux (mg N ₂ O m ⁻² day ⁻¹)	Total Emissions (g N ₂ O day ⁻¹)
11/5/12 11:45	0	1	-23.97	4.42 ± 2.85	6.34 ± 8.33	14.8 ± 7.5	25.5 ± 11.5	2.35 ± 1.06
11/7/12 10:00	2	0	46.56	5.91 ± 4.37	12.1 ± 4.9	16.7 ± 6.8	34.6 ± 9.5	3.15 ± 0.86
11/7/12 13:20	2	1	46.56	5.23 ± 2.91	-0.11 ± 8.73	4.15 ± 11.23	9.27 ± 14.52	0.77 ± 1.21
11/9/12 9:50	4	0	-29.43	15.14 ± 3.81	20.3 ± 3.8	0.35 ± 4.04	35.8 ± 6.7	2.98 ± 0.56
11/9/12 15:30	4	1	-29.43	-7.96 ± 1.58	-14.1 ± 2.7	-9.04 ± 1.87	-31.1 ± 3.6	-2.74 ± 0.32
11/12/1 2 9:30	7	0	-36.79	13.8 ± 2.6	7.71 ± 5.70	8.59 ± 3.61	30.1 ± 7.2	2.65 ± 0.64
11/12/1 2 14:30	7	1	-36.79	13.1 ± 2.8	14.7 ± 15.9	-5.33 ± 7.77	22.5 ± 17.9	1.93 ± 1.53
11/14/1 2 12:50	9	1	-18.84	5.26 ± 2.09	5.27 ± 8.30	12.5 ± 6.1	23.1 ± 10.5	1.89 ± 0.86
11/19/1 2 10:45	14	0	16.18	22.4 ± 3.8	23.0 ± 1.7	29.4 ± 1.8	74.7 ± 4.5	5.93 ± 0.36
11/19/1 2 13:45	14	1	16.18	15.7 ± 2.6	18.6 ± 2.2	22.9 ± 0.8	57.1 ± 3.5	5.11 ± 0.31
11/23/1 2 15:45	18	0	-0.58	-1.02 ± 1.95	14.1 ± 10.7	4.99 ± 5.94	18.1 ± 12.4	1.62 ± 1.11
11/27/1 2 11:00	22	0	-2.35	-1.00 ± 2.11	14.2 ± 5.6	19.2 ± 9.1	32.4 ± 10.9	2.90 ± 0.98
11/27/1 2 13:40	22	1	-2.35	2.09 ± 3.14	-5.30 ± 4.51	-4.95 ± 4.52	-8.16 ± 7.12	-0.65 ± 0.57
11/27/1 2 15:30	22	2	-2.35	34.2 ± 5.5	11.9 ± 2.8	-2.90 ± 4.12	43.1 ± 7.5	3.46 ± 0.60
12/3/12 9:55	28	0	-30.69	-1.05 ± 0.74	11.0 ± 2.9	13.1 ± 4.3	23.1 ± 5.2	1.83 ± 0.42

12/7/12 10:12	32	0	-9.16	13.9 ± 3.5	22.5 ± 5.1	24.2 ± 0.3	60.6 ± 6.2	4.78 ± 0.49
12/11/1 2 11:25	36	0	17.71	15.3 ± 1.3	25.8 ± 1.7	26.4 ± 4.4	67.6 ± 4.9	5.27 ± 0.38
12/11/1 2 14:10	36	1	17.71	37.7 ± 17.7	48.1 ± 28.3	20.5 ± 4.0	106 ± 34	8.90 ± 2.81
12/14/1 2 11:30	39	0	-11.67	-0.91 ± 1.66	8.84 ± 5.61	22.6 ± 10.3	30.5 ± 11.8	2.55 ± 0.99
12/18/1 2 12:00	43	0	-4.85	13.0 ± 3.1	24.6 ± 2.3	28.2 ± 4.1	65.8 ± 5.7	5.51 ± 0.47

*0: no turn or pre turn, 1: post-turn, 2: 2.5hrs post-turn

**Controls for Experiment II and III are the same for both before the turn and after the turn when they occur on the same day.

Table A.2.6: N₂O Flux Data from Experiment III for each sampling day. These values have been adjusted by the fraction of the total surface area that they contain (contribution ratio). The total flux is the sum of each of these fluxes in (g N₂O m⁻² day⁻¹). The total emissions in g/day is the total flux multiplied by the total calculated surface area for that day.

Experiment III - Nitrous Oxide Flux Densities and Emissions								
Date and Time	Age of Pile in Days	Turning Mark *	Daily Flux-Control (mg N ₂ O m ⁻² day ⁻¹)**	Daily Flux-Top (A) (mg N ₂ O/m ² day ⁻¹)	Daily Flux-Upper Side (B) (mg N ₂ O m ⁻² day ⁻¹)	Daily Flux-Lower Side (C) (mg N ₂ O m ⁻² day ⁻¹)	Total Daily Flux (mg N ₂ O m ⁻² day ⁻¹)	Total Emissions (g N ₂ O day ⁻¹)
2/21/13 12:00	0	1	12.69	67.3 ± 21.5	145 ± 72	47.3 ± 13.7	259.7 ± 76.8	26.6 ± 7.9
2/22/13 15:25	1	1	20.17	310 ± 29	28.3 ± 0.6	37.2 ± 3.5	375.4 ± 29.3	40.8 ± 3.18
2/26/13 12:15	5	1	29.04	80.8 ± 29.2	53.5 ± 10.1	39.7 ± 2.1	174 ± 31	16.6 ± 3.0
2/28/13 11:22	7	1	-15.72	11.7 ± 3.1	13.2 ± 4.5	16.1 ± 1.6	41.0 ± 5.7	3.59 ± 0.50
3/5/13 12:15	12	0	61.03	30.0 ± 5.1	28.1 ± 3.7	36.4 ± 2.6	94.4 ± 6.8	8.24 ± 0.59
3/7/13 11:20	14	1	-15.97	11.0 ± 1.6	20.3 ± 3.8	39.0 ± 6.3	70.4 ± 7.5	6.54 ± 0.70
3/12/13 11:03	19	0	-20.58	-3.8 ± 0.8	6.45 ± 3.89	23.3 ± 2.9	25.9 ± 4.9	2.41 ± 0.46
3/12/13 14:03	19	1	-20.58	-2.24 ± 2.58	-2.59 ± 1.20	5.66 ± 6.86	0.84 ± 7.43	0.07 ± 0.61

3/14/13 11:40	21	0	-32.94	-4.46 ± 3.12	-1.05 ± 4.40	11.3 ± 13.9	5.77 ± 14.93	0.47 ± 1.22
3/15/13 13:08	22	0	11.56	9.10 ± 2.82	15.7 ± 5.0	13.7 ± 0.7	38.5 ± 5.8	3.15 ± 0.48
3/19/13 11:17	26	0	-10.86	1.00 ± 1.94	14.4 ± 3.1	30.1 ± 8.7	45.4 ± 9.4	3.73 ± 0.77
3/21/13 12:50	28	0	9.25	11.7 ± 2.9	18.4 ± 5.8	37.2 ± 6.1	67.3 ± 8.9	5.58 ± 0.74
3/26/13 9:55	33	0	-3.56	8.9 ± 0.9	16.5 ± 2.0	26.1 ± 3.4	51.4 ± 4.1	4.27 ± 0.34
3/26/13 13:05	33	1	-3.56	2.9 ± 1.6	4.75 ± 4.93	3.98 ± 3.51	11.7 ± 6.3	0.84 ± 0.45
3/28/13 12:05	35	0	0.22	14.8 ± 7.9	14.4 ± 3.8	24.6 ± 3.5	53.8 ± 9.4	3.86 ± 0.68
4/2/13 10:32	40	0	-27.65	-1.40 ± 4.77	1.31 ± 2.94	10.6 ± 5.1	10.5 ± 7.6	0.75 ± 0.54
4/2/13 14:20	40	1	-27.65	-5.53 ± 0.93	-18.6 ± 4.7	-13.2 ± 0.4	-37.3 ± 4.8	-2.67 ± 0.34
4/5/13 13:15	43	0	-26.96	-2.59 ± 1.04	-2.79 ± 3.48	-1.09 ± 4.32	-6.48 ± 5.64	-0.46 ± 0.40
4/9/13 13:40	47	0	5.70	8.30 ± 1.40	18.4 ± 4.5	29.7 ± 3.2	56.4 ± 5.7	4.05 ± 0.41
4/11/13 9:43	49	0	124.46	21.1 ± 0.61	48.7 ± 1.7	52.4 ± 2.0	122 ± 3	8.75 ± 0.20
4/11/13 12:19	49	1	124.46	23.6 ± 2.1	50.1 ± 4.7	52.6 ± 2.3	126 ± 6	7.87 ± 0.35
4/16/13 10:15	54	0	14.20	14.2 ± 1.8	24.9 ± 1.8	32.8 ± 2.0	71.8 ± 3.2	4.48 ± 0.20

*0: no turn or pre turn, 1: post-turn, 2: 2.5hrs post-turn

**Controls for Experiment II and III are the same for both before the turn and after the turn when they occur on the same day.

Table A.2.7: Summary of integration data for CH₄ from each experiment.

	Experiment I	Experiment II	Experiment III
Days Integrated (Days)	57	43	54
Control Emissions (kg CH ₄)	0.65	0.27	0.61
A, Top Emissions (kg CH ₄)	16 ± 1.7	150 ± 25	20 ± 1.4
B, Upper Side Emissions, (kg CH ₄)	3.0 ± 1.4	17 ± 1.5	3.4 ± 1.3
C, Lower Side Emissions, (kg CH ₄)	2.5 ± 0.48	5.2 ± 0.17	0.70 ± 0.06
Total Emissions (kg CH ₄)	22 ± 2.3	170 ± 25	24 ± 1.9
Total Emissions per day (g CH ₄ day ⁻¹)	410 ± 120	3900 ± 1400	580 ± 110
Total Emissions per day per ton of DW* (g CH ₄ day ⁻¹ Mg ⁻¹ DW)	30 ± 10	340. ± 120	56± 11

*DW – Dry weight compost starting material

Table A.2.8: Summary of integration data for N₂O from each experiment.

	Experiment I	Experiment II	Experiment III
Days Integrated (Days)	57	43	54
Control Emissions (g N ₂ O)	12	-24	23
A, Top Emissions (g N ₂ O)	320 ± 92	34 ± 6.7	150 ± 6.9
B, Upper Side Emissions, (g N ₂ O)	170 ± 37	52 ± 5.3	62 ± 3.3
C, Lower Side Emissions, (g N ₂ O)	172 ± 9.3	52 ± 3.0	82 ± 2.4
Total Emissions (g N ₂ O)	660 ± 100	140 ± 9.1	290 ± 8.0
Total Emissions per day (g N ₂ O day ⁻¹)	15 ± 3.9	2.8 ± 0.54	5.8 ± 0.64
Total Emissions per day per ton of DW* (mg N ₂ O day ⁻¹ Mg ⁻¹ DW)	1100 ± 300	240 ± 47	550 ± 61

*DW – Dry weight compost starting material

Table A.2.9: Summary of the annual N₂O and CH₄ emissions calculation.

Experiment (Date/ Days)	CH ₄ Emissions			N ₂ O Emissions					
	(g/d-t)	Uncertainty (g/d-t)		(mg/d-t)	Uncertainty		Account ing for turning (mg/d-t)	Com- bined Uncer- tainty (mg/d-t)	
		Com- bined	Expan- ded		Com- bined	Expan- ded			
Avg. Daily*									
1 (May – June)	30.9	4.6	9.2	1100.0	148.5	296.9	-	-	
2 (Nov. – Feb.)	340.0	59.8	119.6	240.8	23.3	46.5	102.1	10.8	
3 (Feb. – April)	55.5	5.3	10.7	548.2	30.4	60.8	-	-	
Total**									
1 - 57 days	2027.5	302.7	605.4	72.1	9.7	19.5			
2 – 43 days	16,804. 6	2956.8	5913.5	11.9	1.2	2.3	5047.8	535.7	1071.5
3 – 54 days	3444.6	330.5	661.1	34.0	1.9	3.8			
Total per year	22,277	2991	5981	118	10	20	10,520	699	1397

* Average daily flux was calculated based on the cumulative GHG emissions of the pile divided by the pile composting days under the assumption that the combined standard uncertainty is normally distributed.

**Total statewide emissions were calculated based on the assumption that compost feedstock statewide totals 5,000,000 metric tons/year with a moisture content of 45 percent, which equals a statewide feedstock dry weight of 3,448,275.9 metric tons/year, or 1,149,425.3 metric tons/four-month time period.

Table A.2.10: Summary of Experiment I: moisture, nitrate/nitrite, ammonium, dissolved organic carbon, and carbon nitrogen ratio.

Experiment I – Compost Analysis Study					
Date	Moisture Percent*	{Nitrate +Nitrite}- N $\mu\text{g g}^{-1}$ DW	Ammonium-N $\mu\text{g g}^{-1}$ DW	Dissolved Organic Carbon, $\mu\text{g g}^{-1}$ DW	Carbon Nitrogen Ratio
5/22/2012	40.2% \pm 0.7%	32.8 \pm 18.2	156 \pm 64	11894 \pm 281	31.5 \pm 1.5
5/24/2012	50.4% \pm 1.5%	35.5 \pm 2.6	397 \pm 115	10195 \pm 2756	29.9 \pm 1.0
5/28/2012	52.8% \pm 1.2%	1.4 \pm 0.2	11 \pm 2	14548 \pm 1997	27.2 \pm 0.8
5/30/2012	49.8% \pm 1.5%	7.7 \pm 4.0	242 \pm 121	10060 \pm 971	27.1 \pm 0.6
6/1/2012	42.8% \pm 1.6%	5.9 \pm 2.5	257 \pm 81	9518 \pm 714	28.2 \pm 0.7
6/5/2012	43.6% \pm 1.1%	3.6 \pm 2.8	77 \pm 39	9405 \pm 1340	27.8 \pm 0.7
6/14/2012	47.4% \pm 1.8%	2.7 \pm 1.9	132 \pm 75	8511 \pm 1819	26.6 \pm 1.1
6/27/2012	43.4% \pm 1.5%	1.2 \pm 0.2	91 \pm 47	5485 \pm 967	24.5 \pm 0.6
7/6/2012	44.6% \pm 2.1%	0.9 \pm 0.2	59 \pm 23	3988 \pm 802	23.7 \pm 0.7
7/12/2012	48.2% \pm 1.2%	0.6 \pm 0.1	97 \pm 18	3352 \pm 197	21.7 \pm 0.2
7/19/2012	44.0% \pm 0.9%	0.5 \pm 0.1	179 \pm 4	3439 \pm 275	21.9 \pm 0.4

\pm indicates standard error of five samples

* Moisture was taken after turning events. At times this included watering days, which may artificially make the moisture appear higher

Table A.2.11: Summary of Experiment II: moisture, nitrate/nitrite, ammonium, dissolved organic carbon, and carbon nitrogen ratio.

Experiment II – Compost Analysis Study					
Date	Moisture Percent	{Nitrate +Nitrite}- N $\mu\text{g g}^{-1}$ DW	Ammonium-N $\mu\text{g g}^{-1}$ DW	Dissolved Organic Carbon, $\mu\text{g g}^{-1}$ DW	Carbon Nitrogen Ratio
11/5/2012	43.2% \pm 0.9%	8.8 \pm 0.8	1064 \pm 26	29010 \pm 785	30.1 \pm 0.4
11/7/2012	40.0% \pm 1.6%	6.5 \pm 0.6	926 \pm 59	25220 \pm 1961	29.3 \pm 0.7
11/9/2012	39.4% \pm 0.8%	4.5 \pm 0.1	880 \pm 23	21941 \pm 1097	28.3 \pm 0.6
11/12/2012	36.6% \pm 1.3%	3.1 \pm 0.3	797 \pm 53	19120 \pm 1657	27.8 \pm 0.7
11/14/2012	36.8% \pm 1.1%	2.4 \pm 0.3	788 \pm 58	18688 \pm 1658	27.9 \pm 0.4
11/19/2012	48.6% \pm 1.5%	1.8 \pm 0.2	37 \pm 8	10983 \pm 1847	24.4 \pm 0.2
11/27/2012	46.0% \pm 1.9%	Below detection	37 \pm 6	9961 \pm 1080	24.5 \pm 0.3
12/11/2012	53.4% \pm 1.7%	Below detection	7 \pm 5	3925 \pm 559	20.4 \pm 0.2
12/18/2012	51.4% \pm 2.4%	Below detection	44 \pm 12	2646 \pm 366	19.5 \pm 0.2

\pm indicates standard error of five samples

Table A.2.12: Summary of Experiment III: moisture, nitrate/nitrite, ammonium, dissolved organic carbon, and carbon nitrogen ratio.

Experiment III - Compost Analysis Study					
Date	Moisture Percent	{Nitrate +Nitrite}- N $\mu\text{g g}^{-1}$ DW	Ammonium-N $\mu\text{g g}^{-1}$ DW	Dissolved Organic Carbon, $\mu\text{g g}^{-1}$ DW	Carbon Nitrogen Ratio
2/21/2013	53.0% \pm 1.0%	Below detection	1.9 \pm 0.1	6608 \pm 389	27.5 \pm 0.2
2/26/2013	56.8% \pm 1.2%	Below detection	12.5 \pm 9.7	3364 \pm 178	26.5 \pm 0.7
2/28/2013	53.4% \pm 1.6%	Below detection	5.5 \pm 3.5	3099 \pm 173	25.3 \pm 0.3
3/5/2013	50.8% \pm 1.5%	Below detection	9.0 \pm 3.2	2675 \pm 93	24.9 \pm 0.1
3/7/2013	49.0% \pm 0.8%	Below detection	13.1 \pm 2.7	2690 \pm 162	24.7 \pm 0.3
3/12/2013	46.0% \pm 0.0%	Below detection	13.9 \pm 2.2	2311 \pm 83	24.2 \pm 0.1
3/19/2013	42.4% \pm 1.5%	Below detection	1.9 \pm 1.3	1776 \pm 32	23.6 \pm 0.6
3/26/2013	46.6% \pm 0.7%	Below detection	Below detection	1663 \pm 62	21.6 \pm 0.5
4/2/2013	43.6% \pm 1.8%	Below detection	9.5 \pm 4.0	1594 \pm 81	22.2 \pm 0.3
4/11/2013	42.6% \pm 0.9%	Below detection	19.3 \pm 5.6	1557 \pm 76	21.9 \pm 0.4
4/16/2013	38.4% \pm 0.2%	Below detection	15.3 \pm 3.6	1418 \pm 33	21.7 \pm 0.4

\pm indicates standard error of five samples (except 2/21/13, which had only four samples for nitrate/nitrite, ammonium, and dissolved organic carbon)

Table A.2.13: Calculated surface area for Experiment I for each location and total surface area.

Experiment I – Surface area				
Date and Time	Top (A) m²	Upper Side (B) m²	Lower Side (A) m²	Total
5/24/12 12:00	15.0	34.4	42.0	91.4
5/26/12 13:00	15.2	34.9	42.7	92.9
5/28/12 12:20	17.6	38.5	47.1	103.2
5/30/12 11:30	16.1	35.3	43.2	94.6
6/1/12 12:00	17.6	37.4	45.8	100.8
6/5/12 10:30	17.6	37.4	45.8	100.8
6/5/12 13:00	18.7	39.0	47.8	105.5
6/6/12 14:00	18.7	37.9	46.5	103.0
6/8/12 10:30	18.7	37.9	46.5	103.0
6/11/12 14:30	18.7	36.8	45.1	100.6
6/13/12 10:00	18.7	36.8	45.1	100.6
6/14/12 9:00	18.7	36.8	45.1	100.6
6/14/12 12:15	19.0	37.0	45.4	101.4
6/20/12 10:00	19.0	35.9	44.2	99.0
6/27/12 8:45	19.0	34.9	42.9	96.8
6/27/12 11:45	19.4	35.3	43.5	98.2
7/6/12 9:00	19.4	34.3	42.3	96.0
7/6/12 12:00	19.2	33.8	41.7	94.7
7/11/12 9:30	19.2	33.8	41.7	94.7
7/12/12 9:30	19.2	32.9	40.6	92.7
7/12/12 13:30	13.1	28.2	34.8	76.1
7/18/12 8:45	13.1	28.2	34.8	76.1

Table A.2.14: Calculated surface area for Experiment II for each location and total surface area.

Experiment II – Surface Area				
Date and Time	Top (A) m²	Upper Side (B) m²	Lower Side (A) m²	Total
11/5/12 11:45	18.2	33.8	40.3	92.2
11/7/12 10:00	18.2	33.1	39.6	90.9
11/7/12 13:20	14.7	30.3	38.2	83.3
11/9/12 9:50	14.7	30.3	38.2	83.3
11/9/12 15:30	19.6	31.4	37.1	88.2
11/12/12 9:30	19.6	31.4	37.1	88.2
11/12/12 14:30	18.5	29.9	37.2	85.7
11/14/12 12:50	16.7	29.4	36.0	82.1
11/19/12 10:45	16.7	28.1	34.5	79.4
11/19/12 13:45	16.7	32.5	40.1	89.4
11/23/12 15:45	16.7	32.5	40.1	89.4
11/27/12 11:00	16.7	32.5	40.1	89.4
11/27/12 13:40	19.0	28.5	32.8	80.2
11/27/12 15:30	19.0	28.5	32.8	80.2
12/3/12 9:55	19.0	28.2	32.4	79.5
12/7/12 10:12	19.0	27.8	32.0	78.8
12/11/12 11:25	19.0	27.5	31.6	78.0
12/11/12 14:10	18.1	29.3	36.3	83.7
12/14/12 11:30	18.1	29.3	36.3	83.7
12/18/12 12:00	18.1	29.3	36.3	83.7

Table A.2.15: Calculated surface area for Experiment III for each location and total surface area.

Experiment III- Surface Area				
Date and Time	Top (A) m²	Upper Side (B) m²	Lower Side (A) m²	Total
2/21/13 12:00	21.2	37.7	43.6	102.4
2/22/13 15:25	17.7	41.7	49.3	108.7
2/26/13 12:15	21.1	34.7	39.6	95.4
2/28/13 11:22	17.4	32.6	37.6	87.5
3/5/13 12:15	19.9	31.6	35.8	87.2
3/7/13 11:20	19.4	34.3	39.3	93.0
3/12/13 11:03	19.4	34.3	39.3	93.0
3/12/13 14:03	20.5	28.9	32.5	82.0
3/14/13 11:40	20.5	28.9	32.5	82.0
3/15/13 13:08	20.5	28.9	32.5	82.0
3/19/13 11:17	20.5	28.9	32.5	82.0
3/21/13 12:50	17.0	30.3	35.6	83.0
3/26/13 9:55	17.0	30.3	35.6	83.0
3/26/13 13:05	17.3	25.5	28.9	71.7
3/28/13 12:05	17.3	25.5	28.9	71.7
4/2/13 10:32	17.3	25.5	28.9	71.7
4/2/13 14:20	12.5	27.4	31.8	71.7
4/5/13 13:15	12.5	27.4	31.8	71.7
4/9/13 13:40	12.5	27.4	31.8	71.7
4/11/13 9:43	12.5	27.4	31.8	71.7
4/11/13 12:19	12.5	23.4	26.3	62.3
4/16/13 10:15	12.5	23.4	26.3	62.3

Table A.2.16: Weight measurements of compost piles for each experiment.

Experiment	Experiment I		Experiment II		Experiment III	
Dates	5/22/12	7/19/12	11/5/12	12/18/12	2/21/13	4/16/13
Material	Input	Output	Input	Output	Input	Output
Material, Mg (WW*)	24.375	18.71	22.48	23.96	24.53	23.58
Material, Mg (DW**)	13.2	9.5	11.6	10.6	10.5	13.2

*Raw Wet Weight reported from Northern Recycling.

**Dry weight calculated using moisture measurements taken after turning.

A.4 Appendix for Chapter 4

A.4.1 Materials and Methods Supplemental Information

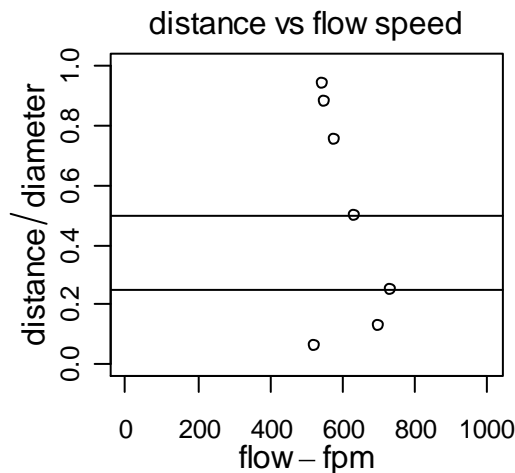
A.4.1.1 Pipe Flow Averaging Method for Biofilter Equations

To estimate the flux of trace gases from the source compost pile and corresponding emissions from the biofilter itself, the average flow velocity in the feeder pipe is needed. Flow velocities in pipes vary with distance from the pipe wall, generally with the maximum flow velocity at the pipe center, but at the wall itself, the flow velocity is assumed to be zero (the so-called “no slip” boundary condition). One method to obtain the average flow velocity would be to sample flow velocities at various radial distances and directions from the centerline and then average these velocities. To take such velocity profiles every time a biofilter experiment was implemented would have been very time-consuming. Therefore a method was developed to take a single centerline flow velocity for each experiment, and then from that calculate the average flow velocity.

This method involved taking the profile of the flow velocity in the pipe twice: once near the beginning of the biofilter experiments (5/21/13), and once near the end (7/5/13). These profiles were combined with theoretical analysis of the flow and radial integration calculus to arrive at the average flow velocity given the centerline velocity. First, the method to characterize the flow velocity as a function of position in the pipe is described. Then, the method of determining the average flow velocity factor, which, when multiplied by the centerline velocity, yields the average flow velocity, is described.

The velocity profile measurements showed an asymmetric flow profile, with an off-center maximum flow velocity (Figure A.4.1).

Figure A.4.1: Flow velocity in feet per minute plotted against normalized distance from the sample port, showing the asymmetric flow profile. Three sections of flow are demarcated by horizontal lines at $y=0.25$ and $y=0.50$.



This profile could be characterized by dividing the pipe flow in three cross sections: One semicircular cross section, with a classical turbulent pipe flow equation fit to the centerline to the pipe walls; the second semicircular cross section (the part that has the peak pipe flow velocity off center), split up into the wall to $\frac{1}{2}$ the radius as another conventional turbulent flow equation fit; and the centerline to the $\frac{1}{2}$ radius position approximated as a linear velocity profile. See the figure below of the cross section of the pipe, with the flow regimes labeled as A, B, and C, corresponding to equations presented below in A.4.2, A.4.3, and A.4.4.

Figure A.4.2: Cross-sectional view of the flow regimes used for the integration method.



The engineering equation for turbulent pipe flow was used (Prieve, 2000), requiring a velocity profile shape coefficient n , which is usually between six and ten, typically seven. $u'(r')$ is the normalized velocity (velocity u divided by centerline [maximum] velocity U_{max}) as a function of the normalized radial position r' (radial position r divided by pipe radius R):

$$u'(r') = (1 - r')^{\frac{1}{n}} \quad \text{[EQ A.4.1]}$$

Equation EQ A.4.1 was used to solve for n using a log-transform regression, given the measured flow profile. For characterizing the flow from the pipe wall to the centerline, (a) for the half of the pipe cross section that does not have the asymmetric maximum, and for the asymmetric maximum half (b), for the pipe wall to $\frac{1}{2}$ the pipe radius, this equation was solved for by regression to get the parameter n . For the flow segment on the asymmetric half of the pipe, between the centerline and the $\frac{1}{2}$ radius point, which had the absolute maximum flow, linear equation (c) was used.

- (a) For quasi-symmetric half, with assumption the flow looks like the centerline measurement is the maximum; no other relative maximums in velocity exist between the centerline and the pipe wall; this expression is valid for r' from 0 to 1.0.

$$u' = (1 - r')^{\frac{1}{n_a}}$$

$$\ln(u') = \frac{1}{n_a} \ln(1 - r')$$

[EQ A.4.2]

regression form:

$$y = mx + b$$

$$y = \ln(u')$$

$$x = \ln(1 - r')$$

$$n_a = \frac{1}{m}$$

- (b) For the asymmetric half, with assumption the flow has an “idealized” maximum in the centerline, although the measurements do not formally support this; so the equation was used from the wall ($r = 1.0$) to $r = 0.5$; an idealized centerline velocity maximum is estimated in this method, occurring at $r = 0.0$, although this formulation is considered valid only between $r = 0.5$ to 1.0 .

$$\frac{u}{u_{b \max}} = (1 - r')^{\frac{1}{n_b}}$$

$$\ln(u) - \ln(u_{\max}) = \frac{1}{n_b} \ln(1 - r')$$

[EQ A.4.3]

regression form:

$$y = mx + b$$

$$y = \ln(u)$$

$$x = \ln(1 - r')$$

$$n_b = \frac{1}{m}$$

$$b = \ln(u_{b \max})$$

- (c) For asymmetric half, in the problematic zone where the maximum velocity is offset from the centerline, a linear velocity profile (linear with radial distance) is assumed between the centerline velocity (at $r = 0$) and the peak velocity (at $r = 0.5$). This is a dimensional equation for the velocity, although the radial distance is still expressed as a non-dimensional, normalized variable, as opposed to (1a), where both u' and r' are non-dimensional.

$$u(r') = mr' + b \quad \text{[EQ A.4.4]}$$

Mass flow balance concepts are used to solve for the average face velocity for use in the other biofilter equations. u_{avg} represents the equivalent, average face velocity that gives the same mass flow as the actual velocity profile times the cross-section area A of the pipe. The radial positions (r') are defined as the radial position r divided by the pipe radius R . The integration in EQ A.4.5 represents an annular ring integration from the center of the pipe ($r'=0$) outward to the pipe walls (at $r'=R'=1$).

$$u_{avg} A = \int_0^{A/2} u_a dA + \int_0^{A/2} u_b dA = \int_0^{R'} u_a \pi r' dr' + \int_0^{R'/2} u_b \pi r' dr' + \int_{R'/2}^{R'} u_c \pi r' dr'$$

but $A = \pi R'^2$ and $R'=1$, so $A = \pi$;

$$u_{avg} = \int_0^{R'} u_a r' dr' + \int_0^{R'/2} u_b r' dr' + \int_{R'/2}^{R'} u_c r' dr' \quad [\text{EQ A.4.5}]$$

Substituting the flow equations in EQ A.4.2, EQ A.4.3, and EQ A.4.5, into u_a , u_c , and u_b :

$$u_{avg} = u_{amax} \int_0^1 (1-r')^{n_a} r' dr' + \int_0^{0.5} (mr'+b) r' dr' + u_{bmax} \int_{0.5}^1 (1-r')^{n_b} r' dr' \quad [\text{EQ A.4.6}]$$

By analyzing the middle integral, then using numerical methods to integrate the first and last integrals with a Fortran program, and finally dividing by the centerline velocity u_{amax} , one gets the multiplication factor that one would multiply by the centerline velocity to get the average velocity.

$$\frac{u_{avg}}{u_{amax}} = \int_0^1 (1-r')^{n_a} r' dr' + \frac{1}{u_{amax}} \left(\frac{m}{24} + \frac{b}{8} \right) + \frac{u_{bmax}}{u_{amax}} \int_{0.5}^1 (1-r')^{n_b} r' dr' \quad [\text{EQ A.4.7}]$$

Two velocity profiles were measured near the beginning and the end of the biofilter experiments (Table A.4.1), and they were substituted into equation EQ A.4.7 (also shown as EQ 3.12 in the materials and methods) after obtaining the flow shape coefficients (Tables A.4.2 and A.4.3) from the earlier equations. The average velocity ratio from EQ A.4.7 was 0.8814, with values of 0.89895 and 0.86384 respectively. Then the ratio 0.8814 was used to multiply by the centerline velocity to get the average pipe flow velocity (see Table A.4.7).

Table A.4.1. Raw measurements in fpm, and fractions of pipe diameter, starting from the sample port to the opposite pipe wall.

Diameter position, starting at port	U measured (fpm) from near beginning of Experiments	U measured (fpm) from near end of Experiments; average of 5 measurements
1/16	440	522.7
1/8	550	699.1
1/4	580	731.4
1/2	558	634.6
1/4	510	579.9
1/8	490	549.1
1/16	500	546.1

Table A.4.2. Coefficients from profile near beginning of study.

Regime/ r' range	Slope m and intercept b Or u_{max}	Exponent n	R^2 Regression fit
Semicircle A/ $r'=0-1.0$	$u_{max} = 558$ fpm	12.98429	0.6971
Segment B/ $r'=0-0.5$	$m=44$ fpm; $b = 558$ fpm	n/a	n/a
Segment C/ $r'=0.5-1.0$	$u_{max}= 685.05$ fpm	5.0182	0.88787

Table A.4.3. Coefficients for the velocity profile taken near end of experiments.

Regime/r' range	Slope m and intercept b Or u_{\max}	Exponent n	R^2 Regression fit
Semicircle A/ $r'=0-1.0$	$u_{\max} = 634.6$ fpm	12.027551	0.8761
Segment B/ $r'=0-0.5$	$m=193.6$ fpm; $b = 634.6$ fpm	n/a	n/a
Segment C/ $r'=0.5-1.0$	$u_{\max}= 901.4$ fpm	4.12575	0.8487

Table A.4.4. All biofilter CH₄ concentrations for each sampling day.

Date and Start Time	Avg. Biofilter Conc. North (g CH₄/L)	Avg. Biofilter Conc. South (g CH₄/L)	Avg. Biofilter Conc. Side (g CH₄/L)	Tot. Avg. Biofilter Conc. (g CH₄/L)	Pipe Concentration (g CH₄/L)	Ambient Concentration (g CH₄/L)
5/21/2013 12:15	1.13E-05 ± 1.89E-06	2.15E-05 ± 5.85E-06	7.93E-06 ± 2.19E-06	1.36E-05 ± 4.08E-06	2.32E-04 ± 2.28E-05	1.17E-06 ± 2.10E-08
5/23/2013 12:00	1.05E-05 ± 3.13E-06	8.00E-06 ± 1.91E-06	7.61E-06 ± 5.27E-06	8.70E-06 ± 9.05E-07	3.53E-05 ± 5.49E-07	1.68E-06 ± 5.09E-07
5/24/2013 10:00	7.33E-06 ± 1.33E-06	1.20E-05 ± 3.20E-06	9.41E-06 ± 6.03E-07	9.58E-06 ± 1.35E-06	2.67E-05 ± 4.85E-07	3.33E-06 ± 3.46E-07
5/29/2013 13:20	4.33E-06 ± 1.00E-06	9.19E-06 ± 5.26E-07	2.19E-06 ± 1.08E-06	5.24E-06 ± 2.07E-06	2.00E-05 ± 5.82E-07	1.08E-06 ± 3.79E-09
5/30/2013 15:33	3.81E-06 ± 2.16E-07	7.49E-06 ± 2.04E-06	6.71E-06 ± 3.01E-06	6.00E-06 ± 1.12E-06	1.95E-05 ± 4.96E-07	1.09E-06 ± 1.91E-08
5/31/2013 10:40	5.70E-06 ± 2.43E-06	4.86E-06 ± 1.53E-06	5.38E-06 ± 3.30E-06	5.31E-06 ± 2.45E-07	2.17E-05 ± 8.90E-07	1.27E-06 ± 9.37E-08
6/4/2013 11:18	4.31E-06 ± 2.22E-07	3.50E-06 ± 5.44E-07	4.98E-06 ± 1.97E-06	4.26E-06 ± 4.28E-07	1.81E-05 ± 4.16E-07	1.10E-06 ± 4.73E-09
6/6/2013 11:09	4.00E-06 ± 4.95E-07	6.71E-06 ± 2.17E-06	3.84E-06 ± 1.57E-06	4.85E-06 ± 9.31E-07	1.59E-05 ± 7.22E-07	1.10E-06 ± 1.22E-08
6/7/2013 10:35	7.47E-06 ± 3.04E-06	7.39E-06 ± 1.29E-06	4.90E-06 ± 1.22E-06	6.59E-06 ± 8.44E-07	1.95E-05 ± 2.74E-07	1.12E-06 ± 1.31E-08
7/10/2013 15:10	2.69E-06 ± 2.16E-07	2.52E-06 ± 3.55E-07	2.17E-06 ± 3.97E-07	2.46E-06 ± 1.53E-07	8.26E-06 ± 2.07E-07	1.42E-06 ± 1.42E-08

A.4.2 Supplemental Data

All data presented throughout the report is done with standard error as (\pm SE) unless otherwise noted.

Table A.4.5. All biofilter N₂O concentrations for each sampling day.

Date and Start Time	Avg. Biofilter North (mg N ₂ O/ L)	Avg. Biofilter South (mg N ₂ O/ L)	Avg. Biofilter Side (mg N ₂ O/ L)	Tot. Avg. Biofilter Conc. (mg N ₂ O/ L)	Pipe Concentration (mg N ₂ O/ L)	Ambient Concentration (mg N ₂ O/ L)
5/21/2013 12:15	5.01E-04 \pm 1.87E-05	5.08E-04 \pm 7.38E-06	4.96E-04 \pm 1.76E-05	5.02E-04 \pm 3.48E-06	7.59E-04 \pm 2.61E-05	5.00E-04 \pm 1.19E-05
5/23/2013 12:00	7.14E-04 \pm 7.85E-05	5.89E-04 \pm 2.24E-05	6.96E-04 \pm 4.03E-05	6.66E-04 \pm 3.90E-05	7.00E-04 \pm 2.87E-05	4.82E-04 \pm 2.75E-05
5/24/2013 10:00	5.82E-04 \pm 7.42E-05	7.20E-04 \pm 1.10E-04	5.76E-04 \pm 3.62E-05	6.26E-04 \pm 4.70E-05	7.32E-04 \pm 3.11E-05	4.89E-04 \pm 2.17E-05
5/29/2013 13:20	4.69E-04 \pm 5.40E-05	6.60E-04 \pm 7.83E-05	4.52E-04 \pm 3.75E-05	5.27E-04 \pm 6.67E-05	8.93E-04 \pm 3.07E-05	5.25E-04 \pm 2.73E-05
5/30/2013 15:33	6.13E-04 \pm 5.26E-05	6.92E-04 \pm 7.01E-05	6.61E-04 \pm 1.35E-04	6.55E-04 \pm 2.30E-05	9.65E-04 \pm 2.42E-05	5.70E-04 \pm 2.65E-05
5/31/2013 10:40	5.68E-04 \pm 5.42E-05	5.90E-04 \pm 6.81E-05	5.91E-04 \pm 3.91E-05	5.83E-04 \pm 7.51E-06	7.79E-04 \pm 2.49E-05	4.79E-04 \pm 4.12E-05
6/4/2013 11:18	5.97E-04 \pm 4.57E-05	5.62E-04 \pm 1.05E-04	5.22E-04 \pm 1.08E-04	5.60E-04 \pm 2.17E-05	1.08E-03 \pm 2.81E-05	5.11E-04 \pm 2.43E-05
6/6/2013 11:09	7.58E-04 \pm 9.48E-05	6.42E-04 \pm 1.02E-04	5.72E-04 \pm 1.02E-04	6.57E-04 \pm 5.42E-05	1.20E-03 \pm 3.67E-05	4.03E-04 \pm 4.51E-05
6/7/2013 10:35	9.04E-04 \pm 2.86E-04	7.24E-04 \pm 9.32E-05	6.86E-04 \pm 1.06E-04	7.71E-04 \pm 6.72E-05	1.42E-03 \pm 3.77E-05	5.27E-04 \pm 2.18E-05
7/10/2013 15:10	7.72E-04 \pm 3.07E-05	6.67E-04 \pm 5.89E-05	5.92E-04 \pm 6.64E-05	6.77E-04 \pm 5.22E-05	1.97E-03 \pm 1.88E-04	5.19E-04 \pm 5.75E-06

Table A.4.6. Wind speed for the time period of sampling from the Esparto, Calif., CIMIS site.

Date and Start Time	Wind Speed, Esparto, CA (m s ⁻¹)
5/21/2013 12:15	4.1
5/23/2013 12:00	2.4
5/24/2013 10:00	1.5
5/29/2013 13:20	1.7
5/30/2013 15:33	1.7
5/31/2013 10:40	3.85
6/4/2013 11:18	1.4
6/6/2013 11:09	1.2
6/7/2013 10:35	1.75
7/10/2013 15:10	3

Table A.4.7. Average of the measured pipe velocity by day and those values after being converted using information given in Appendix A.4.1.1 and then to m³ min⁻¹.

Date and Start Time	Measured Pipe Velocity (ft min⁻¹)	Average Pipe Flow converted (m³ min⁻¹)
5/21/2013 12:15	539 ± 19	22.01 ± 0.08
5/23/2013 12:00	887 ± 7	36.20 ± 0.03
5/24/2013 10:00	877 ± 12	35.80 ± 0.05
5/29/2013 13:20	670 ± 42	27.36 ± 0.17
5/30/2013 15:33	677 ± 56	27.63 ± 0.23
5/31/2013 10:40	710 ± 26	28.99 ± 0.11
6/4/2013 11:18	617 ± 17	25.18 ± 0.07
6/6/2013 11:09	655 ± 15	26.75 ± 0.06
6/7/2013 10:35	683 ± 1	27.90 ± 0.00
7/10/2013 15:10	572 ± 0	23.34 ± 0.00

Table A.4.8. CO₂ Entrainment Factors for each section and the average daily R factor. Calculated using equation EQ 3.11.

Date and Start Time	Calculated CO₂ Entrainment Factor (R) North	Calculated CO₂ Entrainment Factor (R) South	Calculated CO₂ Entrainment Factor (R) Side	Average Daily Calculated CO₂ Entrainment Factor (R)
5/21/2013 12:15	12.13	10.42	21.11	14.55 ± 3.32
5/23/2013 12:00	2.07	3.19	4.05	3.10 ± 0.57
5/24/2013 10:00	2.89	1.13	2.55	2.19 ± 0.54
5/29/2013 13:20	3.29	1.16	11.36	5.27 ± 3.11
5/30/2013 15:33	4.19	1.77	1.50	2.49 ± 0.86
5/31/2013 10:40	4.16	5.73	5.48	5.12 ± 0.49
6/4/2013 11:18	3.16	2.38	3.09	2.88 ± 0.25
6/6/2013 11:09	1.12	1.25	5.42	2.59 ± 1.41
6/7/2013 10:35	1.71	2.21	4.70	2.88 ± 0.92
7/10/2013 15:10	2.03	6.05	15.24	7.77 ± 3.91

Table A.4.9. All biofilter CH₄ filter efficiencies (f_i) for each section and average for each sampling day calculated using equation EQ 3.9. Filter efficiency of 1 is equal to no filtration, and 0 is equal to total filtration. $RE_e = 1-f_i$.

Date and Start Time	Avg. Filter Efficiency - North	Avg. Filter Efficiency-South	Avg. Filter Efficiency – Side	Tot. Avg. Biofilter Filter Efficiency
5/21/2013 12:15	0.60 ± 0.12	1.01 ± 0.29	0.68 ± 0.20	0.76 ± 0.12
5/23/2013 12:00	0.83 ± 0.25	0.83 ± 0.20	0.91 ± 0.63	0.86 ± 0.03
5/24/2013 10:00	0.78 ± 0.14	0.84 ± 0.22	0.95 ± 0.07	0.86 ± 0.05
5/29/2013 13:20	0.79 ± 0.18	0.94 ± 0.06	0.84 ± 0.41	0.85 ± 0.04
5/30/2013 15:33	0.82 ± 0.05	0.97 ± 0.27	0.79 ± 0.36	0.86 ± 0.05
5/31/2013 10:40	1.09 ± 0.47	1.13 ± 0.36	1.22 ± 0.75	1.15 ± 0.04
6/4/2013 11:18	0.83 ± 0.05	0.57 ± 0.09	0.95 ± 0.38	0.78 ± 0.11
6/6/2013 11:09	0.50 ± 0.06	0.87 ± 0.28	1.13 ± 0.46	0.83 ± 0.18
6/7/2013 10:35	0.95 ± 0.38	1.08 ± 0.19	1.13 ± 0.28	1.05 ± 0.05
7/10/2013 15:10	0.73 ± 0.06	1.05 ± 0.15	1.18 ± 0.22	0.99 ± 0.13

Table A.4.10. All biofilter N₂O filter efficiencies (f_i) for each section and average for each sampling day calculated using equation EQ 3.9. Filter efficiency of 1 is equal to no filtration, and 0 is equal to total filtration. $RE_e = 1 - f_i$.

Date and Start Time	Avg. Filter Efficiency - North	Avg. Filter Efficiency - South	Avg. Filter Efficiency - Side	Tot. Avg. Biofilter Filter Efficiency
5/21/2013 12:15	0.44 ± 0.04	0.45 ± 0.03	0.43 ± 0.04	0.44 ± 0.00
5/23/2013 12:00	0.52 ± 0.15	0.41 ± 0.06	0.47 ± 0.10	0.47 ± 0.03
5/24/2013 10:00	0.22 ± 0.14	0.34 ± 0.19	0.22 ± 0.07	0.26 ± 0.04
5/29/2013 13:20	0.45 ± 0.09	0.66 ± 0.12	0.42 ± 0.08	0.51 ± 0.08
5/30/2013 15:33	0.58 ± 0.09	0.66 ± 0.10	0.64 ± 0.19	0.62 ± 0.03
5/31/2013 10:40	0.48 ± 0.12	0.49 ± 0.15	0.49 ± 0.11	0.49 ± 0.00
6/4/2013 11:18	0.55 ± 0.08	0.51 ± 0.16	0.48 ± 0.17	0.51 ± 0.02
6/6/2013 11:09	0.66 ± 0.13	0.56 ± 0.14	0.51 ± 0.21	0.58 ± 0.04
6/7/2013 10:35	0.73 ± 0.33	0.60 ± 0.12	0.59 ± 0.16	0.64 ± 0.05
7/10/2013 15:10	0.48 ± 0.06	0.45 ± 0.09	0.41 ± 0.11	0.44 ± 0.02

Table A.4.11. All biofilter CH₄ emissions originating from the compost source for each section and average for each sampling day calculated using formula EQ 3.10a.

Date and Start Time	Avg. Emissions -North (g CH₄ day⁻¹)	Avg. Emissions -South (g CH₄ day⁻¹)	Avg. Emissions - Side (g CH₄ day⁻¹)	Tot. Avg. Biofilter Emissions (g CH₄ day⁻¹)
5/21/2013 12:15	4430 ± 952	7395 ± 2248	5023 ± 1538	5616 ± 906
5/23/2013 12:00	1529 ± 459	1518 ± 369	1680 ± 1167	1576 ± 52
5/24/2013 10:00	1080 ± 200	1155 ± 310	1307 ± 95	1181 ± 67
5/29/2013 13:20	621 ± 145	737 ± 52	661 ± 327	673 ± 34
5/30/2013 15:33	638 ± 42	752 ± 207	617 ± 278	669 ± 42
5/31/2013 10:40	988 ± 424	1022 ± 327	1102 ± 679	1037 ± 34
6/4/2013 11:18	546 ± 33	375 ± 59	622 ± 247	514 ± 73
6/6/2013 11:09	303 ± 42	534 ± 176	690 ± 285	509 ± 112
6/7/2013 10:35	741 ± 302	847 ± 149	884 ± 221	824 ± 43
7/10/2013 15:10	203 ± 17	293 ± 42	327 ± 60	274 ± 37

Table A.4.12. All biofilter N₂O emissions originating from the compost source for each section and average for each sampling day calculated using formula EQ 3.10b.

Date and Start Time	Avg. Emissions - North (g N₂O day⁻¹)	Avg. Emissions - South (g N₂O day⁻¹)	Avg. Emissions - Side (g N₂O day⁻¹)	Tot. Avg. Biofilter Emissions (g N₂O day⁻¹)
5/21/2013 12:15	10.6 ± 1.1	10.8 ± 0.7	10.4 ± 1.0	10.6 ± 0.1
5/23/2013 12:00	19.2 ± 5.5	14.9 ± 2.3	17.1 ± 3.6	17.0 ± 1.2
5/24/2013 10:00	8.2 ± 5.3	12.9 ± 7.0	8.4 ± 2.8	9.8 ± 1.5
5/29/2013 13:20	15.9 ± 3.3	23.4 ± 4.2	14.9 ± 2.8	18.1 ± 2.7
5/30/2013 15:33	22.1 ± 3.4	25.4 ± 4.0	24.4 ± 7.2	24.0 ± 1.0
5/31/2013 10:40	15.7 ± 4.0	16.0 ± 4.9	16.1 ± 3.5	15.9 ± 0.1
6/4/2013 11:18	21.3 ± 3.0	20.1 ± 6.1	18.7 ± 6.6	20.0 ± 0.8
6/6/2013 11:09	30.5 ± 6.0	25.9 ± 6.5	23.7 ± 9.7	26.7 ± 2.0
6/7/2013 10:35	41.9 ± 19.1	34.0 ± 6.8	33.4 ± 9.0	36.4 ± 2.7
7/10/2013 15:10	31.9 ± 4.9	29.5 ± 6.5	27.0 ± 7.8	29.4 ± 1.4

Bibliography

- Abbasi M.K., and W.A. Adams. 2000. Gaseous N emission during simultaneous nitrification-denitrification associated with mineral N fertilization to a grassland soil under field conditions. *Soil Biol. Biochem.*32: 1251-1259.
- Akdeniz, N., and K. A. Janni. 2012. Full-scale biofilter reduction efficiencies assessed using portable 24-hour sampling units. *J. Air & Waste Mgmt. Assoc.* 62 (2): 170-182.
- Alluvione F., C. Bertora, L. Zavattaro, and C. Grignani. 2010. Nitrous oxide and carbon dioxide emissions following green manure and compost fertilization in corn. *Soil Sci. Soc.Am. J.* 74: 384-395.
- Alsina, Maria Mar, Ana Clara Fanton-Borges, and David R. Smart. 2013. "Spatiotemporal Variation of Event Related N₂O and CH₄ Emissions during Fertigation in a California Almond Orchard." *Ecosphere*: 1–21.
- Andersen, J., Boldrin, A., Samuelsson, J., Christensen, T., Scheutz, C., 2010. Quantification of greenhouse gas emissions from windrow composting of garden waste. *J. Environ. Qual.* 39, 713–724.
- Bailey, S. 2013. Greenhouse gas emissions from composting: a study of two methods. Master's Thesis. University of California, Davis.
- Barraclough, D., 1995. The use of 15N pool dilution and enrichment to separate the heterotrophic and autotrophic pathways of nitrification. *Soil Biol. Biochem* 27, 6.
- Bateman E.J., and E.M. Baggs. 2005. Contributions of nitrification and denitrification to N₂O emissions from soils at different water-filled pore space. *Biol. Fert. Soils.* 41: 379-388.
- Beauchamp, E., Kidd, G., Thurtell, G., 1978. Ammonia volatilization from sewage sludge applied in the field. *J. Environ. Qual.* 7, 141–146.
- Beck-Friis, B., Pell, M., Sonesson, U., Jonsson, H., Kirchmann, H., 2000. Formation and emission of N₂O and CH₄ from compost heaps of organic household waste. *Environ. Monit. Assess.* 62, 317–331.
- Beck-Friis, B., S. Smårs, H. Jönsson, Y. Eklind, and H. Kirchmann. 2003. Composting of source-separated household organics at different oxygen levels: gaining an understanding of emission dynamics. *Compost Sci. Util.* 11(1): 41-50.
- Bengtsson G., S. Fronaeus, and L. Bengtsson-Kloo. 2002. The kinetics and mechanism of oxidation of hydroxylamine by iron (III). *J Chem. Soc. Dalton.* 12: 2548-2552.
- Bogner, J.E., Spokas, K.A., Chanton, R.P., 2011. Seasonal Greenhouse Gas Emissions (Methane, Carbon Dioxide, Nitrous Oxide) from Engineered Landfills: Daily, Intermediate, and Final California Cover Soils. *J. Environ. Qual.* 40, 1010–1020.
- Bohn, H. 1992. Consider biofiltration for decontaminating gases. *Chem. Eng. Progress.* 88: 34–40.

- Bollmann A., and R. Conrad. 1998. Influence of O₂ availability on NO and N₂O release by nitrification and denitrification in soils. *Glob. Change Biol.* 4: 387-396.
- Bouwman A.F., L.J.M. Boumans, and N.H. Batjes. 2002. Modeling global annual N₂O and NO emissions from fertilized fields. *Glob. Biogeochem. Cycles.* 16(4): 1080.
- Bouwman A.F., Fung, I., Matthews, E., John, J. 1993. Global analysis of the potential for N₂O production in natural soils. *Global Biogeochem Cycles.* 7: 557-597.
- Bremner, J.M., Blackmer, A.M., and Waring, S.A. 1980. Formation of nitrous oxide and dinitrogen by chemical decomposition of hydroxylamine in soils. *Soil Biol. Biochem.* 12: 263-269.
- Bremner, J.M., and Blackmer, A.M.. 1979. Effects of acetylene and soil-water content on emission of nitrous oxide from soils. *Nature.* 280: 380-381.
- Bremner, J.M. 1997. Sources of nitrous oxide in soils. *Nutr Cycl Agroecosys.* 49: 7-16.
- Bremner, J.M., Blackmer, A.M., Waring, S.A. 1980. Formation of nitrous oxide and dinitrogen by chemical decomposition of hydroxylamine in soils. *Soil Biol Biochem.* 12: 263-269.
- Bremner, J.M., Heintze, S.G., Mann, P.J.G., Lees, H. 1946. Metallo-organic complexes in soil. *Nature.* 158: 790-791.
- Brooks, P.D., Stark, J.M., McInteer, B.B., Preston, T. 1989. Diffusion Method to Prepare Soil Extracts for Automated N-15 Analysis. *Soil Science Society of America Journal* 53, 1707-1711.
- Brown, H., Wagner-Riddle, C., Thurtell G. 2002. Nitrous oxide flux from a solid dairy manure pile measured using a micrometeorological mass balance method. *Nut. Cycl. Agroecosys.* 62, 53–60.
- Brown, S., Kruger, C., Subler, S. 2008. Greenhouse gas balance for composting operations. *J. Environ. Qual.* 37, 1396–1410.
- Burger, M., and R. Venterea. 2011. "Effects of Nitrogen Fertilizer Types on Nitrous Oxide Emissions." In *Understanding Greenhouse Gas Emissions from Agricultural Management*, 1072:179–202. ACS Symposium Series. American Chemical Society.
- Burger, M., L. E. Jackson, E. J. Lundquist, D. T. Louie, R. L. Miller, D. E. Rolston, and K. M. Scow. 2005. "Microbial Responses and Nitrous Oxide Emissions during Wetting and Drying of Organically and Conventionally Managed Soil under Tomatoes." *Biology and Fertility of Soils* 42 (2): 109–118.
- Butnor, J. R. and K. H. Johnsen. 2004. Calibrating soil respiration measures with a dynamic flu apparatus using artificial soil media of varying porosity. *Eur. J. Soil Sci.* 55: 639-647.
- Buyuksonmez, F. 2011. Prepared for San Joaquin Valleywide Pollution Study Agency: *Comparison of mitigation measures for reduction of emissions resulting from*

greenwaste composting. San Diego State University, San Diego, CA. [Viewed July 31, 2013]. Available from: <http://www.calrecycle.ca.gov/Organics/Air/> or http://www.valleyair.org/busind/pto/emission_factors/criteria/criteria/composting/final-compost-study-report.pdf.

California Energy Commission, 2005. Research roadmap for greenhouse gas inventory

Calrecycle, 2012. <http://www.calrecycle.ca.gov/Laws/Regulations/title14/ch31.htm>. Accessed on May 20, 2012.

CalRecycle. 2010. Climate Change and Solid Waste Management: Organics. Accessed 2012. [Available online at <http://www.calrecycle.ca.gov/Climate/Organics/default.htm>]

CARB. 2011. "California Greenhouse Gas Emissions Inventory: 2000-2009". Sacramento, CA: California Air Resources Board, California Environmental Protection Agency. <http://www.arb.ca.gov/cc/inventory/data/data.htm>.

Chen, L., and S. J. Hoff. 2009. Mitigating Odors from Agricultural Facilities: A Review of Literature Concerning Biofilters. *Appl. Eng. Agric.* 25(5): 751-766.

Churchill, D.B., W.R. Horwath, L.F. Elliott, and D.M. Bilsland. 1995. Perennial Ryegrass Response to Application of Composted Grass Seed Straw. *J. Applied Seed Prod.* 13:16-21.

Contreras-Ramos S.M., D. Alvarez-Bernal, J.A. Montes-Molina, O. Van Cleemput, and L. Dendooven. 2009. Emission of nitrous oxide from hydrocarbon contaminated soil amended with waste water sludge and earthworms. *Appl. Soil Ecol.* 41: 69-76.

Coyne M.S., and J.M. Tiedje. 1990. Induction of denitrifying enzymes in oxygen-limited achromobacter-cycloclastes continuous culture. *Fems Microbiol. Ecol.*73: 263-270.

Dalal R.C., I. Gibson, D.E. Allen, and N.W. Menzies. 2010. Green waste compost reduces nitrous oxide emissions from feedlot manure applied to soil. *Agr. Ecosyst. Environ.* 136: 273-281.

Davidson, E.A., 1991. Fluxes of nitrous oxide and nitric oxide from terrestrial ecosystems, in *Microbial Production and Consumption of Greenhouse Gases: Methane, Nitrogen Oxides and Halomethanes*. Edited by J. E. Rogers and W. B. Whitman.

Davidson, E.A., 2011. Poorly known roles of iron and other metals in the nitrogen cycle. *Abstracts of Papers of the American Chemical Society* 242.

Denmead, O. 2008. Approaches to measuring fluxes of methane and nitrous oxide between landscapes and the atmosphere. *Plant Soil.* 309: 5–24.

Denmead, O. T., 1995. Novel meteorological methods for measuring trace gas fluxes. *Phil. Trans.: Phys. Sci. Eng.* 351, 383–396.

Dever, S.A., G.E. Swarbrick, and R.M. Stuetz. 2007. Passive drainage and biofiltration of landfill gas: Australian field trial. *Waste Management.* 27:277-286.

Dixit, R.M., S.C. Deshmuh, A.A. Gadhe, G.S. Kannade, S.K. Lokhande, R.A. Pandey, A.N. Vaidya, S.N. Mudliar, and M.A. Deshusses. 2012. Treatment of mixtures of toluene and n-propanol vapours in a compost–woodchip-based biofilter. *Environmental technology*. 33(7): 751-760.

Doane T.A., and W.R. Horwath. 2003. Spectrophotometric determination of nitrate with a single reagent. *Anal. Lett.* 36: 2713-2722.

Dobbie, K.E., I.P. McTaggart, and K.A. Smith. 1999. Nitrous oxide emissions from intensive agricultural systems: Variations between crops and seasons, key driving variables, and mean emission factors. *Journal of Geophysical Research-Atmospheres* 104:26891-26899.

Dominik, P., Kaupenjohann, M. 2000. Simple spectrophotometric determination of Fe in oxalate and HCl soil extracts. *Talanta* 51: 701-707.

Edis, R.B., D. Chen, G. Wang, D.A. Turner, K. Park, M. Meyer, and C. Kirkby. 2008. Soil nitrogen dynamics in irrigated maize systems as impacted on by nitrogen and stubble management. *Australian Journal of Experimental Agriculture* 48:382-386.

Engineered Compost Systems (ECS). 2011. *Aerated Static Pile Systems*. [Viewed June 2013]. Available from: <http://www.compostsystems.com/systems/ac-composter>

Esposito Vinzi V. 2010. *Handbook of partial least squares: concepts, methods and applications*. Springer, New York.

Firestone M.K., R.B. Firestone, and J.M. Tiedje. 1980. Nitrous oxide from soil denitrification - factors controlling its biological production. *Science*. 208: 749-751.

Flesch, T., Wilson, J., Yee, E., 1995. Backward-time Lagrangian stochastic dispersion models and their application to estimate gaseous emissions. *J. Appl. Meteorol.* 34, 1320–1332.

Fortuna, A.M., Honeycutt, C.W., Vandemark, G., Griffin, T.S., Larkin, R.P., He, Z.Q., Wienhold, B.J., Sistani, K.R., Albrecht, S.L., Woodbury, B.L., Torbert, H.A., Powell, J.M., Hubbard, R.K., Eigenberg, R.A., Wright, R.J., Alldredge, J.R., Harsh, J.B., 2012. Links among Nitrification, Nitrifier Communities, and Edaphic Properties in Contrasting Soils Receiving Dairy Slurry. *Journal of Environmental Quality* 41, 262-272.

Fowler, D., Coyle, M., Flechard, C., Hargreaves, K., Nemitz, E., Storeton-West, R., Sutton, M., Erisman, J., 2001. Advances in micrometeorological methods for the measurement and interpretation of gas and particle nitrogen fluxes. *Plant Soil* 228, 117–129.

Gao, F., and S. R. Yates. 1998. Laboratory study of closed and dynamic flux chambers: Experimental results and implications for field applications. *J. Geophys. Res.* 103(D20): 26,115-26,125.

- Gao, F., Yates, S. R., Yates, M. V., Gan, J., Ernest, F. F. 1997. Design, fabrication, and application of a dynamic chamber for measuring gas emission from soil. *Environ. Sci. Technol.* 37: 148-153.
- Garland, Gina M., Emma Suddick, Martin Burger, W.R. Horwath, and Johan Six. 2011. "Direct N₂O Emissions Following Transition from Conventional till to No-till in a Cover Cropped Mediterranean Vineyard (*Vitis Vinifera*).” *Agriculture, Ecosystems & Environment* 144 (1) (November): 423–428.
- Glass J.B., and V.J. Orphan. 2012. Trace metal requirements for microbial enzymes involved in the production and consumption of methane and nitrous oxide. *Front. Microbio.* 3: 61.
- Goodroad, L.L., Keeney, D.R., 1984. Nitrous-Oxide Production in Aerobic Soils under Varying pH, Temperature and Water-Content. *Soil Biology & Biochemistry* 16, 39-43.
- Goreau T.J., W.A. Kaplan, S.C. Wofsy, M.B. Mcelroy, F.W. Valois, and S.W. Watson. 1980. Production of NO₂- and N₂O by nitrifying bacteria at reduced concentrations of oxygen. *Appl. Environ. Microb.* 40: 526-532.
- Hellebrand, H. J. 1998. Emission of nitrous oxide and other trace gases during composting of grass and green waste. *J. Agric. Eng. Res.* 69: 365-375.
- Hellmann, B., L. Zelles, A. Palojärvi and Q. Bai. 1997. Emission of climate- relevant trace gases and succession of microbial communities during open-windrow composting. *Appl. Environ. Microbiol.* 63(3): 1011-1018.
- Hobsen, A.M., J. Frederickson, and N.B. Dise. 2005. CH₄ and N₂O from mechanically turned windrow and vermicomposting systems following in-vessel pre-treatment. *Waste Management.* 25: 345-352
- Hong, J.H., and K.J. Park. 2005. Compost biofiltration of ammonia gas from bin composting. *Bioresour. Technol.* 96: 741-745.
- Hood R., R. Merckx, E.S. Jensen, D. Powlson, M. Matijevic, and G. Hardarson. 2000. Estimating crop N uptake from organic residues using a new approach to the 15N isotope dilution technique. *Plant Soil.* 223: 33-44.
- Horwath WR. 2007. Carbon Cycling and Formation of Soil Organic Matter. E.A. Paul, Ed. In: *Soil Microbiology, Ecology and Biochemistry*. Academic Press, New York, pp. 303-339.
- Horwath, W.R. and L.F. Elliott. 1996. Microbial C and N dynamics during mesophilic and thermophilic incubations of ryegrass. *Biol. Fertil Soils* 22:1-9.
- Huang, Q., Q. Zhang, N. Cicek, and D. Mann. 2011. Biofilter: a promising tool for mitigating methane emission from manure storage. *J. Arid Land.* 3(1):61-70.
- Hutchinson, G.L., and A.R. Mosier. 1981. Improved soil cover method for field measurement of nitrous oxide fluxes. *Soil Science Society of America Journal* 45:311-316.

Hutchinson, G.L., and G.P. Livingston. 1993. Use of chamber systems to measure trace gas fluxes, *In* D. E. Rolston, ed. *Agricultural Ecosystem Effects on Trace Gases and Global Climate Change*. ASA Special Publication no. 55, Madison, WI.

Inubushi K., S. Goyal, K. Sakamoto, Y.Wada, K.Yamakawa, and T. Arai, 2000. Influences of application of sewage sludge compost on N₂O production in soils. *Chemosphere*. 2: 6.

IPCC. 2007. Mitigation of climate change. In: B. Metz et al., editors, *Contribution of working group III to the fourth assessment report of the intergovernmental panel on climate change*, Cambridge Univ Press, Cambridge, UK. p. 105.

Jäckel, U., Thummes, K., and Kämpfer, P. 2005. Thermophilic methane production and oxidation in compost. *FEMS Microbiol. Ecol.* 52: 175-184.

Kallenbach, C.M., Rolston, D.E., and Horwath, W.R. 2010. "Cover Cropping Affects Soil N₂O and CO₂ Emissions Differently Depending on Type of Irrigation." *Agriculture, Ecosystems & Environment* 137: 251–260.

Kampschreur, M.J., Kleerebezem, R., de Vet, W.W.J.M. and van Loosdrecht, M.C.M. 2011. Reduced iron induced nitric oxide and nitrous oxide emission. *Water Res.* 45: 5945-5952.

Kent, E.R. 2012. Micrometeorological measurements of greenhouse gas emissions from composting yard-waste. Master's Thesis. University of California, Davis.

Khalil, K., Mary, B., Renault, P. 2004. Nitrous oxide production by nitrification and denitrification in soil aggregates as affected by O₂ concentration. *Soil Biology & Biochemistry* 36, 687-699.

Khan, R. Z., Muller, C., Sommer, S. G. 1997. Micrometeorological mass balance technique for measuring CH₄ emission from stored cattle slurry. *Biol. Fertil. Soils* 24, 442–444.

Kochendorfer, J. and Paw U, K.T. 2011. Field estimates of scalar advection across a canopy edge. *Agric. Forest Meteorol.* 151:585-594.

Kong, Angela Y.Y., Steven J. Fonte, Chris van Kessel, and Johan Six. 2009. "Transitioning from Standard to Minimum Tillage: Trade-Offs between Soil Organic Matter Stabilization, Nitrous Oxide Emissions, and N Availability in Irrigated Cropping Systems." *Soil and Tillage Research* 104 (2) (July): 256–262.

Laughlin, R.J., Stevens, R.J., 2002. Evidence for fungal dominance of denitrification and codenitrification in a grassland soil. *Soil Science Society of America Journal* 66, 1540-1548.

Lee, Juhwan, Jan W. Hopmans, Chris van Kessel, Amy P. King, K. Jeannie Evatt, Dianne Louie, Dennis E. Rolston, and Johan Six. 2009. "Tillage and Seasonal Emissions of CO₂, N₂O and NO across a Seed Bed and at the Field Scale in a Mediterranean Climate." *Agriculture, Ecosystems & Environment* 129: 378–390.

- Leson, G., and A. M. Winer. 1991. Biofiltration: an innovative air pollution control technology for VOC emissions. *J. Air & Waste Mgmt. Assoc.* 41(8): 1045-1054.
- Linn, D.M., and Doran, J.W. 1984. Effect of water-filled pore space on carbon dioxide and nitrous oxide production in tilled and nontilled soils. *Soil Science Society of America Journal* 48:1267-1272.
- Loveland, P.J., and Digby, P. 1984. The extraction of Fe and Al by 0.1 M-pyrophosphate solutions - a comparison of some techniques. *J. Soil Sci.* 35: 243-250.
- Lovley, D.R., Phillips, E.J.P. 1987 Rapid assay for microbially reducible ferric iron in aquatic sediments. *Appl Environ Microbiol* 53: 1536-1540.
- Lynch, N.J., and Cherry, R.S. 1996. Design of passively aerated compost pile: Vertical air velocities between the pipes. *Biotechnol. Prog.* 41(5): 624-629
- Marsh, R. 1992. Biofiltration History, Theoretical Model and Practice, North Western Branch Papers. *Inst. of Chemical Eng.* 3:13.1-13.14.
- Martinec, M., Hartung, E., Jungbluth, T., Schneider, F., and Wieser, P.H. 2001. Reduction of gas, odor, and dust emissions from swine operations with biofilters. ASAE Paper No. 014079 St. Joseph, Mich.: ASAE.
- McGinn, S., 2006. Measuring greenhouse gas emissions from point sources in agriculture. *Canad. J. Soil Sci.* 86, 355–371.
- McNevin, D., and J. Barford. 2000. Biofiltration as an odour abatement strategy. *J. Biochem. Eng.* 5:231 - 242.
- McSwiney, C.P., and G.P. Robertson. 2005. Nonlinear response of N₂O flux to incremental fertilizer addition in a continuous maize (*Zea mays* L.) cropping system. *Global Change Biology* 11:1712-1719.
- Meiklejohn, J. 1953. Iron and the nitrifying bacteria. *J Gen Microbiol* 8: 58-65.
- Mondini C., M.L. Cayuela, T. Sinicco, F. Cordaro, A. Roig, and M.A. Sanchez-Monedero. 2007. Greenhouse gas emissions and carbon sink capacity of amended soils evaluated under laboratory conditions. *Soil Biol. Biochem.* 39: 1366-1374.
- Morgan-Sagastume, J.M., and A. Noyola. 2006. Hydrogen sulfide removal by compost biofiltration: Effect of mixing the filter media on operational factors. *Bioresour. Technol.* 97:1546-1553.
- Mueller, J.C. 1988. Biofiltration of gases - A mature technology for control of a wide range of air pollutants, British Columbia Res. Corp., Vancouver, B.C., Canada, 1
- Mulvaney, R.L., Khan, S.A., Mulvaney, C.S., 1997. Nitrogen fertilizers promote denitrification. *Biology and Fertility of Soils* 24, 211-220.
- Namkoong, W., Park, J-S., VanderGheynst, J.S. 2003. Biofiltration of gasoline vapor by compost media. *Environ. Pollution.* 121:181-187.

- Nicolai, R.E., and Janni, K.A.. 2001. Biofilter media mixture ratio of wood chips and compost treating swine odors. *Water Science and Technology*. 44:261-267.
- Nikiema, J., Bibeau, L., Lavoie, J. 2005. Biofiltration of methane: an experimental study. *Chem Eng. J.* 113:111-117.
- Nikiema, J., R. Brzezinski, and M. Heitz. 2007. Elimination of methane generated from landfills by biofiltration: a review. *Reviews in Environmental Science and Biotechnology*. 6:261-284.
- Norman, J. M., Kucharik, C. J., Gower, S. T., Baldocchi, D. D., Crill, P. M., Rayment, M., Savage, K., Striegl, R. G. 1997. A comparison of six methods for measuring soil-surface carbon dioxide fluxes. *J. Geophys. Res.* 102(D24): 28,771-28,777.
- Pagans, E., Font, X., and Sanchez, A. 2006. Emission of volatile organic compounds from composting of different solid wastes: Abatement by biofiltration. *J. Hazardous Materials*. B131:179-186.
- Pagans, E., Font, X., and Sanchez, A.. 2007. Coupling composting and biofiltration for ammonia and volatile organic compound removal. *Biosystems engineering*. 97:491-500.
- Park, K.-H., and Wagner-Riddle, C. 2010b. Methane Emission Patterns from Stored Liquid Swine Manure. *Asian Australas. J. Anim. Sci.* 23: 1229–1235.
- Park, K., Wagner-Riddle, C., and Gordon, R. 2010a. Comparing methane fluxes from stored liquid manure using micrometeorological mass balance and floating chamber methods. *Agric. For. Meteorol.* 150: 175–181.
- Park, S-J., S-I. Nam, and E-S. Choi. 2001. Removal of odor emitted from composting facilities using a porous ceramic biofilter. *Water Science and Technology*. 44:301-308.
- Park, Y.S., Paw U, K.T., 2004. Numerical estimations of horizontal advection inside canopies. *J. Appl. Meteorol.* 43:1530-1538.
- Playa Vista Development, City of Los Angeles, Department of Building and Safety. 2001. *Regional geochemical assessment of methane, BTEX, CO₂ and H₂S gas occurrences*. [Viewed September 2011]. Available from: <http://www.eti-geochemistry.com/Regional>.
- Poth M., and Focht, D.D. 1985. 15N Kinetic analysis of N₂O production by nitrosomonas-europaea - an examination of nitrifier denitrification. *Appl. Environ. Microb.* 49: 1134-1141.
- Poudel, D.D., Horwath, W.R., Mitchell, J.P., and Temple, S.R. 2001. Impacts of cropping systems on soil nitrogen storage and loss. *Agricultural Systems* 68:253-268.
- Poudel, D.D., Horwath, W.R., Lanini, W.T., Temple, S.R., and van Bruggen. A.H.C. 2002. Comparison of soil N availability and leaching potential, crop yields and weeds in organic, low-input and conventional farming systems in northern California. *Agriculture, Ecosystems and Environment* 90:125-137.

Powell, S.J., Prosser, J.I., 1991. Protection of Nitrosomonas-Europaea Colonizing Clay-Minerals from Inhibition by Nitrapyrin. *Journal of General Microbiology* 137, 1923-1929.

Prieve, D.C. 2000. *A course in fluid mechanics with vector field theory*. Carnegie Mellon University, Department of Chemical Engineering, course 06-703, Fall 2000, Pittsburgh, PA. 219 pp. [Viewed August 2013] Available from:
<http://www.andrew.cmu.edu/course/06-703/Book2000.PDF>

Pumpanen, J., Ilvesniemi, H., Keronen, P., Nissinen, A., Pohja, T., Vesala, T., and Hari, P. 2001. An open chamber system for measuring soil surface CO₂ efflux: Analysis of error sources related to the chamber system. *J. Geophys. Res.* 106(D8): 7985-7992.

R Development Core Team. 2010. R: A language and environment for statistical computing. R Foundation for Statistical Computing, Vienna, Austria. ISBN 3-900051-07-0. [Available online at <http://www.R-project.org>]

Renault P., and Sierra, J. 1994. Modeling oxygen diffusion in aggregated soils .2. Anaerobiosis in topsoil layers. *Soil Sci. Soc. Am. J.* 58: 1023-1030.

Rene, E.R., Murthy, D.V.S., and Swaminathan, T. 2005. Performance evaluation of a compost biofilter treating toluene vapours. *Process Biochemistry.* 40:2771-2779.

Rynk, R. et al. 1992. *On-Farm Composting Handbook*. Ithaca, NY: Northeast Regional Agricultural Engineering Service.

Sadaka, S., Magura, C.R., and Mann, D.D. 2002. Vertical and horizontal airflow characteristics of wood/compost mixtures. *Appl. Eng. Agric.* 18:735-741.

Sall J., Creighton, L., and Lehman, A. 2005. *JMP start statistics: a guide to statistics and data analysis using JMP and JMP in software*. Thomson Brooks/Cole, Pacific Grove, Calif.

Schellenberg, D.L., Alsina, M.M., Muhammad, S., Stockert, C.M., Wolff, M.W., Sanden, B.L., Brown, P.H., and Smart, D.R. 2012. "Yield-Scaled Global Warming Potential from N₂O Emissions and CH₄ Oxidation for Almond (*Prunus Dulcis*) Irrigated with Nitrogen Fertilizers on Arid Land." *Agriculture, Ecosystems & Environment* 155: 7-15.

Schmidt, D., Janni, K., and Nicolai, R. 2004. Biofilter design information. University of Minnesota Extension Biosystems and Agricultural Engineering Update BAEU-18. 25pp.

Schuppli, P.A., Ross, G.J., McKeague, J.A. 1983. The effective removal of suspended materials from pyrophosphate extracts of soil from tropical and temperate regions. *Soil Sci Soc Am J* 47: 1026-1032.

Seligman N.G., Feigenbaum, S., Feinerman, D., and Benjamin, R.W. 1986. Uptake of nitrogen from high C-to-N Ratio, 15N labeled organic residues by spring wheat grown under semiarid conditions. *Soil Biol. Biochem.* 18: 303-307.

Senbayram, M., Chen, R.R., Muhling, K.H., Dittert, K., 2009. Contribution of nitrification and denitrification to nitrous oxide emissions from soils after application of biogas waste and other fertilizers. *Rapid Communications in Mass Spectrometry* 23, 2489-2498.

Simojoki, A., and Jaakkola, A. 2000. Effect of nitrogen fertilization, cropping and irrigation on soil air composition and nitrous oxide emission in a loamy clay. *European Journal of Soil Science* 51:413-424.

Smart, David R.; Alsina, M. Mar; Wolff, Michael W. 2011. N₂O Emissions and Water Management in California Perennial Crops. Edited by: Guo, L; Gunasekara, AS; McConnell, LL ACS symposium series. 1072: 227-255.

Solomon, S., Qin, D., Manning, M., Chen, Z., Marquis, M., Averyt, K.B., Tignor, M., and Miller, H.L. (eds.). 2007. Summary for Policymakers. In: *Climate Change 2007: The Physical Science Basis. Contribution of Working Group I to the Fourth Assessment Report of the Intergovernmental Panel on Climate Change*. Cambridge Univ. Press, Cambridge, United Kingdom and New York, NY, USA.

Sommer, S., McGinn, S., Hao, X., Larney, F. 2004. Techniques for measuring gas emissions from a composting stockpile of cattle manure. *Atmos. Env.* 38, 4643–4652.

Spokas, K., Bogner, J., Chanton, J.P., Morcet, M., Aran, C., Graff, C., Moreau-Le Golvan, Y., Hebe, I. 2006. Methane mass balance at three landfill sites: What is the efficiency of capture by gas collection systems? *Waste Manage.* 26, 516–525.

Staley, B.F., Barlaz, M.A. 2009. Composition of Municipal Solid Waste in the United States and Implications for Carbon Sequestration and Methane Yield. *Journal of Environmental Engineering-Asce* 135, 901-909.

Stark J.M., and Firestone, M.K. 1995. Mechanisms for soil moisture effects on activity of nitrifying bacteria. *Appl. Environ. Microb.* 61: 218-221.

Steenwerth, Kerri, and Belina, K.M. 2008. “Cover Crops and Cultivation: Impacts on Soil N Dynamics and Microbiological Function in a Mediterranean Vineyard Agroecosystem.” *Applied Soil Ecology* 40: 370–380.

Stehfest E., and Bouwman, L. 2006. N₂O and NO emission from agricultural fields and soils under natural vegetation: summarizing available measurement data and modeling of global annual emissions. *Nutr. Cycl. Agroecos.* 74: 207-228. Tenenhaus M., V.E. Vinzi, Y.M. Chatelin, and C. Lauro. 2005. PLS path modeling. *Comput.Stat. Data An.* 48: 159-205.

Suddick, E. C.; Steenwerth, K.; Garland, G. M. 2011. Discerning Agricultural Management Effects on Nitrous Oxide Emissions from Conventional and Alternative Cropping Systems: A California Case Study.; et al. Edited by: Guo, L; Gunasekara, AS; McConnell, LL ACS symposium series. 1072: 203-226.

Swanson, W.J. and Loehr, R.C. 1997. Biofiltration: fundamentals, design and operations principles and applications. *J. Environ. Eng.* 123:538-546.

Tenenhaus M., Vinzi V.E., Chatelin, Y.M., Lauro, C. 2005. PLS path modeling. *Comput Stat Data Anal* 48: 159-205.

- Thauer, R.K., Jungermann, K., Decker, K. 1977. Energy-Conservation in Chemotropic Anaerobic Bacteria. *Bacteriological Reviews* 41, 100-180.
- Trotsenko, Y.A., and Khmelenina, V.N. 2002. Biology of extremophilic and estremotolerant methanotrophs. *Archiv. Microbiol.* 177: 123-131.
- U.S. Environmental Protection Agency (USEPA). 2013. Inventory of greenhouse gas emissions and sinks: 1990-2011. EPA 430-R-13-001
- USDA. 1992. Soil Survey Laboratory Method Manual. Soil Survey Investigations Report no. 42, 8.
- USEPA. 2006. Solid waste management and greenhouse gases: a lifecycle assessment of emissions and sinks. 3rd edition. Washington, DC: USEPA.
- VanCleemput, O., Samater, A.H. 1996. Nitrite in soils: Accumulation and role in the formation of gaseous N compounds. *Fertilizer Research* 45, 81-89.
- VanderGheynst, J.S., Cogan, D.J., Defelice, P.J., Gossett, J.M., and Walker, L.P. 1998. Effect of process management on the emission of organosulfur compounds and gaseous antecedents from composting processes. *Environ. Sci. Technol.* 32: 3713-3718
- VanderZaag, A. C., Wagner-Riddle, C., Park, K.H., Gordon, R. J. 2011. Methane emissions from stored liquid dairy manure in a cold climate. *Anim. Feed Sci. Technol.* 166-67, 581–589.
- Vaughan S.M., Dalal, R.C., Harper, S.M., and Menzies, N.W. 2011. Effect of fresh green waste and green waste compost on mineral nitrogen, nitrous oxide and carbon dioxide from a vertisol. *Waste Manage.* 31: 1720-1728.
- Veihmeyer, F.J., Hendrickson, A.H. 1931. The moisture equivalent as a measure of the field capacity of soils. *Soil Sci* 32: 181-193.
- Venterea, R.T. 2007. Nitrite-driven nitrous oxide production under aerobic soil conditions: kinetics and biochemical controls. *Glob. Change Biol.* 13: 1798-1809.
- Venterea, R.T., Dolan, M.S., Ochsner, T.E. 2010. Urea Decreases Nitrous Oxide Emissions Compared with Anhydrous Ammonia in a Minnesota Corn Cropping System. *Soil Science Society of America Journal* 74, 407-418.
- Venterea, R.T., Rolston, D.E. 2000. Nitric and nitrous oxide emissions following fertilizer application to agricultural soil: Biotic and abiotic mechanisms and kinetics. *Journal of Geophysical Research-Atmospheres* 105, 15117-15129.
- Verdouw H., Vanechteld, C.J.A., and Dekkers, E.M.J. 1978. Ammonia determination based on indophenol formation with sodium salicylate. *Water Res.*12: 399-402.
- Wagner-Riddle, C., Park, K.H., Thurtell, G.W. 2006. A micrometeorological mass balance approach for greenhouse gas flux measurements from stored animal manure. *Agric. For. Meteorol.* 136, 175–187.

- Weier, K.L., Doran, J.W., Power, J.F., Walters, D.T. 1993. Denitrification and the Dinitrogen Nitrous-Oxide Ratio as Affected by Soil-Water, Available Carbon, and Nitrate. *Soil Science Society of America Journal* 57, 66-72.
- Widén, B. and Lindroth, A. 2003. A calibration system for soil carbon-dioxide-efflux measurement chambers: description and application. *Soil Sci. Soc. Am. J.* 67:327-334
- Williams, E.J., Hutchinson, G.L., Fehsenfeld, F.C. 1992. NO_x and N₂O emissions from soil. *Global Biogeochem Cycles* 6: 351-388.
- Wilson, J.D., Shum, W.K.N. 1992. A re-examination of the integrated horizontal flux method for estimating volatilization from circular plots. *Agric. For. Meteorol.* 57, 281–295.
- Wold, S. 1995. Chemometrics; What do we mean with it, and what do we want from it? *Chemometr. Intell. Lab.* 30: 109-115.
- Wrage N., Velthof, G.L., van Beusichem, M.L., and Oenema, O. 2001. Role of nitrifier denitrification in the production of nitrous oxide. *Soil Biol. Biochem.* 33: 1723-1732.
- Wright A.L., Provin, T.L., Hon, F.M., Zuberer, D.A., and White, R.H. 2008. Compost impacts on dissolved organic carbon and available nitrogen and phosphorus in turfgrass soil. *Waste Manage.* 28: 1057-1063.
- Yasuda, T., K. Kuroda, Y. Fukumoto, D. Hanajima, and K. Suzuki. 2009. Evaluation of full-scale biofilter with rockwool mixture treating ammonia gas from livestock composting. *Bioresour. Technol.* 100:1568-1572.
- Zhang, J., Cai, Z., Zhu, T. 2011. N₂O production pathways in the subtropical acid forest soils in China. *Environ Res* 111, 643-649.
- Zhu, X., Burger, M., Doane, T.A., Horwath, W.R. 2013a. Ammonia oxidation pathways and nitrifier denitrification are significant sources of N₂O and NO under low oxygen availability. *Proceedings of the National Academy of Sciences of the United States of America* 110, 6.
- Zhu, X., Silva, L.C., Doane, T.A., Horwath, W.R. 2013b. Iron: the forgotten driver of nitrous oxide production in agricultural soil. *PLoS One* 8, e60146.
- Zhu, X., Silva, L.C.R., Doane, T.A., Wu, N., Horwath, W.R. 2013c. Quantifying the Effects of Green Waste Compost Application, Water Content and Nitrogen Fertilization on Nitrous Oxide Emissions in 10 Agricultural Soils. *Journal of Environmental Quality* 42, 912-918.